

Dissertation zur Erlangung des Doktorgrades der Fakultät für Chemie und Pharmazie
der Ludwig-Maximilians-Universität München

**Structural analysis of stalled ribosomal complexes and
their respective rescue mechanisms by Cryo-Electron
Microscopy**



Paul Huter
aus Zams, Österreich
2018

Erklärung:

Diese Dissertation wurde im Sinne von §7 der Promotionsordnung vom 28.November 2011 von Herrn Prof. Dr. Daniel Wilson betreut.

Eidesstaatliche Erklärung:

Diese Dissertation wurde eigenständig und ohne unerlaubte Hilfe erarbeitet.

München, am 08.05.2018

Paul Huter

Dissertation eingereicht am 08.05.2018

- 1.Gutachter: Herr Prof. Dr. Daniel Wilson
- 2.Gutachter: Herr Prof. Dr. Roland Beckmann

Mündliche Prüfung am 20.06.2018

Table of Contents

Table of Contents	1
Acknowledgments	2
List of Original Publications	4
Abbreviations	7
Summary	9
1 Introduction	10
1.1 Central Dogma of molecular biology.....	10
1.2 Structure of the <i>E. coli</i> ribosome.....	11
1.3 Translation cycle.....	13
1.3.1 Initiation.....	14
1.3.2 Elongation	18
1.3.3 Termination	31
1.3.4 Recycling	36
1.4 Rescue of translational stalled ribosomes	38
1.4.1 <i>Trans</i> -translation, ArfA and ArfB	39
1.4.2 Polyproline mediated stalling and rescue by elongation factor P	49
2 Objectives of these Studies	54
3 Cumulative Thesis: Summary of Publications	56
3.1 Structures of the orthosomycin antibiotics avilamycin and evernimicin in complex with the bacterial 70S ribosome (Publication 1).	56
3.2 Cryo-EM structure of the spinach chloroplast ribosome reveals the location of plastid-specific ribosomal proteins and extensions (Publication 2).....	57
3.3 Structural basis for ArfA-RF2 mediated translation termination on mRNAs lacking stop codons (Publication 3).	57
3.4 Structural basis for ribosome rescue in bacteria (Publication 4).....	58
3.5 Structural basis for polyproline-mediated ribosome stalling and rescue by the elongation factor P (Publication 5).....	59
4 Discussion	61
4.1 Rescue of 'non-stop' complexes with focus on ArfA.....	61
4.2 Structural insights into polyproline-mediated ribosome stalling and rescue by EF-P 70	
5 References	83
6 Publications	108

Acknowledgments

First of all, I want to thank Prof. Dr. Daniel Wilson for giving me the opportunity to join his lab in Munich. I am grateful that he, despite my “starting problems”, gave me enough time to learn and understand the world of cryo-EM. Moreover, I am extremely happy that he gave me the opportunity to work on the ArfA and EF-P project. Hopefully, I was able to pay you back with the impact factor of the publications, but more important, with the choice of whiskey for celebrating them, which reminds me that the EF-P bottle is still closed. Nearly as important as Daniel for my PhD is Dr. Stefan Arenz. I want to thank him for his patient supervision, for his effort in trying to order my chaos and for helping me out whenever needed. It was an enjoyable time working with you, especially when I remember our late-night working sessions. Thanks for everything. In line with that I also have to thank Michael for dealing with all the annoying operational, computational, administrative and bureaucratic *things*, which allowed me to operate smoothly in the background my project and ‘make *things* great again’. Furthermore, I want to thank all the people, of AG Wilson, namely Daniel Sohmen, Bertl, Fabian, Claudia, Maha, Maxi, Aga, Caillan, our guest scientist Mario Mardirossian and Sabine, who saved me a lot of work. Hopefully I did not forget anyone.

I also want to thank the AG Beckmann, especially Prof. Dr. Roland Beckmann. For his interest in our work and for providing us with an awesome infrastructure, which does not only include the electron microscope, but also all the little chemicals, stocks and consumables we were allowed to take. Having said that, I still hope he considers the AG Wilson/AG Beckmann relationship as symbiotic, not parasitic. Talking about provided chemicals, I want to thank Heidi, Joanna, Andrea, Charlotte and Susi, the latter two for making nice EM-grids for me, the former for letting me take an aliquot now and then. Last but not least, I also want to thank Otto and Andre for providing an extremely efficient pipeline and the latter one especially for having a sympathetic ear for any computational issues. I also want to thank Dr. Christian Schmidt for providing the “How to make and validate a model” section, it saved me a lot of time. Also thanks to Dr. Andrea Vaiana for contribution for the EF-P manuscript and the real Italian coffee experience in Erice.

Furthermore, I need to thank my old supervisor Dr. Matthias Erlacher, who was always very supportive and caring. Thanks a lot.

Acknowledgements

I am also grateful for the support of my friends at home. It nice to know that I can always return home and have someone to hang out with, helping me to forget the problems you have outside of Oetz.

Further I thank Chaitali, not only for correcting my thesis, but even more for her support and for always saying the right thing when I lose my composure.

Last but not least, I am absolutely grateful to my family. I struggle every day of homesickness. Thanks for your everlasting support.

List of Original Publications

Publication 1

Arenz, S., Juette, M.F., Graf, M., Nguyen, F., **Huter, P.**, Polikanov, Y.S., Blanchard, S.C., and Wilson, D.N. (2016). Structures of the orthosomycin antibiotics avilamycin and evernimicin in complex with the bacterial 70S ribosome. **Proc. Natl. Acad. Sci. U. S. A.** 113.

Publication 2

Graf, M., Arenz, S., **Huter, P.**, Dönhöfer, A., Nováček, J., and Wilson, D.N. (2017). Cryo-EM structure of the spinach chloroplast ribosome reveals the location of plastid-specific ribosomal proteins and extensions. **Nucleic Acids Res.** 45.

Publication 3

Huter, P., Müller, C., Beckert, B., Arenz, S., Berninghausen, O., Beckmann, R., and Wilson, D.N. (2017). Structural basis for ArfA–RF2-mediated translation termination on mRNAs lacking stop codons. **Nature** 541, 546–549.

Publication 4

Huter, P., Müller, C., Arenz, S., Beckert, B., and Wilson, D.N. (2017). Structural Basis for Ribosome Rescue in Bacteria. **Trends Biochem. Sci.** 42, 669–680.

Publication 5

Huter, P., Arenz, S., Bock, L.V., Graf, M., Frister, J.O, Heuer, A., Peil, L., Starosta, A.L., Wohlgemuth, I., Peske, F., et al. (2017). Structural Basis for Polyproline-Mediated Ribosome Stalling and Rescue by the Translation Elongation Factor EF-P. **Mol. Cell** 68, 515–527.e6.

Publication 6*

Schrode, P.**, **Huter, P.****, Clementi, N., and Erlacher, M. (2017). Atomic mutagenesis at the ribosomal decoding site*. **RNA Biol.** 14, 104–112.

Publication 7

Mardirossian, M., Pérébasquine, N., Benincasa, M., Gambato, S., Hofmann, S., **Huter, P.**, Müller, C., Hilpert, K., Innis, C.A., Tossi, A., et al. (2018). The Dolphin Proline-Rich Antimicrobial Peptide Tur1A Inhibits Protein Synthesis by Targeting the Bacterial Ribosome. **Cell Chem. Biol.**

Publication 8

Graf, M., **Huter P.**, Maracci, C., Peterek M., Rodnina, V.M., Wilson, D.N. (2018) Visualisation of translation termination intermediates during RF3-mediated recycling of RF1. **Nature Communication (accepted).**

*This publication was part of my master thesis ** These authors contributed equally to this work

Contributions Report

This dissertation includes work of my PhD research (07/2014-06/2018) in the lab of Prof. Dr. Daniel Wilson at the Gene Center of the Ludwig-Maximilians University Munich as well as at the University of Hamburg. These projects involved collaborations with experts of the field including Roland Beckmann (Munich, Germany), Yury Polikanov (Chicago, USA), Scott Blanchard (New York, USA), Helmut Grubmüller as well as Marina Rodnina (Göttingen, Germany) and Axel Innis (Bordeaux, Germany).

Publication 1 (Arenz et al., 2016)

This publication reports the structure of two orthosomycin antibiotics, namely evernimycin and avilamycin in complex with the ribosome. The study reveals a unique binding site for both antibiotics on the ribosome comprising interactions with helices 89 and 91 of the 23S rRNA as well as ribosomal protein L16. I was able to provide a high-resolution structure of the orthosomycin evernimycin for the publication.

Publication 2 (Graf et al., 2017)

This publication comprises one of the first structures of the complete ribosome of the spinach chloroplast. I was involved in modelling of the LSU. Furthermore, I helped analyzing the data.

Publication 3 (Huter et al., 2017)

This publication reports the cryo-EM reconstruction of the *Escherichia coli* 70S ribosome stalled on a truncated mRNA in the presence of alternative rescue factor A and release factor 2. I created and isolated stalled ribosomal complexes bearing a truncated mRNA, to which ArfA and RF2 were bound. Furthermore, I was involved in processing of the cryo-EM data, I modeled and validated the atomic model. Additionally, I was involved in interpretation and preparation of the manuscript, including preparation of all the main figures (Figures 1-4) and supplementary figures.

Publication 4 (Huter et al., 2017)

This publication summarizes the mode of action of the so far known rescue factors that operate on stalled non-stop complexes with focus on ArfA. We discussed their shared properties as well as their difference in mediating peptide release. I was involved in preparing the manuscript as well as Figures 1 and 3.

Publication 5 (Huter et al., 2017)

This publication reports several high-resolution cryo-EM structures of polyproline stalled ribosomes in the absence and presence of elongation factor P. I prepared all the SRCs, performed cryo-EM analysis, reconstructed and refined the complexes and built the models. Furthermore, I assisted in purifying the EF-P variants and performed the Firefly Luciferase Assay to assess the contribution of critical residues within domain 3 of EF-P. I prepared all the figures and contributed to data interpretation as well as manuscript preparation.

Abbreviations

30PIC	30S preinitiation complex
30PIC	30S preinitiation complex
30S	small ribosomal subunit
30SIC	30S initiation complex
30SIC	30S initiation complex
50S	large ribosomal subunit
70SIC	70S initiation complex
AA	Amino Acids
aa-tRNA	aminoacyl transfer ribonucleic acid
ArfA	alternative rescue factor A
ArfB	alternative rescue factor B
ASL	anticodon stem loop
CCW	counter clock-wise
CTD	C-terminal domain
CW	clock-wise
C	cytosine
cryo-EM	cryo electron microscopy
DC	decoding center
DNA	deoxyribonucleic acid
<i>E. coli</i>	<i>Escherichia coli</i>
EF-G	elongation factor G
EF-Tu	elongation factor thermo unstable
fMet	formyl-methionine
GTP	Guanosine-5'-triphosphate
G	guanine
<i>H. marismortui</i>	<i>haloarcula marismortui</i>
h#	Helix of the 16S rRNA
H#	Helix of the 23S rRNA
IF	initiation factor
kDA	kilodalton
LSU	large ribosomal subunit

Abbreviations

mDA		megadalton
miRNA		micro ribonucleic acid
mRNA		messenger ribonucleic acid
NC		nascent polypeptide chain
ncRNA		non coding ribonucleic acid
NTD		N-terminal domain
ORF		open reading frame
POST		post-translocation
PoTC		post termination complex
PRE		pre-translocation
PTC		peptidyl-transferase center
RF		release factor
RNA		ribonucleic acid
RNC		ribosome nascent chain complex
rProteins		ribosomal proteins
RRF		ribosomal recycling factor
rRNA		ribosomal ribonucleic acid
SD sequence		Shine-Dalgarno sequence
SRC		stalled ribosome complex
SSU		small ribosomal subunit
TIR		translation initiation region
tmRNA		trans-messenger RNA
tRNA		transfer ribonucleic acid
	A-tRNA	acceptor transfer ribonucleic acid
	P-tRNA	peptidyl transfer ribonucleic acid
	E-tRNA	exit transfer ribonucleic acid
T		thymine
U		uracil

Summary

The ribosome is a multifunctional ribonucleoprotein complex responsible for the translation of the genetic code into proteins. It consists of two subunits, the small ribosomal subunit and the large ribosomal subunit. During initiation of translation, both subunits join and form a functional 70S ribosome that is capable of protein synthesis. In the course of elongation, the ribosome synthesizes proteins according to the codons on the mRNA until it encounters a stop codon leading to the recruitment of release factors 1 or 2 followed by release of the nascent chain. Upon release of the polypeptide chain the subunits dissociate from each other and can be recruited for another round of translation.

There are two scenarios that interfere with active translation, namely the formation of so called 'non-stop' or 'no-go' complexes. In both cases, ribosomes pause translation and without interference of additional factors, they would become stalled. Accumulation of such events leads to a decrease of ribosomal subunits that can be recruited for translation, ultimately resulting in the death of the cell. Using cryo-electron microscopy (cryo-EM), we obtained the structure of alternative rescue factor A (ArfA) together with release factor 2 bound to a 'non-stop' complex. Our reconstructions showed that the C-terminal domain of ArfA occupies the empty mRNA channel on the SSU, whereas the N-terminal domain provides a platform for recruiting RF2 in a stop codon-independent way. Thereby, ArfA stabilizes a unique conformation of the switch loop of RF2, responsible for directing the catalytically important GGQ motif towards the PTC. The high-resolution structure of ArfA allowed us to compare its mode of action with *trans*-translation and alternative rescue factor B, two other factors operating on 'non-stop' complexes. A second project focused on elongation factor P (EF-P), a factor that alleviates stalling on polyproline stalled ribosomes. Applying cryo-EM, we were able to show that in the absence of EF-P, the nascent chain is destabilized as the polyproline moiety attached to the P-tRNA is not able to accommodate within the ribosomal tunnel. Binding of modified EF-P to the polyproline stalled complex stabilizes the P-site tRNA and especially the CCA, thereby forcing the nascent chain to adopt an alternative conformation that is favorable for translation to proceed.

1 Introduction

1.1 Central Dogma of molecular biology

Conservation of the genome, its transfer and faithful implementation of the information stored within, are fundamentally important steps in every cell. About 50 to 60 years ago the central dogma of molecular biology gained prominence for establishing the sequential occurrence of these vital events and their interconnectedness (Crick, 1958, 1970). The classical view describes a consecutive order of events, in which deoxyribonucleic acid (DNA) can either replicate itself to maintain the genomic integrity (Replication) or transfer its information onto ribonucleic acid (RNA) molecules (Transcription), which in turn serve as templates for the synthesis of proteins (Translation). Together replication, transcription and translation form the three founding pillars of the dogma of molecular biology. This model is valid to this day, however extensive studies over the decades have broadened our understanding of the molecular mechanisms behind it. Both replication and transcription require the recruitment of macromolecular machines. While replication of the genome requires the action of DNA polymerases, transcription of information from DNA to RNA is mediated by RNA polymerases. RNA molecules are a heterogeneous population that fulfill various roles in a cell and can be divided into two major classes, namely non-coding RNA (ncRNA) and messenger RNA (mRNA). Recent studies have shown that ncRNAs pursue different functions such as catalysis of chemical reactions (e.g. ribosomal RNA, rRNA), serving as adaptor molecules (e.g. transfer RNA, tRNA) or structural scaffolds (e.g. rRNA) and regulating gene expression (e.g. micro RNA, miRNA) (Dogini et al., 2014; Hüttenhofer et al., 2005). On the other hand, mRNAs contain the information of genes, which can be decoded and translated into proteins. This process is called translation and is mediated by ribosomes. In contrast to the other two molecular machines, the ribosome mainly consists predominantly of rRNA and the structural and mechanistic themes of the core components are conserved among the three phylogenetic kingdoms of life. However, there are certain differences between and as well as within each kingdom concerning size, regulation and composition to name a few (Graf et al., 2017; Melnikov et al., 2012). My work is focused exclusively on the prokaryotic ribosomal machinery of *Escherichia Coli* (*E. coli*). Unless mentioned otherwise, all ribosomes within this thesis refer to the *E. coli* ribosome.

1.2 Structure of the *E. coli* ribosome

The ribosome is a multifunctional cellular complex with an approximately molecular mass of 2.3 MDa. It consists out of two separate subunits, namely the large subunit (50S, LSU) and the small subunit (SSU, 30S), together forming a complete 70S ribosome. Both of the subunits are made out of rRNA and proteins.

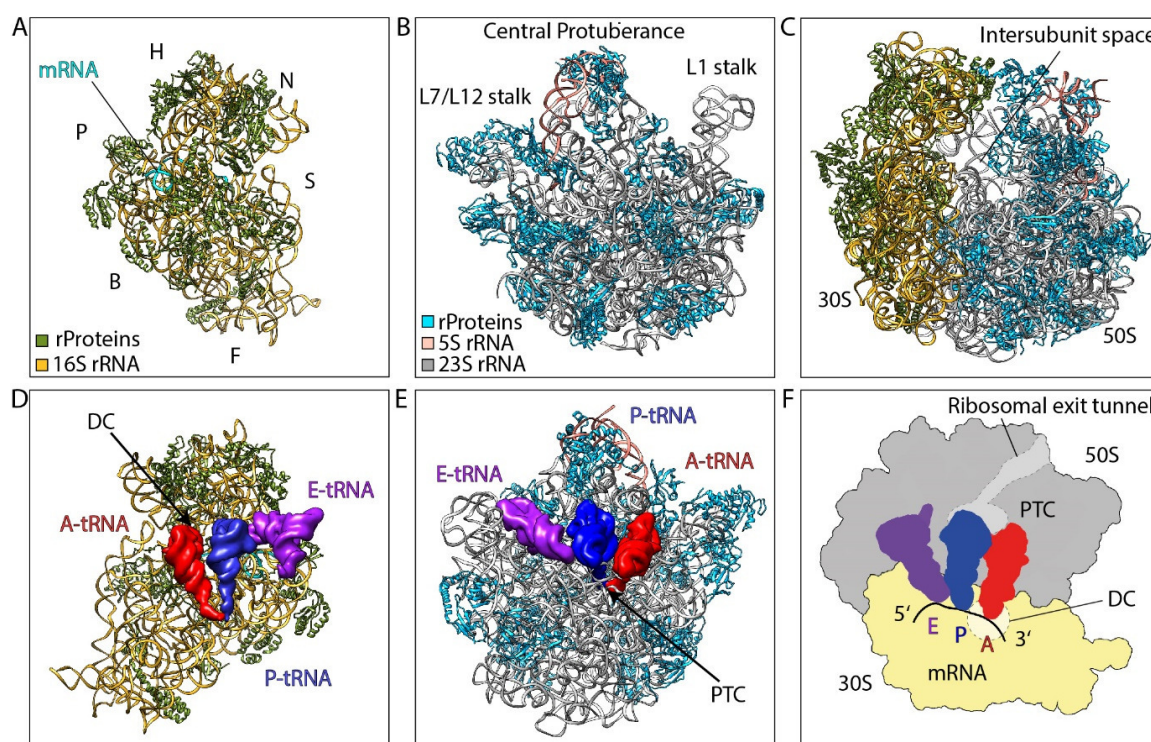


Figure 1. Structural overview of the bacterial ribosome. (A) View of the structure of the SSU from the solvent side. The 16S rRNA (gold), rProteins (green) of the SSU and mRNA (cyan) are indicated. The major subdivision are indicated: H, head; N, neck; B, body; P, platform; S, shoulder; F, foot and T, toe (also known as spur). (B) View of the structure of the LSU from the solvent side. 23S rRNA (grey), 5S rRNA (salmon) and the rProteins (blue) are indicated. (C) Overview of a vacant 70S ribosome with the intersubunit space indicated. (D) View of the structure of the SSU from the interface with A-, P- and E-tRNAs (red, blue, purple). (E) View of the structure of the LSU from the interface with A-, P- and E-tRNAs bound (red, blue, purple). (F) Schematic representation of the 70S ribosome showing the 50S (grey), 30S (yellow), A-, P- and E-tRNAs (red, blue, purple) and mRNA (black). The side of the decoding center (DC) on the SSU, the peptidyl-transferase center (PTC) as well as the ribosomal exit tunnel on the LSU are depicted as dashed-lined.

The 30S is composed of the 16S rRNA and 21 ribosomal proteins (rProteins) forming the typical morphological shape of the SSU, which can be divided into Head, Neck and Body. The body itself can be further segmented into Shoulder, Platform, Foot and Toe (also known as spur) (Figure 1A) (Schluenzen et al., 2000).

The LSU includes the 23S rRNA, 5S rRNA and 33 rProteins. It forms a rounded base with three protuberances called the L1 stalk, the central protuberance and the L7/L12 stalk (**Figure 1B**) (Yusupov et al., 2001).

Both subunits join by forming intermolecular bridges providing an intersubunit space important for the accommodation of tRNAs (**Figure 1C**). The ribosome possesses three binding sites for tRNAs, namely the acceptor site (A-site), the peptidyl site (P-site) and the exit site (E-site) (Yusupov et al., 2001). All three tRNAs associate with the ribosome by forming contacts with the 30S as well as 50S (**Figure 1D-F**).

Each of the subunits harbors a crucial functional core. The SSU comprises the decoding center (DC), where the correct tRNA is selected according to the information stored within the mRNA (**Figure 1D,F**) (Rozov et al., 2016a). The LSU contains the peptidyl transferase center (PTC), which links amino acids (aa) to a nascent polypeptide chain (NC) which passes through the ribosomal exit tunnel (**Figure 1E,F**) (Polacek and Mankin, 2005; Rodnina et al., 2007). High resolution structures revealed that both functional cores are made of rRNA with the closest ribosomal proteins being too far-off to participate in their respective enzymatic reaction, leading to the suggestion that the ribosome is a ribozyme (Ban et al., 2000; Demeshkina et al., 2012; Hansen et al., 2002a; Harms et al., 2001; Loveland et al., 2017; Ogle et al., 2001, 2002; Polikanov et al., 2014; Schlunzen et al., 2000; Schlünzen et al., 2001; Voorhees et al., 2009a). This is supported by a vast amount of biochemical data, revealing that translation can occur in the absence of translation factors as well as many ribosomal proteins (Dabbs, 1986; Gavrilova et al., 1976; Leder and Nirenberg, 1964; Lill et al., 1986; Nomura et al., 1969). While mutations in rProteins are widely tolerated, manipulation of highly conserved rRNA residues, in contrast, results in inactivation of ribosomes (Dabbs, 1986; Lind et al., 2010)⁻³³. Therefore, the ribosome should be indeed considered as a classical ribozyme (Noller, 2012). The role of the rProteins, on the other hand, is to improve efficiency and accuracy of translation, binding of tRNAs and translation factors as well as folding the rRNA in its functional state (Davies and Nomura, 1972; Hoang et al., 2004; Nomura et al., 1969).

1.3 Translation cycle

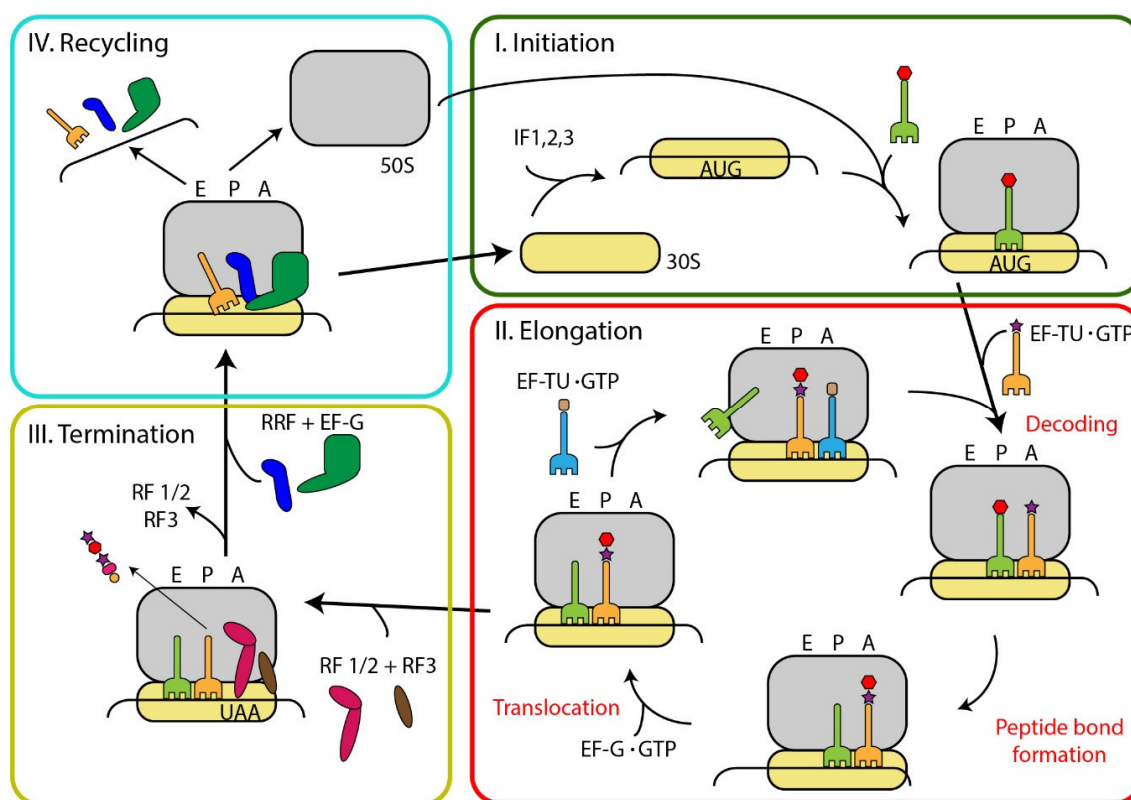


Figure 2. The translation cycle. During Initiation (green) the 30S subunit incorporates the mRNA together with initiation factor (IF) 1,2 and 3 followed by the binding of 50S subunit and positioning of the initiator tRNA by IF2 to form the 70S Initiation complex (70SIC). This step is followed by Elongation (red), during which tRNAs are delivered to the A-site of the ribosome. After establishing a correct interaction between the anticodon of the tRNA and the codon on the mRNA (decoding), the ribosome catalyzes the transfer of the peptide from the P-site tRNA onto the A-site tRNA, (peptide bond formation), prolonging the NC by an additional aa. Subsequently, elongation-factor G (EF-G) binds and translocates the tRNAs from the A- to the P-site and P- to the E-site, respectively. This leads to an empty A-site, allowing another round of elongation until the appearance of a stop codon in the A-site of the ribosome (termination, beige). Stop codons are either recognized by RF1 or RF2 (release factor), which hydrolyze the ester bond between the tRNA and the nascent chain, allowing the polypeptide chain to be released. RF3 mediates the release of the RF1/2 and allow EF-G and RRF (ribosomal recycling factor) to split the ribosome (recycling, cyan). After dissociation of the subunits from each other, they can participate in another round of translation.

Translation is the most energy-consuming pathway in a growing *E.coli* cell. Approximately 50% of the energy in form of ATP and GTP are consumed during protein synthesis (Buttgereit and Brand, 1995; Russell and Cook, 1995). Due to the enormous energy costs, translation is a tightly regulated and monitored process as errors during protein synthesis would have devastating effects. Therefore, ribosomes not only

interact with mRNAs or tRNAs but also with many different protein factors like elongation factors or rescuing factors, which ensure fast and accurate translation. The order, in which ribosomes interact with these different factors is dictated by the four steps of translation. These steps are: (i) Initiation, (ii) Elongation, which can be further subdivided into Decoding, Peptide bond formation and Translocation, (iii) Termination as well as (iv) Recycling (Figure 2). It is worth noting that the last step, recycling, and the first step, initiation, are connected, as the dissociation of both subunits from each other allows them to participate in another round of initiation. Hence, translation should be imagined as a circular process and the order of events is often described as the translation cycle. Each single step and the corresponding sub-steps will be described in more detail in the following sections.

1.3.1 Initiation

Initiation of translation in bacteria starts either during transcription of mRNA or primarily on full length transcripts (Passalacqua et al., 2009). It involves the formation of the 30S preinitiation complex (30PIC) (i), during which the mRNA, the initiator-tRNA and the initiation factors (IF) 1, 2 and 3 bind to the small subunit. After establishing a correct interaction between the anticodon of the initiator-tRNA and the start codon on the mRNA, the 30PIC gets converted to a functional 30S initiation complex (30SIC) (ii), capable of recruiting the 50S subunit. The newly formed 70S initiation complex (70SIC) (iii) allows peptide bond formation between the initiator-tRNA and the incoming tRNA in the A-site. Although having a limited set of factors involved, initiation is a slow process. The assembly of ribosomes on the mRNA can last for several seconds, whereas elongation repeats itself 20 times per second (Fluitt et al., 2007; Young and Bremer, 1976). Therefore initiation is the rate-limiting step of translation (Gualerzi and Pon, 1990; Laursen et al., 2005).

Formation of the 30PIC. After dissociation of the two subunits during recycling, IF3 binds the 30S subunit either before or after release of the mRNA and tRNA (Milón et al., 2012). IF3 binds at the platform of the small subunit and adopts an open conformation (Carter et al., 2001; Milón et al., 2012). The N-terminal domain (NTD) is located close to the binding site of the initiator-tRNA, whereas the C-terminal domain (CTD) interacts with loop 790 (h24) (Figure 3A) (Hussain et al., 2016; Milón et al., 2012). Binding of IF3 prevents re-association of the 50S subunit before binding of the

remaining IFs, mRNA and initiator-tRNA (Dallas and Noller, 2001; Karimi et al., 1999). Subsequently, IF2 binds and forms a short-lived complex together with IF3 and the SSU, which becomes stabilized by the binding of IF1. IF2 consists of three major parts, namely the N-terminal region, the central “G-domain” and the C-terminal part. On the 30S subunit the NTD of IF2 contacts IF1 and S12 and is thought to be in charge for the binding of IF2 to the small subunit (Julián et al., 2011; Moreno et al., 1998, 1999). The C-terminal part of IF2 is responsible for the interaction with the 3' end of the initiator-tRNA as well as with its fMet moiety (Figure 3A) (Caban et al., 2017; Guennegues et al., 2000; Hussain et al., 2016). The GTP-binding domain or G-domain contains the structural elements for binding and hydrolysis of GTP (Gualerzi et al., 1991; Wienk et al., 2012). IF1 is a small protein that binds to the ribosomal A-site in vicinity to h44 and the 530 loop and stabilizes IF2 and IF3 on the small subunit (Figure 3A) (Hussain et al., 2016). After the initial binding of the IFs on the 30S, IF1 and 3 synergistically induce conformational changes within the small subunit, reminiscent of the conformation of a rotated ribosome (Figure 3B) (Julián et al., 2011; Simonetti et al., 2008). 30S bound IF2 is responsible for recruiting the initiator-tRNA, which is a tRNA different from the bulk of elongating tRNAs. The initiator-tRNA is aminoacylated with methionine, whose α NH₂-group gets formylated by formyl-methyl-transferase (FMT). The modification of the α NH₂-group leads to a specificity for the initiator-tRNA towards IF2 and discrimination against EF-Tu (Antoun et al., 2006; Boelens and Gualerzi, 2002).

Recruitment of the mRNA. Binding of the mRNA to the 30S subunit can happen any time during 30PIC formation and is therefore independent of the composition of the complex (Milón et al., 2012; Studer and Joseph, 2006). The recruitment rather depends on inherited features of the mRNA itself, which are (i) the secondary structure of the translation initiation region (TIR), (ii) the ability of the TIR to interact with the ribosomal protein S1 and (iii) the presence of a Shine-Dalgarno sequence (SD-sequence) (Boni et al., 1991; Shine and Dalgarno, 1974; Skorski et al., 2006; Sørensen et al., 1998; Studer and Joseph, 2006).

The docking site or “entrance” of the mRNA is located around the platform of the 30S (h26, h28, h40) and is made up of several positively charged ribosomal proteins, that are able to interact with differently folded mRNAs (Figure 3C) (Allen et al., 2005; Jenner et al., 2005; Kaminishi et al., 2007; Marzi et al., 2007). It was shown that weak secondary structures favor translation initiation, however also highly

structured mRNAs are able to be recruited to the docking site (Allert et al., 2010; Kudla et al., 2009; Nakamoto, 2006). This suggests, although all mRNAs have the same docking site, that the strength of folding influences the details of recruitment (Milón and Rodnina, 2012). Recruitment of the mRNA to the 30S subunit is further facilitated by A/U rich sequences and SD-sequence upstream of the start codon. A/U rich sequences are recognized by the ribosomal protein S1, which interacts with the mRNA upstream of the SD sequence and thereby facilitates docking and unfolding of the mRNA (Demo et al., 2017a; Komarova et al., 2002; Marzi et al., 2007; Sengupta et al., 2001). The SD sequence can be found around seven to ten bases upstream of the start codon and has the consensus sequence AGGAGG. It assists placing the start codon of the mRNA into the P-site of the ribosome by forming interactions with the anti-SD sequence, located at the interface of the ribosomal head and back of the platform, where it base pairs with the 3'-end of the 16S rRNA (Figure **3C,D**) (Jacob et al., 1987; Kaminishi et al., 2007; Ma et al., 2002; Skorski et al., 2006; Yusupova et al., 2006).

It is noteworthy that not all mRNAs contain all the above-mentioned features. In this context, there are three different kind of mRNAs, namely one that have a SD-sequence upstream of the start codon (SD-led mRNAs), one that do not have a SD-sequence upstream of the start codon and ,dependent on the bacterial species, also leaderless mRNAs that directly start with AUG. The abundance of these types can change significantly (Chang et al., 2006; Ma et al., 2002; Scharff et al., 2011a). SD-led mRNAs are the most favorable mRNAs for translation, as they inherit every feature needed for fast initiation. On the other hand non SD-led mRNAs do not contain a SD-sequence in proximity to the start codon. It remains elusive how ribosomes, programmed with these mRNAs, are able to faithfully position the start codon at the P-site, despite forming a stable complex with the 30S subunit (Milon et al., 2008; Scharff et al., 2011a). Last but not least, leaderless mRNAs lack the 5'-end upstream of start codon. It was shown that they mainly associate with 70S rather than 30S (Grill et al., 2000). Moreover they do not require the interaction of S1 and other proteins that form the initial docking site of the mRNA (Kaberina et al., 2009; Moll et al., 2002).

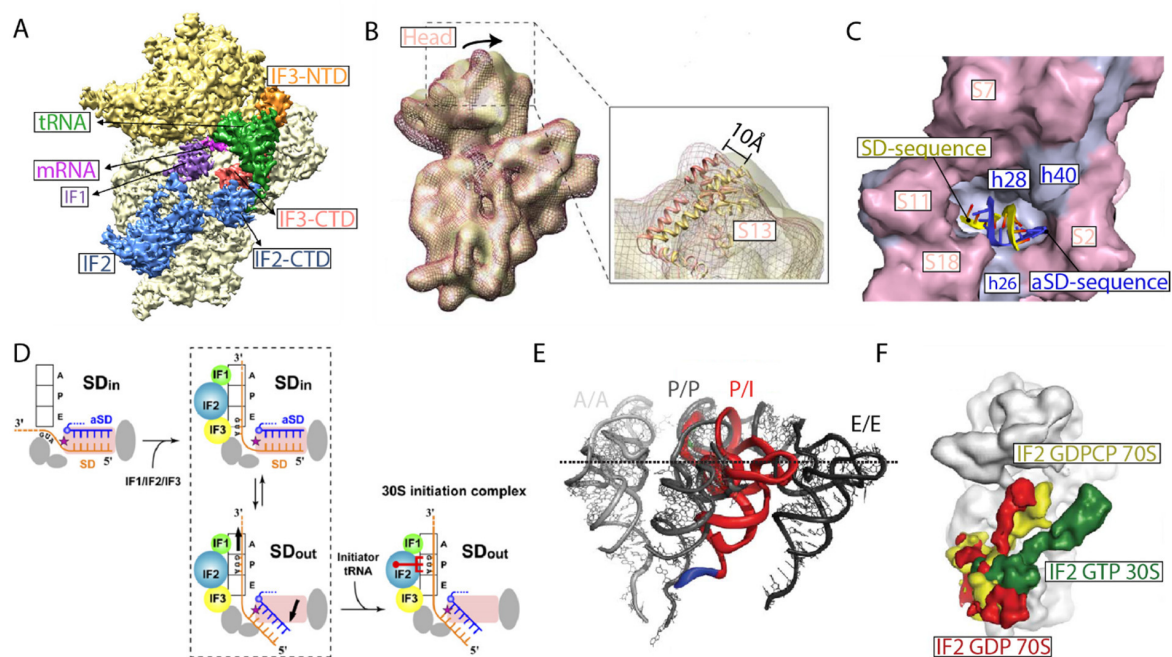


Figure 3. Main events during formation of the 70S initiation complex. (A) Cryo-EM reconstruction of the 30PIC containing IF1 (purple), IF2 (blue), IF3 (NTD, orange; CTD, brick red), mRNA (pink), initiator-tRNA (green) (adapted from (Hussain et al., 2016)). (B) Cryo-EM reconstruction of a 30S subunit in complex with mRNA in the absence of tRNA and IFs (red mesh) or presence of tRNA and IFs (30SIC, semitransparent yellow). Indicated is the clockwise rotation of the 30S head towards the platform. The inset shows the positions of protein S13 indicating a shift of 10 Å during rotation (adapted from (Julián et al., 2011)). (C) View on the SD helix (SD-sequence, yellow; aSD-sequence, blue) on the 30S with the surrounding proteins (purple) and helices (blue) indicated (adapted from (Kaminishi et al., 2007)). (D) Model for the accommodation of the start codon AUG in the ribosomal P-site in cooperation with IFs (IF1, green; IF2, blue; IF3, yellow) and SD helix (SD-sequence, orange; aSD-sequence, blue) (adapted from (Kaminishi et al., 2007)). (E) Comparison of several tRNA positions from a 70S post-initiation complex and the P/I (red) state that forms during the formation of the 30SIC adapted from (Julián et al., 2011)). (F) Positions of IF2 during several states of translation initiation (IF2·GTP 30SIC, green; IF2·GDPNP 70SIC, yellow; IF2·GDP 70SIC, red) (adapted from (Simonetti et al., 2008)).

Formation of the 30SIC. The main event during transition to the 30SIC is the formation of an interaction between the anticodon of the initiator-tRNA and the start codon of the mRNA. It requires the correct positioning of a start codon into the ribosomal P-site. This process is facilitated by the formation of a SD-aSD pairing, but does not necessarily rely on this interaction, as non-SD led mRNA and leaderless mRNA are still able to initiate translation (Calogero et al., 1988; Van Etten and Janssen, 1998; Milon et al., 2008; Scharff et al., 2011b). Presumably, the SD helix helps to increase the concentration of start codon triplets near the P-site, whereas its recognition is achieved kinetically by IFs (Figure 3D) (Calogero et al., 1988; Canonaco et al., 1989; Kaminishi et al., 2007). In bacteria, all start codon triplets share a U at the second position. AUG, GUG and UUG are the most common one with AUG being the most

avored (Sussman et al., 1996). Recruitment of the correct tRNA to the ribosomal P-site is mediated by the CTD of IF2, that specifically recognizes the blocked αNH_2 -group as well as by IF1 and IF3, which dissociate incorrect tRNAs from the ribosome (Antoun et al., 2006; Caban et al., 2017; Hartz et al., 1989; Hussain et al., 2016; Wintermeyer and Gualerzi, 1983). Recognition of the correct start codon and tRNA allows placement of the initiator-tRNA in its P/I state (peptidyl/initiation state) by forming contacts between the ASL and stop codon (Figure 3E) (Allen et al., 2005; Julián et al., 2011; Simonetti et al., 2008; Sprink et al., 2016). Thereby, the 30S·IF1·IF2·initiator-tRNA complex gets further stabilized, whereas IF3 gets destabilized (Milón and Rodnina, 2012; Milon et al., 2008). IF3 interferes with the binding of the 50S subunit as it occupies a space important for the formation of an intersubunit bridge. Thereby, destabilization of IF3 might work as the trigger for 50S association (Antoun et al., 2006; Dallas and Noller, 2001; Julián et al., 2011; Milon et al., 2008).

Formation of the 70SIC. The large subunits binds the 30S in its rotated state with all IFs and the initiator-tRNA attached to it (Allen et al., 2005; Milon et al., 2008). First of all, IF3 dissociates from the complex before GTP hydrolysis (Goyal et al., 2015). Next, IF2 interacts with the Sarcin-Ricin loop (SRL) inducing the hydrolysis of GTP bound to IF2, causing several structural rearrangements (Figure 3F) (Qin et al., 2009; La Teana et al., 2001). As a first step, IF2 undergoes a conformational change that loosens its contacts with both subunit as well as with the initiator-tRNA (Goyal et al., 2015; Myasnikov et al., 2005). Secondly, IF1 leaves the complex (Milon et al., 2008). Subsequently, the transition of the 30S from a rotated-state to an unrotated-state occurs and thereby the initiator-tRNA get rearranged in its P/P position (Julián et al., 2011; Marshall et al., 2009; Myasnikov et al., 2005; Sprink et al., 2016). Lastly, IF2 leaves the ribosome committing the 70SIC for elongation (Marshall et al., 2009; Myasnikov et al., 2005).

1.3.2 Elongation

During elongation, the ribosome has to translate the genetic code into amino acid sequences. It starts with the dissociation of IF2 from the 70SIC, leaving an empty A-site behind. The vacant A-site is recognized by a so called ternary complex, which consists of elongation factor thermo unstable (EF-Tu), an aminoacyl-tRNA (aa-tRNA) and guanosine-5'-triphosphate (GTP).

Based on the complementarity between the anticodon of the tRNA and the codon of the mRNA, the ternary complex gets either rejected or is allowed to accommodate in the ribosomal A-site (**decoding**). Once the correct tRNA is selected, the ribosome transfers the growing peptide chain to the aa-tRNA in the A-site and thereby elongates the nascent chain by one additional amino acid (**peptide bond formation**). Subsequently, EF-G binds to the ribosome and translocates the mRNA in 3'direction by one codon, causing the now deacylated tRNA to move to the E site and the A-site tRNA to the P-site, respectively (**translocation**). Hence, the A-site is vacant, allowing the next ternary complex to enter. The three main steps of elongation continue until the ribosome encounters a stop codon at the A-site, marking the end of elongation and initiating termination. In the next following sections these three steps of elongation will be described in more detail.

Decoding. Throughout elongation the ribosome discriminates between correct and incorrect ternary complexes, dictated by the mRNA codon in the ribosomal A-site. These ternary complexes contain EF-Tu, GTP and one of 50 different aa-tRNAs matching one or more of the 61 canonical codons on the mRNA (Rodnina and Wintermeyer, 2001). The basis for the discrimination is the base-complementarity of the anticodon stem loop (ASL) of the tRNA and the codon on the mRNA. Taking the “wobble hypothesis” into consideration which states that the first two positions of the codon create the coding specificity (explanation follows later), three possibilities arise to describe the complementarity between the mRNA and the tRNA (Crick, 1966). A tRNA can be either cognate (no mismatch between the first and second position), near-cognate (one mismatch between the first and second position) or non-cognate (no match between the first and second position) (Ogle et al., 2001; Plant et al., 2007). However, studies showed that base pairing alone is not sufficient to account for the average misincorporation rate of 3×10^{-3} (Eisinger et al., 1971; Lofffield, 1963; McLaughlin et al., 1966; Sugimoto et al., 1986). Moreover, antibiotics as well as mutations affecting the ribosome can induce miscoding, demonstrating that the ribosome augments to the obtained fidelity rates (Brink et al., 1994; Moazed and Noller, 1987; O'Connor et al., 1997; Rodnina et al., 2000).

The kinetic proofreading model describes a two-step mechanism during accommodation of the A-site tRNA, in which the ribosome discriminates between cognate and near-cognate tRNAs (Rodnina et al., 1994, 1995). Under physiological conditions it was shown that non-cognate tRNAs are not accepted by the ribosome

and therefore are excluded from the discussions in the following section (Pape et al., 1999).

Initial selection begins with binding of the ternary complex to the A-site in a codon-independent manner, followed by codon recognition. Dependent on the complementarity of the anticodon/codon helix, the ternary complex gets either rejected or undergoes a conformational change triggering EF-Tu bound GTP hydrolysis (Voorhees et al., 2010). EF-Tu rearranges in the GDP-bound conformation and dissociates from the tRNA (Liu et al., 2015; Pape et al., 1998, 1999; Rodnina et al., 1996). Release of EF-Tu from the ternary complex marks the second proofreading step. Dependent on the nature of the anticodon-codon helix the tRNA is rejected or accommodates within the ribosomal A-site followed by instantaneous peptide bond formation (Pape et al., 1999).

First molecular details on how decoding works are based on X-ray structures of isolated 30S subunit crystals programmed with either cognate or near-cognate ASLs (Ogle et al., 2001, 2002). Binding of the ASL to the mRNA results in a double helical structure (anticodon-codon helix). This induces universally conserved nucleotides A1492 and A1493 to flip out of the internal loop of helix 44 and interact with the minor groove of the anticodon-codon helix reminiscent of A-minor motifs (Ogle et al., 2001, 2002). These motifs consist of consecutive adenines that insert into the minor groove of RNA helices and thus contribute to their stability (Lescoute and Westhof, 2006).

Additionally, G530 switches from the *syn* conformation to the *anti* conformation. The structural rearrangements allow A1493 to interact with the first base pair, whereas A1492 acts together with G530 to monitor the second position. Interactions with the third position is less stringent as it involves fewer hydrogen bonds providing a structural explanation for the wobble hypothesis (**Figure 4A-C**, upper panel) (Crick, 1966; Ogle et al., 2001, 2002). The energy derived from a cognate interaction prevents the tRNA to dissociate from the ribosome and induces domain closure, a movement of the head towards the shoulder of the 30S, triggering hydrolysis of EF-Tu bound GTP (Ogle et al., 2001, 2002). However, a near-cognate interaction leads to a disturbed geometry within the anticodon/codon helix, disrupting important hydrogen bonds between A1492, A1493, G530 and the ASL/codon interaction and displacing them from each other (Ogle et al., 2001). The resulting energy penalty leads to the dissociation of the near-cognate tRNA and prevents domain closure (Ogle et al., 2001, 2002).

X-ray analysis of 70S ribosomes programmed with cognate or near-cognate tRNAs and longer mRNAs further refined the understanding of the decoding process (Demeshkina et al., 2012; Rozov et al., 2015). In complex with 70S ribosomes near-cognate anticodon/codon helices adopt base pairs reminiscent of canonical Watson-Crick pairs (**Figure 4A-C**). Moreover, nucleotides G530, A1492 and A1493 seem to adopt the same conformation relative to the anticodon/codon helix as in the case of a cognate interaction (**Figure 4D**) (Demeshkina et al., 2012).

A possible explanation for the differences in those structures can be attributed to the set up used for the 30S subunit crystal. The 30S crystals were soaked with a hexanucleotide RNA (U6) mimicking mRNA. Moreover, the P-site codon was occupied by the 3' end of the 16S rRNA, forcing the U6 mRNA to the A-site, resulting in a discontinuous mRNA. This creates an artificial situation as the P/A kink cannot form, which is an interaction between the P-tRNA, the 16S rRNA, a metal ion and the mRNA kink. As a result the mRNA is less stabilized. Furthermore, density for the near-cognate ASL was only observed in the presence of paromomycin, an antibiotic that induces the “out” position of A1492 and A1493 (Ogle et al., 2001, 2002; Rozov et al., 2016a). Thus, there is a general flexibility within the A-site of the 30S structures that allows wobble base pairing (Rozov et al., 2016a).

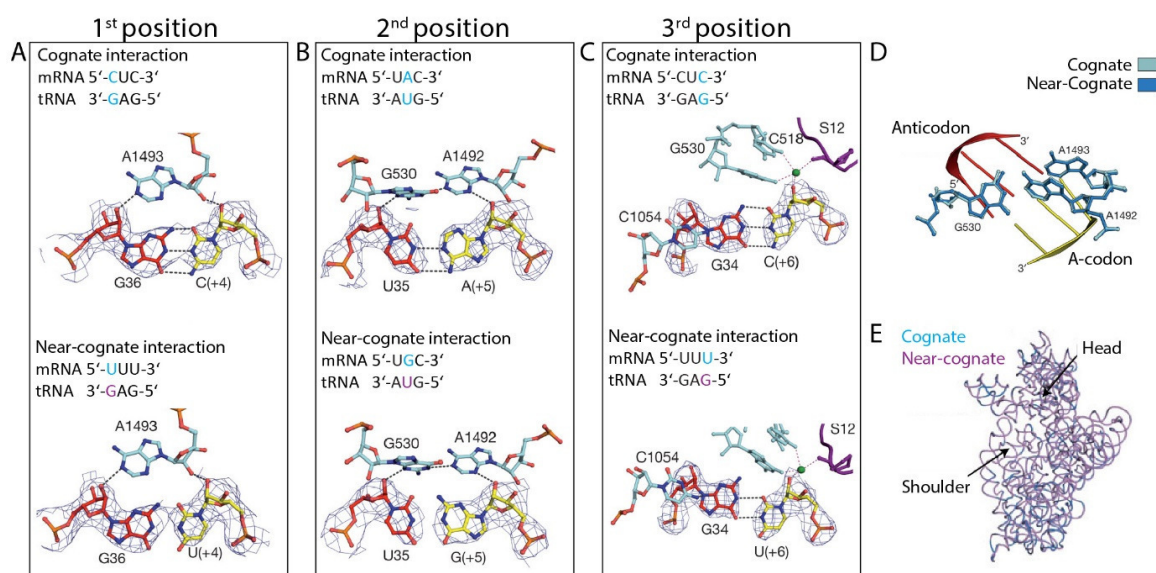


Figure 4. Codon-anticodon interactions inside the decoding centre. (A-C) Codon-anticodon (mRNA, yellow; tRNA, red) interactions at the first (A), second (B) and third (C) position for cognate as well as near-cognate tRNAs. **(D)** Superimposition of residues G530, A1492 and A1493 relative to the codon/anticodon helix comparing the cognate (cyan) with the near cognate structure (blue). **(E)** Superimposition of the 16S rRNA comparing the cognate (blue) with the near-cognate structure (purple) shows identical domain closure in both cases (adapted from (Demeshkina et al., 2012)).

Based on these observations, decoding errors derive from mismatched anticodon-codon helices that mimic a Watson-Crick shape. The energy costs of mimicking a Watson-Crick like geometry requires a keto-enol tautomerization, pushing the equilibrium towards dissociation of the near-cognate ternary complex (Demeshkina et al., 2012; Rozov et al., 2015, 2016a, 2016b). This is also a *bona fide* explanation why non-cognate tRNAs never surpass the initial selection checkpoint as the energy penalty would be even higher (Rozov et al., 2015, 2016b).

Recognition of the codon is followed by domain closure, which is identical for cognate and near-cognate interactions mimicking Watson-Crick geometry (**Figure 4E**) (Demeshkina et al., 2012; Loveland et al., 2017). Recent cryo-EM structures explain the necessity of the Watson-Crick geometry for domain closure. Near-cognate interaction with a G U base pair fail to stabilize G530 to an extent that is favorable for domain closure and thereby keeps the ribosome in an open conformation (Loveland et al., 2017).

During domain closure, the ternary complexes gets pushed towards the sarcin ricin loop (SRL) of the 50S. This allows the catalytic important His84 of EF-Tu to interact with A2662 of the SRL, hydrolyzing GTP by coordinating a water molecule for nucleophilic attack on the γ -phosphate of GTP (Loveland et al., 2017; Voorhees et al., 2010). Hydrolysis and release of the inorganic phosphate induces conformational changes within EF-Tu and its release from the ribosome. Following the release of EF-Tu, the aa-tRNA shifts from its EF-Tu bound state (A/T state) to the A/A state, a movement that includes the accommodation of the aminoacyl end of the tRNA into the PTC (Blanchard et al., 2004; Nissen et al., 2000; Schmeing et al., 2009; Voorhees et al., 2010). It was recently shown that the conversion from the A/T state to the A/A state can be inhibited by the orthosomycins evernimicin and avilamycin (Arenz et al., 2016). Both antibiotics interact with H89 and H91 of the 23S rRNA as well with L16. This binding site overlaps with the elbow region of fully accommodated A-site tRNA but not A/T tRNA

tRNA accommodation is fast for cognate tRNAs, but slow for near-cognate tRNAs therefore providing an evidence for the second proofreading step during tRNA selection (Pape et al., 1998, 1999). Structural insights that explain the different accommodation rates are lacking, however misalignment of the anticodon-codon helix as well as sterical restrains imposed by the ribosome are likely (Fischer et al., 2016; Rodnina and Wintermeyer, 2001).

Peptide bond formation. Formation of a peptide bond between the aa-tRNA and peptidyl-tRNA is the main chemical reaction during protein synthesis. It involves the aminolysis of the ester bond that links the nascent chain to the ribose of the P-site tRNA and transfer of the chain on to the A-site tRNA adding an additional residue (Satterthwait and Jencks, 1974). This happens in a stepwise manner. After the accommodation of the aa-tRNA, a nucleophilic attack of the α -amine of the aa-tRNA on to the carbonyl carbon of the peptidyl-tRNA occurs. This leads to the formation of a transition state, the rate-limiting step of peptide bond formation (Hiller et al., 2011; Satterthwait and Jencks, 1974). In comparison, the transition state decomposes fast on the ribosome while it accumulates in solution. Hence, the ribosome catalyses this reaction by 10^5 - 10^7 fold faster compared to reactions in solution, highlighting the significance of the translation apparatus (Sievers et al., 2004). Fast breakdown of the transition state results in a deacylated tRNA in the P-site and a peptidyl-tRNA in the A-site (Hiller et al., 2011).

Structural as well as biochemical studies point out that the reaction on the ribosome is RNA-driven (Ban et al., 2000; Maden and Monro, 1968; Nissen et al., 2000; Schmeing et al., 2005a; Wohlgemuth et al., 2006). Hence it is not surprising that the peptidyl transferase center (PTC), the catalytical center of peptide bond formation, is comprised of a cluster of universally conserved rRNA nucleotides located within the central loop of domain V of the 23S rRNA (Ban et al., 2000; Nissen et al., 2000). These residues form a tight cavity that serves as a platform for the accommodation of the CCA-ends of the A and P-site tRNAs bringing them in close contact and shielding them from the close surrounding. This is in line with experiments showing that the 50S subunit alone is capable of peptide bond formation (Maden and Monro, 1968; Okuda et al., 2005; Schmeing et al., 2002; Seila et al., 2005; Wohlgemuth et al., 2006).

Crystal structures of *Haloarcula marismortui* 50S subunits provided a first detailed picture. In the absence of A-site tRNA the PTC adopts the uninduced state. C74 and C75 of the P-site tRNA form Watson Crick base pairing with G2251 and G2252 holding the acceptor end in place. A76 is stacking on to A2451 and is in hydrogen bond distant to A2450 (Kim and Green, 1999; Nissen et al., 2000; Polikanov et al., 2014; Voorhees et al., 2009a). Nucleotides C2063, A2451 and U2585 form a pocket around the ester group of the peptidyl-tRNA to sterically exclude water that would otherwise hydrolyze the ester bond (Schmeing et al., 2005a, 2005b). G2583 forms a G U wobble pair together with U2506 blocking the A-site pocket. Binding of the

A-site tRNA causes an induced fit that is a conformational change in the PTC (referred as the induced state). A-tRNA nucleotides C74 stacks with U2555, C75 base pairs with G2253 and A76 forms an A-minor motif with G2583 (**Figure 5A**) (Kim and Green, 1999; Nissen et al., 2001; Schmeing et al., 2005a, 2005b). The latter interaction leads to disruption of the G2583-U2506 wobble base pair, shifting U2506 away from the A-site pocket. Hence, the CCA end gets stabilized leading to positioning of the amino acid moiety that allows formation of hydrogen bonds with the N3 and 2'-OH of A2451 as well as the 2'-OH of A76. Accompanied by the A-tRNA accommodation is a shift of A2602 and U2585 exposing the peptidyl-tRNA ester for a nucleophilic attack (Schmeing et al., 2005a, 2005b). Thus, the PTC mainly functions as an entropic trap leading to a significant reduction of the reaction entropy (Schmeing et al., 2005a, 2005b; Sievers et al., 2004).

Most enzymes contribute to chemical reactions in two ways. The first contribution is to arrange the substrates in close proximity, allowing them to react. The second step involves the functional groups of the enzyme that influence the chemistry of the reaction. The contribution of both steps can differ significantly from one enzyme to the other. An important question is whether the peptidyl-transfer reaction is solely dependent on substrate alignment or if functional groups within the PTC exist that influence the chemical reactivity (Polacek and Mankin, 2005). Biochemical experiments as well as the crystal structures of *H. marismortui* 50S suggested a general acid/base mechanism involving the N3 of A2451. However, mutations of this adenine as well as neighboring nucleotides did not lead to a significant reduction in peptide bond formation (Hansen et al., 2002b; Muth et al., 2000; Nissen et al., 2001; Polacek et al., 2001; Thompson et al., 2001). Furthermore, using full length tRNA substrates for kinetic experiments, showed no pH-dependency for peptide bond formation (Beringer et al., 2005; Youngman et al., 2004).

Therefore, a substrate assisted mechanism was proposed with the 2'-OH group of A76 of the P-site tRNA being the main candidate (Dorner et al., 2003; Erlacher et al., 2006; Weinger et al., 2004). The α -amino group of the aa-tRNA forms an extensive network of hydrogen bonds with the N3 of A2451 and the 2'-OH group of A76 (Schmeing et al., 2005a, 2005b). As it was demonstrated that the former is neglectable, a substrate assisted mechanism was suggested, in which a proton is transferred from the nucleophile to the 2'-OH group to the 3'-OH group of A76 (Dorner et al., 2003; Schmeing et al., 2005a, 2005b). Indeed, deletion of the 2'-OH of the A76 showed at

least a decrease of activity by 100-fold (Aqvist et al., 2012; Huang and Sprinzl, 2011; Weinger et al., 2004; Zaher et al., 2011). Hence, a proton shuttling mechanism was proposed, either as a six or eight membered mechanism, in which two or three protons together with a water molecule coordinate the attack of the nucleophile in a fully concerted manner. (Hiller et al., 2011; Kuhlenkoetter et al., 2011; Schmeing et al., 2005b; Wallin and Aqvist, 2010).

Recent high resolution structures of pre-attack and post-catalysis states 70S ribosomes of *Thermus thermophilus* provided further molecular details (Polikanov et al., 2014; Voorhees et al., 2009a). Owing to the higher resolution the position of three water molecules (W1-3) inside the PTC could be identified. These water molecules are coordinated by A2451, U2584, C2063 and A2602, the N-terminal part of L27 as well as with the A76 of both tRNAs. Based on this findings a proton wire mechanism is suggested in which residues of the PTC and both tRNAs obtain a catalytical role by activating the water molecules (**Figure 5A+B**) (Polikanov et al., 2014).

A tight network of hydrogen bonds between the N6 of A2602, the phosphate oxygen of A76 of the A-site tRNA, the 2'OH of A2451 and the N-terminus of L27 coordinates W1 to the attacking amine and shields W1 from exchange with the bulk solvent (**pre-attack**). This guarantees a geometry that allows the concerted attack by the α -amine of the aa-tRNA onto the carbonyl-carbon of the peptidyl-tRNA via transfer of the proton from the nucleophile via A76 2'OH of the P-site tRNA to the A2451 2'OH to W1 (Hiller et al., 2011; Kingery et al., 2008; Polikanov et al., 2014). This results in the tetrahedral intermediate state, which is stabilized by the donation of a proton to the negatively charged ester carbonyl carbon by W2. The ribosome facilitates the fast break down of this state to prevent premature termination by hydrolysis (Hiller et al., 2011; Polikanov et al., 2014; Satterthwait and Jencks, 1974). On the basis of the 70S structure a transfer of a proton from the positively charged W1 to W3 to form a H_3O^+ ion is suggested, that catalyzes the hydrolysis of the intermediate state into their respective products (Polikanov et al., 2014). Thus the ribosome provides a prearranged proton-transfer network that contributes to the reaction besides being an entropic trap (**Figure 5D**) (Polikanov et al., 2014; Sievers et al., 2004).

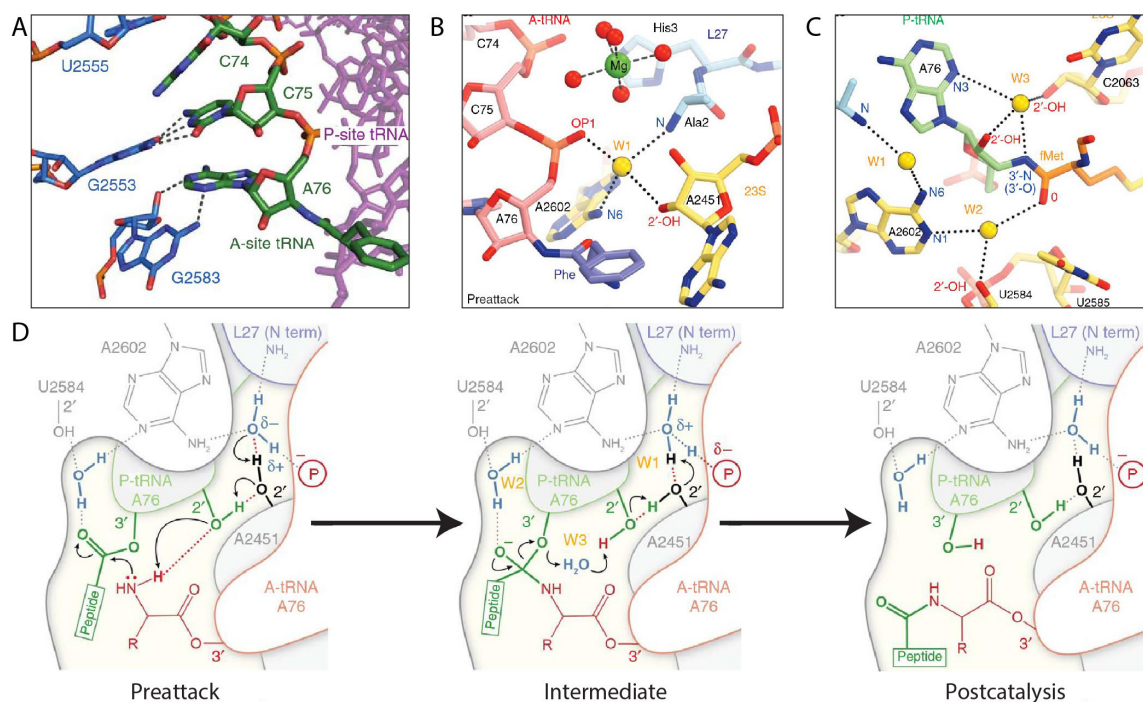


Figure 5. Conformation of residues involved in the proton wire of the PTC. (A) Interactions between the CCA end of A-site tRNA (green) with residues of the A-loop of the 23S rRNA (blue) (from (Voorhees et al., 2009b)). (B+C) Coordination of water molecules in the PTC involving the A-site tRNA acceptor stem (pink), residues of the 23S rRNA (yellow), L27 (cyan) and P-site tRNA (green). Possible hydrogen bonds are indicated as dashed lines. (D) Model for proton wire mechanism in presence of three trapped water molecules (yellow) inside the PTC. Adapted from (Polikanov et al., 2014)

Another question raised from that study is the contribution of L27 in peptide bond formation. L27 represents the closest ribosomal protein to the PTC. From crystal and cryo-EM structures it was shown that, upon accommodation of the A-site, the last three N-terminal residues protrude into the PTC, which is not the case for complexes that are not committed for peptide bond formation (Huter et al., 2017a; Polikanov et al., 2014; Voorhees et al., 2009a). Thus, L27 stabilizes residues of the 23S rRNA and both tRNAs upon accommodation of the A-site tRNA (Polikanov et al., 2014; Voorhees et al., 2009a; Wang and Xiao, 2012; Wang et al., 2014). Additionally it is suggested to coordinate the W1 molecule and together with the A-tRNA A76 and the 5' phosphate oxygen of A2451, is the source responsible for the deprotonation of the α -amine (Polikanov et al., 2014). In contrast to structural studies, biochemical studies show a contradicting picture. Whereas some groups reported that ribosome lacking L27 showed no defect in peptide bond formation, another group demonstrated that deletion of the three N-terminal residues leads to a decreased rate of translation (Maguire et al., 2005; Maracci et al., 2015). Further biochemical and kinetic experiments are

needed to further address the contribution of L27. However, it is not entirely incorrect to assume that L27 facilitates the peptidyl-transfer activity.

Translocation. Following peptide bond formation the ribosome is occupied with a deacylated tRNA in the P-site and a peptidyl-tRNA in the A-site (**PRE-state**). In order to allow translation to continue, the ribosome has to translocate the bound tRNAs together with their associated mRNA codons from the P- to the E-site and A- to the P-site, respectively. As a result, the ribosome provides a vacant A-site programmed with the next codon of the mRNA (**POST-state**).

Translocation happens in a stepwise manner, with the acceptor ends of tRNAs moving first with respect to the 50S subunit (A/P, P/E) followed by a movement of the tRNA with respect to the 30S subunit (P/P, E/E) (Blanchard et al., 2004). The driving force behind translocation are large conformational changes of the SSU that coordinate the movement of mRNA and tRNAs to their respective place (Frank and Agrawal, 2000). The ribosome possesses the capability to perform this movements on its own. However, in the absence of factors, this process is bidirectional, meaning the ribosome translocates backward and forward (Konevega et al., 2007; Shoji et al., 2006). It requires the assistance of EF-G and GTP that drives translocation into a unidirectional process by acting like a pawl and therefore preventing backtranslocation (Konevega et al., 2007; Liu et al., 2014; Shoji et al., 2006).

Researchers in recent years revealed the underlying mechanisms and could dissect the events of translocation in a sequential order. Following peptide bond formation the CCA ends of the tRNAs spontaneously move from the P- to the E site and A- to the P-site on the 50S (A/P and P/E hybrid states) (**Figure 6D**) (Fu et al., 2011; Munro et al., 2007). The driving force for these movements is the deacylated state of the P-site tRNA, as the E-site tRNA sterically occludes the accommodation of a peptidyl-tRNA (Rheinberger and Nierhaus, 1983; Schmeing et al., 2003). This, on the other hand, results in a vacant 50S P-site, which has a strong affinity for peptidyl-tRNAs (Semenkov et al., 1992; Sharma et al., 2004).

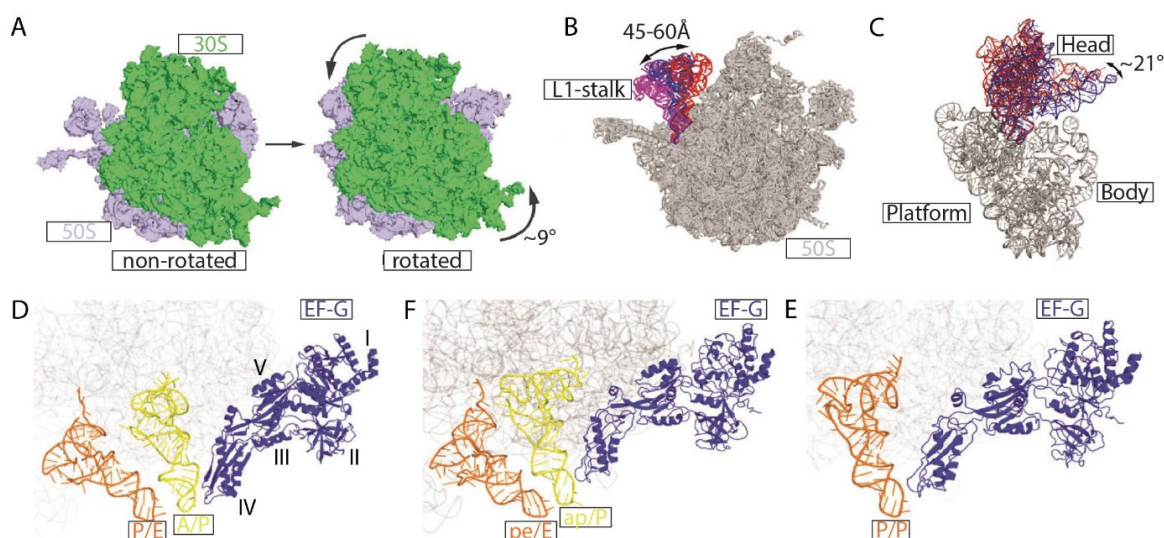


Figure 6. Structural rearrangements of the ribosome and EF-G during translocation. (A) Structural comparison between a non-rotated classical state (PDB 4V9D) and a rotated, hybrid state (PDB 4V7C) ribosome reveals a CCW rotation of the SSU (green) relative to the LSU (grey). (B) Conformation of the L1 stalk shown in the open (magenta), semi-closed (blue) and closed (blue) position. (C) Comparison of a non-rotated with a partially rotated ribosome depicting the CCW swiveling of the head. (D-F) Progressive movement of domain IV of EF-G (blue) from a rotated-hybrid state (PDB 4V7D) to a partially rotated state (PDB 4W29) to a non-rotated posttranslocation state (PDB 4V5F) and their corresponding states of the deacylated (orange) and peptidyl (yellow) tRNA are depicted. Adapted from (Ling and Ermolenko, 2016).

Coupled to the movement of the acceptor stem of the deacylated tRNA on the 50S is a counterclockwise (CCW) rotation of the platform and body domains of the SSU relative to the LSU ($\sim 3\text{-}10^\circ$), often referred to as ‘ratcheting’ (Figure 6A) (Agirrezabala et al., 2008; Dunkle et al., 2011; Ermolenko et al., 2007a; Julián et al., 2008). In the absence of EF-G, kinetic studies observed a back and forth fluctuation between the classic non-rotated state and the rotated-hybrid state. Interestingly, EF-G can bind both states (Blanchard et al., 2004; Cornish et al., 2008; Munro et al., 2007). The binding of EF-G, however, accelerates the formation of the rotated-hybrid state, driving the reaction towards the formation of the POST-complex (P/P, E/E) (Belardinelli et al., 2016; Chen et al., 2011).

Rotation of the small subunit moves domain 1 of EF-G in close proximity to the SRL. Domain 1 is structurally similar to other translational GTPases (traGTPase), comprising the important G subdomain required for the hydrolysis of GTP (Maracci and Rodnina, 2016). Hence, the close proximity to the SRL triggers GTP hydrolysis and thereby the release of inorganic phosphate (Belitsina et al., 1975; Koch et al., 2015; Moazed et al., 1988; Rodnina et al., 1997). Akin for EF-Tu during decoding, the energy released by hydrolysis does not have an influence on translocation per se, but is stored

to dissociate EF-G after translocation. This is exemplified by the fact, that in presence of non-hydrolysable GTP analogues a single round of translocation can occur (Pan et al., 2007; Rodnina et al., 1997).

Binding of EF-G triggers an additional independent movement of the 30S termed the head swivel (Guo and Noller, 2012). During head swiveling, the head of the 30S subunits rotates CCW towards the platform (**Figure 6C**). Thereby it frees the path for the movement of tRNAs on the 30S subunit, which is usually blocked by the head domain (Dunkle et al., 2011). Translocation of the mRNA is passive and dependent on the movement of A- and P-tRNAs (Joseph and Noller, 1998). This is exemplified by the fact that tRNA can translocate in the absence of mRNA (Belitsina et al., 1981). However, translocation of mRNA cannot be observed in the presence of only a deacylated tRNA in the P-site (Joseph and Noller, 1998).

Simultaneously with the CCW movement of the head, the body and platform start to inverse their movement in a CW direction (Guo and Noller, 2012; Ratje et al., 2010). The exact time point of this reverse rotation is not known. Cryo-EM and crystallographic studies were able to capture an intermediate state, with body-platform being backrotated to 3.5°, while the head swivel reaches its maximum rotation. The tRNA in the complex are configured in an ap/P and pe/E state (**Figure 6F**). These states are characterized by accommodated acceptor stems in the 50S as well ASL in on the 30S in their respective tRNA binding sites. However, on the 30S some tRNA elements still interact with residues of the A- and P-sites on the 30S head domain (Ratje et al., 2010; Zhou et al., 2013, 2014). This might represent a late stage intermediate showing that reverse rotation of the 30S body and platform is initiated before head swiveling reaches its maximum. Followed by positioning of the ASL and mRNA in the 30S is a back swivel of the head and further reverse rotation of the 30S body and platform transforming the ribosome in its classic non-rotated state with a vacant A-site (POST-state; P/P, E/E) (Guo and Noller, 2012).

Coupled to the movements of the small subunit and tRNAs is the conformation of the L1 stalk of the LSU, that compromises parts of helices 76, 77 and 78 of 23S rRNA, as well as the L1 protein. Dependent on the rotation of body and platform, the L1 stalk was visualized in three different conformations. In the non-rotated classic state, the L1 configuration can be described as outwards or open, directed away from the ribosomal core (Cornish et al., 2008; Dunkle et al., 2011; Fei et al., 2009). In the rotated hybrid state, the L1 stalks undergoes a 45-60 Å movement interacting with the

elbow of P/E tRNA (Cornish et al., 2008; Dunkle et al., 2011; Fei et al., 2009). Upon completion of translocation the L1 is still contacting the now fully accommodated E-tRNA, but only differs by 20 Å difference compared to the open conformation (**Figure 6B**) (Cornish et al., 2008). Dissociation of the deacylated tRNA moves the L1 stalk back to its open position. Based on these observed conformations it is likely that the L1 stalk facilitates the movement of the E-site tRNA at different stages as suggested by Bock et al (Bock et al., 2013).

Not only the ribosome but also EF-G undergoes conformational changes throughout translocation. Structural studies with EF-G in solution and bound to different states of translocation reveal a transition from a free conformation in solution into an extended conformation on the ribosome (Brilot et al., 2013; Czworkowski et al., 1994; Gao et al., 2009; Lin et al., 2015; Ramrath et al., 2013; Zhou et al., 2014). Notably, one X-ray structure observed the compacted form of EF-G on the ribosome. However, the observed compact form might have been the result of fusing EF-G to L9 of the neighboring ribosome and/or the usage of the antibiotic dityromycin trapping EF-G and therefore does not represent a physiological state (Lin et al., 2015).

The extension of EF-G is driven by the progressive movement of domain IV, resulting in docking of this domain in the A-site of the 30S as observed in non-rotated post-translocation complexes (Brilot et al., 2013; Gao et al., 2009; Zhou et al., 2014). Structures of intermediate states showed that domain IV contacts the ASL of the peptidyl-tRNA still bound to the 30S A-site as well as important residues of the decoding center (**Figure 6D+E**) (Brilot et al., 2013; Gao et al., 2009; Ramrath et al., 2013; Zhou et al., 2014). These contacts might form barriers which need to be destabilized by EF-G for fast translocation. The fully accommodated domain IV in the POST-state might on the other hand, work as a barrier or pawl that prevents backtranslocation of the peptidyl-tRNA from the P-site to the A-site (**Figure 6F**) (Ling and Ermolenko, 2016).

1.3.3 Termination

The presence of one of three stop codons within the A-site terminates protein synthesis by releasing the nascent chain from the ribosome. These three stop codons are encoded as UAG, UAA and UGA. In contrary to canonical codons, stop codons are recognized by Class I release factors that mediate the hydrolysis of the ester bond of the peptidyl-tRNA. Release factor 1 (RF1) thereby recognizes UAG and UAA codons, whereas release factor 2 (RF2) is specific for UGA and UAA. After release of the peptide, the class II release factor RF3 binds the ribosome and dissociates RF1/2 from the ribosome.

RF1/2 share highly conserved regions and consist of four domains with domains 2,3 and 4 of the factors overlapping with the binding site of A-site tRNA.(Zhou et al., 2012a). For a long time, it remained elusive how these decoding factors are capable of discriminating between the different stop codons or if they indirectly recognize stop codons through interactions with the ribosome. Swapping of conserved domains between RF1 and RF2 revealed the presence of a crucial tripeptide motif, namely P(A/V)T in RF1 and SPF in RF2, located in a loop of domain 2 (Ito et al., 2000). Exchanging these motifs between both RFs changes the specificity towards the stop codon suggesting that the tripeptide motif efficiently deciphers stop codons, in an anticodon-like manner (Ito et al., 2000; Nakamura et al., 2000).

Four high-resolution crystal structures of RF1/2 bound to both their respective stop codons explain the molecular mechanism behind deciphering stop codons (Ito et al., 2000; Korostelev et al., 2008, 2010; Laurberg et al., 2008). P(A/V)T/SPF motives are located in loops that are directed towards the decoding site, interacting with the stop codon. The stop codon itself adopts an unusual conformation with the first two bases stacking and the third base being sandwiched between G530 and residues of the release factors. Surprisingly, only a single amino acid in both motifs is in direct contact with the second position of the respective stop codon, namely the T186 for RF1 and the S206 for RF2 (Korostelev et al., 2008, 2010; Laurberg et al., 2008; Weixlbaumer et al., 2008). This is in agreement with studies from Ito et al., showing a prerequisite of those two aa in overexpressed RF1/2 mutants in Δ RF1 or Δ RF2 strains (Ito et al., 2000). The acceptance of an A and a G for RF2 might be due to the potential of serine to interact with A and G at this position.

U1 position of the stop codon is recognized by backbone elements of the decoding factors that interact with N3 of uridine and explains the restriction to U at this position (Korostelev et al., 2008, 2010; Laurberg et al., 2008; Weixlbaumer et al., 2008). Due to the backbone interaction, mutations failed to confirm this interaction. However, by introducing non-canonical RNA residues at the first position, Erlacher and coworkers were able to show that this interaction relies on the exocyclic group of uridine, explaining its exclusiveness at this position (Hoernes et al., 2018). RF1 monitors the third position via interactions of Thr194 and Q181, whereas RF2 interaction depends on T194 (Korostelev et al., 2008, 2010; Laurberg et al., 2008; Weixlbaumer et al., 2008). Mutational studies show that exchange of aa adjacent to the tripeptide motif can change the specificity of RF1/2 (Ito et al., 1998; Korkmaz and Sanyal, 2017; Young et al., 2010). These findings, however, should not question the importance of the tripeptide motives, but rather highlight an elaborate network of interactions in which the P(A/V)T/SPF motif is a prerequisite (**Figure 7A+B**).

Using metal ion fluorescence resonance energy transfer, Trappl et al could show that upon recognition of the stop codon, RF1 opens from a closed to an open extended conformation on the ribosome. In contrast, this induced fit does not happen in the presence of a sense codon (Trappl and Joseph, 2016). Structures of the isolated decoding factors reveal a tight packing of domain 2 and 3 against each other, whereas bound to the ribosome, domain 3 escapes this packing and is orientated towards the PTC (Korostelev et al., 2008, 2010; Laurberg et al., 2008; Shin et al., 2004; Vestergaard et al., 2001; Weixlbaumer et al., 2008). Opening of domain 3 requires a rearranged state of a switch loop within RF1/2, connecting domain 3 and 4. This rearranged state of the switch loop is stabilized by residues of the decoding site that adopt an alternative conformation upon stop codon recognition by release factors (**Figure 7C**) (Korostelev et al., 2010; Laurberg et al., 2008). Thus, recognition of the stop codon is coupled to the opening of release factors on the ribosome (**Figure 7D**).

Sequence alignments between all kingdoms showed the abundance of a GGQ motif in all release factors (Frolova et al., 1999). In bacteria this motif is found within the tip of domain 3, placing it next to A76 of the peptidyl-tRNA upon release factor opening. Mutations affecting the first and second glycine abolished hydrolysis, whereas mutations of glutamine were tolerated, indicating a direct involvement of the motif for hydrolysis (Frolova et al., 1999; Shaw and Green, 2007). This came as a surprise as the glutamine is post-translationally methylated *in vivo* leading to enhanced

activity for peptide release (Dincbas-Renqvist et al., 2000; Heurgué-Hamard et al., 2002). From structural analysis it came apparent that the side chain of Gln of the GGQ motif in RF1 is orientated away from A76 and the catalytic center. The backbone NH, however, is in hydrogen bonding distance to the 3'OH of A76. Mutation of Gln to Pro in RF1 eliminates the NH backbone interaction and thereby abolishes the activity of RF1 (**Figure 7E**) (Santos et al., 2013; Shaw and Green, 2007). Recent structures, that used release factors carrying the methylated glutamine, showed a tighter packing of the glutamine against its neighboring residues and thereby additionally stabilizing the backbone of the glutamine (Pierson et al., 2016; Zeng and Jin, 2016). The two glycines, on the other hand, are not directly involved in catalysis but are important for the conformation and integrity of the loop (Laurberg et al., 2008; Shaw and Green, 2007).

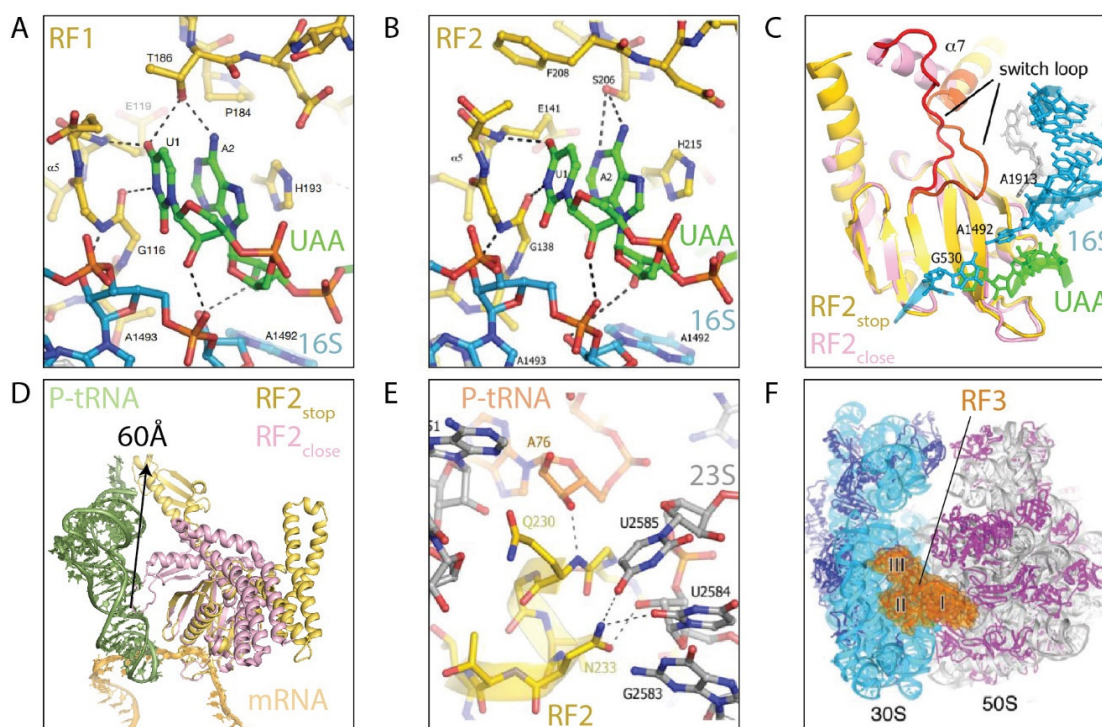


Figure 7. Termination of translation in the presence of a stop codon. (A) Decoding of the stop codon (green) by the P(A/V)T motif of RF1 (yellow). **(B)** Same as (A) but in the presence of RF2 and the corresponding SPF motif. **(C)** Comparison of the switch loop region of RF2 (red) in its open, ribosome bound conformation (yellow) and closed conformation (pink) as observed in solution. Remodeling of the switch loop on the ribosome involves stacking interaction between A1492 (16S, blue) and the switch loop. **(D)** After remodeling of the switch loop of RF2 (yellow) the tip of domain III gets positioned into the PTC. This involves a movement of 60 Å compared to the closed RF2 conformation (pink). **(E)** Backbone interaction between the catalytic important Q230 of RF2 (yellow) and A76 of P-tRNA (orange) is shown. **(F)** Crystal structure of RF3 (orange) bound to a rotated ribosome. Pictures adapted from (Laurberg et al., 2008; Zhou et al., 2012b)

Likewise, during peptide bond formation, the presence of an A-site substrate induces a similar conformational change within the PTC (Shaw and Green, 2007). In the presence of RF1/2 this includes residues U2506, which overlaps with the binding site of RFs and U2585 which moves away from the ester bond allowing its hydrolysis by a water molecule (Shaw and Green, 2007; Schmeing et al., 2005b). This leads to the following situation: Accommodation of domain 3 and conformational changes within the PTC allow the activation of an attacking water molecule. The backbone of Gln interacts via its NH-group with the 3'OH of A76, whereas its side chain is shielding the PTC from other nucleophiles larger than water (**Figure 7E**) (Jin et al., 2010; Korostelev et al., 2008, 2010; Laurberg et al., 2008; Shaw and Green, 2007; Shaw et al., 2012; Weixlbaumer et al., 2008). Similar to peptide bond formation, this reaction proceeds through a tetrahedral intermediate (Korostelev et al., 2008, 2010; Laurberg et al., 2008; Trobro and Åqvist, 2009; Weixlbaumer et al., 2008). Break down of this state results in deacylated tRNA and free peptide. In contrast to peptide bond formation, hydrolysis of the peptide is less understood. One model suggests that 2'OH of A76 acts as a proton shuttle by accepting a proton from the nucleophilic water and subsequently transferring it to the leaving group on the 3'OH, that is stabilized by the main chain amide of the glutamine (Schmeing et al., 2005a; Shaw et al., 2012; Sievers et al., 2004; Trobro and Åqvist, 2009; Weinger et al., 2004). Other models suggest a step-wise proton transfer with only one proton moving at the same time (Kuhlenkoetter et al., 2011).

After hydrolysis the class II release factor RF3 binds the ribosome and stimulates the release of RF1/2 (Freistroffer et al., 1997; Goldstein and Caskey, 1970). Like EF-Tu and EF-G, RF3 is a translational GTPase (traGTPase) and binds the ribosome preferentially in complex with GTP (**Figure 7F**) (Adio et al., 2018; Koutmou et al., 2014a; Peske et al., 2014). Additionally, the binding site of RF3 overlaps with their position on the ribosome (Gao et al., 2007; Jin et al., 2011; Pallesen et al., 2013; Zhou et al., 2012a, 2012c). Hence, a direct interaction between RF3 and RF1/2 is unlikely as there is no overlap in the binding site, suggesting that RF3 promotes dissociation of RF1/2 indirectly (Gao et al., 2007; Jin et al., 2011; Pallesen et al., 2013; Zhou et al., 2012a, 2012c). From crystal structures it is evident that in the absence of RF3, but presence of RF1/2, the ribosome adopts a non-rotated state (Jin et al., 2010; Korostelev et al., 2008; Laurberg et al., 2008; Weixlbaumer et al., 2008). By contrast, it could be shown that in the presence of RF3, but absence of RF1/2, the ribosome is in a rotated state (Gao et al., 2007; Jin et al., 2011; Zhou et al., 2012c). Hence, it is

likely that RF3 dissociates RF1/2 by inducing subunit rotation. Recent biophysical studies further refined the understanding for this process. Like EF-Tu, RF3 binds the ribosome preferentially in complex with GTP (Adio et al., 2018; Koutmou et al., 2014b; Peske et al., 2014). Binding of RF3 facilitates the transition from non-rotated RF1/2-bound state to a rotated state and thereby removing the decoding factors (Adio et al., 2018; Ermolenko et al., 2007b; Sternberg et al., 2009). The conversion from a non-rotated to a rotated state seems to be dependent on the presence of GTP bound to RF3, as non-hydrolysable analogues showed a reduced rate in conversion (Adio et al., 2018; Shi and Joseph, 2016). Interestingly, RF3 mutants that are able to bind GTP but are deficient in hydrolysis are also able to induce this transformation, suggesting that the presence of the hydrolysable analogue is needed but not its hydrolysis (Adio et al., 2018; Shi and Joseph, 2016). It rather seems that hydrolysis is needed to reset ribosomes back to a non-rotated state by dissociating RF3 from the ribosome (Adio et al., 2018; Peske et al., 2014; Shi and Joseph, 2016).

Last but not least it should be noted that cells lacking RF3, show no growth defect (Grentzmann et al., 1994; O'Connor, 2015). Even more, RF3 is only found in a subset of bacteria suggesting that RF3 is not part of a conserved mechanism but an auxiliary factor fine tuning the RNA machinery (Margus et al., 2007).

1.3.4 Recycling

Dissociation of RF1/2 results in a post termination complex (PoTC) programmed with a deacylated tRNA and mRNA. To return the ribosomal subunits to the pool of translating ribosome, the ribosome has to be disassembled into its individual components. Recycling is mediated by three factors, namely the ribosome recycling factor (RRF), EF-G and IF3.

RRF binds the ribosome in its rotated state.(Fu et al., 2016; Prabhakar et al., 2017; Sternberg et al., 2009). Binding of RRF to the ribosomal A-site prevents reassociation of RF1/2, as evident from single molecule Förster resonance energy transfer (smFRET) experiments. While binding of RF1/2 converts the ribosome to a non-rotated state, increasing concentrations of RRF stabilize the rotated state. This is also in agreement with structural studies showing that binding of RRF to a physiological PoTC was only observed in the rotated state (Dunkle et al., 2011; Fu et al., 2016; Gao et al., 2005). Notably, there was also a structure of RRF bound to a non-rotated ribosome. however, in this crystal structure the ASL of a P-tRNA was used, thereby allowing accommodation of RRF as it would otherwise clash with the body of the tRNA (Weixlbaumer et al., 2007). RRF consists of two domains connected by a linker and binds the A- and P-site cleft of the 50S. Domain II is contacting S12 and intersubunit bridge B2a on the SSU while domain I forms several contacts with 23S rRNA on the 50S subunit with domain I, including the SRL and L7/L12 stalk (Agrawal et al., 2004; Barat et al., 2007; Fu et al., 2016; Gao et al., 2005).

Binding of RRF alone is not sufficient to split subunits but requires EF-G to do so (Frank et al., 2007; Hirokawa et al., 2006; Peske et al., 2005; Zavialov et al., 2005). Reconstructions of time-resolved cryo-electron microscopy showed a conformational change of RRF upon binding of EF-G that directs domain II towards domain I bringing it in closer contact to the intersubunit bridge B2a (Fu et al., 2016; Zhang et al., 2015). This structural rearrangement together with domain IV of EF-G is thought to split B2a and thereby facilitates subunit dissociation (Dunkle et al., 2011; Fu et al., 2016; Pai et al., 2008; Yokoyama et al., 2012; Zhang et al., 2015). It is noteworthy to mention that a crystal structure of *T. thermophilus* RRF together with *E. coli* EF-G on the *E. coli* ribosome exists (Yokoyama et al., 2012). However, biochemically assays revealed that this complex is not functional and therefore is not physiological relevant. Experimentally it was shown that additionally to the presence of RRF and EF-G

recycling requires the hydrolysis of GTP bound to EF-G to split subunits (Borg et al., 2016; Prabhakar et al., 2017). However, it remains elusive if hydrolysis or resulting Pi release trigger the above mentioned structural changes or if they are required to dissociate EF-G from the ribosome.

Upon subunit dissociation, RRF and EF-G leave the ribosome and IF3 binds the ribosome preventing rebinding of the 50S (Hirokawa et al., 2005; Karimi et al., 1999; Peske et al., 2005; Prabhakar et al., 2017). Furthermore, it was shown that binding of IF3 accelerates the departure of P-site tRNA and thereby indirectly causes the dissociation of the mRNA (Karimi et al., 1999; Prabhakar et al., 2017). Thus, IF3 facilitates the departure of tRNA and mRNA, but also connects recycling with translation initiation by preventing reassociation of the 50S.

Noteworthy, the above described pathway of recycling might just be one possible way to split subunits. There are many possibilities described in the literature how this might be achieved. For example a recent paper suggests that in presence of RRF and EF-G, the mRNA is first to leave the 70S, followed by the tRNA and delayed subunit dissociation. However, in presence of an upstream SD-sequence, mRNA and tRNA dissociate after 70S splitting (Chen et al., 2017). Interestingly, mRNAs used for recycling experiments mostly contain a start codon followed by a stop codon with an upstream SD-sequence, pushing the experimental outcome towards prior splitting followed by tRNA/mRNA dissociation. On the other hand the absence of a SD-sequence would provide a pool of vacant 70S that can be used to initiate translation (Chen et al., 2017; Grill et al., 2000; Qin et al., 2016; Yamamoto et al., 2016). Another model suggests that EF-G translocates RRF into the P-site and thereby dissociates tRNA and hence indirectly the mRNA (Hirokawa et al., 2005). This would again provide a vacant 70S pool. Another explanation for the discrepancy in experimental outcomes is the presence of different Mg^{2+} concentrations. The lower the Mg^{2+} concentration is, the more likely it is to observe a 70S splitting event. In summary, there might be several pathways to return ribosomes to the translation pool.

1.4 Rescue of translational stalled ribosomes

Translation is a pivotal event in every single cell and thus cells invest considerable amounts of energy to produce, recycle and provide ribosomes and other translation factors. Interventions that disturb a smooth running translation cycle would lead to increased energy consumption and as a consequence, death of the cell (Buttgereit and Brand, 1995; Russell and Cook, 1995). There are two scenarios that interfere with active translation, namely the formation of a 'non-stop' or 'no-go' complex, both of them leading to stalled ribosomes (Giudice and Gillet, 2013). Non-stop complexes derive from the lack of a stop signal, leading to stalled ribosomes at the 3' end of mRNA bearing a vacant A-site (Giudice and Gillet, 2013; Keiler, 2015). On the other hand, 'no-go' complexes derive e.g. from rare codon stretches, amino acid starvation, stalling peptides/motifs and antibiotics (Giudice and Gillet, 2013; Himeno et al., 2015; Keiler, 2015; Li et al., 2005; Roche and Sauer, 1999; Starosta et al., 2014a; Wilson, 2014; Wilson and Beckmann, 2011).

Bacteria have evolved various mechanisms to cope with these stress situations and alleviate stalled ribosomes. Non-stop complexes are resolved by a rescue mechanism called *trans*-translation, the protein alternative rescue factor ArfA or ArfB (Giudice and Gillet, 2013; Himeno et al., 2015; Huter et al., 2017b; Keiler, 2015). By contrast, 'no-go' complexes are alleviated by a variety of factors that depend on the cause of stalling. One way is to convert the 'no-go' complex into a 'non-stop' complex by an A-site specific cleavage, making it a *bona fide* target for *trans*-translation (Buskirk and Green, 2017; Hayes and Sauer, 2003; Ivanova et al., 2004; Janssen et al., 2013). Other possibilities include rescue factors that help to continue translation instead of terminating it. The so called ribosome protection proteins (RPP) alleviate drug-induced stalling by binding to the ribosome and displacing the drug from the ribosome (Arenz et al., 2015; Farrell et al., 2011; Nguyen et al., 2014). Another scenario is caused by translation of consecutive proline motifs that arrest ribosomes. Binding of elongation factor P (EF-P) restores translation on those 'no-go' complexes (Doerfel et al., 2013; Huter et al., 2017a; Ude et al., 2013). The sum of reasons for 'no-go' complexes and their respective mechanisms make it impossible to describe them all within this thesis. Hence, only those that were directly related to my research during my PhD will be described

Last but not the least, it is worth mentioning that stalling is not always harmful to the cell but can also be used as a tool to regulate the expression of genes (Wilson and Beckmann, 2011). These 'physiological' stalling events, also known as translation attenuation, often occur on small open reading frames and thereby influence the expression of downstream genes

1.4.1 *Trans*-translation, ArfA and ArfB

Studies in *E. coli* reveal that 2-4% of translating ribosomes are stalled due to the formation of a 'non-stop' complex at any one time (Ito et al., 2011). Reasons for the appearance of non-stop complexes are manifold. They can derive from random events like mRNA damage, premature termination of transcription or exonucleolytic cleavage. This causes the lack of the 3'-located stop codon resulting in a non-stop complex with the very 3'-end of the mRNA in the P-site and a vacant A-site (Hong et al., 2007; Svetlanov et al., 2012). Miscoding inducing antibiotics, frameshift events and nonsense suppression (readthrough of a stop codon), although not physically removing the stop codon, lead to the formation of the same complex by suppressing the stop signal and thereby promoting translation to the 3' end of the mRNA (Abo et al., 2002; Ueda et al., 2002).

However, reaching the 3' end of an mRNA is not the only way to create a non-stop complex. It was shown that *trans*-translation is also active on ribosomes that are stalled on intact mRNAs, e.g. after encountering rare codons or stalling sequences (Roche and Sauer, 1999; Wilson and Beckmann, 2011). In such cases the mRNA might be exposed to exonucleases like RNase II, which specifically cleaves the A-site to make the complex a target for *trans*-translation (Garza-Sánchez et al., 2008; Janssen et al., 2013). Similar to that is the toxin-antitoxin system RelBE. Upon amino acid starvation the antitoxin RelB becomes degraded, leading to the activation of RelE toxin that on the other hand cleaves mRNAs in the ribosomal A-site (Neubauer et al., 2009; Starosta et al., 2014a). Hence, rescue of 'non-stop' complexes are even part of regulatory circuits.

The first line of defense against non-stop complexes is *trans*-translation mediated by a molecule called tmRNA. Remarkably, tmRNA or its encoding gene *ssrA* has been found in all sequenced prokaryotes (Gueneau de Novoa and Williams, 2004). Deletion of *ssrA* is either lethal in many medically relevant species or results in severe

phenotypes including defects in virulence (Brunel and Charpentier, 2016; Huang et al., 2000; Personne and Parish, 2014; Ramadoss et al., 2013a; Thibonnier et al., 2008). However, other species like *E. coli*, show rather mild phenotypes upon deletion of *ssrA*, due to the existence of back-up systems like ArfA or ArfB (Abo et al., 2002; Chadani et al., 2010). Indeed, deletion of tmRNA and ArfA is synthetically lethal in *E. coli*, despite the presence of ArfB. However, if ArfB is overexpressed, it can rescue the synthetic lethal effect of $\Delta ssrA\Delta arfA$ (Chadani et al., 2010, 2011a). On the other hand, deletion of tmRNA from *Neisseria gonorrhoeae* is lethal despite the presence of ArfA (Schaub et al., 2012). Deletion of tmRNA in *Bacillus subtilis* is not lethal, despite the apparent absence of ArfA and ArfB, suggesting the presence of other yet unknown rescue mechanisms (Muto et al., 2000; Shin and Price, 2007; Wiegert and Schumann, 2001). Hence, it is likely that at least one rescue mechanism is required for the viability of the cell, pointing out the importance of resolving stalling on non-stop complexes. *Trans*-translation, rescue by ArfA and ArfB will be discussed further in the following sections.

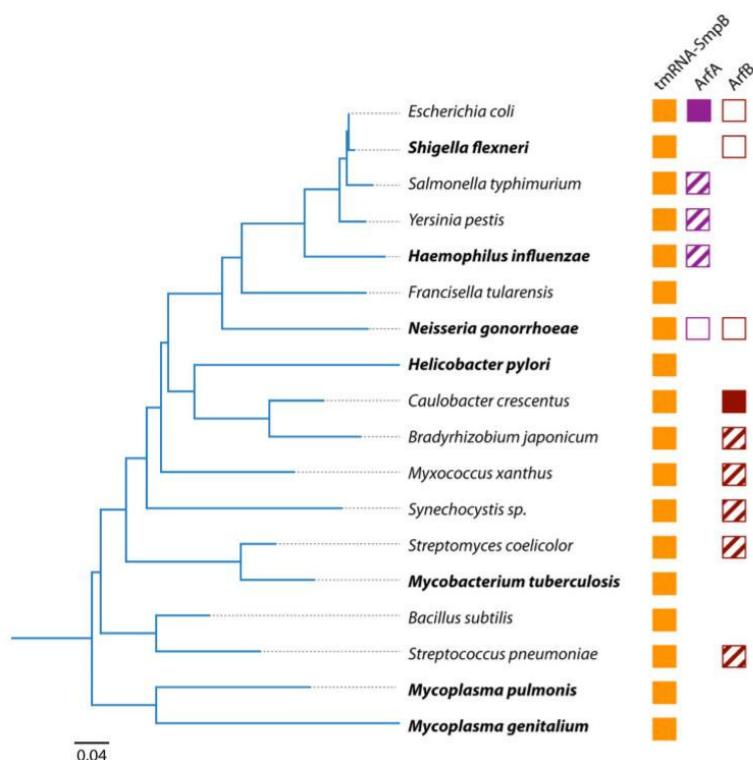


Figure 8. Phylogenetic distribution of tmRNA, ArfA and ArfB based on the sequence of the 16S rRNA. For organisms in bold, *trans*-translation is essential and cannot be compensated by ArfA or ArfB. Filled boxes for ArfA or ArfB means that the alternative rescue factor is capable of compensating the loss of *trans*-translation. Hashed boxes indicate that it hasn't been shown so far to be essential or not. Adapted from (Keiler and Feaga, 2014).

Trans-translation. *trans*-translation is mediated by a ribonucleoprotein complex made out of tmRNA and SmpB. Both molecules are required to rescue non-stop complexes. While SmpB is a small RNA binding protein, tmRNA is a specialized RNA molecule. tmRNA is comprised of a tRNA-like domain (TLD) and a messenger-like domain (MLD), which are connected by a series of pseudoknots (**Figure 9A**) (Felden et al., 1996; Karzai et al., 1999a; Keiler et al., 1996, 2000; Komine et al., 1994; Ushida et al., 1994). In most bacterial lineages tmRNA comprises a single RNA molecule of about 350 nt in length. The secondary structure is conserved throughout bacteria, however some lineages use two RNA transcripts to produce a functional two-piece tmRNA (Keiler et al., 2000). The TLD of the RNA molecule form structures reminiscent of tRNA^{Ala}, allowing it to be charged by alanyl-tRNA synthetase and interact with EF-Tu, but is lacking the ASL (Moore and Sauer, 2007). The lack of the ASL is compensated by SmpB. SmpB is a small 160 amino acids containing protein with a globular core and a C-terminal tail that remains unstructured in solution (Dong et al., 2002; Karzai et al., 1999b). Together with the TLD, SmpB functionally and structurally mimics a tRNA molecule. The MLD part of the tmRNA contains an open reading frame (ORF) that encodes 8-35 aa long degradation tag, which helps to restore translation by providing a template (**Figure 9A**) (Moore and Sauer, 2007).

The vacant A-site is recognized by a quaternary complex, consisting of tmRNA, SmpB and EF-Tu·GTP with the SmpB-tmRNA module in the A/T site of the 70S (Kaur et al., 2006; Valle et al., 2003). An X-ray structure revealed that the C-terminus of SmpB binds in close proximity to the decoding bases A1492, A1493 and G530 and extends into the mRNA entry channel forming a α -helix that would overlap with the position of a full-length mRNA (Neubauer et al., 2012). This is in agreement with biochemical studies showing a decrease in peptidyl transfer to tmRNA with increasing length of the 3'-end of the mRNA from the P-site (Kurita et al., 2014a; Miller and Buskirk, 2014). Interestingly, it could be shown that GTP hydrolysis occurs independent of the length of the 3'-extension, suggesting that hydrolysis of GTP serves as a proofreading step that rejects the quaternary complex upon encountering an extended mRNA (Himeno et al., 2015). In case of an empty channel GTP hydrolysis allows the C-terminal part of SmpB to accommodate within the tunnel and thereby stabilizing the tmRNA/SmpB complex permitting the CCA end to interact with the PTC (Kurita et al., 2014a; Miller and Buskirk, 2014; Neubauer et al., 2012). Hence, peptide

bond formation between the nascent chain and alanine of tmRNA can occur. While the TLD and SmpB undergo conformational changes within these early steps, the pseudoknots and MLD remain static, forming an “arc” around the 30S subunit (Himeno et al., 2015).

Subsequently, EF-G binds the ribosome and translocates SmpB and the TLD from the A-site to the P-site, placing the first codon of the MLD into the A-site (Ramrath et al., 2012). Comparing cryo-EM reconstructions of preaccommodated tmRNA/SmpB with fully translocated tmRNA/SmpB revealed that in both states the tmRNA maintains its “arc” structure, raising the question how the MLD can be placed into the decoding site (Kaur et al., 2006; Valle et al., 2003; Weis et al., 2010).

A cryo-EM reconstruction together with fusidic acid was able to stall the ribosome in concert with tmRNA/SmpB and EF-G (Ramrath et al., 2012). The resulting structure was similar to a translocation intermediate, but revealed an additional movement of the head. While the translocation intermediate showed 30S rotation of 4° and a head swivel of 18°, this reconstruction showed an extra movement of the head, parallel to the path of the mRNA (**Figure 9B**) (Ramrath et al., 2012; Ratje et al., 2010). This tilt opens the intersubunit bridge B1A and allows translocation of the tmRNA. On the solvent side of the 30S, S2 and S3 are interacting with elements of the tmRNA suggesting that these interactions work as a pivot point for placing the MLD into the decoding center. Accompanying the large head movements is the opening of the decoding site around G530 allowing the placement of the new ORF into the mRNA entry channel (**Figure 9C**). Hence, the head movements open the intersubunit space around B1A, the decoding center and together with fixation of the tmRNA through S2 and S3, allow the MLD to move freely and place the ORF into the mRNA channel (**Figure 9D**) (Ramrath et al., 2012). Another observation that could be made is that the conformation of EF-G is similar to that observed in canonical POST complexes. Domain IV interacts with SmpB close to the DC, detaching SmpB from the channel and thus allowing accommodation of the MLD (Ramrath et al., 2012; Ratje et al., 2010). These structural rearrangements allow translation to proceed on the ORF of the MLD until a stop codon is encountered, recruiting RF1/2 which leads to termination of translation and recycling of the ribosome (Keiler et al., 1996). The ORF, when translated, incorporates a degradation tag at the C-terminus of the polypeptide, which is recognized by Clp and other proteases (Withey and Friedman, 1999). Hence, the faulty protein is degraded upon release from the ribosome (Keiler et al., 1996). It is

worth to mention that recycling of the ribosome and not degradation of the protein is the essential part of *trans*-translation (Huang et al., 2000). This was shown by Huang et al., who altered the MLD sequence of tmRNA in a way that it cannot be recognized by the degradation machinery anymore. Cells expressing this altered tmRNA were still viable, whereas when they used a tmRNA defective of amino acid charging the effect was lethal.

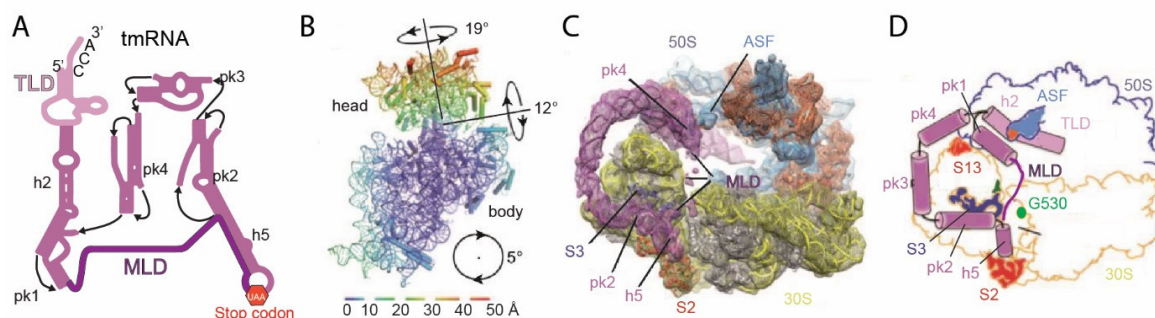


Figure 9. Rescue of non-stop complexes by tmRNA. (A) Secondary structure of tmRNA, with the TLD (light purple), MLD (dark purple) and its connecting helices and pseudoknots (purple). (B) Rotational analysis of the 30S movement during translocation of tmRNA. An additional “tilt” of the head is observed, resulting in an additional opening of the intersubunit space. (C) Cryo-EM map of a translocation intermediate in concert with tmRNA revealing the mechanism of MLD placement into the SSU. (D) Schematic representation of the conformation of the elements of tmRNA and the interplay with elements on the 50S (light blue) and 30S (yellow). Adapted from (Ramrath et al., 2012).

ArfB. The third discovered ribosome rescue factor working on non-stop ribosomal complexes is ArfB (former YaeJ) (Chadani et al., 2011b; Handa et al., 2011). The very first hints that ArfB alleviates stalling on non-stop complexes came from a screening in $\Delta ssrA\Delta arfA$ mutants. In those studies it was shown that ArfB can rescue the phenotype, however, only when overexpressed (Chadani et al., 2011b). Further analysis revealed that its N-terminal domain contains a GGQ motif, reminiscent of other release factors, suggesting that the factor alone is sufficient in peptidyl-tRNA hydrolysis. Indeed, mutations within the GGQ motif abolished its capability to hydrolyze the peptidyl-tRNA, suggesting that ArfB on its own is capable of rescuing non-stop complexes (Chadani et al., 2011b; Handa et al., 2011). This observation is further supported by the crystal structure of ArfB bound to the ribosome. ArfB consists of two domains, separated by a ~ 12 aa long linker. The globular N-terminal domain is structurally similar to domain III of RF1/2. The C-terminal domain is unstructured in solution but forms a α -helix that reaches into the mRNA channel similar to SmpB (**Figure 10A**) (Gagnon et al., 2012).

Comparable to SmpB and ArfA, accommodation of the C-terminus within the empty mRNA channel is essential for its function. Truncations of the C-terminal domain prohibit binding of ArfB to the ribosome, whereas mutations or truncations in the GGQ domain or linker domain do not decrease binding (Chadani et al., 2011b; Handa et al., 2011; Kogure et al., 2014). Thus, the C-terminal helix monitors the empty mRNA channel and helps to direct the globular domain towards the PTC (**Figure 10B,C**) (Gagnon et al., 2012). Likewise for SmpB, ArfB is more tolerant towards extended mRNAs, as evident from experiments showing that ArfB can resolve stalling upon rare codon stretches (Handa et al., 2011).

Positioning of the C-terminus of ArfB causes rearrangements within the decoding site through stacking interactions of residues of the linker of Arg118 on G530 and Pro110 on A1493. These interactions might help to guide the globular domain towards the PTC by determining the path of the linker region (**Figure 10B,C**) (Gagnon et al., 2012). Indeed, progressive truncations of the linker region severely decrease peptidyl-tRNA hydrolysis (Handa et al., 2011; Kogure et al., 2014). Positioning of the GGQ motif into the PTC results in hydrolysis. Superimposing the ArfB model with the model of RF2 bound to the ribosomes reveals an identical conformation of the GGQ motif and PTC residues, suggesting a similar mechanism of peptide release (see **1.3.3**) (Gagnon et al., 2012; Zhou et al., 2012b).

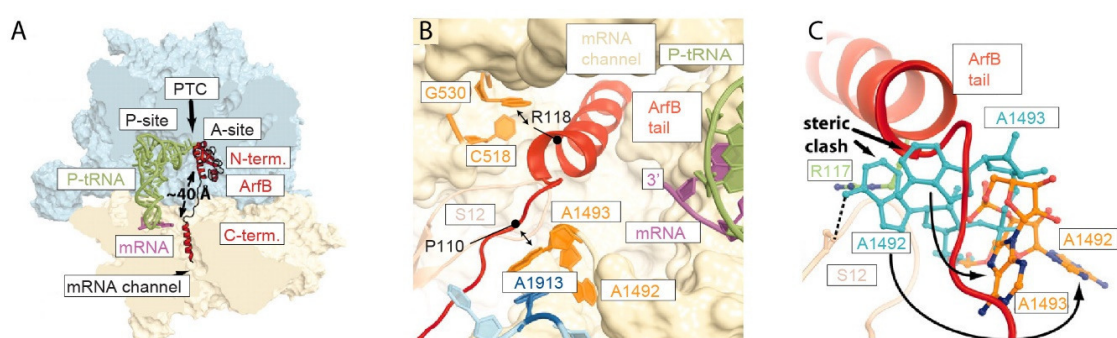


Figure 10. Interaction of ArfB with a non-stop ribosomal complex. (A) Overview of the ArfB binding site (red) on the 70S ribosome (50S, blue; 30S, yellow) in complex with P-tRNA (green) and truncated mRNA (purple). (B) Accommodation of the C-terminus of ArfB within the mRNA entry channel. Stacking interactions between R118 and G530 (orange) as well as between P110 and A1493 (orange) are indicated. (C) Accommodation of the C-terminus of ArfB induces conformational changes within A1492/A1493 (orange) that are different to the position during decoding of a sense codon (blue). These reorientations allow to place the N-terminus of ArfB into the PTC. Taken from (Gagnon et al., 2012).

Homologs of ArfB exist in organelles of eukaryotes with the best-characterized one being the human mitochondrial immature colon carcinoma transcript 1 (ICT-1) (Akabane et al., 2014; Duarte et al., 2012; Feaga et al., 2016; Kogure et al., 2014). Like ArfB, ICT-1 has a GGQ domain and a similar C-terminal tail and can restore cell viability in $\Delta ssrA\Delta arfA$ strains, when overexpressed (Kogure et al., 2014). *Vice versa*, the knockdown of ICT-1 in eukaryotes can be rescued by the expression of bacterial ArfB (Feaga et al., 2016). This suggest that ArfB and ICT-1 are functional interchangeable (Akabane et al., 2014).

ArfA. ArfA, a 72 aa long protein, was initially identified in genetic screens as a factor that is essential for cell viability in $\Delta ssrA$ background in *E. coli* (Chadani et al., 2010). In more detail, the amino acid substitution A18T, found within this study, caused a loss-of-function mutation within ArfA and thereby displayed a severe growth defect. Although both variants, wt ArfA and A18T ArfA co-localize with the ribosome, only wt ArfA was able to rescue non-stop complexes in an S30 lysate (Chadani et al., 2010). Indirect proof for ArfA working on non-stop complexes came from studies revealing that the expression of ArfA is dependent on *trans*-translation (Chadani et al., 2011c; Garza-Sánchez et al., 2011). The mRNA of *arfA* contains secondary structures that can either cause premature transcription termination or are cleaved by RNase III at defined positions within the ORF (Chadani et al., 2011c; Garza-Sánchez et al., 2011; Schaub et al., 2012). Thus, translation of *arfA* results in a non-stop ribosomal complex which is rescued by *trans*-translation and targets ArfA for degradation (Chadani et al., 2011c; Garza-Sánchez et al., 2011). Even if the ribosome is able to synthesize full-length ArfA, it is prone for aggregation due to the hydrophobicity of the C-terminus (Chadani et al., 2011a). However, if tmRNA is absent or overwhelmed a truncated version of ArfA lacking the terminal 17-18 aa is released. Remarkably, the truncated version retains its rescue activity, making the C-terminus dispensable for its function, which is in line with its poor conservation (Chadani et al., 2011c; Garza-Sánchez et al., 2011; Schaub et al., 2012). Overexpression of ArfA in wt cells on the other hand has an inhibitory effect on cell growth (Chadani et al., 2010). Hence, ArfA serves as a back-up system for *trans*-translation which is only active when *trans*-translation is hampered.

The mode of action of ArfA however remained obscure. Although it was able to rescue non-stop complexes in a S30 lysate, it failed to do so on isolated ribosomal complexes, indicating that additional factors are involved (Chadani et al., 2010, 2011a).

Experiments in a reconstituted cell-free translation system identified RF2, but not RF1, as the factor cooperating with ArfA. Rescue activity was strictly dependent on the GGQ motif of RF2, but not on the SPF motif (1.3.3) (Chadani et al., 2010; Shimizu, 2012). Hydroxyl-radical probing on ribosomal non-stop complexes showed that binding of the C-terminus of ArfA exposes nucleotides that are close to the mRNA entry channel and the decoding site overlapping with the position of SmpB, whereas the N-terminus appeared to be flexible. Binding of RF2 to the 70S-ArfA complex changed the mode of interaction of ArfA with the ribosome. Location of the C-terminus did not change significantly, however the N-terminus caused a more defined cleavage pattern (Kurita et al., 2014b).

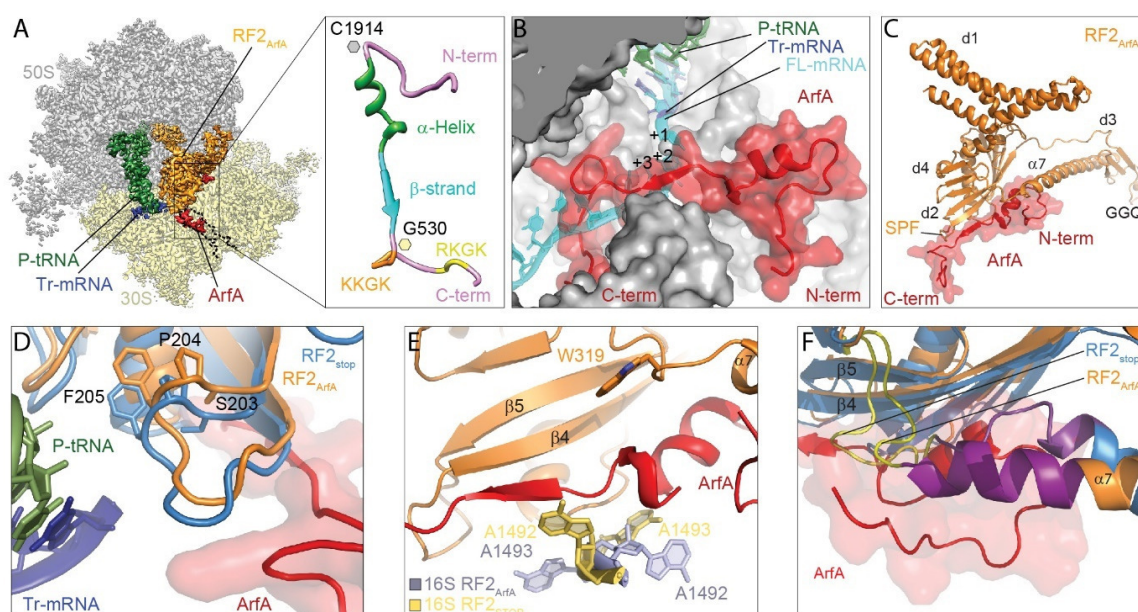


Figure 11. Interactions of ArfA and RF2 on a non-stop ribosomal complex. (A) Transverse section of the cryo-EM reconstruction of ArfA-RF2-SRC, highlighting the 30S (yellow), 50S (grey), P-tRNA (green), RF2 (orange), ArfA (red) and truncated mRNA (dark blue). Zoom in showing the model for ArfA with secondary structures (a-helix, green; b-strand, blue) and motifs highlighted (RKGK, yellow; KKGK orange). Additionally position of G530 of 16S rRNA (pale yellow) and C1914 (grey) of 23S rRNA are indicated. (B) Position of ArfA within the mRNA entry channel revealing a steric clash with a superimposed full-length mRNA (FL-mRNA, cyan) compared to truncated mRNA (Tr-mRNA). (C) Overview of the interaction surface between ArfA and RF2_{ArfA}. (D) Superimposition of RF2_{stop} (blue, PDB 4V5E) with ArfA and RF2_{ArfA} from the ArfA-RF2-structure. (E) Interaction of ArfA with W319 of RF2_{ArfA} and conformation of decoding nucleotides A1492/A1493 in the presence of ArfA (pale blue) or presence of RF2_{stop} (yellow). (F) Remodeling of the switch loop (yellow) and $\alpha 7$ helix (purple) of domain 3 of RF2 (orange) by ArfA (red) compared to the conformation of RF2 when decoding a canonical stop codon (blue).

Recently, five different groups were able to resolve cryo-EM structures of truncated ArfA in interplay with RF2 on 70S non-stop complexes (see Discussion) (**Figure 11A**). The outcome of all reconstructions was nearly identical. Hence, the following sections will describe the common conclusions of these studies, whereas differences will be discussed in the discussion section (Demo et al., 2017b; Huter et al., 2017c; James et al., 2016; Ma et al., 2017; Zeng et al., 2017).

In line with hydroxyl-radical probing, the C-terminus resides within the mRNA entry channel with clear density observed up to position 46-48 and lack of density for the remaining C-terminal residues, in agreement with their poor conservation (**Figure 11B**) (Demo et al., 2017b; Huter et al., 2017c; James et al., 2016; Kurita et al., 2014b; Ma et al., 2017; Zeng et al., 2017). In contrast to the C-termini of SmpB or ArfB that form helices and follow the predetermined path of the mRNA channel, the C-terminus of ArfA appears to rather block the tunnel. Comparing the path of full-length mRNA with the position of C-terminus of ArfA shows that only up to two to three nucleotides are allowed to accommodate within the mRNA channel in presence of ArfA (**Figure 11B**) (Demo et al., 2017b; Huter et al., 2017c; James et al., 2016; Ma et al., 2017; Zeng et al., 2017). This is in line with biochemical data, showing that mRNA extended by more than 3 nt. reduces the efficiency of rescue with nearly no rescue activity observed if the mRNA is extended by six or more nucleotides (Chadani et al., 2011c; Kurita et al., 2014b; Zeng and Jin, 2016).

Furthermore, the C-terminus of ArfA contains two highly conserved positively charged stretches (KKGK₃₃₋₃₆; RKGK₄₁₋₄₄) that anchor the C-terminus into the channel by forming contacts with the surrounding 16S rRNA. It is worth to mention that single mutations within these stretches do not have an effect on the rescue activity by ArfA, suggesting a redundancy in their interaction network (Kurita et al., 2014b; Ma et al., 2017; Zeng et al., 2017). Proceeding from the mRNA entry channel towards the N-terminus, the C-terminal loop makes a 90° turn around G530, placing the N-terminus in a pocket formed by decoding center, h18, h44 and S12. The only contact with the LSU is through Lys12 of ArfA contacting C1914 of H69 resulting in a ~180° bend that directs the very N-terminus towards S12. The described conformation of ArfA creates a platform for the interaction with RF2 (Demo et al., 2017b; Huter et al., 2017c; James et al., 2016; Ma et al., 2017; Zeng et al., 2017).

Recruitment of RF2 to the non-stop complex results in an overall similar conformation as seen upon canonical termination (**Figure 11C**). However, a small shift

is observed within the decoding domain 2/4 affecting the SPF motif. Importantly, the SPF does not interact with ArfA, demonstrating that ArfA does not mimic a stop codon (**Figure 11D**). This is further highlighted by the fact that mutations within the SPF motif do not interfere with rescue of non-stop complexes (Chadani et al., 2012). The conformation of ArfA rather provides an interface for RF2, involving residues 15-31 of ArfA that interact with β 4- β 5 strands of domain 2 and the distal end of α -helix α 7 of domain of RF2. ArfA thereby augments a β -strand to the β -sheet of RF2 domain 2/4 (**Figure 11C,E**) (Demo et al., 2017b; Huter et al., 2017c; James et al., 2016; Ma et al., 2017; Zeng et al., 2017).

During canonical termination, the transition of the closed to the open state of RF2 is mediated by rearrangements within the switch loop between domain III and IV of RF2 (**1.3.3**). Through stacking interactions between the switch loop and the decoding nucleotides A1492/A1493, the α -helix α 7 becomes extended by two or three turns, when compared to the close conformation of RF2 (**Figure 11E,F**) (Jin et al., 2010; Korostelev et al., 2008, 2010; Laurberg et al., 2008; Weixlbaumer et al., 2008; Zhou et al., 2012b). However, in the presence of ArfA, A1492/A1493 adopt distinct conformations restricting interactions with the switch loop (**Figure 11E**). Instead, ArfA itself stabilizes an alternative conformation of the switch loop. These interactions include a hydrophobic patch within the α -helical region of ArfA and Trp319 of RF2. Hence, the α 7 of domain III of RF2 adopts a similar conformation as seen upon canonical termination (**Figure 11E,F**). These movements help to direct the GGQ motif towards the PTC (Demo et al., 2017b; Huter et al., 2017c; James et al., 2016; Ma et al., 2017; Zeng et al., 2017).

Additionally, two groups reported reconstructions of RF2 in an intermediate state but bound to the 70S-ArfA complex. While James et al. were able to obtain this intermediate state using independent reconstructions, one with ArfA A18T bound to the 70S-RF2 complex and the other one with *T. thermophilus* RF2 bound to 70S-ArfA complex, Demo et al. were able to obtain this state as a subpopulation of their 70S-ArfA-RF2 reconstruction (Demo et al., 2017b; James et al., 2016). The overall conformation of RF2 in those reconstructions reflects the conformation of closed RF2 in solution with the GGQ motif being 70 Å away from its respective target (Vestergaard et al., 2001; Zoldák et al., 2007). Interestingly, in all of those reconstructions the N-terminus of ArfA as well as the switch loop of RF2 was disordered. Hence, it seems plausible that the opening of RF2 is dependent on the ordering of the switch loop by

the N-terminus of ArfA and that the observed states represent a preaccommodation state of RF2 (see Discussion) (Demo et al., 2017b; James et al., 2016).

Hence, biochemical and structural studies lead to the following model (Chadani et al., 2012; Demo et al., 2017b; Huter et al., 2017c; James et al., 2016; Kurita et al., 2014b; Ma et al., 2017; Zeng et al., 2017). ArfA binds the ribosome and probes the empty mRNA entry channel with its C-terminus, similar to SmpB. Accommodation of ArfA recruits RF2 that transits from a closed to open conformation upon stabilization of the switch loop by the N-terminus of ArfA. Similar to canonical termination, opening of the release factor places the catalytic important GGQ motif into the PTC and allows release of the nascent chain.

1.4.2 Polyproline mediated stalling and rescue by elongation factor P

Translation elongation proceeds with an average speed of 12-20 aa/s⁻¹ under optimal conditions (Bilgin et al., 1992; Proshkin et al., 2010). This rate, however, can strongly vary and is dependent on several factors like tRNA abundance, the availability of amino acids, structural features of the translated mRNA and many other parameters (Bullwinkle and Ibba, 2016; Moine et al., 1988; Yanofsky and Horn, 1994). Interestingly, it was shown that the nature of amino acids themselves can influence the rate of elongation, implicating that not every amino acid is a perfect substrate for peptide bond formation (Johansson et al., 2011; Pavlov et al., 2009). Of particular interest is the amino acid proline that is distinct from the other 19 proteinogenic amino acids as it is a secondary amine with a pyrrolidine ring as a side chain, curving back from the C_α to the nitrogen of the amine (**Figure 12A**). It was shown that proline is a poor A-site acceptor as well as a poor donor when present in the P-site, as judged by its strongly reduced reactivity with puromycin when compared to other amino acids (Doerfel et al., 2013; Muto and Ito, 2008; Wohlgemuth et al., 2008). Hence, proline significantly reduces the rate of peptide bond formation when compared to other amino acids. *In vitro* experiments showed that this effect is most severe when ribosomes encounter a stretch of consecutive prolines, as it leads to the arrest of translation (Doerfel et al., 2013; Ude et al., 2013). Surprisingly, such polyproline motifs are quite abundant in every living organism, despite their effect on translation. For example roughly 2% of all genes in *E.coli* contain polyproline coding motifs with increasing numbers as the genome gets larger (Starosta et al., 2014b). Presumably every

organism, including archaea and eukaryotes, has at least one polyproline-containing gene which is the *valS* gene coding for the Val-tRNA synthetase (Starosta et al., 2014b). Mutation within the proline triplet leads to the formation of mischarged Thr-tRNA^{Val} *in vitro* and interferes with viability in *E.coli*.

Given the importance and abundance of such triplets, this raises the question of the advantage of prolines over other amino acids. Indeed, due to the cyclic structure of the side chain, prolines show an exceptional conformational rigidity (Morris et al., 1992). Hence, prolines restrain their own conformational freedom as well as the conformation of neighboring residues and act as a structural disruptor of secondary structure elements within α -helices and β -sheets and are often found at the start or end of such elements. On the other hand, proline can be found as *cis* and *trans* isomers, altering the torsion angle of peptide bonds by 180°, whereas all other amino acids prefer the *trans* conformation (Lu et al., 2007; Yaron et al., 1993).

Thus, prolines display properties that are crucial for the architecture of proteins. However, the fact that sequential prolines can arrest translation *in vitro* but are crucial for the viability of an organism implies that cells utilize additional mechanisms to alleviate those stalling events.

EF-P was initially described as a factor that associates with the ribosome and promotes peptide bond formation between fMet-tRNA^{fMet} and puromycin (Glick and Ganoza, 1975; Glick et al., 1979). Phylogenetically, EF-P is ubiquitously distributed throughout bacteria and has orthologous in eukaryotes and archaea (eIF5a and aIF5a, respectively) (Kyrpides and Woese, 1998). Crystal structures of EF-P alone revealed a three-domain architecture and an overall conformation mimicking the L-shape of a tRNA (**Figure 12B**) (Choi and Choe, 2011; Hanawa-Suetsugu et al., 2004; Kristensen and Laurberg, 2002; Yanagisawa et al., 2010). Domain 2 and 3 exhibit oligonucleotide-binding folds responsible for DNA/RNA binding. Domain 1, on the other hand, occupies the most conserved region within EF-P located at the tip of a loop. Further insights on the mode of action of EF-P came from a crystal structure of *Thermus thermophilus* EF-P-70S structure programmed a short mRNA and tRNA^{fMet} (Blaha et al., 2009). EF-P binds between the P and E-site of the ribosome and interacts with both subunits. Domain 3 is orientated towards the SSU but lacks density in this structure for its loop close to the mRNA. Domain 2 interacts with the L1 protein leading to a conformation of the L1 stalk/protein that is similar to the position during translocation. The highly conserved loop of domain 1 interacts with the CCA-end of the P-tRNA with the closest

residue being Arg32 (analogous to Lys34 in *E.coli*). From that structure it was concluded that EF-P helps to position the fMet-tRNA and hence assists in formation of the first peptide bond.

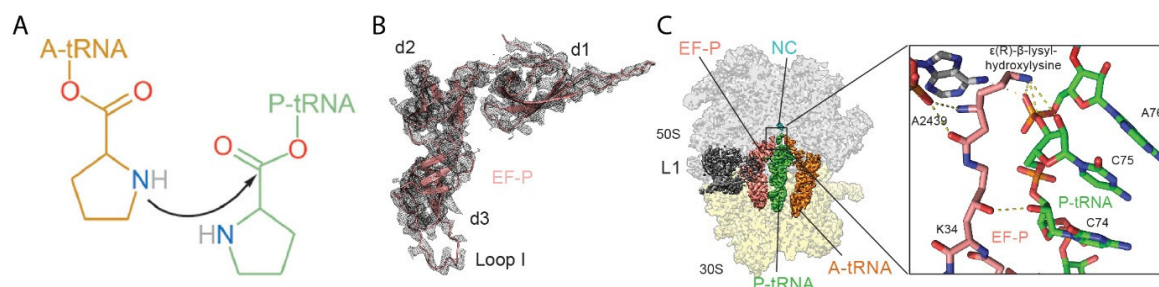


Figure 12. EF-P alleviates proline-induced stalling by contacting the CCA-end of the peptidyl-tRNA. (A) The α -amino group of the proline attached to the A-site tRNA nucleophilically attacks the carbonyl carbon of the proline attached to the P-site tRNA during peptide bond formation. (B) Cryo-EM density with molecular model for *E.coli* EF-P (salmon) with domains 1-3 (d1-d3) indicated. (C) Representation of a PPP-stalled ribosomal complex in presence of A-site tRNA (orange), P-site (green) tRNA and EF-P. Further indicated are the 30S (yellow), 50S (grey) and the 'in' position of the L1 protein (dark grey). Inlet shows the interaction of the ϵ (R)- β -lyssyl-hydroxylysine modification contacting the backbone of the CCA-end of P-site tRNA.

Studies by Doerfel et al. as well as Ude et al. further refined the understanding for EF-P (Doerfel et al., 2013; Ude et al., 2013). In their studies both groups could show that consecutive prolines, but no other amino acid, arrest ribosomal translation *in vitro* and that rescue of those ribosomes is strictly dependent on EF-P. In support of that, ribosomal profiling data as well as proteomic analysis by mass spectrometry in absence of EF-P identified additional pausing motifs containing diprolyl motifs, thus expanding the range of sequences that require EF-P (Elgamal et al., 2014; Peil et al., 2013; Woolstenhulme et al., 2015). Interestingly, not every diprolyl motif requires the help of EF-P. It was shown that the accumulation of ribosomes on diprolyl motifs was dependent on the amino acid preceding or following the PP sequence (Elgamal et al., 2014; Peil et al., 2013; Woolstenhulme et al., 2015). Following *in vitro* studies also confirmed the influence of the upstream amino acid on proline triplets (Starosta et al., 2014c).

A commonality between those stalling motifs is that the ribosome arrests with the second proline in the P-site and that this state is recognized by EF-P (Doerfel et al., 2013). Indeed, biochemical studies could show that EF-P recognizes a specific architecture of the D-loop that is shared by all isomers of tRNA^{Pro} in *E.coli* (Kato et

al., 2016). Interestingly, tRNA^{fMet} has the same D-loop architecture explaining the beneficial effect of EF-P on the first peptide bond formation.

Other studies revealed that endogenous EF-P bears a posttranslational modification at the tip of the highly conserved loop of domain 1 (**Figure 12B**) (Aoki et al., 2008). In *E.coli* this leads to an additional mass of +144 Da at position of Lys34 resulting from the activity of three modification enzymes (Bailly and de Crécy-Lagard, 2010; Navarre et al., 2010; Peil et al., 2012; Yanagisawa et al., 2010). In a first step the enzyme EpmB, a 2,3 - aminomutase converts (S)- α -lysine to (R)- β -lysine, which is ligated to the ϵ -amino group of Lys34 by EpmA (Bailly and de Crécy-Lagard, 2010; Navarre et al., 2010; Peil et al., 2012; Yanagisawa et al., 2010). In a last step EpmC completes the posttranslational modification by hydroxylation of C5 of Lys34 resulting in a ϵ (R)- β -lysyl-hydroxylysine modification (Peil et al., 2012). Interestingly, deletion of the modification enzymes EpmB and EpmA lead to similar phenotypes as observed upon deletion of EF-P, indicating that the cellular function of EF-P is dependent on those modification enzymes (Zou et al., 2012a, 2012b). Indeed, Doerfel et al and Ude et al could show that only modified EF-P is capable of alleviating polyproline stalled ribosomes (Doerfel et al., 2013; Ude et al., 2013). In more detail it was shown that the action of EpmB and EpmA is essential, whereas the final hydroxylation by EpmC is dispensable for the function of EF-P. It is noteworthy to mention that only a subset of bacteria have the above mentioned modification enzymes. Other bacteria use unrelated different posttranslational modification systems that lead to the addition of, for example, rhamnosylation of Arg32 in *Pseudomonas aeruginosa* or 5-aminopentanol moiety at Lys32 in *Bacillus subtilis* (Lassak et al., 2015a; Rajkovic and Ibba, 2017). So far such pathways have only been discovered in 35% of available bacterial genomes. Hence it is not clear, if the posttranslational modification of EF-P is a general strategy or just utilized by a subset of bacteria (Lassak et al., 2015a; Rajkovic and Ibba, 2017).

Despite these insights it remained unclear as to how consecutive prolines perturb translation and on how modified EF-P is contributing to the rescue of the arrested ribosomes. From the crystal structure of *Tth*. 70S-EF-P complex it was hard to deduce any information in this regard as the ribosomes were not programmed with prolines and EF-P was lacking the modification (Blaha et al., 2009). Biochemical experiments using proline analogues as a substrate revealed that the steric properties of proline rather than its electrophilic nature make it a poor substrate for peptide bond

formation as it interferes with the precise positioning of substrates within the PTC (Doerfel et al., 2015). Furthermore, it was concluded that the modification might stabilize the CCA end of the peptidyl-tRNA and thereby helps to position the P-site substrates in the PTC. First structural insights on the contribution of the modification came from a cryo-EM reconstruction containing eIF5A (Schmidt et al., 2016). eIF5A contains a hypusinylated lysine at position Lys51 that is analogous to Lys34 in *E.coli* (Zanelli et al., 2006). The modification in this structure reaches towards the PTC contacting the backbone of the CCA-end demonstrating that the modification does not directly contribute to catalysis (Schmidt et al., 2016). Nevertheless, no conclusion on relieving of polyproline-stalled ribosomes could be drawn as the ribosomes resulted from a native pull-out and hence do not represent a defined state.

Recently, Huter and coworkers were able to elucidate the mode of action of EF-P and its modification on polyproline stalled ribosomes using cryo-EM and MD simulations (Huter et al., 2017a). Based on their reconstructions it is suggested that the favorable all-*trans* conformation of consecutive prolines is not possible in context of the ribosomal tunnel. Hence, no density for the nascent chain could be observed in the absence of EF-P, indicating strong flexibility within the growing peptide. Furthermore, the A-site tRNA had severe problems to accommodate within the PTC. However, when EF-P was present the nascent chain and A-site tRNA were stabilized due to EF-P and the modification contacting the peptidyl-tRNA (**Figure 12C**). Based on the density and modelling of the peptidyl-moiety an alternative conformation of prolines is suggested that allows the nascent chain to overcome the sterical restrictions imposed by the ribosomal tunnel. Last but not least, stabilization of the CCA end by the modification leads to an optimal positioning of the substrates for peptide bond formation. Hence, the effect of EF-P is of entropic nature rather than directly contributing to the catalysis of peptide bond formation (Doerfel et al., 2015; Huter et al., 2017a)

2 Objectives of these Studies

Structure of orthosomycins avilamycin and evernimicin (Publication 1).

Most of the medically used antibiotics target the ribosome and thereby inhibit bacterial growth. The rise of multidrug resistance in pathogenic bacteria, however, highlights the need for new therapeutic agents. The orthosomycin antibiotics, avilamycin and evernimicin were shown to be promising candidates as they do not display any cross-resistance with other classes of antibiotics that target the ribosome (Buzzetti et al., 1968; Wright, 1979). Biochemical experiments suggested binding of these agents around H89 and H91 of the 23S rRNA, indicating that they bind to a unique site of the ribosome (Belova et al., 2001; Kofoed and Vester, 2002). The aim of the study was to determine the binding site of avilamycin and evernimicin on the 70S ribosome using cryo-EM. The study was complemented with smFRET data to unravel the mode of action of those two orthosomycins.

Structure of the spinach chloroplast ribosome (Publication 2).

Recent advances in cryo-EM have led to procurement of high-resolution structures of bacterial as well eukaryotic ribosomes. However, high-resolution structures of the chloroplast ribosome had been lacking. Chlororibosomes are very specialized as they only translate a limited number of proteins encoded in the chloroplast genome. Sequence alignments imply high structural and mechanistic similarities between chlororibosomes and the translation machinery of other bacteria, for example *Escherichia coli*. On the other hand, proteomic studies identified six plastic-specific ribosomal proteins. The aim of the study was to obtain a high-resolution structure of the chlororibosomes to gain deeper insights into the architecture of the chlororibosome as well as the location of the plastic-specific ribosomal proteins.

Structural insights into ribosome rescue by trans-translation, ArfA and ArfB (Publication 3 and 4).

Ribosomes stall on the 3' end of messenger RNAs without a stop codon (Giudice and Gillet, 2013; Keiler and Feaga, 2014). These 'non-stop' complexes are rescued by tmRNA, the alternative factor A (ArfA) or B (ArfB). While all of these factors recognize such stalled ribosomes, they use different strategies to recycle them. tmRNA resumes translation on the tmRNA open reading frame, that encodes for a degradation tag and includes a stop codon, allowing canonical termination and recycling. ArfB, on the other hand, provides its own GGQ motif capable of peptidyl-tRNA hydrolysis. ArfA rescues stalled ribosomes together with release factor 2. Our aim was to understand how ArfA cooperates with RF2 to alleviate stalling on 'non-stop' complexes. Therefore, we sought to obtain a high-resolution reconstruction of 70S ribosomes stalled on truncated mRNAs in the presence of ArfA and RF2. Based on our results, we were able to structurally compare and summarize the available structures of all three rescue factors.

Structural basis for polyproline-induced stalling and rescue by EF-P (Publication 5).

It was shown that the amino acid proline is a poor substrate for peptide bond formation as it is a suboptimal A-site acceptor and P-site donor (Doerfel et al., 2013; Johansson et al., 2011; Muto and Ito, 2008; Pavlov et al., 2009; Wohlgemuth et al., 2008). Thus, prolines significantly reduce the speed of translation. This effect becomes even more pronounced, when ribosomes try to translate a consecutive stretch of prolines, leading to arrest of translation *in vitro* (Doerfel et al., 2013; Ude et al., 2013). Recent studies showed that EF-P is required to alleviate stalling on such polyproline-arrested ribosomes. Furthermore, EF-P needs to be posttranslationally modified to restore translation.

Structural insights into the mode of action of EF-P on polyproline stalled ribosomes have been lacking. Thus, the aim of this study was to obtain high resolution structures of ribosomes stalled on consecutive proline sequences in the absence and presence of EF-P, to understand why polyprolines are stalling ribosomes and to explain the mode of action of EF-P and its modification to rescue such stalling events.

3 Cumulative Thesis: Summary of Publications

3.1 Structures of the orthosomycin antibiotics avilamycin and evernimicin in complex with the bacterial 70S ribosome (Publication 1).

Stefan Arenz, Manuel F. Juetz, Michael Graf, Fabian Nguyen, Paul Huter, Yury S. Polikanov, Scott C. Blanchard and Daniel N. Wilson

Proceedings of the National Academy of Sciences. 113, 7527-7532 (2016)

Increasing multidrug resistance in pathogenic bacteria highlights the need for new antibiotics. Two promising candidates are the orthosomycins avilamycin and evernimicin as they utilize a unique binding position on the ribosome. Thus, they do not show any cross-resistance with other classes of antibiotics and therefore might be clinically relevant. In this paper, we present two cryo-EM reconstructions of avilamycin and evernimicin bound to the *E. coli* 70S ribosome. The reconstructions show that both antibiotics bind the LSU close to the minor groove of H89 and H91 and interact with arginine residues of L16. This binding site suggests that the presence of either avilamycin or evernimicin interferes with the transition of IF2-30S conformation to the IF2-70S conformation. Furthermore, complementing smFRET data demonstrated that avilamycin and evernimicin prevent accommodation of aa-tRNA at the A-site of the ribosome.

3.2 Cryo-EM structure of the spinach chloroplast ribosome reveals the location of plastid-specific ribosomal proteins and extensions (Publication 2).

Michael Graf, Stefan Arenz, Paul Huter, Alexandra Dönhofer, Jiri Novacek and Daniel N. Wilson

Nucleic Acids Research. 45, 2887-2896 (2017)

Recent advances in cryo-EM allowed the visualization of a variety of ribosomes of different species. However, insights into the architecture of chloroplast ribosomes have so far been missing. Sequence comparison show a high degree of similarity between the translation machinery of chloroplasts and other bacteria, including cyanobacteria and γ -proteobacteria, however chloroplast additionally have six non-orthologous proteins termed 'plastid-specific ribosomal proteins' (PSRP). This works comprises a cryo-EM structure of the spinach chlororibosome at 3.6 Å resolution for the LSU and 5.4 Å resolution for the SSU. With respect to the *E. coli* 70S ribosome, the structure shows that most differences are located in the periphery of the ribosome, whereas the functional core remains highly similar. Furthermore, we were able to allocate the binding site of PSRPs. Last but not least, we identified a group of protein extension at the back of the LSU that might assist in binding of the chlororibosome to the thylakoid membrane.

3.3 Structural basis for ArfA-RF2 mediated translation termination on mRNAs lacking stop codons (Publication 3).

Paul Huter, Claudia Müller, Bertrand Beckert, Stefan Arenz, Otto Berninghausen, Roland Beckmann and Daniel N. Wilson

Nature. 541, 546-549 (2017)

Ribosomes that stall at the 3' end of mRNAs get rescued by either tmRNA, ArfA or ArfB. While structures of such stalled complexes together with tmRNA or ArfB have been obtained, information on the interplay of ArfA with the ribosome and RF2 have been lacking. By using the same A-site truncated SRC as for EF-P, we were able to bind ArfA together with RF2 to the stalled complex and subject the sample for cryo-EM analysis, resulting in a reconstruction at 3.1 Å. As evident from the structure, ArfA binds

close to the decoding site of the A-site. The C-terminus of ArfA resides within the mRNA entry channel, a position that would overlap with a 3' extended mRNA. Proceeding from the mRNA entry channel towards the N-terminus, the C-terminal loop makes a 90° turn around G530, placing the N-terminus in a pocket formed by the decoding center, h18, h44 and S12. The only contact with the LSU is via Lys12 of ArfA contacting C1914 of H69 resulting in a ~180° bend that directs the very N-terminus towards S12. The described conformation of ArfA creates a large interaction interface with RF2, augmenting a β -strand to the β -sheet of domain 2/4 of RF2. The overall position of RF2 in complex with ArfA is similar to that observed during canonical termination. Surprisingly, the conserved SPF motif of RF2, does not contact ArfA and therefore ArfA does not mimic a stop codon. Instead, ArfA interacts with the switch loop of RF2. These interactions extend the α -helix α 7 of domain 3 by several turns, thereby facilitating the opening of RF2 and placement of the catalytical important GGQ motif at the PTC. Hence, our structure demonstrates that ArfA not only recruits RF2 in a codon-independent manner, but also induces conformation changes that direct domain 3 towards the PTC.

3.4 Structural basis for ribosome rescue in bacteria (Publication 4).

Paul Huter, Claudia Müller, Stefan Arenz, Bertrand Beckert and Daniel N. Wilson
Trends in Biochemical Sciences. 42, 669-680 (2017)

Ribosomes that get stuck at the 3' end of mRNA require the interaction of tmRNA, ArfA or ArfB. Based on our previous structure on ArfA, we could compare the mode of action of other rescue factors that operate on non-stop complexes. tmRNA is dependent on a small protein called SmpB, which probes the empty mRNA entry channel and thereby recruits tmRNA. Thus, tmRNA is able to resume translation on its provided ORF that leads to canonical termination and degradation of the faulty protein. ArfB probes the empty mRNA entry channel via its C-terminus and provides its own GGQ motif allowing it to hydrolyse the peptidyl tRNA. ArfA, on the other hand, was shown to be a back-up system for tmRNA. Under circumstances, when tmRNA is overwhelmed, a truncated version of ArfA is translated, which is capable of recognizing stalled complexes via its C-terminus. Binding of ArfA provides a platform for RF2 recruitment that allows translation to terminate in a codon-independent manner.

3.5 Structural basis for polyproline-mediated ribosome stalling and rescue by the elongation factor P (Publication 5).

Paul Huter, Stefan Arenz, Lars V. Bock, Michael Graf, Jan Ole Frister, Andre Heuer, Lauri Peil, Agata L. Starosta, Ingo Wohlgemuth, Frank Peske, Jiri Novacek, Otto Berninghausen, Helmut Grubmüller, Tanel Tenson, Roland Beckmann, Marina V. Rodnina, Andrea C. Vaiana and Daniel N. Wilson

Prolines are suboptimal substrates for peptide bond formation, as evident by biochemical studies showing that they are poor A-site acceptors as well as P-site donors. This effect is even more pronounced, when ribosomes encounter stretches of consecutive prolines leading to the arrest of translation *in vitro*. Those polyproline-arrested ribosomes are rescued by EF-P, which requires a posttranslational modification to be functional. By using a previously characterized reporter mRNA as a template for translation, we were able to stall ribosomes on a consecutive proline stretch in the absence of EF-P. The stalled ribosomes were isolated from the translation reaction and subjected for cryo-EM analysis in the absence of EF-P. This dataset revealed two major subclasses with resolution ranging from 3.6 to 3.9 Å. In both of the reconstructions, it was evident, that the quality of density for the tRNAs was progressively deteriorating from the SSU to the PTC. Furthermore, no density for the nascent chain could be observed, indicating that polyproline containing nascent chains cannot accommodate within the peptide tunnel in the absence of EF-P. As a result, consecutive prolines destabilize the peptidyl-tRNA and prevent accommodation of the A-site tRNA, which leads to ribosomal stalling. Our second dataset in the presence of exogenous modified EF-P showed that the tRNAs are more stably bound due contact between EF-P and the body of the P-site tRNA. Furthermore, we could show that the modification of EF-P contacts the CCA end of the P-site tRNA. We also observed density for the nascent chain, however, due to the presence of EF-P the density was fused to the A-site tRNA and therefore no conclusions on the conformation of polyprolines in the peptide tunnel could be made.

Hence we created a third SRC that was based on the above described reporter mRNA but was truncated after the second proline. Thus, by eliminating the codon at the A-site we could exclude any interference by the A-site tRNA. Subjecting this SRCs for cryo-EM analysis resulted in a reconstruction at 3.1 Å in the presence of P-tRNA and EF-P. Using this approach, we could show that the conformation of the diprolyl moiety

deviates from the favored all-*trans* conformation of prolines. EF-P stabilizes the P-site tRNA and most importantly the CCA end via its modification, thereby stabilizing the nascent chain by forcing it into an alternative conformation. MD simulations complemented this result showing that in presence of EF-P the alignment of substrates for peptide bond formation is restored. However, in the absence of EF-P or its modification the substrates have an unfavorable geometry and thus peptide bond formation is prevented.

The high-resolution structure also allowed us to describe critical interactions of EF-P with the P-site tRNA as well as the E-site codon and S7. Based on our reconstructions we could confirm the result of Katoh et al. showing that the extended D-loop architecture of tRNA^{Pro} is critical for the recognition of polyproline-stalled ribosomes by EF-P. Furthermore, we could show that Tyr183 and Arg186 interact with residues of the 16S rRNA as well as the ASL of the P-site tRNA. Using our well-established firefly luciferase translation assay, we could show that mutation of these two residues abolished the activity of EF-P on stalling.

Additionally, we observed interactions of domain 3 of EF-P with the E-site codon and ribosomal protein S7. Based on our structural insights, we suggested that this loop region of domain 3 might recognize the nature of the E-site codon. Surprisingly, mutations of residues of domain 3 that interact with the E-site codon and S7 did not significantly reduce the rescue activity of EF-P, raising the question about the importance of these interactions. Further biochemical experiments will be needed to elucidate the role of those interactions.

4 Discussion

4.1 Rescue of 'non-stop' complexes with focus on ArfA

The five recently published structures on 'non-stop' ribosomal complexes in the presence of ArfA and RF2 allow us to not only complete the picture of the ArfA-RF2 rescue mechanism, but also provides the opportunity to compare the different rescue pathways with each other (Demo et al., 2017b; Huter et al., 2017c; James et al., 2016; Ma et al., 2017; Zeng et al., 2017). The structures are in excellent agreement with each other, despite the different strategies used for the formation of the SRCs. These different approaches will be discussed in the following section.

Four out of five 'non-stop' complexes were formed by incubating 70S ribosomes with a small mRNA containing SD-sequence, linker sequence and an AUG start codon (Demo et al., 2017b; James et al., 2016; Ma et al., 2017; Zeng et al., 2017). This led to programmed ribosomes with the AUG codon in the ribosomal P-site and a vacant A-site. Furthermore, these complexes were incubated with either deacylated tRNA^{fMet} or non-hydrolysable fMet-NH-tRNA^{fMet} together with C-terminal truncated ArfA and RF2. These reconstructions resulted in one major population of 70S ribosomes within the cryo-EM datasets that were programmed with P-site tRNA, RF2 and ArfA. One exception is the dataset of Demo et al. that revealed, besides the presence of E-site tRNA, a second major class with RF2 in its closed form (42% after subtraction of junk particles compared to 34% with RF2 in its open conformation on the ribosome).

Huter et al. created a truncated mRNA based on the *nlpD* ORF, leading to stalled ribosomes that are programmed with a peptidyl-tRNA^{Pro} in the P-site and a vacant A-site when translated (see EF-P) (Huter et al., 2017a, 2017c). These stalled ribosomes were also incubated with C-terminally truncated ArfA but contrary to other studies RF2-GAQ was used. Hence, this experimental set up represents the only 'non-stop' ribosomal complex, as the other SRCs are rather initiation complexes. Nevertheless, sorting of this cryo-EM dataset resulted in two major subclasses after *in silico* sorting. One class was programmed with peptidyl-tRNA^{Pro} in the P-site, C-terminal truncated ArfA and RF2 (49% of particles of the dataset after subtraction of junk particles), the other class had additional density for E-site tRNA (40% of particles

of the dataset after subtraction of junk particles). However, besides the presence of the E-site tRNA, the two classes do not differ in context to ArfA-mediated rescue.

The different approaches for creating the SRCs in the presence of ArfA and RF2 resulted in two observed states dependent on the nature of tRNA and RF2 used (Demo et al., 2017b; Huter et al., 2017c; James et al., 2016; Ma et al., 2017; Zeng et al., 2017). While the usage of deacylated tRNA mimics a post-hydrolysis state, using RF2-GAQ or non-hydrolyzable P-tRNA mimics a pre-hydrolysis state. Nevertheless, these two different states did not lead to changes within domain 3 of RF2 at the PTC and therefore the same conclusions could be made from all the studies. Remarkably, none of the applied strategies resulted in a ribosomal complex with only ArfA bound, indicative for a high affinity of RF2 for the ribosome once ArfA is recruited.

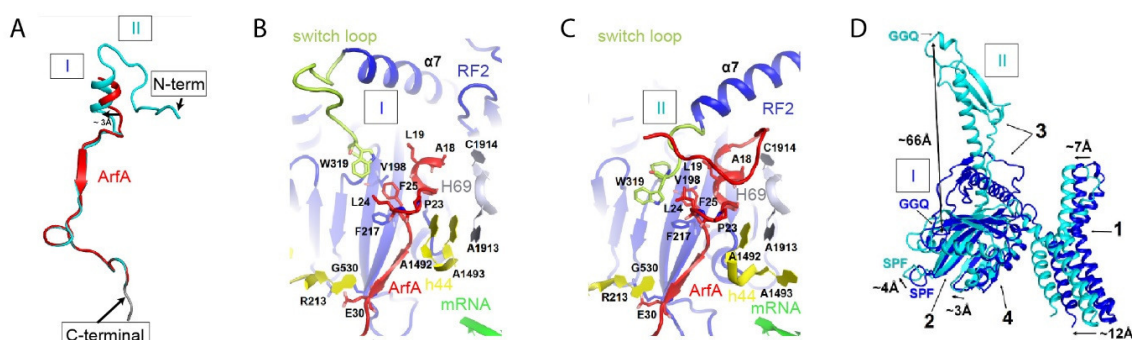


Figure 13. Transition of RF2 from a closed to an open state on the ribosome in presence of ArfA. (A) Conformation of the N-terminus of ArfA in presence of closed (red, I) and open RF2 (blue, II). (B) Interaction of ArfA (red) with elements of the decoding center in presence of closed RF2 (blue, I) with the switch loop highlighted in pale yellow. (C) Interaction of ArfA (red) with elements of the decoding center in presence of open RF2 (blue, II) with the switch loop highlighted in pale yellow. (D) Superposition of RF2 in its closed (blue) and open conformation (cyan) in context of ArfA mediated rescue. Taken from (Demo et al., 2017b)

Lastly, James et al. created two additional SRCs, one with ArfA-A18T and RF2 and another one with ArfA but *T. thermophilus* rather than *E. coli* RF2 resulting in the closed conformation of RF2 bound to the ribosome that is similar to the compact conformation of RF2 in solution (James et al., 2016; Vestergaard et al., 2001). The observed closed conformation of RF2 in those two independent datasets as well as in the dataset of Demo et al. is nearly identical, revealing several interesting points (Demo et al., 2017b; James et al., 2016). In all of those structures, the N-terminus of ArfA as well as the switch loop of RF2 remained disordered, whereas the contacts between the β -strand of ArfA and β -strand β 4 of domain 2 of RF2 are already established (**Figure 13A+B**). Hence, the observed closed conformations might be a

pre-accommodated conformation of RF2 as proposed for canonical termination. Furthermore, decoding nucleotides A1492 and A1493 of h44 adopt a different conformation when compared to the open conformation of RF2 in complex with ArfA (**Figure 13B+C**). The nucleotides reside inside helix 44 and are sandwiched between A1913 of H69 and Pro23 of ArfA. In presence of the open conformation of RF2, however, A1493 flips out and allows A1913 of H69 to stack on A1492. This newly established interaction brings H69 closer to the SSU and thereby allows C1914 to stabilize the N-terminal domain of ArfA and coordinate its 180° turn to establish interactions with S12 (**Figure 13C**) (Demo et al., 2017b; Huter et al., 2017c; James et al., 2016; Ma et al., 2017; Zeng et al., 2017). The ArfA inactivating mutant A18T fails to stabilize the N-terminus but does not interfere with RF2 binding (James et al., 2016). Ala18 resides within the α -helix of ArfA but does neither interact with the ribosome nor RF2. Instead, the residue is in close proximity to Ile11 of ArfA that is located in the N-terminal part of ArfA that runs antiparallel to the α -helix, when stabilized. Hence, a polar Thr cannot pack against Ile11 and would interfere with the placement of the N-terminus of ArfA.

Positioning of the N-terminal domain of ArfA allows it to interact with elements of the switch loop (Demo et al., 2017b; Huter et al., 2017c; James et al., 2016; Ma et al., 2017; Zeng et al., 2017). Especially a hydrophobic patch formed by residues Leu19, Leu 24 and Phe25 of the α -helical part of ArfA interact with Trp319 of the switch loop, inducing an alternative conformation of the latter element (**Figure 13C**). This is in line with the observed closed conformation in presence of *T.thermophilus* RF2, as it has a distinct switch loop composition failing to interact with the hydrophobic patch (James et al., 2016). Thus, the α 7 of domain 3 of RF2 gets extended similar to the conformation during canonical termination. This leads to the positioning of domain 3 into the PTC (**Figure 13D**).

The five cryo-EM reconstructions also provide a structural basis on how ArfA is able to discriminate between RF1 and RF2 (Demo et al., 2017b; Huter et al., 2017c; James et al., 2016; Ma et al., 2017; Zeng et al., 2017). Comparing the sequence of RF1 and RF2 as well as aligning RF1 on to RF2 in complex with ArfA identifies several residues within the switch loop and domain 2 of RF1 that might interfere with the recruitment by ArfA. Especially the hydrophobic interface between by Ile16, Leu20 and Phe25 of Arfa and Val198, Phe217 and Phe 221 of β 5 element of RF2 would be disrupted as the latter amino acids would be substituted to Gly, Ala and Ala. As

previously mentioned this hydrophobic interface is important for the initial recruitment of RF2. This is in line with biochemical studies showing that RF1 cannot even bind to the ribosome in presence of ArfA.

An interesting question that is raised by the amount of cryo-EM reconstructions is the fact that Demo et al. could obtain the closed conformation of RF2 using wt RF2 and ArfA (Demo et al., 2017b). On the one hand, this indicates that the closed conformation might represent a *bona fide* intermediate state as it represents a major subpopulation within their reconstruction. On the other hand, four out of five groups were not able to detect this conformation, probably due to differences within the experimental set-up. Indeed, Demo et al. were the only group that used the FREALIGN software for processing the dataset, whereas the other groups used RELION or a FREALIGN/RELION combination (Demo et al., 2017b; Huter et al., 2017c; James et al., 2016; Ma et al., 2017; Zeng et al., 2017). However, differences between those two softwares cannot account for the fact that there was no trace of the closed conformation within four out of five reconstructions. Even more, classification of the dataset of Huter et al was performed with FREALIGN. Additionally, the percentage of particles analyzed after the initial 3D classification is comparable for Demo et al. and Huter et al, with approximately 60% of particles being further classified (Demo et al., 2017b; Huter et al., 2017c). The remaining 40% of particles were discarded as they either showed no relevant programming of ribosomes with respect to ArfA and RF2 or due to poor particle alignment. Furthermore, James et al used 82% of particles after initial 3D classification for further analysis (James et al., 2016). Thus, it seems unlikely that particles programmed with the closed conformation of RF2 were discarded during processing of the datasets. In this respect, the data of Ma et al. and Zeng et al could not be further analyzed as the sorting schemes lack the necessary details (Ma et al., 2017; Zeng et al., 2017).

Hence, additional factors might have contributed. One possibility is the different buffer conditions used for preparing the cryo-EM grids, as different concentrations of Mg^{2+} or other ions might have an effect. In this regard, it is interesting that Demo et al. used by far the highest $MgCl_2$ concentration (20 mM of $MgCl_2$). High Mg^{2+} concentrations result in more rigid ribosomes (Yamamoto et al., 2010). Thus, the rigid conformation of the ribosome might have led to a prolonged transition time from the closed to open conformation for RF2. Another interesting possibility is that only Huter et al. and Demo et al. used an N-terminal His₆-tag, whereas the other groups removed

the N-terminal tags during purification of the protein. The His-tag itself might have led to stabilization of the closed conformation in the case of Demo et al. but did not in the case of Huter et al, as they had an additional 3C-protease cleavage tag between the His-tag and the first amino acid of ArfA. A counter argument is the fact that there is no density for the N-terminal His-tag of ArfA in presence of closed RF2. It is important to mention, that both groups showed biochemically, that the purified proteins are active in rescuing 'non-stop' complexes. To summarize, there might be many reasons why the closed conformation was only observed by Demo et al. However, the high number of particles occupied with RF2 might not reflect a physiological situation and is most likely caused by the experimental set up changing the equilibrium between closed and open conformation. It would be interesting to further elucidate the reason behind that as it would provide a possible tool to visualize intermediate states that otherwise would be too transient for cryo-EM.

Another difference within the five different reconstructions was the length of the ArfA protein (Demo et al., 2017b; Huter et al., 2017c; James et al., 2016; Ma et al., 2017; Zeng et al., 2017). As described in the introduction, full length ArfA is 72 aa but aggregates *in vivo* due to its hydrophobic C-terminus. Moreover, it is mainly C-terminal truncated ArfA that is active on non-stop ribosomes *in vivo*. Hence, C-terminal truncated versions of ArfA were used, that either lacked 12 (60 aa length in total) or 17 aa (55 aa length in total). These truncated versions were also shown to be functional in previous biochemical investigations (Chadani et al., 2012; Kurita et al., 2014b). Interestingly, in every reconstruction only up to 48 aa could be modelled, indicating that the very C-terminal residues do not contribute to the functionality of ArfA (**Figure 13A**) (Demo et al., 2017b; Huter et al., 2017c; James et al., 2016; Ma et al., 2017; Zeng et al., 2017). In line with that is the poor sequence conservation of the very C-terminus (Kurita et al., 2014b).

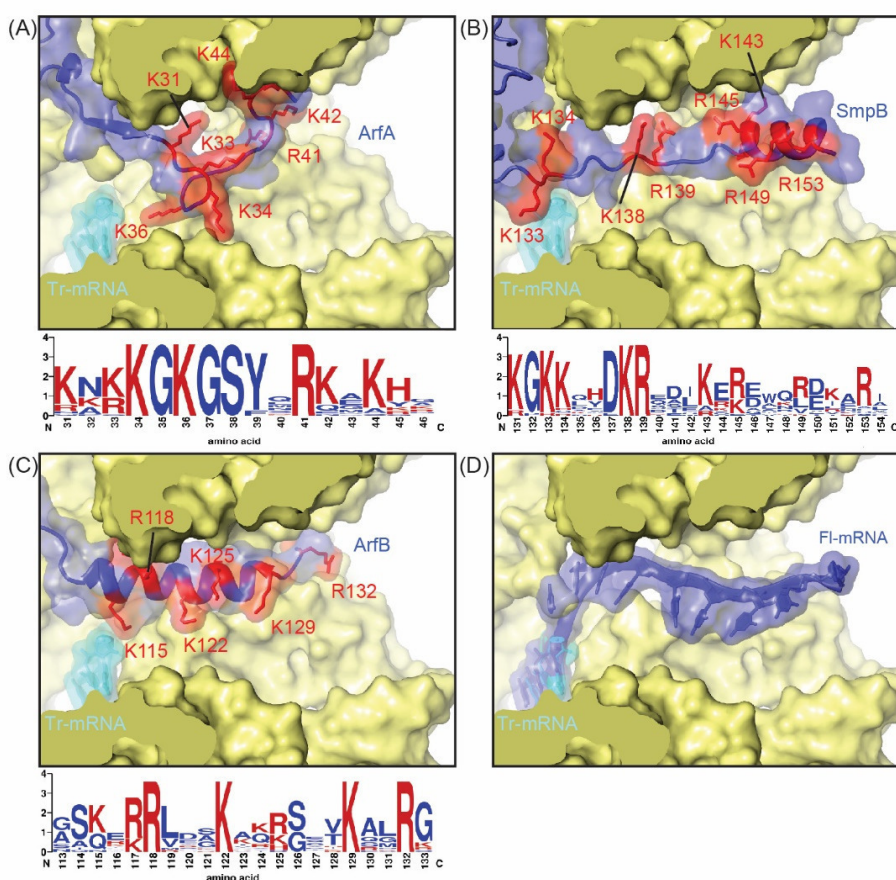


Figure 14. Monitoring of the vacant mRNA entry channel by the C-termini of ribosome rescue factors. (A) Probing of the mRNA entry channel by ArfA. (B) Probing of the mRNA entry channel by SmpB. (C) Probing of the mRNA entry channel by ArfB. (D) Superimposition of full-length mRNA on to the 70S-ArfA-RF2 ribosome. Positively charged residues are highlighted in red. Conservation of the respective C-terminus is represented as a Weblogo. Taken from (Huter et al., 2017b)

The visualization of the C-terminal domain of ArfA allows us to compare it with the C-termini of SmpB and ArfB (**Figure 14A-C**). Both of them, SmpB and ArfB, probe the mRNA entry channel by forming an α -helix (Gagnon et al., 2012; Neubauer et al., 2012). Like for ArfA, the respective C-terminal domains are enriched in conserved positively charged stretches that help to place the C-termini inside the mRNA channel (Huter et al., 2017b). The importance of these conserved stretches is underlined by mutational studies. In case of SmpB, triple alanine substitution within these positive stretches interfere with recycling activity, whereas it is tolerant towards single substitutions (Miller et al., 2011; Sundermeier et al., 2005). The C-terminal domain of ArfB is even more sensitive as the substitution of a single positively charged residue already abolishes its activity (Kogure et al., 2014). For the C-terminus of ArfA, the mutational studies are a bit unambiguous. While one group reports that single

mutations of positively charged residue to Cys (e.g R41C) does not interfere with its activity, other groups report a severe decrease in activity (Kurita et al., 2014b; Ma et al., 2017; Zeng et al., 2017). Furthermore, evidences for triple substitutions, like in the case of SmpB, are missing. However, it seems likely that such a mutation would interfere with the anchoring of the C-terminal tail of ArfA, as judged by the cryo-EM reconstructions.

In contrast to the C-termini of SmpB or ArfB that form helices and follow the predetermined path of the mRNA channel, the C-terminus of ArfA appears to rather block the tunnel and therefore is less tolerant towards 3' extended mRNAs (**Figure 14B-D**) (Huter et al., 2017b). In more detail, the C-terminal domain would overlap with the second or third nucleotide of the A-site codon (Demo et al., 2017b; Huter et al., 2017c; James et al., 2016; Ma et al., 2017; Zeng et al., 2017). Indeed, these structural observations are in agreement with biochemical data. The efficiency in ribosomal recycling by ArfA-RF2 decreases with extended mRNA by up to four residues into the A-site, with nearly no activity after six nucleotides (Shimizu, 2012; Zeng and Jin, 2016). By contrast, SmpB and ArfB are more tolerant towards extended 3' mRNAs (Asano et al., 2005; Ivanova et al., 2004; Kurita et al., 2014a; Shimizu, 2012). *In vitro* data showed that *trans*-translation and ArfB are active up to 9-15 nt. downstream from the P-site codon. The length dependency is less restricted *in vivo*, as pausing in the middle of mRNAs possibly induces nucleolytic cleavage that generates non-stop complexes (Janssen et al., 2013). Thus, combining the structural and biochemical data it seems likely that the C-termini of those rescue factors compete with the presence of mRNA in the mRNA entry channel. Accommodation of the C-terminus in the mRNA channel is essential for stable binding of the rescue complex. Notably, biochemical assays could show that ArfA and RF2 can bind to the ribosome regardless of the length of the 3'extension of the mRNA but remains inactive concerning recycling activity (Kurita et al., 2014b). It seems that the C-terminus in such a case fails to stably bind the mRNA channel and induce a favorable conformation.

Upon stabilization of the C-termini within the mRNA entry channel all of the three factors form contacts with the universally conserved nucleotides G530, A1492 and/or A1493 (Huter et al., 2017b). All three factors interact with G530 via interactions of Glu30 of ArfA, Arg118 of ArfB or His136 of SmpB. In contrast, the conformation of A1492 and A1493 differs depending on the rescue factor. In the presence of ArfA or SmpB, A1493 is flipped out of helix 44 and a stacking interaction between A1492 and

A1913 of the 23S rRNA can be established. Binding of ArfB on the other hand induces a conformation in which A1493 remains inside the helix and is sandwiched between Pro110 of ArfB and A1913. Mutations effecting decoding nucleotides (G530A, A1492G and A1493G) are lethal in the context of aa-tRNA accommodation but seem to be tolerated in the case of tmRNA recycling (Miller et al., 2011; Schrode et al., 2017). Such data is lacking for ArfA and ArfB. However, amino acid substitutions of residues that interact with decoding nucleotides (Pro23Cys, Glu30Cys for ArfA, Pro110Ala and Arg118Lys for ArfB) do not significantly impair their function (Kogure et al., 2014; Kurita et al., 2014b; Ma et al., 2017; Zeng et al., 2017). It is important to mention that mutation of His136Ala of SmpB reduces the rate of GTP hydrolysis by EF-Tu, but is not essential for peptidyl transfer (Kurita et al., 2014a; Miller and Buskirk, 2014). Therefore, it seems plausible that the decoding residues do not actively contribute to the positioning of the factors, but rather adopt conformations that do not interfere with the positioning of the rescue factors.

Taken together, the recently published cryo-EM structures on ArfA, as well as structural studies on ArfB and tmRNA/SmpB revealed molecular details on how those factors recognize a 'non-stop' ribosomal complex and mediate ribosome recycling (Huter et al., 2017b). All of those factors monitor the empty mRNA channel via their respective C-termini, thereby showing different degree of tolerance towards 3'extended mRNA. Accommodation of the C-termini induces conformational changes. In the case of SmpB this leads to the stabilization of the tmRNA/SmpB complex resulting in the positioning of the CCA end of tmRNA into the PTC. Hence, peptide bond formation between the peptidyl-tRNA and the Ala charged tmRNA in the A-site can occur. Translocation replaces the ORF of tmRNA with the aberrant mRNA and translation can continue until the ribosome encounters the stop codon on the MLD of mRNA, inducing canonical termination via class 1 release factors and subsequent recycling of subunits. The ORF provided by the MLD encodes for a degradation tag, which is recognized by specific proteases resulting in degradation of the faulty protein

ArfB, on the other hand, provides its own GGQ motif making it independent of class 1 release factors. Upon stabilization of the C-terminus, the N-terminus gets placed towards the PTC allowing the GGQ motif to mediate peptidyl-hydrolysis.

ArfA again utilizes a different approach to mediate rescue of non-stop complexes. Interaction of the C-terminus with the empty mRNA channel induces conformational changes within ArfA. Thereby, ArfA provides a platform for RF2

recruitment that permits RF2 to transit from a closed to an open conformation placing the catalytic important domain 3 towards the PTC.

Although the molecular mechanisms behind 'non-stop' mediated rescue is well understood, their distribution and interplay among species remains puzzling (Keiler and Feaga, 2014). While it is clear that *trans*-translation plays an essential role in nearly all bacteria, the interplay with ArfA and ArfB remains elusive. This is best exemplified in *Neisseria gonorrhoeae* (Huang et al., 2000). In this organisms *trans*-translation is essential despite the presence of ArfA. On the other hand, *N.gonorrhoeae* ArfA is able to compensate the $\Delta ssrA\Delta arfA$ double deletion in *E.coli* (Schaub et al., 2012). In contrast to that, ArfB is present in *E.coli* but can compensate the lethality of $\Delta ssrA\Delta ArfA$ only if overexpressed (Chadani et al., 2011a). In *Caulobacter crescentus*, however, chromosomally encoded ArfB is able to compensate the lack of tmRNA despite the absence of ArfA (Keiler and Feaga, 2014). It is hard to draw general conclusions as all findings are based on a limited set of examined species. Hence, it is impossible to explain, why sometimes ArfA can compensate for the loss of *trans*-translation *in vivo*, but not ArfB and *vice versa*. Last but not least, the deletion of *ssrA* in *Bacillus subtilis* is not lethal (Wiegert and Schumann, 2001). Although it is likely that yet unknown rescue factors compensate for the loss of tmRNA, there is no certainty. On the other hand it raises the question of yet undiscovered alternative rescue factors (Keiler and Feaga, 2014). Last but not least, these studies were all carried out under controlled laboratory conditions, which might favor the importance of one factor over the other. One needs a systematic approach, in different bacterial systems as well as under varying environmental conditions, to fully understand the interplay of these factors.

Finally, due to the importance of recycling of non-stop ribosomal complexes in bacteria, these factors would be preferable targets for antimicrobial agents. Moreover, eukaryotic cells utilize different pathways to deal with 'non-stop' complexes (Buskirk and Green, 2017). Indeed, agents that target *trans*-translation have already been discovered (Alumasa and Keiler, 2015; Macé et al., 2017; Ramadoss et al., 2013b). It is noteworthy to mention that the initially described inhibitor KKL-35 turned out to not specifically target *trans*-translation (Macé et al., 2017). On the other hand, it was demonstrated that antisense RNAs targeting the MLD of tmRNA or small proteins mimicking SmpB are an effective agent to silence *trans*-translation.

Nevertheless, as already mentioned above, the loss of one system can often be compensated by another one. Thus, such agents might be used as an adjuvant in combination with other antibiotics but not as a main therapy.

4.2 Structural insights into polyproline-mediated ribosome stalling and rescue by EF-P

Prolines harbor physical and chemical properties that interfere with peptide bond formation. This effect is most dramatic, when ribosomes encounter stretches of consecutive prolines, as it leads to arrest of translation *in vitro* (Doerfel et al., 2013; Ude et al., 2013). It was shown that EF-P is responsible for alleviating stalling on polyproline stretches, however, the mode of action of EF-P on unlocking these arrested ribosomes remained elusive. Biochemical studies could show that the activity of EF-P is dependent on the posttranslational modification of a conserved residue (Lys34 in *E. coli*) within the tip of the loop of domain 1 (Doerfel et al., 2013; Ude et al., 2013). In *E. coli*, this posttranslational modification system comprises the sequential action of three enzymes, namely EpmB, EpmA and EpmC, resulting in a ϵ (R)- β -lysyl-hydroxylysine modification at position Lys34 (Bailly and de Crécy-Lagard, 2010; Navarre et al., 2010; Peil et al., 2012; Yanagisawa et al., 2010).

On the basis of the structure of Blaha et al. using unmodified EF-P bound to the 70S ribosome it was suggested that the modification extends towards the PTC and is either directly involved in the catalysis or indirectly by stabilization of the peptidyl-tRNA (Blaha et al., 2009; Doerfel et al., 2015; Lassak et al., 2016). In the light of new biochemical insights and the absence of modified EF-P, interpretation of the structure is limited as it was based on the assumption that EF-P is an initiation factor. Thus, we sought to obtain high-resolution structures of polyproline-stalled ribosomes in absence and presence of modified EF-P using single particle cryo-EM. The study was complemented with molecular dynamics simulations to gain further insights into the mechanism of EF-P (Huter et al., 2017a). The applied strategies and the resulting observations and conclusions as well as an outlook will be given in the following sections

To elucidate the mechanism of polyproline induced stalling and the mode of action of EF-P to alleviate this arrest, we created RNCs based on a reporter mRNA coding for NlpD-PPP in the absence of EF-P. To enhance the efficiency of stalling we

introduced an Arg upstream of the PPP motif as was demonstrated by Starosta et al. (Starosta et al., 2014c). The resulting SRCs were subjected to cryo-EM in the absence (Dataset 1) or presence of EF-P (Dataset 2). *In silico* sorting of dataset 1 revealed two major subpopulations comprising 70S ribosomes that were either programmed with a peptidyl-tRNA^{Pro} in the P-site or a peptidyl-tRNA^{Pro} in the P-site and a Pro-tRNA^{Pro} in the A-site. Sorting of dataset 2 revealed 70S ribosomes that were either programmed with a peptidyl-tRNA^{Pro} or peptidyl-tRNA^{Pro} in the P-site, a Pro-tRNA^{Pro} in the A-site as well as EF-P being located in between the P and E-site of the ribosome, spanning both subunits.

By comparing both datasets, the following conclusions could be made. In the absence of EF-P, the density for the P-site tRNA was less uniform and strong as compared to the volume of dataset 2 containing A-tRNA, P-tRNA and EF-P. In more detail, while the density around the ASL of the P-tRNA was comparable to the density of the 30S, it progressively deteriorated towards the 50S. Furthermore, the CCA end was less resolved. This effect was even more pronounced in the case of the A-site tRNA in dataset 1, with no density for the CCA end even at low threshold. In line with the continuous decline of map quality for the tRNAs was the lack of a defined density for the nascent chain in absence of EF-P, which came as a surprise. So far, all cryo-EM structures of stalled ribosome nascent chain complexes (RNCs) showed clear density for the nascent chain (Ito and Chiba, 2013; Su et al., 2017; Wilson et al., 2016). Secondly, prolines are restrained in their conformational freedom and restrict the possible conformation of its neighboring residues, thus one should expect a defined density for the nascent chain (Morris et al., 1992). However, the lack of density in two independently processed volumes indicates that the nascent chain is flexible and therefore could not be resolved.

From the class containing EF-P, the following observations could be made. EF-P occupied the same position as was observed in the Tth 70S ribosome (Blaha et al., 2009). In this position, EF-P does stabilize the CCA end via its modification as well as the body of the peptidyl-tRNA as apparent by the uniform quality of density and local resolution calculations for the P-site tRNA. Furthermore, the quality for the density of A-site tRNA improved significantly. Consistent with this notion, the very N-terminus of L27 could be resolved, whereas density for the N-terminus of L27 was lacking in presence of A-site tRNA in dataset 1. This is indicative of a productive conformation of the PTC in the presence of EF-P (Polikanov et al., 2014; Voorhees et al., 2009b).

Additionally, although density for the nascent chain could be observed, it was rather fused to the A-site tRNA than the P-site tRNA. Hence, we concluded that the volume represents a post peptide bond formation state with a deacylated tRNA in the P-site and a peptidyl-tRNA in the A-site. Thus, no conclusions on the conformation of prolines in context of stalling could be made as the nascent chain was transferred.

However, comparing the two different SRCs revealed several interesting facts. First of all, in the absence of EF-P the nascent chain appears to be flexible and parts of the A-site tRNA that are close to the PTC remained disordered. Thus, one can conclude that polyproline stretches destabilize the peptidyl-tRNA and thereby indirectly prevent A-tRNA accommodation. Or in other words, the flexibility of the nascent chain interferes with proper alignment of substrates within the PTC. EF-P, on the other hand, stabilizes the peptidyl-tRNA and especially the CCA end via its modification resulting in a conformation of the PTC favorable for peptide bond formation.

Another interesting observation is the high proportion of empty ribosomes in both datasets (30% of particles in dataset 1, 19% of particles in dataset 2). This might have been a result of the purification procedure of the SRCs after elution from the Talon beads, however, no vacant 70S class could be detected in dataset 3 (will be described later), although the same procedure was applied to purify those SRCs. An alternative and highly speculative explanation is peptidyl-tRNA drop-off as a result of translational stalling. Peptidyl-tRNAs that carry short nascent peptides can dissociate from the ribosome (Cruz-Vera et al., 2004; Gonzalez de Valdivia and Isaksson, 2005), whereas peptidyl-tRNAs that carry more than five amino acids are stably associated with the ribosome (Ivanova et al., 2005). Although we use a template for our SRCs that causes stalling at position corresponding to the 72 aa of the ORF, the flexibility of the nascent chain as well as the resulting destabilization of the P-site tRNA and prolonged arrest might allow peptidyl-tRNA drop-off. This is in agreement with dataset 3, as the interaction of the stably bound peptidyl-tRNA and nascent chain hold the complex tightly together and thereby prevent drop-off (Ivanova et al., 2005). Thus, due to the absence of any cellular factors like tmRNA and the resulting prolonged arrest, peptidyl-tRNA drop-off might occur.

Nevertheless, as explained no conclusions on the conformation on prolines could be made due to flexibility of the nascent chain in absence and post-peptide bond state in the presence of EF-P. Furthermore, the resolution of the class containing EF-P in dataset 2 was not good enough to unambiguously model EF-P and its modification.

To further gain insights we created a third SRC based on a variant of the previously used NlpD template. In more detail, we truncated the ORF after the second proline of the triple proline motif. This resulted in ribosomes being programmed with the peptidyl-tRNA at the second proline, but additionally bearing a vacant A-site. Moreover, we bound the antibiotic evernimycin to the SRC which is known to bind to a site of the ribosomal A-site that would overlap with the elbow region of an A-site tRNA and hence would be an additional sterical hinderance for the presence of A-site tRNA (Arenz et al., 2016). By doing this we were able to eliminate the influence of the A-site tRNA allowing us to catch translation in a pre-peptide bond formation situation. Furthermore, the homogeneity of the sample was increased, enhancing the average resolution of reconstructions. It is important to mention, that this SRCs were created using the PURExpress *In Vitro* Protein Synthesis Kit (NEB) and not in the *E. coli* lysate based translation system as mentioned before. The lysate based translation system comprises rescue factors like tmRNA, ArfA and ArfB that would immediately recycle the 'non-stop' complex (Huter et al., 2017b).

In silico sorting revealed two major subpopulations being programmed with either P-site tRNA and EF-P or P-site tRNA and E-site tRNA. The obtained resolution allowed us to generate a molecular model of EF-P as well as of its modification. Based on this several critical residues could be identified.

For example, we observed a possible backbone interaction of Asp69 with residue U17a of the D-loop of tRNA^{Pro}. The presence of this additional residue within the D-loop is unique to the isomers of tRNA^{Pro} as well as tRNA^{fMet} but is lacking in all other tRNAs (Katoh et al., 2016). Additionally, it was shown to be an essential recognition element for EF-P. Notably, we do observe the same interaction in the *Tth*. EF-P ribosome structure of Blaha et al (Blaha et al., 2009). On the other hand, such an interaction cannot be established in the presence of other tRNAs as they lack this additional nucleotide. Remarkably, the extended D-loop structure of tRNA^{Pro} is a conserved feature among prokaryotic species indicating that recognition of the additional D-loop nucleotide by EF-P is a general mechanism (Katoh et al., 2016). Moreover, this interaction is similar to the interaction of EttA, an ABC-F protein that binds to 70SIC and thereby regulates the entry into translation elongation cycle in energy-depleted cells (Boël et al., 2014). Böel et al could show biochemically that Etta has specificity for tRNA^{fMet}. Additionally, low resolution cryo-EM reconstructions provide a structural evidence for the interaction of Etta with the extended conformation

of tRNA^{fMet} (Chen et al., 2014). Hence, D-loop recognition is a property shared by those two factors that bind in the ribosome E-site. It remains to be determined if other E-site associated ribosomal factors utilize similar recognition elements.

eIF5A on the other hand might not rely on such a recognition motif, as first of all, the tRNA^{Pro} isomers in eukaryotes do not have an extended D-loop and secondly, recent ribosome profiling data revealed a diverse range of stalling motifs, not restricted to polyprolines, that are alleviated by eIF5A (Pelechano and Alepuz, 2017; Schuller et al., 2017). Thus, it seems likely that eIF5A uses a more general mechanism to recognize stalled ribosomes. Indications for such a mechanism come from the study of Schmidt et al. using the elongation inhibitor cycloheximide to arrest cells (Schmidt et al., 2016). In the presence of this drug, the E-site tRNA cannot bind and allows eIF5A to bind (Buskirk and Green, 2017; Schmidt et al., 2016; Schneider-Poetsch et al., 2010). Indeed, as eIF5A and EF-P need to enter the ribosome through the E-site, dissociation of the E-site tRNA upon prolonged stalling might allow eIF5A to recognize arrested ribosomes. The same mechanism can be applied for EF-P. Nevertheless, EF-P might require additional recognition motifs as the speed of translation elongation is faster in bacteria than in eukaryotes and requires a more coordinated response.

Other important contacts can be found within domain 3 of EF-P that interacts with the SSU as well as the P-site tRNA. In particular, two conserved residues Tyr183 and Arg186 are interacting with A42 of the P-site tRNA as well as G1338 of the 16S rRNA. Interestingly, G1338 and A1339 are part of an interaction network that interacts with the ASL, including residue A42 of the P-site tRNA and thereby stabilizing the tRNA and prevent movement into the E-site (Abdi and Fredrick, 2005; Blaha et al., 2009; Selmer et al., 2006). On the other hand, it was suggested that interactions between the ASL and this part of the 16S rRNA need to be disrupted during translocation, probably by movements of the head (Dunkle et al., 2011; Selmer et al., 2006). Hence, we generated two variants of modified EF-P bearing the substitution of Tyr183Ala or Arg186Ala. Indeed, translation of a firefly luciferase (Fluc) reporter mRNA bearing a triple proline motif in presence of those mutants showed no activity. This suggests that those two residues are critical for the activity of EF-P. However, based on the limitation of this assay, we cannot address if the inactivity is due to the loss of stabilization of the P-site tRNA or might result from other events for example like translocation.

Furthermore, we observed contacts of loop 1 of domain 3 of EF-P with the E-site codon of the mRNA as well as ribosomal protein S7, which is in clear contrast to

the previously determined *Tth*. EF-P-ribosome structure, where the loop was disordered (Blaha et al., 2009). Especially highly conserved residues Gly144, Asp145 and Thr146 (GDT motif) form backbone interactions with the E-site codon and Arg78 of S7. In this conformation of the loop, S7 shifts about 7 Å towards the E-site codon, when compared to the volume of dataset 2 without EF-P but is essentially the same in the presence of E-site tRNA (from dataset 3). Based on our structural insights we designed various mutants addressing the role of loop 1 of domain 3 and concluded that the loop might be able to recognize proline codons (CCX). We rationalized this assumption as the *Tth* EF-P ribosome complex was programmed with a short mRNA displaying an AAA codon in the E-site and thus failed to interact with loop 1 as the AAA codon would sterically overlap with the path of our modeled loop 1. The same scenario would be true for a GGG codon when occupying the E-site. On the other hand, CUG (leucine codon) and CCG (proline codon) would not interfere with the position of loop 1 and the difference between these two codons would be the presence of an additional interaction of the side chain of Asp₁₄₅ with the second nucleotide of the E-site codon (**Figure 15A+B**). In contrast to that, eIF5A lacks domain 3 and its function is not limited to proline stalled ribosomes as revealed by ribosomal profiling (Pelechano and Alepuz, 2017; Schuller et al., 2017). We concluded that loop 1 might recognize the nature of the codon and together with the D-loop interaction cause specificity for proline stalled ribosomes.

Retrospectively seen, there might be an alternative explanation for the absence of loop 1 within the *Tth* EF-P ribosome structure. Jenner et al. compared the conformation of the E-site of the 30S in 70SIC as well as for elongating ribosomes (Jenner et al., 2007, 2010). Based on their observation, 70SIC programmed with mRNAs containing a SD-sequence are in a rather 'tense' conformation, which makes the E-site codon less favorable for codon-anticodon interactions. This is most likely due to the close proximity of the SD-anti-SD helix to the E-site codon. Additionally it makes sense from a biological point of view as an initiation complex does not have an E-site tRNA. However, the mRNA in an elongating complex is in a relaxed conformation due to the increased distance of the E-site codon and SD-sequence. Therefore, the disordered loop 1 as observed in the crystal structure of *Tth* EF-P ribosome complex might be a result of the tense conformation of the mRNA rather than the presence of the AAA codon.

In our experiments it was shown that despite the high degree of conservation of the GDT motif substitution to ${}_{144}\text{AAA}_{146}$ failed to dramatically reduce the activity of EF-P, probably due to the nature of mainly backbone interactions. Hence, it seems unlikely that the nature of the codon in the E-site is critical for the rescue activity on polyproline stalled ribosomes. It might be that GDT is an optimal amino acid sequence because it facilitates an active backbone architecture of loop 1. Thus, the importance of loop 1 might not directly correlate with specific recognition of the E-site codon.

Binding of loop 1 induces structural rearrangements within the 30S E-site that are comparable to the structural rearrangements in presence of E-site tRNA, for example the placement of the tip of S7 towards the E-site codon (**Figure 15C**) (Jenner et al., 2007; Yusupova et al., 2006). Indeed, mimicking the role of the E-site tRNA on the 30S might have an important physiological role. For example it was shown that truncations within the region of S7 ($\Delta\text{Arg77-Tyr84}$) that are normally contacting the E-site codon as well as the E-site tRNA stimulate -1 and +1 frameshifting (Devaraj et al., 2009; Márquez et al., 2004). It was suggested that these mutations increase the dissociation of E-site tRNA and thereby increase the possibility of having an unoccupied A and E-site at the same time, resulting in a single codon/anticodon interaction to hold the register of the mRNA. Alternatively, these mutations destabilize the E-site codon and thereby prevent interaction of the ASL of E-site tRNA with the codon.

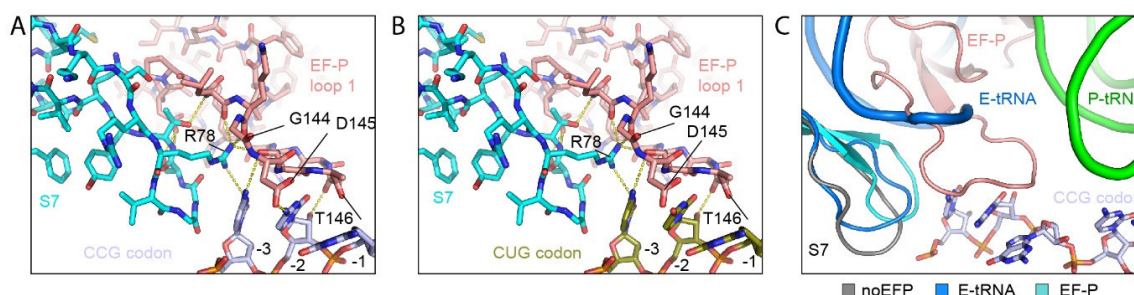


Figure 15. Interaction of loop 1 of domain 3 of EF-P with the E-site codon. (A) Interaction between loop 1 of domain 3 of EF-P (salmon) with a proline codon in the E-site (light blue) and S7 (cyan). **(B)** Interaction between loop 1 of domain 3 of EF-P with a leucine codon (beige) in the E-site and S7. Interaction of the GDT motif with CUG lacks the side chain interaction of D145 with the -2 nucleotide of the E-site codon. **(C)** Comparison of the 30S E-site in presence of EF-P (salmon) and E-site tRNA based on the model of dataset 3. Binding of any ligand to the 30S E-site involves a movement of the tip of S7 (cyan, EF-P; blue, E-site tRNA (PDB:4V8U), grey, no EF-P) towards the E-site codon.

From the point of our structure, these deletions, especially of residue Arg78 would abolish the interaction network between S7, the E-site codon and the loop 1 of EF-P (**Figure 15**). Thus, one can envision that the lack of loop 1 of EF-P has the same effect. In line with that is the recent finding that the presence of EF-P suppresses frameshifting in a situation where a proline codon (CCC-C) is located at the P-site, adjacent to the start codon in the E-site (Gamper et al., 2015). Dependent on the incoming aa in the A-site, this might lead to a prolonged stalling time relative to peptide bond formation, allowing the mRNA to shift out of register upon elimination of EF-P. Based on our structure one can assume that EF-P inherits the same function on ribosomes that are arrested in the middle of an ORF. Thus, prolonged stalling and the resulting dissociation of the E-site tRNA destabilizes the arrested ribosome. EF-P recognizes those stalled complexes and through interactions of its loop 1 with the E-site codon contributes additional energy to prevent frameshifting. eIF5A, on the other hand, does lack domain 3. It remains to be determined if eukaryotes have a compensatory mechanism.

The obtained high-resolution structure allowed us to model the ϵ (R)- β -lysyl-hydroxylysine modification at position Lys34 of domain 1. The (R)-lysyl moiety forms several contacts with the backbone of the CCA-end especially with the backbone of A76 and 2'OH of the ribose of C75 but is also in hydrogen bond distance to the conserved nucleotide A2439 of the 23S rRNA. Last but not least, the hydroxyl group at position Lys34 that is added by the enzyme EpmC interacts with the 2'OH group of C74. Nevertheless, this interaction does not seem to be critical for the alleviation of polyproline-stalled ribosomes. However, such a modification might be able to enhance the stability or solubility of a protein. These interactions are in contrast to the previously observed interaction of *Tth* EF-P, which lacks the modification and hence is unable to contact the CCA-end (Blaha et al., 2009). On the other hand, the hypusine modification of yeast eIF5A seems to utilize similar interactions to contact the CCA-end of the peptidyl-tRNA as well as residue A2808, the eukaryotic counterpart of A2439 (Melnikov et al., 2016a; Schmidt et al., 2016).

As mentioned in the introduction, the modification ϵ (R)- β -lysyl-hydroxylysine is found within a small subset of bacteria as judged by the presence of the corresponding modification enzymes (Lassak et al., 2016; Rajkovic and Ibba, 2017). We know of other modifications like rhamnosylation of an Arg32 that is the equivalent position to Lys34 in bacteria like *Pseudomonas aeruginosa* and *Neisseria meningitidis* (Lassak et al.,

2015b). In contrast to that, *B. subtilis* has a 5-aminopentanol moiety attached to Lys32 of EF-P (Rajkovic et al., 2016). Like for $\epsilon(R)$ - β -lysyl-hydroxylysine, these modifications were shown to be essential for alleviating polyproline-arrested ribosomes.

By contacting the CCA end of the peptidyl-tRNA, the modification seems to indirectly stabilize the nascent chain as judged by the presence of density for the nascent chain within the ribosomal exit tunnel. However, density for the nascent chain still appeared flexible as evident from local resolution calculations. Nevertheless, it allowed us to place a model the four C-terminal residues. Surprisingly, we observed a conformation of the diprolyl moiety that is distinct to the favored *all-trans* conformation deviating in its Phi angle by roughly 30°. It is noteworthy to mention that the estimates dihedral angles within this structure are rough estimations as the resolution is too limiting within this region. This diprolyl-positioning was unexpected as proline-proline bonds lack the rotatory freedom around the Psi and Phi angle (Morris et al., 1992). However, this deviation in the conformation seems to be necessary, as evident by comparing our conformation of the diprolyl moiety with the one observed in the crystal structure of Melnikov et al (Melnikov et al., 2016b). On the basis of their modelled *all-trans* diprolyl conformation, the N-terminus would be orientated towards the tunnel wall, thus directing the upstream amino acid into it, whereas in our structure the N-terminus is directed towards the lumen of the tunnel, following the path of other stalled nascent chains. Indeed, an *in silico* modelled triprolyl peptide in the *all-trans* conformation (also known as a *trans*-polyproline helix or P_{II}-helix) attached to the P-site tRNA would not be possible in the context of the ribosomal tunnel as it would direct the most N-terminal Pro into the tunnel wall. Similar to that, an *all-cis* conformation (also known as a *cis*-polyproline helix or P_I-helix) would interfere with ribosomal translation as it would interfere with the position of the A-site tRNA. The observed flexibility of the nascent chain in the absence of EF-P might be due to the prolyl moiety trying to adopt its favored configuration, which is prevented by the peptide passage, leading to destabilization of the peptidyl-tRNA. On the other hand, stabilization by EF-P and its modification forces the prolyl moiety to adopt an alternative conformation that is compatible with the path of the tunnel.

These observations raise several interesting questions. First of all, the favored *all-trans* conformation is not possible in the heart of the PTC. However, P_{II}-helix are one of the most abundant secondary structure elements beside α -helices and β -sheets (Chebrek et al., 2014; Saha and Shamala, 2012). Moreover, prolines can also adopt a

cis-conformation as evident by the presence of peptidylprolyl isomerase enzymes present in prokaryotes and eukaryotes (Fischer et al., 1984; Lu et al., 2007; Yaron et al., 1993). Our results counter argue against a mechanism suggesting that these parameters are already adopted during peptide bond formation. Furthermore, there are genes like AmiB that have eight consecutive prolines which are efficiently synthesized in presence of EF-P (Doerfel et al., 2013; Ude et al., 2013). Even though it was shown that α -helices can form inside the ribosomal tunnel, it is unlikely that a conformational rigid polyproline helix can be passed through the ribosomal tunnel without interfering with peptide bond formation.

Secondly, as stated in the introduction, prolines also restrain the conformation of their neighboring residues. Although we lack the resolution for placing side chains for the amino acids following the PP sequence, it seems likely that the presence of unfavorable residues immediately upstream of the proline moiety further restrict the rotatory and conformational freedom. Based on the chemical and physical properties of amino acids, there appears to be no shared attributes between the groups of amino acids that cause strong stalling. Unfortunately, our reconstructions also do not allow us to make conclusions as to why some amino acids in the A-site enhance stalling whereas others do not.

There are known arrest peptides that have a proline codon either at the P-site codon (TnaC) or A-site codon (SecM) (Gong and Yanofsky, 2002; Ito et al., 2010; Nakatogawa and Ito, 2002). It was shown that stalling within these peptides critically rely on the presence of prolines, but as well as on the residue located further upstream of proline. Nevertheless, those stalling events cannot be alleviated by EF-P as the upstream residues interact with the ribosomal tunnel and provide enough energy to block peptidyl-transfer or peptide release and thereby overcome the effect of EF-P (Buskirk and Green, 2017). Furthermore, they are also resistant to tagging by *trans*-translation as well as rescue by ArfA and ArfB (Cruz-Vera et al., 2005; Garza-Sánchez et al., 2006). A possible explanation for the resistance of those leader peptides is that they all stall with a ligand in a non-reactive state in the A-site. In the case of SecM this would be Pro-tRNA^{Pro}, whereas TnaC would have RF2 bound (Bhushan et al., 2011; Bischoff et al., 2014).

Finally, it needs to be determined at which time point EF-P leaves the ribosome. As described, the modification contacts the backbone of the CCA end of the deacylated P-tRNA after peptide bond formation. This position would interfere with early

movements during translocation when the acceptor arm has to move from the P- to the E-site in respect to the 50S (Blanchard et al., 2004). It seems likely that EF-P leaves the ribosome during the onset of the rotation of platform in parallel with opening of the L1 stalk.

In many cases, the activity of EF-P is dependent on its posttranslational modification. However, given the fact that so far in only 35% of bacterial genomes the posttranslational modification systems have been identified, it is conceivable that some bacteria might lack such systems. Especially genomes that comprise a small number of polyproline coding genes might not depend on these modifications (Starosta et al., 2014b). One example is *Lactobacillus jensenii* that has only one polyproline coding gene (Rajkovic and Ibba, 2017). Deletion of EF-P in such small genomes cause a more pronounced phenotype as deletion of modification systems for EF-P in other bacteria. This indicates that unmodified EF-P has some residual capacity of alleviating polyproline stalled ribosomes *in vivo*, as was also shown by Doerfel et al *in vitro* (Doerfel et al., 2013; Lassak et al., 2015b). In the light of our results, it might be that the stabilization effect of EF-P on the peptidyl-tRNA body might be enough to overcome the arrest. Another strategy for such organisms might be to prevent unfavorable residues that are upstream or downstream of the proline induced stalling site. Indeed, such a selection against strong staller might explain that the loss of EF-P is not lethal in many bacteria such as *E. coli*, *B. subtilis* or *Shewanella oneidensis* (Baba et al., 2006; Lassak et al., 2015b; Ohashi et al., 2003). On the other hand, the loss of EF-P is lethal in organisms like *Mycobacterium tuberculosis* (Sasseti et al., 2003). Comparison between the genome of *E. coli* and *M. tuberculosis* reveals that although both genomes have comparable numbers of coding sequences, *M. tuberculosis* has approximately 420 proteins with a proline stalling sequence whereas *E. coli* only has 100 proteins (Lassak et al., 2016; Sasseti et al., 2003; Starosta et al., 2014b). In line with that is the lethal effect of the deletion of eIF5A in eukaryotes, as those genomes contain more than 10% of polyproline containing genes (Ude et al., 2013; Wöhl et al., 1993). On the other hand, the dependency on EF-P and especially modified EF-P might also be influenced by the importance of certain polyproline containing genes under stress conditions.

Examples of such genes that depend on functional EF-P are the transcriptional activator CadC, the short ORF *mgtP* that is part of the *mgtCBR* leader RNA or the *vaIs* gene as described in the introduction (Nam et al., 2016; Starosta et al., 2014b; Ude et

al., 2013). Both of these genes contain stretches of consecutive prolines and regulate the expression of downstream genes in response to stress conditions. For example, activation of CadC requires two stimuli, exogenous lysine and mild acidic conditions to induce the downstream operon *cadBA*, that codes for proteins helping to maintain the intracellular pH (Ude et al., 2013). Removal of the polyproline cluster in CadC makes translation independent of EF-P, thereby increasing the copy number of CadC protein and thus leading to a dysregulation of the *cadBA* operon.

Consecutive proline codons at *mgtP* are critical for the downstream ORF of *mgtC* (Nam et al., 2016). In the absence of EF-P, ribosomes stall at the polyproline motif, thereby uncoupling transcription from translation. Hence, an alternative stem-loop is formed that allows induction of the *mgtC* coding region. Substitution of the consecutive prolines to glycine inhibits expression of *mgtC*.

Given the abundance of ORFs encoding polyproline sequences it is likely that regulation of the expression of EF-P is a *bona fide* regulatory mechanism within cells. However, direct evidence for the regulation of expression of EF-P is lacking. An alternative mechanism to regulate the expression of ORFs encoding consecutive prolines might be through regulation of the modification enzymes or by limiting or increasing the amounts of substrates that are needed for the respective modification. For example, the modification enzyme EpmA is also able to α -lysinylate EF-P, which causes an inactive form of EF-P (Gilreath et al., 2011; Roy et al., 2011). Thus, downregulation of EpmB would decrease the pool of available β -lysine and increase the probability of α -lysinylated EF-P. Moreover, modification enzymes might compete with other cellular processes for substrates. Rhamnosylation requires dTDP-L-rhamnose, which is a substrate for different cellular processes like production of rhamnolipids or glycosylated flagellin (Lassak et al., 2015b; Rajkovic and Ibba, 2017). Hence, competition with other enzymes might be a part of regulating the modification pathway. Another possibility arises from recent studies in *B. subtilis*. Briefly, in *B. subtilis* the modification enzyme *ymfl* reduces 5-aminopentanone to 5-aminopentanol in the final step of EF-P modification (Hummels et al., 2017; Witzky et al., 2018). It was shown that deletion of *ymfl* results in the same phenotype as the deletion of *efp*, whereas modified EF-P and EF-P with the amino acids substitution (Lys32Arg) and hence unmodified EF-P, suppressed the phenotype. It is possible that such intermediate modification alter the activity of EF-P. However, it is not clear in how far such intermediate states are stable and relevant under physiological conditions.

A recent report by Alejo et al expands the range of applications for EF-P (Alejo and Blanchard, 2017). Based on pre-steady-state smFRET imaging, it was shown that EF-P was able to rescue translocation defects that derived from mismatched peptidyl-tRNA anticodon/mRNA codon interactions. In more detail, during translocation of mismatched peptidyl-tRNAs from the A- to the P-site, the translocation process arrests at a stage before translocation is complete but after the dissociation of the deacylated tRNA from the E-site. This would represent a state where the head domain of the SSU displays a swivel-like motion of 18-20°, whereas the body of the SSU shows a partial rotation of 2-4° (Borg et al., 2015; Ramrath et al., 2013; Zhou et al., 2013). The P-site tRNA resides in an ap/P state. As discussed above, prolonged pausing and a free E-site allows EF-P to bind. Given the fact that the translocation defect arises from a mismatched anticodon/codon base pairing and the beneficial effect of EF-P to alleviate this arrest, an interaction between domain 3 and the ASL of the P-site tRNA is likely. Especially residues Tyr183 and Arg186 of EF-P might play a critical role, as they contact the ASL and the 16S rRNA in our structure. Thus, it is likely that EF-P establishes similar contacts with the P-site tRNA as judged by alignments of our 70S-EF-P structure compared to the 70S-fusidic acid-EF-G structure of Ramrath et al. (Ramrath et al., 2013).

5 References

- Abdi, N.M., and Fredrick, K. (2005). Contribution of 16S rRNA nucleotides forming the 30S subunit A and P sites to translation in *Escherichia coli*. *RNA* *11*, 1624–1632.
- Abo, T., Ueda, K., Sunohara, T., Ogawa, K., and Aiba, H. (2002). SsrA-mediated protein tagging in the presence of miscoding drugs and its physiological role in *Escherichia coli*. *Genes Cells* *7*, 629–638.
- Adio, S., Sharma, H., Senyushkina, T., Karki, P., Maracci, C., Holtkamp, W., Peske, F., and Rodnina, M. V. (2018). Dynamics of ribosomes and release factors during translation termination in *E. coli*. *bioRxiv* 243485.
- Agirrezabala, X., Lei, J., Brunelle, J.L., Ortiz-Meoz, R.F., Green, R., and Frank, J. (2008). Visualization of the hybrid state of tRNA binding promoted by spontaneous ratcheting of the ribosome. *Mol. Cell* *32*, 190–197.
- Agrawal, R.K., Sharma, M.R., Kiel, M.C., Hirokawa, G., Booth, T.M., Spahn, C.M.T., Grassucci, R.A., Kaji, A., and Frank, J. (2004). Visualization of ribosome-recycling factor on the *Escherichia coli* 70S ribosome: functional implications. *Proc. Natl. Acad. Sci. U. S. A.* *101*, 8900–8905.
- Akabane, S., Ueda, T., Nierhaus, K.H., and Takeuchi, N. (2014). Ribosome Rescue and Translation Termination at Non-Standard Stop Codons by ICT1 in Mammalian Mitochondria. *PLoS Genet.* *10*, e1004616.
- Alejo, J.L., and Blanchard, S.C. (2017). Miscoding-induced stalling of substrate translocation on the bacterial ribosome. *Proc. Natl. Acad. Sci.* *114*, 201707539.
- Allen, G.S., Zavialov, A., Gursky, R., Ehrenberg, M., and Frank, J. (2005). The Cryo-EM Structure of a Translation Initiation Complex from *Escherichia coli*. *Cell* *121*, 703–712.
- Allert, M., Cox, J.C., and Hellinga, H.W. (2010). Multifactorial Determinants of Protein Expression in Prokaryotic Open Reading Frames. *J. Mol. Biol.* *402*, 905–918.
- Alumasa, J.N., and Keiler, K.C. (2015). Clicking on trans-translation drug targets. *Front. Microbiol.* *6*, 498.
- Antoun, A., Pavlov, M.Y., Lovmar, M., and Ehrenberg, M. (2006). How Initiation Factors Maximize the Accuracy of tRNA Selection in Initiation of Bacterial Protein Synthesis. *Mol. Cell* *23*, 183–193.
- Aoki, H., Xu, J., Emili, A., Chosay, J.G., Golshani, A., and Ganoza, M.C. (2008). Interactions of elongation factor EF-P with the *Escherichia coli* ribosome. *FEBS J.* *275*, 671–681.
- Aqvist, J., Lind, C., Sund, J., and Wallin, G. (2012). Bridging the gap between ribosome structure and biochemistry by mechanistic computations. *Curr. Opin. Struct. Biol.* *22*, 815–823.
- Arenz, S., Nguyen, F., Beckmann, R., and Wilson, D.N. (2015). Cryo-EM structure of the tetracycline resistance protein TetM in complex with a translating ribosome at 3.9-Å resolution. *Proc. Natl. Acad. Sci. U. S. A.* *112*, 5401–5406.
- Arenz, S., Juette, M.F., Graf, M., Nguyen, F., Huter, P., Polikanov, Y.S., Blanchard, S.C., and Wilson, D.N. (2016). Structures of the orthosomycin antibiotics avilamycin and evernimicin in complex with the bacterial 70S ribosome. *Proc. Natl. Acad. Sci. U. S. A.* *113*.

- Asano, K., Kurita, D., Takada, K., Konno, T., Muto, A., and Himeno, H. (2005). Competition between trans-translation and termination or elongation of translation. *Nucleic Acids Res.* **33**, 5544–5552.
- Baba, T., Ara, T., Hasegawa, M., Takai, Y., Okumura, Y., Baba, M., Datsenko, K.A., Tomita, M., Wanner, B.L., and Mori, H. (2006). Construction of *Escherichia coli* K-12 in-frame, single-gene knockout mutants: the Keio collection. *Mol. Syst. Biol.* **2**.
- Bailly, M., and de Crécy-Lagard, V. (2010). Predicting the pathway involved in post-translational modification of Elongation factor P in a subset of bacterial species. *Biol. Direct* **5**, 3.
- Ban, N., Nissen, P., Hansen, J., Moore, P.B., and Steitz, T.A. (2000). The complete atomic structure of the large ribosomal subunit at 2.4 Å resolution. *Science* **289**, 905–920.
- Barat, C., Datta, P.P., Raj, V.S., Sharma, M.R., Kaji, H., Kaji, A., and Agrawal, R.K. (2007). Progression of the ribosome recycling factor through the ribosome dissociates the two ribosomal subunits. *Mol. Cell* **27**, 250–261.
- Belardinelli, R., Sharma, H., Peske, F., Wintermeyer, W., and Rodnina, M. V. (2016). Translocation as continuous movement through the ribosome. *RNA Biol.* **13**, 1197–1203.
- Belitsina, N. V., Glukhova, M.A., and Spirin, A.S. (1975). Translocation in ribosomes by attachment-detachment of elongation factor G without GTP cleavage: evidence from a column-bound ribosome system. *FEBS Lett.* **54**, 35–38.
- Belitsina, N. V., Tnalina, G.Z., and Spirin, A.S. (1981). Template-free ribosomal synthesis of polylysine from lysyl-tRNA. *FEBS Lett.* **131**, 289–292.
- Belova, L., Tenson, T., Xiong, L., McNicholas, P.M., and Mankin, A.S. (2001). A novel site of antibiotic action in the ribosome: interaction of evernimicin with the large ribosomal subunit. *Proc. Natl. Acad. Sci. U. S. A.* **98**, 3726–3731.
- Beringer, M., Bruell, C., Xiong, L., Pfister, P., Bieling, P., Katunin, V.I., Mankin, A.S., Böttger, E.C., and Rodnina, M. V. (2005). Essential Mechanisms in the Catalysis of Peptide Bond Formation on the Ribosome. *J. Biol. Chem.* **280**, 36065–36072.
- Bhushan, S., Hoffmann, T., Seidelt, B., Frauenfeld, J., Mielke, T., Berninghausen, O., Wilson, D.N., and Beckmann, R. (2011). SecM-stalled ribosomes adopt an altered geometry at the peptidyl transferase center. *PLoS Biol.* **9**, e1000581.
- Bilgin, N., Claesens, F., Pahverk, H., and Ehrenberg, M. (1992). Kinetic properties of *Escherichia coli* ribosomes with altered forms of S12. *J. Mol. Biol.* **224**, 1011–1027.
- Bischoff, L., Berninghausen, O., and Beckmann, R. (2014). Molecular basis for the ribosome functioning as an L-tryptophan sensor. *Cell Rep.* **9**, 469–475.
- Blaha, G., Stanley, R.E., and Steitz, T.A. (2009). Formation of the first peptide bond: the structure of EF-P bound to the 70S ribosome. *Science* **325**, 966–970.
- Blanchard, S.C., Kim, H.D., Gonzalez, R.L., Puglisi, J.D., and Chu, S. (2004). tRNA dynamics on the ribosome during translation. *Proc. Natl. Acad. Sci.* **101**, 12893–12898.
- Bock, L. V., Blau, C., Schröder, G.F., Davydov, I.I., Fischer, N., Stark, H., Rodnina, M. V., Vaiana, A.C., and Grubmüller, H. (2013). Energy barriers and driving forces in tRNA translocation through the ribosome. *Nat. Struct. Mol. Biol.* **20**, 1390–1396.

References

- Boël, G., Smith, P.C., Ning, W., Englander, M.T., Chen, B., Hashem, Y., Testa, A.J., Fischer, J.J., Wieden, H.-J., Frank, J., et al. (2014). The ABC-F protein EttA gates ribosome entry into the translation elongation cycle. *Nat. Struct. Mol. Biol.* *21*, 143–151.
- Boelens, R., and Gualerzi, C.O. (2002). Structure and function of bacterial initiation factors. *Curr. Protein Pept. Sci.* *3*, 107–119.
- Boni, I. V., Isaeva, D.M., Musychenko, M.L., and Tzareva, N. V (1991). Ribosome-messenger recognition: mRNA target sites for ribosomal protein S1. *Nucleic Acids Res.* *19*, 155–162.
- Borg, A., Holm, M., Shiroyama, I., Hauryliuk, V., Pavlov, M., Sanyal, S., and Ehrenberg, M. (2015). Fusidic acid targets elongation factor G in several stages of translocation on the bacterial ribosome. *J. Biol. Chem.* *290*, 3440–3454.
- Borg, A., Pavlov, M., and Ehrenberg, M. (2016). Complete kinetic mechanism for recycling of the bacterial ribosome. *RNA* *22*, 10–21.
- Brilot, A.F., Korostelev, A.A., Ermolenko, D.N., and Grigorieff, N. (2013). Structure of the ribosome with elongation factor G trapped in the pretranslocation state. *Proc. Natl. Acad. Sci. U. S. A.* *110*, 20994–20999.
- Brink, M.F., Brink, G., Verbeet, M.P., and de Boer, H.A. (1994). Spectinomycin interacts specifically with the residues G1064 and C1192 in 16S rRNA, thereby potentially freezing this molecule into an inactive conformation. *Nucleic Acids Res.* *22*, 325–331.
- Brunel, R., and Charpentier, X. (2016). Trans-translation is essential in the human pathogen *Legionella pneumophila*. *Sci. Rep.* *6*, 37935.
- Bullwinkle, T.J., and Ibba, M. (2016). Translation quality control is critical for bacterial responses to amino acid stress. *Proc. Natl. Acad. Sci.* *113*, 2252–2257.
- Buskirk, A.R., and Green, R. (2017). Ribosome pausing, arrest and rescue in bacteria and eukaryotes. *Philos. Trans. R. Soc. Lond. B. Biol. Sci.* *372*, 20160183.
- Buttgereit, F., and Brand, M.D. (1995). A hierarchy of ATP-consuming processes in mammalian cells. *Biochem. J.* *312 (Pt 1)*, 163–167.
- Buzzetti, F., Eisenberg, F., Grant, H.N., Keller-Schierlein, W., Voser, W., and Zähler, H. (1968). Avilamycin. *Experientia* *24*, 320–323.
- Caban, K., Pavlov, M., Ehrenberg, M., and Gonzalez, R.L. (2017). A conformational switch in initiation factor 2 controls the fidelity of translation initiation in bacteria. *Nat. Commun.* *8*, 1475.
- Calogero, R.A., Pon, C.L., Canonaco, M.A., and Gualerzi, C.O. (1988). Selection of the mRNA translation initiation region by *Escherichia coli* ribosomes. *Proc. Natl. Acad. Sci. U. S. A.* *85*, 6427–6431.
- Canonaco, M.A., Gualerzi, C.O., and Pon, C.L. (1989). Alternative occupancy of a dual ribosomal binding site by mRNA affected by translation initiation factors. *Eur. J. Biochem.* *182*, 501–506.
- Carter, A.P., Clemons, W.M., Brodersen, D.E., Morgan-Warren, R.J., Hartsch, T., Wimberly, B.T., and Ramakrishnan, V. (2001). Crystal structure of an initiation factor bound to the 30S ribosomal subunit. *Science* *291*, 498–501.
- Chadani, Y., Ono, K., Ozawa, S., Takahashi, Y., Takai, K., Nanamiya, H., Tozawa, Y., Kutsukake, K., and Abo, T. (2010). Ribosome rescue by *Escherichia coli* ArfA (YhdL) in the absence of trans-translation system. *Mol. Microbiol.* *78*, 796–808.

- Chadani, Y., Ono, K., Kutsukake, K., and Abo, T. (2011a). *Escherichia coli* YaeJ protein mediates a novel ribosome-rescue pathway distinct from SsrA- and ArfA-mediated pathways. *Mol. Microbiol.* *80*, 772–785.
- Chadani, Y., Ono, K., Kutsukake, K., and Abo, T. (2011b). *Escherichia coli* YaeJ protein mediates a novel ribosome-rescue pathway distinct from SsrA- and ArfA-mediated pathways. *Mol. Microbiol.* *80*, 772–785.
- Chadani, Y., Matsumoto, E., Aso, H., Wada, T., Kutsukake, K., Sutou, S., and Abo, T. (2011c). translation-mediated tight regulation of the expression of the alternative ribosome-rescue factor ArfA in *Escherichia coli*. *Genes Genet. Syst.* *86*, 151–163.
- Chadani, Y., Ito, K., Kutsukake, K., and Abo, T. (2012). ArfA recruits release factor 2 to rescue stalled ribosomes by peptidyl-tRNA hydrolysis in *Escherichia coli*. *Mol. Microbiol.* *86*, 37–50.
- Chang, B., Halgamuge, S., and Tang, S.-L. (2006). Analysis of SD sequences in completed microbial genomes: Non-SD-led genes are as common as SD-led genes. *Gene* *373*, 90–99.
- Chebrek, R., Leonard, S., de Brevern, A.G., and Gelly, J.-C. (2014). PolyprOnline: polyproline helix II and secondary structure assignment database. *Database 2014*, bau102-bau102.
- Chen, B., Boël, G., Hashem, Y., Ning, W., Fei, J., Wang, C., Gonzalez, R.L., Hunt, J.F., and Frank, J. (2014). EttA regulates translation by binding the ribosomal E site and restricting ribosome-tRNA dynamics. *Nat. Struct. Mol. Biol.* *21*, 152–159.
- Chen, C., Stevens, B., Kaur, J., Cabral, D., Liu, H., Wang, Y., Zhang, H., Rosenblum, G., Smilansky, Z., Goldman, Y.E., et al. (2011). Single-Molecule Fluorescence Measurements of Ribosomal Translocation Dynamics. *Mol. Cell* *42*, 367–377.
- Chen, Y., Kaji, A., Kaji, H., and Cooperman, B.S. (2017). The kinetic mechanism of bacterial ribosome recycling. *Nucleic Acids Res.* *45*, 10168–10177.
- Choi, S., and Choe, J. (2011). Crystal structure of elongation factor P from *Pseudomonas aeruginosa* at 1.75 Å resolution. *Proteins* *79*, 1688–1693.
- Clementi, N., Chirkova, A., Puffer, B., Micura, R., and Polacek, N. (2010). Atomic mutagenesis reveals A2660 of 23S ribosomal RNA as key to EF-G GTPase activation. *Nat. Chem. Biol.* *6*, 344–351.
- Cornish, P. V., Ermolenko, D.N., Noller, H.F., and Ha, T. (2008). Spontaneous Intersubunit Rotation in Single Ribosomes. *Mol. Cell* *30*, 578–588.
- Crick, F. (1958). On protein synthesis. *Symp. Soc. Exp. Biol.* *12*, 138–163.
- Crick, F. (1970). Central dogma of molecular biology. *Nature* *227*, 561–563.
- Crick, F.H.C. (1966). Codon—anticodon pairing: The wobble hypothesis. *J. Mol. Biol.* *19*, 548–555.
- Cruz-Vera, L.R., Magos-Castro, M.A., Zamora-Romo, E., and Guarneros, G. (2004). Ribosome stalling and peptidyl-tRNA drop-off during translational delay at AGA codons. *Nucleic Acids Res.* *32*, 4462–4468.
- Cruz-Vera, L.R., Rajagopal, S., Squires, C., and Yanofsky, C. (2005). Features of Ribosome-Peptidyl-tRNA Interactions Essential for Tryptophan Induction of *tna* Operon Expression. *Mol. Cell* *19*, 333–343.
- Czworkowski, J., Wang, J., Steitz, T.A., and Moore, P.B. (1994). The crystal structure of elongation factor G complexed with GDP, at 2.7 Å resolution. *EMBO J.* *13*, 3661–3668.
- Dabbs, E.R. (1986). *Mutant Studies on the Prokaryotic Ribosome*. (Springer, New York, NY), pp. 733–748.

References

- Dallas, A., and Noller, H.F. (2001). Interaction of translation initiation factor 3 with the 30S ribosomal subunit. *Mol. Cell* **8**, 855–864.
- Davies, J., and Nomura, M. (1972). The Genetics of Bacterial Ribosomes. *Annu. Rev. Genet.* **6**, 203–234.
- Demeshkina, N., Jenner, L., Westhof, E., Yusupov, M., and Yusupova, G. (2012). A new understanding of the decoding principle on the ribosome. *Nature* **484**, 256–259.
- Demo, G., Rasouly, A., Vasilyev, N., Svetlov, V., Loveland, A.B., Diaz-Avalos, R., Grigorieff, N., Nudler, E., and Korostelev, A.A. (2017a). Structure of RNA polymerase bound to ribosomal 30S subunit. *Elife* **6**.
- Demo, G., Svidritskiy, E., Madireddy, R., Diaz-Avalos, R., Grant, T., Grigorieff, N., Sousa, D., and Korostelev, A.A. (2017b). Mechanism of ribosome rescue by ArfA and RF2. *Elife* **6**.
- Devaraj, A., Shoji, S., Holbrook, E.D., and Fredrick, K. (2009). A role for the 30S subunit E site in maintenance of the translational reading frame. *RNA* **15**, 255–265.
- Dincbas-Renqvist, V., Engström, A., Mora, L., Heurgué-Hamard, V., Buckingham, R., and Ehrenberg, M. (2000). A post-translational modification in the GGQ motif of RF2 from *Escherichia coli* stimulates termination of translation. *EMBO J.* **19**, 6900–6907.
- Doerfel, L.K., Wohlgemuth, I., Kothe, C., Peske, F., Urlaub, H., and Rodnina, M. V. (2013). EF-P Is Essential for Rapid Synthesis of Proteins Containing Consecutive Proline Residues. *Science* (80-.). **339**, 85–88.
- Doerfel, L.K., Wohlgemuth, I., Kubyskhin, V., Starosta, A.L., Wilson, D.N., Budisa, N., and Rodnina, M. V. (2015). Entropic Contribution of Elongation Factor P to Proline Positioning at the Catalytic Center of the Ribosome. *J. Am. Chem. Soc.* **137**, 12997–13006.
- Dogini, D.B., Pascoal, V.D.B., Avansini, S.H., Vieira, A.S., Pereira, T.C., and Lopes-Cendes, I. (2014). The new world of RNAs. *Genet. Mol. Biol.* **37**, 285–293.
- Dong, G., Nowakowski, J., and Hoffman, D.W. (2002). Structure of small protein B: the protein component of the tmRNA-SmpB system for ribosome rescue. *EMBO J.* **21**, 1845–1854.
- Dorner, S., Panuschka, C., Schmid, W., and Barta, A. (2003). Mononucleotide derivatives as ribosomal P-site substrates reveal an important contribution of the 2'-OH to activity. *Nucleic Acids Res.* **31**, 6536–6542.
- Duarte, I., Nabuurs, S.B., Magno, R., and Huynen, M. (2012). Evolution and Diversification of the Organellar Release Factor Family. *Mol. Biol. Evol.* **29**, 3497–3512.
- Dunkle, J.A., Wang, L., Feldman, M.B., Pulk, A., Chen, V.B., Kapral, G.J., Noeske, J., Richardson, J.S., Blanchard, S.C., and Cate, J.H.D. (2011). Structures of the bacterial ribosome in classical and hybrid states of tRNA binding. *Science* **332**, 981–984.
- Eisinger, J., Feuer, B., and Yamane, T. (1971). Codon-anticodon binding in tRNA_{phe}. *Nat. New Biol.* **231**, 126–128.
- Elgamal, S., Katz, A., Hersch, S.J., Newsom, D., White, P., Navarre, W.W., and Ibba, M. (2014). EF-P Dependent Pauses Integrate Proximal and Distal Signals during Translation. *PLoS Genet.* **10**, e1004553.

References

- Endo, Y., and Wool, I.G. (1982). The site of action of alpha-sarcin on eukaryotic ribosomes. The sequence at the alpha-sarcin cleavage site in 28 S ribosomal ribonucleic acid. *J. Biol. Chem.* *257*, 9054–9060.
- Erlacher, M.D., Lang, K., Wotzel, B., Rieder, R., Micura, R., and Polacek, N. (2006). Efficient Ribosomal Peptidyl Transfer Critically Relies on the Presence of the Ribose 2'-OH at A2451 of 23S rRNA. *J. Am. Chem. Soc.* *128*, 4453–4459.
- Ermolenko, D.N., Spiegel, P.C., Majumdar, Z.K., Hickerson, R.P., Clegg, R.M., and Noller, H.F. (2007a). The antibiotic viomycin traps the ribosome in an intermediate state of translocation. *Nat. Struct. Mol. Biol.* *14*, 493–497.
- Ermolenko, D.N., Majumdar, Z.K., Hickerson, R.P., Spiegel, P.C., Clegg, R.M., and Noller, H.F. (2007b). Observation of Intersubunit Movement of the Ribosome in Solution Using FRET. *J. Mol. Biol.* *370*, 530–540.
- Van Etten, W.J., and Janssen, G.R. (1998). An AUG initiation codon, not codon-anticodon complementarity, is required for the translation of unleadered mRNA in *Escherichia coli*. *Mol. Microbiol.* *27*, 987–1001.
- Farrell, D.J., Castanheira, M., and Chopra, I. (2011). Characterization of Global Patterns and the Genetics of Fusidic Acid Resistance. *Clin. Infect. Dis.* *52*, S487–S492.
- Feaga, H.A., Quickel, M.D., Hankey-Giblin, P.A., and Keiler, K.C. (2016). Human Cells Require Non-stop Ribosome Rescue Activity in Mitochondria. *PLOS Genet.* *12*, e1005964.
- Fei, J., Bronson, J.E., Hofman, J.M., Srinivas, R.L., Wiggins, C.H., and Gonzalez, R.L. (2009). Allosteric collaboration between elongation factor G and the ribosomal L1 stalk directs tRNA movements during translation. *Proc. Natl. Acad. Sci.* *106*, 15702–15707.
- Felden, B., Himeno, H., Muto, A., Atkins, J.F., and Gesteland, R.F. (1996). Structural organization of *Escherichia coli* tmRNA. *Biochimie* *78*, 979–983.
- Fischer, G., Bang, H., and Mech, C. (1984). Determination of enzymatic catalysis for the cis-trans isomerization of peptide binding in proline-containing peptides. *Biomed. Biochim. Acta* *43*, 1101–1111.
- Fischer, N., Neumann, P., Bock, L. V., Maracci, C., Wang, Z., Paleskava, A., Konevega, A.L., Schröder, G.F., Grubmüller, H., Ficner, R., et al. (2016). The pathway to GTPase activation of elongation factor SelB on the ribosome. *Nature* *540*.
- Fluitt, A., Pienaar, E., and Viljoen, H. (2007). Ribosome kinetics and aa-tRNA competition determine rate and fidelity of peptide synthesis. *Comput. Biol. Chem.* *31*, 335–346.
- Frank, J., and Agrawal, R.K. (2000). A ratchet-like inter-subunit reorganization of the ribosome during translocation. *Nature* *406*, 318–322.
- Frank, J., Gao, H., Sengupta, J., Gao, N., and Taylor, D.J. (2007). The process of mRNA-tRNA translocation. *Proc. Natl. Acad. Sci.* *104*, 19671–19678.
- Freistroffer, D. V., Pavlov, M.Y., MacDougall, J., Buckingham, R.H., and Ehrenberg, M. (1997). Release factor RF3 in *E. coli* accelerates the dissociation of release factors RF1 and RF2 from the ribosome in a GTP-dependent manner. *EMBO J.* *16*, 4126–4133.
- Frolova, L.Y., Tsivkovskii, R.Y., Sivolobova, G.F., Oparina, N.Y., Serpinsky, O.I., Blinov, V.M., Tatkov, S.I., and Kisselev, L.L. (1999). Mutations in the highly conserved GGQ motif of class 1 polypeptide release factors abolish ability of human eRF1 to trigger peptidyl-tRNA hydrolysis. *RNA* *5*, 1014–1020.

References

- Fu, J., Munro, J.B., Blanchard, S.C., and Frank, J. (2011). Cryoelectron microscopy structures of the ribosome complex in intermediate states during tRNA translocation. *Proc. Natl. Acad. Sci. U. S. A.* *108*, 4817–4821.
- Fu, Z., Kaledhonkar, S., Borg, A., Sun, M., Chen, B., Grassucci, R.A., Ehrenberg, M., and Frank, J. (2016). Key Intermediates in Ribosome Recycling Visualized by Time-Resolved Cryoelectron Microscopy. *Structure* *24*, 2092–2101.
- Gagnon, M.G., Seetharaman, S. V., Bulkley, D., and Steitz, T.A. (2012). Structural Basis for the Rescue of Stalled Ribosomes: Structure of YaeJ Bound to the Ribosome. *Science* (80-.). *335*, 1370–1372.
- Gamper, H.B., Masuda, I., Frenkel-Morgenstern, M., and Hou, Y.-M. (2015). Maintenance of protein synthesis reading frame by EF-P and m(1)G37-tRNA. *Nat. Commun.* *6*, 7226.
- Gao, H., Zhou, Z., Rawat, U., Huang, C., Bouakaz, L., Wang, C., Cheng, Z., Liu, Y., Zavialov, A., Gursky, R., et al. (2007). RF3 induces ribosomal conformational changes responsible for dissociation of class I release factors. *Cell* *129*, 929–941.
- Gao, N., Zavialov, A. V., Li, W., Sengupta, J., Valle, M., Gursky, R.P., Ehrenberg, M., and Frank, J. (2005). Mechanism for the Disassembly of the Posttermination Complex Inferred from Cryo-EM Studies. *Mol. Cell* *18*, 663–674.
- Gao, Y.-G., Selmer, M., Dunham, C.M., Weixlbaumer, A., Kelley, A.C., and Ramakrishnan, V. (2009). The structure of the ribosome with elongation factor G trapped in the posttranslocational state. *Science* *326*, 694–699.
- Garza-Sánchez, F., Janssen, B.D., and Hayes, C.S. (2006). Prolyl-tRNA(Pro) in the A-site of SecM-arrested ribosomes inhibits the recruitment of transfer-messenger RNA. *J. Biol. Chem.* *281*, 34258–34268.
- Garza-Sánchez, F., Gin, J.G., and Hayes, C.S. (2008). Amino acid starvation and colicin D treatment induce A-site mRNA cleavage in *Escherichia coli*. *J. Mol. Biol.* *378*, 505–519.
- Garza-Sánchez, F., Schaub, R.E., Janssen, B.D., and Hayes, C.S. (2011). tmRNA regulates synthesis of the ArfA ribosome rescue factor. *Mol. Microbiol.* *80*, 1204–1219.
- Gavrilova, L.P., Kostishkina, O.E., Koteliensky, V.E., Rutkevitch, N.M., and Spirin, A.S. (1976). Factor-free ("non-enzymic") and factor-dependent systems of translation of polyuridylic acid by *Escherichia coli* ribosomes. *J. Mol. Biol.* *101*, 537–552.
- Gilreath, M.S., Roy, H., Bullwinkle, T.J., Katz, A., Navarre, W.W., and Ibba, M. (2011). β -Lysine discrimination by lysyl-tRNA synthetase. *FEBS Lett.* *585*, 3284–3288.
- Giudice, E., and Gillet, R. (2013). The task force that rescues stalled ribosomes in bacteria. *Trends Biochem. Sci.* *38*, 403–411.
- Glick, B.R., and Ganoza, M.C. (1975). Identification of a soluble protein that stimulates peptide bond synthesis. *Proc. Natl. Acad. Sci. U. S. A.* *72*, 4257–4260.
- Glick, B.R., Chládek, S., and Ganoza, M.C. (1979). Peptide bond formation stimulated by protein synthesis factor EF-P depends on the aminoacyl moiety of the acceptor. *Eur. J. Biochem.* *97*, 23–28.
- Goldstein, J.L., and Caskey, C.T. (1970). Peptide chain termination: effect of protein S on ribosomal binding of release factors. *Proc. Natl. Acad. Sci. U. S. A.* *67*, 537–543.
- Gong, F., and Yanofsky, C. (2002). Instruction of Translating Ribosome by Nascent Peptide. *Science* (80-.). *297*, 1864–1867.

References

- Gonzalez de Valdivia, E.I., and Isaksson, L.A. (2005). Abortive translation caused by peptidyl-tRNA drop-off at NGG codons in the early coding region of mRNA. *FEBS J.* **272**, 5306–5316.
- Goyal, A., Belardinelli, R., Maracci, C., Milón, P., and Rodnina, M. V (2015). Directional transition from initiation to elongation in bacterial translation. *Nucleic Acids Res.* **43**, 10700–10712.
- Graf, M., Arenz, S., Huter, P., Dönhöfer, A., Nováček, J., and Wilson, D.N. (2017). Cryo-EM structure of the spinach chloroplast ribosome reveals the location of plastid-specific ribosomal proteins and extensions. *Nucleic Acids Res.* **45**.
- Grentzmann, G., Brechemier-Baey, D., Heurgue, V., Mora, L., and Buckingham, R.H. (1994). Localization and characterization of the gene encoding release factor RF3 in *Escherichia coli*. *Proc. Natl. Acad. Sci. U. S. A.* **91**, 5848–5852.
- Grill, S., Gualerzi, C.O., Londei, P., and Bläsi, U. (2000). Selective stimulation of translation of leaderless mRNA by initiation factor 2: evolutionary implications for translation. *EMBO J.* **19**, 4101–4110.
- Gualerzi, C.O., and Pon, C.L. (1990). Initiation of mRNA translation in prokaryotes. *Biochemistry* **29**, 5881–5889.
- Gualerzi, C.O., Severini, M., Spurio, R., La Teana, A., and Pon, C.L. (1991). Molecular dissection of translation initiation factor IF2. Evidence for two structural and functional domains. *J. Biol. Chem.* **266**, 16356–16362.
- Gueneau de Novoa, P., and Williams, K.P. (2004). The tmRNA website: reductive evolution of tmRNA in plastids and other endosymbionts. *Nucleic Acids Res.* **32**, D104-8.
- Guenneugues, M., Caserta, E., Brandi, L., Spurio, R., Meunier, S., Pon, C.L., Boelens, R., and Gualerzi, C.O. (2000). Mapping the fMet-tRNA^{fMet} binding site of initiation factor IF2. *EMBO J.* **19**, 5233–5240.
- Guo, Z., and Noller, H.F. (2012). Rotation of the head of the 30S ribosomal subunit during mRNA translocation. *Proc. Natl. Acad. Sci. U. S. A.* **109**, 20391–20394.
- Hanawa-Suetsugu, K., Sekine, S., Sakai, H., Hori-Takemoto, C., Terada, T., Unzai, S., Tame, J.R.H., Kuramitsu, S., Shirouzu, M., and Yokoyama, S. (2004). Crystal structure of elongation factor P from *Thermus thermophilus* HB8. *Proc. Natl. Acad. Sci. U. S. A.* **101**, 9595–9600.
- Handa, Y., Inaho, N., and Nameki, N. (2011). YaeJ is a novel ribosome-associated protein in *Escherichia coli* that can hydrolyze peptidyl-tRNA on stalled ribosomes. *Nucleic Acids Res.* **39**, 1739–1748.
- Hansen, J.L., Schmeing, T.M., Moore, P.B., and Steitz, T.A. (2002a). Structural insights into peptide bond formation. *Proc. Natl. Acad. Sci.* **99**, 11670–11675.
- Hansen, J.L., Schmeing, T.M., Moore, P.B., and Steitz, T.A. (2002b). Structural insights into peptide bond formation. *Proc. Natl. Acad. Sci. U. S. A.* **99**, 11670–11675.
- Harms, J., Schlutzenzen, F., Zarivach, R., Bashan, A., Gat, S., Agmon, I., Bartels, H., Franceschi, F., and Yonath, A. (2001). High resolution structure of the large ribosomal subunit from a mesophilic eubacterium. *Cell* **107**, 679–688.
- Hartz, D., McPheeters, D.S., and Gold, L. (1989). Selection of the initiator tRNA by *Escherichia coli* initiation factors. *Genes Dev.* **3**, 1899–1912.
- Hayes, C.S., and Sauer, R.T. (2003). Cleavage of the A site mRNA codon during ribosome pausing provides a mechanism for translational quality control. *Mol. Cell* **12**, 903–911.

References

- Heurgué-Hamard, V., Champ, S., Engström, A., Ehrenberg, M., and Buckingham, R.H. (2002). The hemK gene in *Escherichia coli* encodes the N(5)-glutamine methyltransferase that modifies peptide release factors. *EMBO J.* *21*, 769–778.
- Hiller, D.A., Singh, V., Zhong, M., and Strobel, S.A. (2011). A two-step chemical mechanism for ribosome-catalysed peptide bond formation. *Nature* *476*, 236–239.
- Himeno, H., Nameki, N., Kurita, D., Muto, A., and Abo, T. (2015). Ribosome rescue systems in bacteria. *Biochimie* *114*, 102–112.
- Hirokawa, G., Nijman, R.M., Raj, V.S., Kaji, H., Igarashi, K., and Kaji, A. (2005). The role of ribosome recycling factor in dissociation of 70S ribosomes into subunits. *RNA* *11*, 1317–1328.
- Hirokawa, G., Demeshkina, N., Iwakura, N., Kaji, H., and Kaji, A. (2006). The ribosome-recycling step: consensus or controversy? *Trends Biochem. Sci.* *31*, 143–149.
- Hoang, L., Fredrick, K., and Noller, H.F. (2004). Creating ribosomes with an all-RNA 30S subunit P site. *Proc. Natl. Acad. Sci.* *101*, 12439–12443.
- Hoernes, T.P., Clementi, N., Juen, M.A., Shi, X., Faserl, K., Willi, J., Gasser, C., Kreutz, C., Joseph, S., Lindner, H., et al. (2018). Atomic mutagenesis of stop codon nucleotides reveals the chemical prerequisites for release factor-mediated peptide release. *Proc. Natl. Acad. Sci.* *115*, E382–E389.
- Hong, S.-J., Lessner, F.H., Mahen, E.M., and Keiler, K.C. (2007). Proteomic identification of tmRNA substrates. *Proc. Natl. Acad. Sci.* *104*, 17128–17133.
- Huang, Y., and Sprinzl, M. (2011). Peptide Bond Formation on the Ribosome: The Role of the 2'-OH Group on the Terminal Adenosine of Peptidyl-tRNA and of the Length of Nascent Peptide Chain. *Angew. Chemie Int. Ed.* *50*, 7287–7289.
- Huang, C., Wolfgang, M.C., Withey, J., Koomey, M., and Friedman, D.I. (2000). Charged tmRNA but not tmRNA-mediated proteolysis is essential for *Neisseria gonorrhoeae* viability. *EMBO J.* *19*, 1098–1107.
- Hummels, K.R., Witzky, A., Rajkovic, A., Tollerson, R., Jones, L.A., Ibba, M., and Kearns, D.B. (2017). Carbonyl reduction by YmfI in *Bacillus subtilis* prevents accumulation of an inhibitory EF-P modification state. *Mol. Microbiol.* *106*, 236–251.
- Hussain, T., Llácer, J.L., Wimberly, B.T., Kieft, J.S., and Ramakrishnan, V. (2016). Large-Scale Movements of IF3 and tRNA during Bacterial Translation Initiation. *Cell* *167*, 133–144.e13.
- Huter, P., Arenz, S., Bock, L.V., Graf, M., Frister, J.O., Heuer, A., Peil, L., Starosta, A.L., Wohlgemuth, I., Peske, F., et al. (2017a). Structural Basis for Polyproline-Mediated Ribosome Stalling and Rescue by the Translation Elongation Factor EF-P. *Mol. Cell* *68*, 515–527.e6.
- Huter, P., Müller, C., Arenz, S., Beckert, B., and Wilson, D.N. (2017b). Structural Basis for Ribosome Rescue in Bacteria. *Trends Biochem. Sci.* *42*, 669–680.
- Huter, P., Müller, C., Beckert, B., Arenz, S., Berninghausen, O., Beckmann, R., and Wilson, D.N. (2017c). Structural basis for ArfA–RF2-mediated translation termination on mRNAs lacking stop codons. *Nature* *541*, 546–549.
- Hüttenhofer, A., Schattner, P., and Polacek, N. (2005). Non-coding RNAs: hope or hype? *Trends Genet.* *21*, 289–297.

References

- Ito, K., and Chiba, S. (2013). Arrest peptides: cis-acting modulators of translation. *Annu. Rev. Biochem.* **82**, 171–202.
- Ito, K., Uno, M., and Nakamura, Y. (1998). Single amino acid substitution in prokaryote polypeptide release factor 2 permits it to terminate translation at all three stop codons. *Proc. Natl. Acad. Sci. U. S. A.* **95**, 8165–8169.
- Ito, K., Uno, M., and Nakamura, Y. (2000). A tripeptide “anticodon” deciphers stop codons in messenger RNA. *Nature* **403**, 680–684.
- Ito, K., Chiba, S., and Pogliano, K. (2010). Divergent stalling sequences sense and control cellular physiology. *Biochem. Biophys. Res. Commun.* **393**, 1–5.
- Ito, K., Chadani, Y., Nakamori, K., Chiba, S., Akiyama, Y., and Abo, T. (2011). Nascentome Analysis Uncovers Futile Protein Synthesis in *Escherichia coli*. *PLoS One* **6**, e28413.
- Ivanova, N., Pavlov, M.Y., Felden, B., and Ehrenberg, M. (2004). Ribosome Rescue by tmRNA Requires Truncated mRNAs. *J. Mol. Biol.* **338**, 33–41.
- Ivanova, N., Pavlov, M.Y., and Ehrenberg, M. (2005). tmRNA-induced Release of Messenger RNA from Stalled Ribosomes. *J. Mol. Biol.* **350**, 897–905.
- Jacob, W.F., Santer, M., and Dahlberg, A.E. (1987). A single base change in the Shine-Dalgarno region of 16S rRNA of *Escherichia coli* affects translation of many proteins. *Proc. Natl. Acad. Sci. U. S. A.* **84**, 4757–4761.
- James, N.R., Brown, A., Gordiyenko, Y., and Ramakrishnan, V. (2016). Translational termination without a stop codon. *Science* (80-.). **354**, 1437–1440.
- Janssen, B.D., Garza-Sánchez, F., and Hayes, C.S. (2013). A-Site mRNA Cleavage Is Not Required for tmRNA-Mediated *ssrA*-Peptide Tagging. *PLoS One* **8**, e81319.
- Jenner, L., Romby, P., Rees, B., Schulze-Briese, C., Springer, M., Ehresmann, C., Ehresmann, B., Moras, D., Yusupova, G., and Yusupov, M. (2005). Translational Operator of mRNA on the Ribosome: How Repressor Proteins Exclude Ribosome Binding. *Science* (80-.). **308**, 120–123.
- Jenner, L., Rees, B., Yusupov, M., and Yusupova, G. (2007). Messenger RNA conformations in the ribosomal E site revealed by X-ray crystallography. *EMBO Rep.* **8**, 846–850.
- Jenner, L.B., Demeshkina, N., Yusupova, G., and Yusupov, M. (2010). Structural aspects of messenger RNA reading frame maintenance by the ribosome. *Nat. Struct. Mol. Biol.* **17**, 555–560.
- Jin, H., Kelley, A.C., Loakes, D., and Ramakrishnan, V. (2010). Structure of the 70S ribosome bound to release factor 2 and a substrate analog provides insights into catalysis of peptide release. *Proc. Natl. Acad. Sci. U. S. A.* **107**, 8593–8598.
- Jin, H., Kelley, A.C., and Ramakrishnan, V. (2011). Crystal structure of the hybrid state of ribosome in complex with the guanosine triphosphatase release factor 3. *Proc. Natl. Acad. Sci. U. S. A.* **108**, 15798–15803.
- Johansson, M., Jeong, K.-W., Trobro, S., Strazewski, P., Aqvist, J., Pavlov, M.Y., and Ehrenberg, M. (2011). pH-sensitivity of the ribosomal peptidyl transfer reaction dependent on the identity of the A-site aminoacyl-tRNA. *Proc. Natl. Acad. Sci.* **108**, 79–84.
- Joseph, S., and Noller, H.F. (1998). EF-G-catalyzed translocation of anticodon stem-loop analogs of transfer RNA in the ribosome. *EMBO J.* **17**, 3478–3483.

- Julián, P., Konevega, A.L., Scheres, S.H.W., Lázaro, M., Gil, D., Wintermeyer, W., Rodnina, M. V, and Valle, M. (2008). Structure of ratcheted ribosomes with tRNAs in hybrid states. *Proc. Natl. Acad. Sci. U. S. A.* *105*, 16924–16927.
- Julián, P., Milon, P., Agirrezabala, X., Lasso, G., Gil, D., Rodnina, M. V, and Valle, M. (2011). The Cryo-EM structure of a complete 30S translation initiation complex from *Escherichia coli*. *PLoS Biol.* *9*, e1001095.
- Kaberdina, A.C., Szaflarski, W., Nierhaus, K.H., and Moll, I. (2009). An Unexpected Type of Ribosomes Induced by Kasugamycin: A Look into Ancestral Times of Protein Synthesis? *Mol. Cell* *33*, 227–236.
- Kaminishi, T., Wilson, D.N., Takemoto, C., Harms, J.M., Kawazoe, M., Schluenzen, F., Hanawa-Suetsugu, K., Shirouzu, M., Fucini, P., and Yokoyama, S. (2007). A Snapshot of the 30S Ribosomal Subunit Capturing mRNA via the Shine-Dalgarno Interaction. *Structure* *15*, 289–297.
- Karimi, R., Pavlov, M.Y., Buckingham, R.H., and Ehrenberg, M. (1999). Novel roles for classical factors at the interface between translation termination and initiation. *Mol. Cell* *3*, 601–609.
- Karzai, A.W., Susskind, M.M., and Sauer, R.T. (1999a). SmpB, a unique RNA-binding protein essential for the peptide-tagging activity of SsrA (tmRNA). *EMBO J.* *18*, 3793–3799.
- Karzai, A.W., Susskind, M.M., and Sauer, R.T. (1999b). SmpB, a unique RNA-binding protein essential for the peptide-tagging activity of SsrA (tmRNA). *EMBO J.* *18*, 3793–3799.
- Katoh, T., Wohlgemuth, I., Nagano, M., Rodnina, M. V., and Suga, H. (2016). Essential structural elements in tRNA^{Pro} for EF-P-mediated alleviation of translation stalling. *Nat. Commun.* *7*, 11657.
- Kaur, S., Gillet, R., Li, W., Gursky, R., and Frank, J. (2006). Cryo-EM visualization of transfer messenger RNA with two SmpBs in a stalled ribosome. *Proc. Natl. Acad. Sci. U. S. A.* *103*, 16484–16489.
- Keiler, K.C. (2015). Mechanisms of ribosome rescue in bacteria. *Nat. Rev. Microbiol.* *13*, 285–297.
- Keiler, K.C., and Feaga, H.A. (2014). Resolving Nonstop Translation Complexes Is a Matter of Life or Death. *J. Bacteriol.* *196*, 2123–2130.
- Keiler, K.C., Waller, P.R., and Sauer, R.T. (1996). Role of a peptide tagging system in degradation of proteins synthesized from damaged messenger RNA. *Science* *271*, 990–993.
- Keiler, K.C., Shapiro, L., and Williams, K.P. (2000). tmRNAs that encode proteolysis-inducing tags are found in all known bacterial genomes: A two-piece tmRNA functions in *Caulobacter*. *Proc. Natl. Acad. Sci. U. S. A.* *97*, 7778–7783.
- Kim, D.F., and Green, R. (1999). Base-pairing between 23S rRNA and tRNA in the ribosomal A site. *Mol. Cell* *4*, 859–864.
- Kingery, D.A., Pfund, E., Voorhees, R.M., Okuda, K., Wohlgemuth, I., Kitchen, D.E., Rodnina, M. V, and Strobel, S.A. (2008). An uncharged amine in the transition state of the ribosomal peptidyl transfer reaction. *Chem. Biol.* *15*, 493–500.
- Koch, M., Flür, S., Kreutz, C., Ennifar, E., Micura, R., and Polacek, N. (2015). Role of a ribosomal RNA phosphate oxygen during the EF-G-triggered GTP hydrolysis. *Proc. Natl. Acad. Sci.* *112*, E2561–E2568.
- Kofoed, C.B., and Vester, B. (2002). Interaction of avilamycin with ribosomes and resistance caused by mutations in 23S rRNA. *Antimicrob. Agents Chemother.* *46*, 3339–3342.

References

- Kogure, H., Handa, Y., Nagata, M., Kanai, N., Guntert, P., Kubota, K., and Nameki, N. (2014). Identification of residues required for stalled-ribosome rescue in the codon-independent release factor YaeJ. *Nucleic Acids Res.* *42*, 3152–3163.
- Komarova, A. V., Tchufistova, L.S., Supina, E. V., and Boni, I. V (2002). Protein S1 counteracts the inhibitory effect of the extended Shine-Dalgarno sequence on translation. *RNA* *8*, 1137–1147.
- Komine, Y., Kitabatake, M., Yokogawa, T., Nishikawa, K., and Inokuchi, H. (1994). A tRNA-like structure is present in 10Sa RNA, a small stable RNA from *Escherichia coli*. *Proc. Natl. Acad. Sci. U. S. A.* *91*, 9223–9227.
- Konevega, A.L., Fischer, N., Semenov, Y.P., Stark, H., Wintermeyer, W., and Rodnina, M. V (2007). Spontaneous reverse movement of mRNA-bound tRNA through the ribosome. *Nat. Struct. Mol. Biol.* *14*, 318–324.
- Korkmaz, G., and Sanyal, S. (2017). R213I mutation in release factor 2 (RF2) is one step forward for engineering an omnipotent release factor in bacteria *Escherichia coli*. *J. Biol. Chem.* *292*, 15134–15142.
- Korostelev, A., Asahara, H., Lancaster, L., Laurberg, M., Hirschi, A., Zhu, J., Trakhanov, S., Scott, W.G., and Noller, H.F. (2008). Crystal structure of a translation termination complex formed with release factor RF2. *Proc. Natl. Acad. Sci.* *105*, 19684–19689.
- Korostelev, A., Zhu, J., Asahara, H., and Noller, H.F. (2010). Recognition of the amber UAG stop codon by release factor RF1. *EMBO J.* *29*, 2577–2585.
- Koutmou, K.S., McDonald, M.E., Brunelle, J.L., and Green, R. (2014a). RF3:GTP promotes rapid dissociation of the class 1 termination factor. *RNA* *20*, 609–620.
- Koutmou, K.S., McDonald, M.E., Brunelle, J.L., and Green, R. (2014b). RF3:GTP promotes rapid dissociation of the class 1 termination factor. *RNA* *20*, 609–620.
- Kristensen, O., and Laurberg, M. (2002). Expression, refolding and crystallization of *Aquifex aeolicus* elongation factor P. *Acta Crystallogr. D. Biol. Crystallogr.* *58*, 1039–1041.
- Kudla, G., Murray, A.W., Tollervey, D., and Plotkin, J.B. (2009). Coding-Sequence Determinants of Gene Expression in *Escherichia coli*. *Science* (80-). *324*, 255–258.
- Kuhlenkoetter, S., Wintermeyer, W., and Rodnina, M. V (2011). Different substrate-dependent transition states in the active site of the ribosome. *Nature* *476*, 351–354.
- Kurita, D., Miller, M.R., Muto, A., Buskirk, A.R., and Himeno, H. (2014a). Rejection of tmRNA·SmpB after GTP hydrolysis by EF-Tu on ribosomes stalled on intact mRNA. *RNA* *20*, 1706–1714.
- Kurita, D., Chadani, Y., Muto, A., Abo, T., and Himeno, H. (2014b). ArfA recognizes the lack of mRNA in the mRNA channel after RF2 binding for ribosome rescue. *Nucleic Acids Res.* *42*, 13339–13352.
- Kyrpides, N.C., and Woese, C.R. (1998). Universally conserved translation initiation factors. *Proc. Natl. Acad. Sci. U. S. A.* *95*, 224–228.
- Lassak, J., Keilhauer, E.C., Fürst, M., Wuichet, K., Gödeke, J., Starosta, A.L., Chen, J.-M., Søggaard-Andersen, L., Rohr, J., Wilson, D.N., et al. (2015a). Arginine-rhamnosylation as new strategy to activate translation elongation factor P. *Nat. Chem. Biol.* *11*, 266–270.
- Lassak, J., Keilhauer, E.C., Fürst, M., Wuichet, K., Gödeke, J., Starosta, A.L., Chen, J.-M., Søggaard-Andersen, L., Rohr, J., Wilson, D.N., et al. (2015b). Arginine-rhamnosylation as new strategy to activate translation elongation factor P. *Nat. Chem. Biol.* *11*, 266–270.

References

- Lassak, J., Wilson, D.N., and Jung, K. (2016). Stall no more at polyproline stretches with the translation elongation factors EF-P and IF-5A. *Mol. Microbiol.* **99**, 219–235.
- Laurberg, M., Asahara, H., Korostelev, A., Zhu, J., Trakhanov, S., and Noller, H.F. (2008). Structural basis for translation termination on the 70S ribosome. *Nature* **454**, 852–857.
- Laursen, B.S., Sørensen, H.P., Mortensen, K.K., and Sperling-Petersen, H.U. (2005). Initiation of protein synthesis in bacteria. *Microbiol. Mol. Biol. Rev.* **69**, 101–123.
- Leder, P., and Nirenberg, M.W. (1964). RNA CODEWORDS AND PROTEIN SYNTHESIS, 3. ON THE NUCLEOTIDE SEQUENCE OF A CYSTEINE AND A LEUCINE RNA CODEWORD. *Proc. Natl. Acad. Sci. U. S. A.* **52**, 1521–1529.
- Lescoute, A., and Westhof, E. (2006). The A-minor motifs in the decoding recognition process. *Biochimie* **88**, 993–999.
- Li, X., Hirano, R., Tagami, H., and Aiba, H. (2005). Protein tagging at rare codons is caused by tmRNA action at the 3' end of nonstop mRNA generated in response to ribosome stalling. *RNA* **12**, 248–255.
- Lill, R., Robertson, J.M., and Wintermeyer, W. (1986). Affinities of tRNA binding sites of ribosomes from *Escherichia coli*. *Biochemistry* **25**, 3245–3255.
- Lin, J., Gagnon, M.G., Bulkley, D., and Steitz, T.A. (2015). Conformational changes of elongation factor G on the ribosome during tRNA translocation. *Cell* **160**, 219–227.
- Lind, P.A., Berg, O.G., and Andersson, D.I. (2010). Mutational Robustness of Ribosomal Protein Genes. *Science (80-)*. **330**, 825–827.
- Ling, C., and Ermolenko, D.N. (2016). Structural insights into ribosome translocation. *Wiley Interdiscip. Rev. RNA* **7**, 620–636.
- Liu, T., Kaplan, A., Alexander, L., Yan, S., Wen, J.-D., Lancaster, L., Wickersham, C.E., Fredrick, K., Noller, H., Tinoco, I., et al. (2014). Direct measurement of the mechanical work during translocation by the ribosome. *Elife* **3**.
- Liu, W., Chen, C., Kavaliauskas, D., Knudsen, C.R., Goldman, Y.E., and Cooperman, B.S. (2015). EF-Tu dynamics during pre-translocation complex formation: EF-Tu-GDP exits the ribosome via two different pathways. *Nucleic Acids Res.* **43**, 9519–9528.
- Lofffield, R.B. (1963). THE FREQUENCY OF ERRORS IN PROTEIN BIOSYNTHESIS. *Biochem. J.* **89**, 82–92.
- Loveland, A.B., Demo, G., Grigorieff, N., and Korostelev, A.A. (2017). Ensemble cryo-EM elucidates the mechanism of translation fidelity. *Nature* **546**, 113–117.
- Lu, K.P., Finn, G., Lee, T.H., and Nicholson, L.K. (2007). Prolyl cis-trans isomerization as a molecular timer. *Nat. Chem. Biol.* **3**, 619–629.
- Ma, C., Kurita, D., Li, N., Chen, Y., Himeno, H., and Gao, N. (2017). Mechanistic insights into the alternative translation termination by ArfA and RF2. *Nature* **541**, 550–553.
- Ma, J., Campbell, A., and Karlin, S. (2002). Correlations between Shine-Dalgarno sequences and gene features such as predicted expression levels and operon structures. *J. Bacteriol.* **184**, 5733–5745.
- Macé, K., Demay, F., Guyomar, C., Georgeault, S., Giudice, E., Goude, R., Trautwetter, A., Ermel, G., Blanco, C., and Gillet, R. (2017). A Genetic Tool to Quantify trans-Translation Activity in Vivo. *J. Mol. Biol.* **429**, 3617–3625.

References

- Maden, B.E., and Monro, R.E. (1968). Ribosome-catalyzed peptidyl transfer. Effects of cations and pH value. *Eur. J. Biochem.* **6**, 309–316.
- Maguire, B.A., Beniaminov, A.D., Ramu, H., Mankin, A.S., and Zimmermann, R.A. (2005). A protein component at the heart of an RNA machine: the importance of protein I27 for the function of the bacterial ribosome. *Mol. Cell* **20**, 427–435.
- Maracci, C., and Rodnina, M. V. (2016). Review: Translational GTPases. *Biopolymers* **105**, 463–475.
- Maracci, C., Wohlgemuth, I., and Rodnina, M. V (2015). Activities of the peptidyl transferase center of ribosomes lacking protein L27. *RNA* **21**, 2047–2052.
- Margus, T., Remm, M., and Tenson, T. (2007). Phylogenetic distribution of translational GTPases in bacteria. *BMC Genomics* **8**, 15.
- Márquez, V., Wilson, D.N., Tate, W.P., Triana-Alonso, F., and Nierhaus, K.H. (2004). Maintaining the Ribosomal Reading Frame. *Cell* **118**, 45–55.
- Marshall, R.A., Aitken, C.E., and Puglisi, J.D. (2009). GTP Hydrolysis by IF2 Guides Progression of the Ribosome into Elongation. *Mol. Cell* **35**, 37–47.
- Marzi, S., Myasnikov, A.G., Serganov, A., Ehresmann, C., Romby, P., Yusupov, M., and Klaholz, B.P. (2007). Structured mRNAs Regulate Translation Initiation by Binding to the Platform of the Ribosome. *Cell* **130**, 1019–1031.
- McLaughlin, C.S., Dondon, J., Grunberg-Manago, M., Michelson, A.M., and Saunders, G. (1966). Stability of the messenger RNA-sRNA-ribosome complex. *Cold Spring Harb. Symp. Quant. Biol.* **31**, 601–610.
- Melnikov, S., Ben-Shem, A., Garreau de Loubresse, N., Jenner, L., Yusupova, G., and Yusupov, M. (2012). One core, two shells: bacterial and eukaryotic ribosomes. *Nat. Struct. Mol. Biol.* **19**, 560–567.
- Melnikov, S., Mailliot, J., Shin, B.-S., Rigger, L., Yusupova, G., Micura, R., Dever, T.E., and Yusupov, M. (2016a). Crystal Structure of Hypusine-Containing Translation Factor eIF5A Bound to a Rotated Eukaryotic Ribosome. *J. Mol. Biol.* **428**, 3570–3576.
- Melnikov, S., Mailliot, J., Rigger, L., Neuner, S., Shin, B., Yusupova, G., Dever, T.E., Micura, R., and Yusupov, M. (2016b). Molecular insights into protein synthesis with proline residues. *EMBO Rep.* **17**, 1776–1784.
- Miller, M.R., and Buskirk, A.R. (2014). An unusual mechanism for EF-Tu activation during tmRNA-mediated ribosome rescue. *RNA* **20**, 228–235.
- Miller, M.R., Liu, Z., Cazier, D.J., Gebhard, G.M., Herron, S.R., Zaher, H.S., Green, R., and Buskirk, A.R. (2011). The role of SmpB and the ribosomal decoding center in licensing tmRNA entry into stalled ribosomes. *RNA* **17**, 1727–1736.
- Milon, P., Konevega, A.L., Gualerzi, C.O., and Rodnina, M. V (2008). Kinetic checkpoint at a late step in translation initiation. *Mol. Cell* **30**, 712–720.
- Milón, P., and Rodnina, M. V. (2012). Kinetic control of translation initiation in bacteria. *Crit. Rev. Biochem. Mol. Biol.* **47**, 334–348.
- Milón, P., Maracci, C., Filonava, L., Gualerzi, C.O., and Rodnina, M. V (2012). Real-time assembly landscape of bacterial 30S translation initiation complex. *Nat. Struct. Mol. Biol.* **19**, 609–615.
- Moazed, D., and Noller, H.F. (1987). Interaction of antibiotics with functional sites in 16S ribosomal RNA. *Nature* **327**, 389–394.

References

- Moazed, D., Robertson, J.M., and Noller, H.F. (1988). Interaction of elongation factors EF-G and EF-Tu with a conserved loop in 23S RNA. *Nature* 334, 362–364.
- Moine, H., Romby, P., Springer, M., Grunberg-Manago, M., Ebel, J.P., Ehresmann, C., and Ehresmann, B. (1988). Messenger RNA structure and gene regulation at the translational level in *Escherichia coli*: the case of threonine:tRNA^{Thr} ligase. *Proc. Natl. Acad. Sci. U. S. A.* 85, 7892–7896.
- Moll, I., Grill, S., Gründling, A., and Bläsi, U. (2002). Effects of ribosomal proteins S1, S2 and the DeaD/CsdA DEAD-box helicase on translation of leaderless and canonical mRNAs in *Escherichia coli*. *Mol. Microbiol.* 44, 1387–1396.
- Moore, S.D., and Sauer, R.T. (2007). The tmRNA System for Translational Surveillance and Ribosome Rescue. *Annu. Rev. Biochem.* 76, 101–124.
- Moreno, J.M., Kildsgaard, J., Siwanowicz, I., Mortensen, K.K., and Sperling-Petersen, H.U. (1998). Binding of *Escherichia coli* initiation factor IF2 to 30S ribosomal subunits: a functional role for the N-terminus of the factor. *Biochem. Biophys. Res. Commun.* 252, 465–471.
- Moreno, J.M., Drskjøtersen, L., Kristensen, J.E., Mortensen, K.K., and Sperling-Petersen, H.U. (1999). Characterization of the domains of *E. coli* initiation factor IF2 responsible for recognition of the ribosome. *FEBS Lett.* 455, 130–134.
- Morris, A.L., MacArthur, M.W., Hutchinson, E.G., and Thornton, J.M. (1992). Stereochemical quality of protein structure coordinates. *Proteins Struct. Funct. Genet.* 12, 345–364.
- Munro, J.B., Altman, R.B., O'Connor, N., and Blanchard, S.C. (2007). Identification of two distinct hybrid state intermediates on the ribosome. *Mol. Cell* 25, 505–517.
- Muth, G.W., Ortoleva-Donnelly, L., and Strobel, S.A. (2000). A single adenosine with a neutral pKa in the ribosomal peptidyl transferase center. *Science* 289, 947–950.
- Muto, H., and Ito, K. (2008). Peptidyl-prolyl-tRNA at the ribosomal P-site reacts poorly with puromycin. *Biochem. Biophys. Res. Commun.* 366, 1043–1047.
- Muto, A., Fujihara, A., Ito, K.I., Matsuno, J., Ushida, C., and Himeno, H. (2000). Requirement of transfer-messenger RNA for the growth of *Bacillus subtilis* under stresses. *Genes Cells* 5, 627–635.
- Myasnikov, A.G., Marzi, S., Simonetti, A., Giuliodori, A.M., Gualerzi, C.O., Yusupova, G., Yusupov, M., and Klaholz, B.P. (2005). Conformational transition of initiation factor 2 from the GTP- to GDP-bound state visualized on the ribosome. *Nat. Struct. Mol. Biol.* 12, 1145–1149.
- Nakamoto, T. (2006). A unified view of the initiation of protein synthesis. *Biochem. Biophys. Res. Commun.* 341, 675–678.
- Nakamura, Y., Ito, K., and Ehrenberg, M. (2000). Mimicry grasps reality in translation termination. *Cell* 101, 349–352.
- Nakatogawa, H., and Ito, K. (2002). The ribosomal exit tunnel functions as a discriminating gate. *Cell* 108, 629–636.
- Nam, D., Choi, E., Shin, D., and Lee, E.-J. (2016). tRNA^{Pro}-mediated downregulation of elongation factor P is required for mgtCBR expression during *Salmonella* infection. *Mol. Microbiol.* 102, 221–232.
- Navarre, W.W., Zou, S.B., Roy, H., Xie, J.L., Savchenko, A., Singer, A., Edvokimova, E., Prost, L.R., Kumar, R., Ibba, M., et al. (2010). PoxA, YjeK, and Elongation Factor P Coordinately Modulate Virulence and Drug Resistance in *Salmonella enterica*. *Mol. Cell* 39, 209–221.

References

- Neubauer, C., Gao, Y.-G., Andersen, K.R., Dunham, C.M., Kelley, A.C., Hentschel, J., Gerdes, K., Ramakrishnan, V., and Brodersen, D.E. (2009). The structural basis for mRNA recognition and cleavage by the ribosome-dependent endonuclease RelE. *Cell* 139, 1084–1095.
- Neubauer, C., Gillet, R., Kelley, A.C., and Ramakrishnan, V. (2012). Decoding in the absence of a codon by tmRNA and SmpB in the ribosome. *Science* 335, 1366–1369.
- Nguyen, F., Starosta, A.L., Arenz, S., Sohmen, D., Dönhöfer, A., and Wilson, D.N. (2014). Tetracycline antibiotics and resistance mechanisms. *Biol. Chem.* 395, 559–575.
- Nissen, P., Hansen, J., Ban, N., Moore, P.B., and Steitz, T.A. (2000). The structural basis of ribosome activity in peptide bond synthesis. *Science* 289, 920–930.
- Nissen, P., Ippolito, J.A., Ban, N., Moore, P.B., and Steitz, T.A. (2001). RNA tertiary interactions in the large ribosomal subunit: the A-minor motif. *Proc. Natl. Acad. Sci. U. S. A.* 98, 4899–4903.
- Noller, H.F. (2012). Evolution of Protein Synthesis from an RNA World. *Cold Spring Harb. Perspect. Biol.* 4, a003681–a003681.
- Nomura, M., Mizushima, S., Ozaki, M., Traub, P., and Lowry, C. V (1969). Structure and function of ribosomes and their molecular components. *Cold Spring Harb. Symp. Quant. Biol.* 34, 49–61.
- O'Connor, M. (2015). Interactions of release factor RF3 with the translation machinery. *Mol. Genet. Genomics* 290, 1335–1344.
- O'Connor, M., Thomas, C.L., Zimmermann, R.A., and Dahlberg, A.E. (1997). Decoding fidelity at the ribosomal A and P sites: influence of mutations in three different regions of the decoding domain in 16S rRNA. *Nucleic Acids Res.* 25, 1185–1193.
- Ogle, J.M., Brodersen, D.E., Clemons, W.M., Tarry, M.J., Carter, A.P., and Ramakrishnan, V. (2001). Recognition of Cognate Transfer RNA by the 30S Ribosomal Subunit. *Science* (80-). 292, 897–902.
- Ogle, J.M., Murphy, F. V, Tarry, M.J., and Ramakrishnan, V. (2002). Selection of tRNA by the ribosome requires a transition from an open to a closed form. *Cell* 111, 721–732.
- Ohashi, Y., Inaoka, T., Kasai, K., Ito, Y., Okamoto, S., Satsu, H., Tozawa, Y., Kawamura, F., and Ochi, K. (2003). Expression Profiling of Translation-associated Genes in Sporulating *Bacillus subtilis* and Consequence of Sporulation by Gene Inactivation. *Biosci. Biotechnol. Biochem.* 67, 2245–2253.
- Okuda, K., Seila, A.C., and Strobel, S.A. (2005). Uncovering the Enzymatic p K_a of the Ribosomal Peptidyl Transferase Reaction Utilizing a Fluorinated Puromycin Derivative †. *Biochemistry* 44, 6675–6684.
- Pai, R.D., Zhang, W., Schuwirth, B.S., Hirokawa, G., Kaji, H., Kaji, A., and Cate, J.H.D. (2008). Structural Insights into ribosome recycling factor interactions with the 70S ribosome. *J. Mol. Biol.* 376, 1334–1347.
- Pallesen, J., Hashem, Y., Korkmaz, G., Koripella, R.K., Huang, C., Ehrenberg, M., Sanyal, S., and Frank, J. (2013). Cryo-EM visualization of the ribosome in termination complex with apo-RF3 and RF1. *Elife* 2, e00411.
- Pan, D., Kirillov, S. V., and Cooperman, B.S. (2007). Kinetically Competent Intermediates in the Translocation Step of Protein Synthesis. *Mol. Cell* 25, 519–529.
- Pape, T., Wintermeyer, W., and Rodnina, M. V (1998). Complete kinetic mechanism of elongation factor Tu-dependent binding of aminoacyl-tRNA to the A site of the *E. coli* ribosome. *EMBO J.* 17, 7490–7497.

References

- Pape, T., Wintermeyer, W., and Rodnina, M. (1999). Induced fit in initial selection and proofreading of aminoacyl-tRNA on the ribosome. *EMBO J.* *18*, 3800–3807.
- Passalacqua, K.D., Varadarajan, A., Ondov, B.D., Okou, D.T., Zwick, M.E., and Bergman, N.H. (2009). Structure and complexity of a bacterial transcriptome. *J. Bacteriol.* *191*, 3203–3211.
- Pavlov, M.Y., Watts, R.E., Tan, Z., Cornish, V.W., Ehrenberg, M., and Forster, A.C. (2009). Slow peptide bond formation by proline and other N-alkylamino acids in translation. *Proc. Natl. Acad. Sci. U. S. A.* *106*, 50–54.
- Peil, L., Starosta, A.L., Virumäe, K., Atkinson, G.C., Tenson, T., Remme, J., and Wilson, D.N. (2012). Lys34 of translation elongation factor EF-P is hydroxylated by YfcM. *Nat. Chem. Biol.* *8*, 695–697.
- Peil, L., Starosta, A.L., Lassak, J., Atkinson, G.C., Virumäe, K., Spitzer, M., Tenson, T., Jung, K., Remme, J., and Wilson, D.N. (2013). Distinct XPPX sequence motifs induce ribosome stalling, which is rescued by the translation elongation factor EF-P. *Proc. Natl. Acad. Sci. U. S. A.* *110*, 15265–15270.
- Pelechano, V., and Alepuz, P. (2017). eIF5A facilitates translation termination globally and promotes the elongation of many non polyproline-specific tripeptide sequences. *Nucleic Acids Res.* *45*, 7326–7338.
- Personne, Y., and Parish, T. (2014). Mycobacterium tuberculosis possesses an unusual tmRNA rescue system. *Tuberculosis* *94*, 34–42.
- Peske, F., Rodnina, M. V, and Wintermeyer, W. (2005). Sequence of steps in ribosome recycling as defined by kinetic analysis. *Mol. Cell* *18*, 403–412.
- Peske, F., Kuhlenkoetter, S., Rodnina, M. V., and Wintermeyer, W. (2014). Timing of GTP binding and hydrolysis by translation termination factor RF3. *Nucleic Acids Res.* *42*, 1812.
- Pierson, W.E., Hoffer, E.D., Keedy, H.E., Simms, C.L., Dunham, C.M., and Zaher, H.S. (2016). Uniformity of Peptide Release Is Maintained by Methylation of Release Factors. *Cell Rep.* *17*, 11–18.
- Plant, E.P., Nguyen, P., Russ, J.R., Pittman, Y.R., Nguyen, T., Quesinberry, J.T., Kinzy, T.G., and Dinman, J.D. (2007). Differentiating between near- and non-cognate codons in *Saccharomyces cerevisiae*. *PLoS One* *2*, e517.
- Polacek, N., and Mankin, A.S. (2005). The Ribosomal Peptidyl Transferase Center: Structure, Function, Evolution, Inhibition. *Crit. Rev. Biochem. Mol. Biol.* *40*, 285–311.
- Polacek, N., Gaynor, M., Yassin, A., and Mankin, A.S. (2001). Ribosomal peptidyl transferase can withstand mutations at the putative catalytic nucleotide. *Nature* *411*, 498–501.
- Polikanov, Y.S., Steitz, T.A., and Innis, C.A. (2014). A proton wire to couple aminoacyl-tRNA accommodation and peptide-bond formation on the ribosome. *Nat. Struct. Mol. Biol.* *21*, 787–793.
- Powers, T., and Noller, H.F. (1990). Dominant lethal mutations in a conserved loop in 16S rRNA. *Proc. Natl. Acad. Sci. U. S. A.* *87*, 1042–1046.
- Prabhakar, A., Capece, M.C., Petrov, A., Choi, J., and Puglisi, J.D. (2017). Post-termination Ribosome Intermediate Acts as the Gateway to Ribosome Recycling. *Cell Rep.* *20*, 161–172.
- Proshkin, S., Rahmouni, A.R., Mironov, A., and Nudler, E. (2010). Cooperation Between Translating Ribosomes and RNA Polymerase in Transcription Elongation. *Science* (80-.). *328*, 504–508.
- Qin, B., Yamamoto, H., Ueda, T., Varshney, U., and Nierhaus, K.H. (2016). The Termination Phase in Protein Synthesis is not Obligatorily Followed by the RRF/EF-G-Dependent Recycling Phase. *J. Mol. Biol.* *428*, 3577–3587.

References

- Qin, H., Grigoriadou, C., and Cooperman, B.S. (2009). Interaction of IF2 with the Ribosomal GTPase-Associated Center during 70S Initiation Complex Formation. *Biochemistry* **48**, 4699–4706.
- Rajkovic, A., and Ibba, M. (2017). Elongation Factor P and the Control of Translation Elongation. *Annu. Rev. Microbiol.* **71**, 117–131.
- Rajkovic, A., Hummels, K.R., Witzky, A., Erickson, S., Gafken, P.R., Whitelegge, J.P., Faull, K.F., Kearns, D.B., and Ibba, M. (2016). Translation Control of Swarming Proficiency in *Bacillus subtilis* by 5-Amino-pentanolyated Elongation Factor P. *J. Biol. Chem.* **291**, 10976–10985.
- Ramadoss, N.S., Zhou, X., and Keiler, K.C. (2013a). tmRNA Is Essential in *Shigella flexneri*. *PLoS One* **8**, e57537.
- Ramadoss, N.S., Alumasa, J.N., Cheng, L., Wang, Y., Li, S., Chambers, B.S., Chang, H., Chatterjee, A.K., Brinker, A., Engels, I.H., et al. (2013b). Small molecule inhibitors of trans-translation have broad-spectrum antibiotic activity. *Proc. Natl. Acad. Sci.* **110**, 10282–10287.
- Ramrath, D.J.F., Yamamoto, H., Rother, K., Wittek, D., Pech, M., Mielke, T., Loerke, J., Scheerer, P., Ivanov, P., Teraoka, Y., et al. (2012). The complex of tmRNA-SmpB and EF-G on translocating ribosomes. *Nature* **485**, 526–529.
- Ramrath, D.J.F., Lancaster, L., Sprink, T., Mielke, T., Loerke, J., Noller, H.F., and Spahn, C.M.T. (2013). Visualization of two transfer RNAs trapped in transit during elongation factor G-mediated translocation. *Proc. Natl. Acad. Sci.* **110**, 20964–20969.
- Ratje, A.H., Loerke, J., Mikolajka, A., Brünner, M., Hildebrand, P.W., Starosta, A.L., Dönhöfer, A., Connell, S.R., Fucini, P., Mielke, T., et al. (2010). Head swivel on the ribosome facilitates translocation by means of intra-subunit tRNA hybrid sites. *Nature* **468**, 713–716.
- Rheinberger, H.J., and Nierhaus, K.H. (1983). Testing an alternative model for the ribosomal peptide elongation cycle. *Proc. Natl. Acad. Sci. U. S. A.* **80**, 4213–4217.
- Roche, E.D., and Sauer, R.T. (1999). SsrA-mediated peptide tagging caused by rare codons and tRNA scarcity. *EMBO J.* **18**, 4579–4589.
- Rodnina, M. V., and Wintermeyer, W. (2001). Fidelity of aminoacyl-tRNA selection on the ribosome: kinetic and structural mechanisms. *Annu. Rev. Biochem.* **70**, 415–435.
- Rodnina, M. V., Fricke, R., and Wintermeyer, W. (1994). Transient conformational states of aminoacyl-tRNA during ribosome binding catalyzed by elongation factor Tu. *Biochemistry* **33**, 12267–12275.
- Rodnina, M. V., Fricke, R., Kuhn, L., and Wintermeyer, W. (1995). Codon-dependent conformational change of elongation factor Tu preceding GTP hydrolysis on the ribosome. *EMBO J.* **14**, 2613–2619.
- Rodnina, M. V., Pape, T., Fricke, R., Kuhn, L., and Wintermeyer, W. (1996). Initial binding of the elongation factor Tu.GTP.aminoacyl-tRNA complex preceding codon recognition on the ribosome. *J. Biol. Chem.* **271**, 646–652.
- Rodnina, M. V., Savelsbergh, A., Katunin, V.I., and Wintermeyer, W. (1997). Hydrolysis of GTP by elongation factor G drives tRNA movement on the ribosome. *Nature* **385**, 37–41.
- Rodnina, M. V., Pape, T., and Wintermeyer, W. (2000). Conformational switch in the decoding region of 16S rRNA during aminoacyl-tRNA selection on the ribosome. *Nat. Struct. Biol.* **7**, 104–107.
- Rodnina, M. V., Beringer, M., and Wintermeyer, W. (2007). How ribosomes make peptide bonds. *Trends Biochem. Sci.* **32**, 20–26.

References

- Roy, H., Zou, S.B., Bullwinkle, T.J., Wolfe, B.S., Gilreath, M.S., Forsyth, C.J., Navarre, W.W., and Ibba, M. (2011). The tRNA synthetase paralog PoxA modifies elongation factor-P with (R)- β -lysine. *Nat. Chem. Biol.* 7, 667–669.
- Rozov, A., Demeshkina, N., Westhof, E., Yusupov, M., and Yusupova, G. (2015). Structural insights into the translational infidelity mechanism. *Nat. Commun.* 6, 7251.
- Rozov, A., Demeshkina, N., Westhof, E., Yusupov, M., and Yusupova, G. (2016a). New Structural Insights into Translational Miscoding. *Trends Biochem. Sci.* 41, 798–814.
- Rozov, A., Westhof, E., Yusupov, M., and Yusupova, G. (2016b). The ribosome prohibits the G•U wobble geometry at the first position of the codon–anticodon helix. *Nucleic Acids Res.* 44, gkw431.
- Russell, J.B., and Cook, G.M. (1995). Energetics of bacterial growth: balance of anabolic and catabolic reactions. *Microbiol. Rev.* 59, 48–62.
- Saha, I., and Shamala, N. (2012). Investigating diproline segments in proteins: occurrences, conformation and classification. *Biopolymers* 97, 54–64.
- Santos, N., Zhu, J., Donohue, J.P., Korostelev, A.A., and Noller, H.F. (2013). Crystal structure of the 70S ribosome bound with the Q253P mutant form of release factor RF2. *Structure* 21, 1258–1263.
- Sassetti, C.M., Boyd, D.H., and Rubin, E.J. (2003). Genes required for mycobacterial growth defined by high density mutagenesis. *Mol. Microbiol.* 48, 77–84.
- Satterthwait, A.C., and Jencks, W.P. (1974). The mechanism of the aminolysis of acetate esters. *J. Am. Chem. Soc.* 96, 7018–7031.
- Scharff, L.B., Childs, L., Walther, D., and Bock, R. (2011a). Local absence of secondary structure permits translation of mRNAs that lack ribosome-binding sites. *PLoS Genet.* 7, e1002155.
- Scharff, L.B., Childs, L., Walther, D., and Bock, R. (2011b). Local Absence of Secondary Structure Permits Translation of mRNAs that Lack Ribosome-Binding Sites. *PLoS Genet.* 7, e1002155.
- Schaub, R.E., Poole, S.J., Garza-Sánchez, F., Benbow, S., and Hayes, C.S. (2012). Proteobacterial ArfA peptides are synthesized from non-stop messenger RNAs. *J. Biol. Chem.* 287, 29765–29775.
- Schlunzen, F., Tocilj, A., Zarivach, R., Harms, J., Gluehmann, M., Janell, D., Bashan, A., Bartels, H., Agmon, I., Franceschi, F., et al. (2000). Structure of functionally activated small ribosomal subunit at 3.3 angstroms resolution. *Cell* 102, 615–623.
- Schlünzen, F., Zarivach, R., Harms, J., Bashan, A., Tocilj, A., Albrecht, R., Yonath, A., and Franceschi, F. (2001). Structural basis for the interaction of antibiotics with the peptidyl transferase centre in eubacteria. *Nature* 413, 814–821.
- Schmeing, T.M., Seila, A.C., Hansen, J.L., Freeborn, B., Soukup, J.K., Scaringe, S.A., Strobel, S.A., Moore, P.B., and Steitz, T.A. (2002). A pre-translocational intermediate in protein synthesis observed in crystals of enzymatically active 50S subunits. *Nat. Struct. Biol.* 9, 225–230.
- Schmeing, T.M., Moore, P.B., and Steitz, T.A. (2003). Structures of deacylated tRNA mimics bound to the E site of the large ribosomal subunit. *RNA* 9, 1345–1352.
- Schmeing, T.M., Huang, K.S., Strobel, S.A., and Steitz, T.A. (2005a). An induced-fit mechanism to promote peptide bond formation and exclude hydrolysis of peptidyl-tRNA. *Nature* 438, 520–524.
- Schmeing, T.M., Huang, K.S., Kitchen, D.E., Strobel, S.A., and Steitz, T.A. (2005b). Structural Insights into the Roles of Water and the 2' Hydroxyl of the P Site tRNA in the Peptidyl Transferase Reaction. *Mol. Cell* 20, 437–448.

References

- Schmeing, T.M., Voorhees, R.M., Kelley, A.C., Gao, Y.-G., Murphy, F. V., Weir, J.R., and Ramakrishnan, V. (2009). The Crystal Structure of the Ribosome Bound to EF-Tu and Aminoacyl-tRNA. *Science* (80-). 326, 688–694.
- Schmidt, C., Becker, T., Heuer, A., Braunger, K., Shanmuganathan, V., Pech, M., Berninghausen, O., Wilson, D.N., and Beckmann, R. (2016). Structure of the hypusinylated eukaryotic translation factor eIF-5A bound to the ribosome. *Nucleic Acids Res.* 44, 1944–1951.
- Schneider-Poetsch, T., Ju, J., Eyler, D.E., Dang, Y., Bhat, S., Merrick, W.C., Green, R., Shen, B., and Liu, J.O. (2010). Inhibition of eukaryotic translation elongation by cycloheximide and lactimidomycin. *Nat. Chem. Biol.* 6, 209–217.
- Schrode, P., Huter, P., Clementi, N., and Erlacher, M. (2017). Atomic mutagenesis at the ribosomal decoding site. *RNA Biol.* 14, 104–112.
- Schuller, A.P., Wu, C.C.-C., Dever, T.E., Buskirk, A.R., and Green, R. (2017). eIF5A Functions Globally in Translation Elongation and Termination. *Mol. Cell* 66, 194–205.e5.
- Seila, A.C., Okuda, K., Núñez, S., Seila, A.F., and Strobel, S.A. (2005). Kinetic Isotope Effect Analysis of the Ribosomal Peptidyl Transferase Reaction †. *Biochemistry* 44, 4018–4027.
- Selmer, M., Dunham, C.M., Murphy, F. V., Weixlbaumer, A., Petry, S., Kelley, A.C., Weir, J.R., and Ramakrishnan, V. (2006). Structure of the 70S ribosome complexed with mRNA and tRNA. *Science* 313, 1935–1942.
- Semenkov, Y. u, Shapkina, T., Makhno, V., and Kirillov, S. (1992). Puromycin reaction for the A site-bound peptidyl-tRNA. *FEBS Lett.* 296, 207–210.
- Sengupta, J., Agrawal, R.K., and Frank, J. (2001). Visualization of protein S1 within the 30S ribosomal subunit and its interaction with messenger RNA. *Proc. Natl. Acad. Sci.* 98, 11991–11996.
- Senior, B.W., and Holland, I.B. (1971). Effect of colicin E3 upon the 30S ribosomal subunit of *Escherichia coli*. *Proc. Natl. Acad. Sci. U. S. A.* 68, 959–963.
- Sharma, D., Southworth, D.R., and Green, R. (2004). EF-G-independent reactivity of a pre-translocation-state ribosome complex with the aminoacyl tRNA substrate puromycin supports an intermediate (hybrid) state of tRNA binding. *RNA* 10, 102–113.
- Shaw, J.J., and Green, R. (2007). Two Distinct Components of Release Factor Function Uncovered by Nucleophile Partitioning Analysis. *Mol. Cell* 28, 458–467.
- Shaw, J.J., Trobro, S., He, S.L., Åqvist, J., and Green, R. (2012). A Role for the 2' OH of Peptidyl-tRNA Substrate in Peptide Release on the Ribosome Revealed through RF-Mediated Rescue. *Chem. Biol.* 19, 983–993.
- Shi, X., and Joseph, S. (2016). Mechanism of Translation Termination: RF1 Dissociation Follows Dissociation of RF3 from the Ribosome. *Biochemistry* 55, 6344–6354.
- Shimizu, Y. (2012). ArfA recruits RF2 into stalled ribosomes. *J. Mol. Biol.* 423, 624–631.
- Shin, J.-H., and Price, C.W. (2007). The SsrA-SmpB ribosome rescue system is important for growth of *Bacillus subtilis* at low and high temperatures. *J. Bacteriol.* 189, 3729–3737.
- Shin, D.H., Brandsen, J., Jancarik, J., Yokota, H., Kim, R., and Kim, S.-H. (2004). Structural analyses of peptide release factor 1 from *Thermotoga maritima* reveal domain flexibility required for its interaction with the ribosome. *J. Mol. Biol.* 341, 227–239.

References

- Shine, J., and Dalgarno, L. (1974). The 3'-terminal sequence of Escherichia coli 16S ribosomal RNA: complementarity to nonsense triplets and ribosome binding sites. *Proc. Natl. Acad. Sci. U. S. A.* *71*, 1342–1346.
- Shoji, S., Walker, S.E., and Fredrick, K. (2006). Reverse translocation of tRNA in the ribosome. *Mol. Cell* *24*, 931–942.
- Sievers, A., Beringer, M., Rodnina, M. V, and Wolfenden, R. (2004). The ribosome as an entropy trap. *Proc. Natl. Acad. Sci. U. S. A.* *101*, 7897–7901.
- Simonetti, A., Marzi, S., Myasnikov, A.G., Fabbretti, A., Yusupov, M., Gualerzi, C.O., and Klaholz, B.P. (2008). Structure of the 30S translation initiation complex. *Nature* *455*, 416–420.
- Skorski, P., Leroy, P., Fayet, O., Dreyfus, M., and Hermann-Le Denmat, S. (2006). The highly efficient translation initiation region from the Escherichia coli rpsA gene lacks a shine-dalgarno element. *J. Bacteriol.* *188*, 6277–6285.
- Sørensen, M.A., Fricke, J., and Pedersen, S. (1998). Ribosomal protein S1 is required for translation of most, if not all, natural mRNAs in Escherichia coli in vivo. *J. Mol. Biol.* *280*, 561–569.
- Sprink, T., Ramrath, D.J.F., Yamamoto, H., Yamamoto, K., Loerke, J., Ismer, J., Hildebrand, P.W., Scheerer, P., Burger, J., Mielke, T., et al. (2016). Structures of ribosome-bound initiation factor 2 reveal the mechanism of subunit association. *Sci. Adv.* *2*, e1501502–e1501502.
- Starosta, A.L., Lassak, J., Jung, K., and Wilson, D.N. (2014a). The bacterial translation stress response. *FEMS Microbiol. Rev.* *38*, 1172–1201.
- Starosta, A.L., Lassak, J., Peil, L., Atkinson, G.C., Woolstenhulme, C.J., Virumäe, K., Buskirk, A., Tenson, T., Remme, J., Jung, K., et al. (2014b). A conserved proline triplet in Val-tRNA synthetase and the origin of elongation factor P. *Cell Rep.* *9*, 476–483.
- Starosta, A.L., Lassak, J., Peil, L., Atkinson, G.C., Virumäe, K., Tenson, T., Remme, J., Jung, K., and Wilson, D.N. (2014c). Translational stalling at polyproline stretches is modulated by the sequence context upstream of the stall site. *Nucleic Acids Res.* *42*, 10711–10719.
- Sternberg, S.H., Fei, J., Prywes, N., McGrath, K.A., and Gonzalez, R.L. (2009). Translation factors direct intrinsic ribosome dynamics during translation termination and ribosome recycling. *Nat. Struct. Mol. Biol.* *16*, 861–868.
- Studer, S.M., and Joseph, S. (2006). Unfolding of mRNA Secondary Structure by the Bacterial Translation Initiation Complex. *Mol. Cell* *22*, 105–115.
- Su, T., Cheng, J., Sohmen, D., Hedman, R., Berninghausen, O., von Heijne, G., Wilson, D.N., and Beckmann, R. (2017). The force-sensing peptide VemP employs extreme compaction and secondary structure formation to induce ribosomal stalling. *Elife* *6*.
- Sugimoto, N., Kierzek, R., Freier, S.M., and Turner, D.H. (1986). Energetics of internal GU mismatches in ribooligonucleotide helices. *Biochemistry* *25*, 5755–5759.
- Sundermeier, T.R., Dulebohn, D.P., Cho, H.J., and Karzai, A.W. (2005). A previously uncharacterized role for small protein B (SmpB) in transfer messenger RNA-mediated trans-translation. *Proc. Natl. Acad. Sci.* *102*, 2316–2321.
- Sussman, J.K., Simons, E.L., and Simons, R.W. (1996). Escherichia coli translation initiation factor 3 discriminates the initiation codon in vivo. *Mol. Microbiol.* *21*, 347–360.

References

- Svetlanov, A., Puri, N., Mena, P., Koller, A., and Karzai, A.W. (2012). *Francisella tularensis* tmRNA system mutants are vulnerable to stress, avirulent in mice, and provide effective immune protection. *Mol. Microbiol.* *85*, 122–141.
- T. Schmeing, K. Huang, S. Strobel, and T. Steitz (2005). An induced-fit mechanism to promote peptide bond formation and exclude hydrolysis of peptidyl-tRNA. *Nature* *438*, 520–524.
- La Teana, A., Gualerzi, C.O., and Dahlberg, A.E. (2001). Initiation factor IF 2 binds to the alpha-sarcin loop and helix 89 of *Escherichia coli* 23S ribosomal RNA. *RNA* *7*, 1173–1179.
- Thibonnier, M., Thiberge, J.-M., and De Reuse, H. (2008). Trans-translation in *Helicobacter pylori*: essentiality of ribosome rescue and requirement of protein tagging for stress resistance and competence. *PLoS One* *3*, e3810.
- Thompson, J., Kim, D.F., O'Connor, M., Lieberman, K.R., Bayfield, M.A., Gregory, S.T., Green, R., Noller, H.F., and Dahlberg, A.E. (2001). Analysis of mutations at residues A2451 and G2447 of 23S rRNA in the peptidyltransferase active site of the 50S ribosomal subunit. *Proc. Natl. Acad. Sci.* *98*, 9002–9007.
- Trappl, K., and Joseph, S. (2016). Ribosome Induces a Closed to Open Conformational Change in Release Factor 1. *J. Mol. Biol.* *428*, 1333–1344.
- Trobro, S., and Åqvist, J. (2009). Mechanism of the Translation Termination Reaction on the Ribosome. *Biochemistry* *48*, 11296–11303.
- Ude, S., Lassak, J., Starosta, A.L., Kraxenberger, T., Wilson, D.N., and Jung, K. (2013). Translation Elongation Factor EF-P Alleviates Ribosome Stalling at Polyproline Stretches. *Science (80-.)*. *339*, 82–85.
- Ueda, K., Yamamoto, Y., Ogawa, K., Abo, T., Inokuchi, H., and Aiba, H. (2002). Bacterial SsrA system plays a role in coping with unwanted translational readthrough caused by suppressor tRNAs. *Genes Cells* *7*, 509–519.
- Ushida, C., Himeno, H., Watanabe, T., and Muto, A. (1994). tRNA-like structures in 10Sa RNAs of *Mycoplasma capricolum* and *Bacillus subtilis*. *Nucleic Acids Res.* *22*, 3392–3396.
- Valle, M., Gillet, R., Kaur, S., Henne, A., Ramakrishnan, V., and Frank, J. (2003). Visualizing tmRNA entry into a stalled ribosome. *Science* *300*, 127–130.
- Vestergaard, B., Van, L.B., Andersen, G.R., Nyborg, J., Buckingham, R.H., and Kjeldgaard, M. (2001). Bacterial polypeptide release factor RF2 is structurally distinct from eukaryotic eRF1. *Mol. Cell* *8*, 1375–1382.
- Voorhees, R.M., Weixlbaumer, A., Loakes, D., Kelley, A.C., and Ramakrishnan, V. (2009a). Insights into substrate stabilization from snapshots of the peptidyl transferase center of the intact 70S ribosome. *Nat. Struct. Mol. Biol.* *16*, 528–533.
- Voorhees, R.M., Weixlbaumer, A., Loakes, D., Kelley, A.C., and Ramakrishnan, V. (2009b). Insights into substrate stabilization from snapshots of the peptidyl transferase center of the intact 70S ribosome. *Nat. Struct. Mol. Biol.* *16*, 528–533.
- Voorhees, R.M., Schmeing, T.M., Kelley, A.C., and Ramakrishnan, V. (2010). The Mechanism for Activation of GTP Hydrolysis on the Ribosome. *Science (80-.)*. *330*, 835–838.
- Wallin, G., and Åqvist, J. (2010). The transition state for peptide bond formation reveals the ribosome as a water trap. *Proc. Natl. Acad. Sci. U. S. A.* *107*, 1888–1893.

References

- Wang, Y., and Xiao, M. (2012). Role of the ribosomal protein L27 revealed by single-molecule FRET study. *Protein Sci.* *21*, 1696–1704.
- Wang, Y., Xiao, M., and Li, Y. (2014). Heterogeneity of single molecule FRET signals reveals multiple active ribosome subpopulations. *Proteins Struct. Funct. Bioinforma.* *82*, 1–9.
- Weinger, J.S., Parnell, K.M., Dorner, S., Green, R., and Strobel, S.A. (2004). Substrate-assisted catalysis of peptide bond formation by the ribosome. *Nat. Struct. Mol. Biol.* *11*, 1101–1106.
- Weis, F., Bron, P., Giudice, E., Rolland, J.-P., Thomas, D., Felden, B., and Gillet, R. (2010). tmRNA–SmpB: a journey to the centre of the bacterial ribosome. *EMBO J.* *29*, 3810–3818.
- Weixlbaumer, A., Petry, S., Dunham, C.M., Selmer, M., Kelley, A.C., and Ramakrishnan, V. (2007). Crystal structure of the ribosome recycling factor bound to the ribosome. *Nat. Struct. Mol. Biol.* *14*, 733–737.
- Weixlbaumer, A., Jin, H., Neubauer, C., Voorhees, R.M., Petry, S., Kelley, A.C., and Ramakrishnan, V. (2008). Insights into Translational Termination from the Structure of RF2 Bound to the Ribosome. *Science (80-)*. *322*, 953–956.
- Wiegert, T., and Schumann, W. (2001). SsrA-mediated tagging in *Bacillus subtilis*. *J. Bacteriol.* *183*, 3885–3889.
- Wienk, H., Tishchenko, E., Belardinelli, R., Tomaselli, S., Dongre, R., Spurio, R., Folkers, G.E., Gualerzi, C.O., and Boelens, R. (2012). Structural dynamics of bacterial translation initiation factor IF2. *J. Biol. Chem.* *287*, 10922–10932.
- Wilson, D.N. (2014). Ribosome-targeting antibiotics and mechanisms of bacterial resistance. *Nat. Rev. Microbiol.* *12*, 35–48.
- Wilson, D.N., and Beckmann, R. (2011). The ribosomal tunnel as a functional environment for nascent polypeptide folding and translational stalling. *Curr. Opin. Struct. Biol.* *21*, 274–282.
- Wilson, D.N., Arenz, S., and Beckmann, R. (2016). Translation regulation via nascent polypeptide-mediated ribosome stalling. *Curr. Opin. Struct. Biol.* *37*.
- Wintermeyer, W., and Gualerzi, C. (1983). Effect of *Escherichia coli* initiation factors on the kinetics of N-Acph-e-tRNA^{Phe} binding to 30S ribosomal subunits. A fluorescence stopped-flow study. *Biochemistry* *22*, 690–694.
- Withey, J., and Friedman, D. (1999). Analysis of the role of trans-translation in the requirement of tmRNA for lambda^{dimm}P22 growth in *Escherichia coli*. *J. Bacteriol.* *181*, 2148–2157.
- Witzky, A., Hummels, K.R., Tollerson, R., Rajkovic, A., Jones, L.A., Kearns, D.B., and Ibba, M. (2018). EF-P Posttranslational Modification Has Variable Impact on Polyproline Translation in *Bacillus subtilis*. *MBio* *9*, e00306-18.
- Wöhl, T., Klier, H., Ammer, H., Lottspeich, F., and Magdolen, V. (1993). The HYP2 gene of *Saccharomyces cerevisiae* is essential for aerobic growth: characterization of different isoforms of the hypusine-containing protein Hyp2p and analysis of gene disruption mutants. *Mol. Gen. Genet.* *241*, 305–311.
- Wohlgemuth, I., Beringer, M., and Rodnina, M. V (2006). Rapid peptide bond formation on isolated 50S ribosomal subunits. *EMBO Rep.* *7*, 699–703.
- Wohlgemuth, I., Brenner, S., Beringer, M., and Rodnina, M. V (2008). Modulation of the rate of peptidyl transfer on the ribosome by the nature of substrates. *J. Biol. Chem.* *283*, 32229–32235.

References

- Woolstenhulme, C.J., Guydosh, N.R., Green, R., and Buskirk, A.R. (2015). High-Precision Analysis of Translational Pausing by Ribosome Profiling in Bacteria Lacking EFP. *Cell Rep.* *11*, 13–21.
- Wright, D.E. (1979). The orthosomycins, a new family of antibiotics. *Tetrahedron* *35*, 1207–1237.
- Yamamoto, H., Wittek, D., Gupta, R., Qin, B., Ueda, T., Krause, R., Yamamoto, K., Albrecht, R., Pech, M., and Nierhaus, K.H. (2016). 70S-scanning initiation is a novel and frequent initiation mode of ribosomal translation in bacteria. *Proc. Natl. Acad. Sci. U. S. A.* *113*, E1180-9.
- Yamamoto, T., Shimizu, Y., Ueda, T., and Shiro, Y. (2010). Mg²⁺ dependence of 70 S ribosomal protein flexibility revealed by hydrogen/deuterium exchange and mass spectrometry. *J. Biol. Chem.* *285*, 5646–5652.
- Yanagisawa, T., Sumida, T., Ishii, R., Takemoto, C., and Yokoyama, S. (2010). A paralog of lysyl-tRNA synthetase aminoacylates a conserved lysine residue in translation elongation factor P. *Nat. Struct. Mol. Biol.* *17*, 1136–1143.
- Yanofsky, C., and Horn, V. (1994). Role of regulatory features of the trp operon of *Escherichia coli* in mediating a response to a nutritional shift. *J. Bacteriol.* *176*, 6245–6254.
- Yaron, A., Naider, F., and Scharpe, S. (1993). Proline-dependent structural and biological properties of peptides and proteins. *Crit. Rev. Biochem. Mol. Biol.* *28*, 31–81.
- Yokoyama, T., Shaikh, T.R., Iwakura, N., Kaji, H., Kaji, A., and Agrawal, R.K. (2012). Structural insights into initial and intermediate steps of the ribosome-recycling process. *EMBO J.* *31*, 1836–1846.
- Young, R., and Bremer, H. (1976). Polypeptide-chain-elongation rate in *Escherichia coli* B/r as a function of growth rate. *Biochem. J.* *160*, 185–194.
- Young, D.J., Edgar, C.D., Poole, E.S., and Tate, W.P. (2010). The codon specificity of eubacterial release factors is determined by the sequence and size of the recognition loop. *RNA* *16*, 1623–1633.
- Youngman, E.M., Brunelle, J.L., Kochaniak, A.B., and Green, R. (2004). The active site of the ribosome is composed of two layers of conserved nucleotides with distinct roles in peptide bond formation and peptide release. *Cell* *117*, 589–599.
- Yusupov, M.M., Yusupova, G.Z., Baucom, A., Lieberman, K., Earnest, T.N., Cate, J.H., and Noller, H.F. (2001). Crystal structure of the ribosome at 5.5 Å resolution. *Science* *292*, 883–896.
- Yusupova, G., Jenner, L., Rees, B., Moras, D., and Yusupov, M. (2006). Structural basis for messenger RNA movement on the ribosome. *Nature* *444*, 391–394.
- Zaher, H.S., Shaw, J.J., Strobel, S.A., and Green, R. (2011). The 2'-OH group of the peptidyl-tRNA stabilizes an active conformation of the ribosomal PTC. *EMBO J.* *30*, 2445–2453.
- Zanelli, C.F., Maragno, A.L.C., Gregio, A.P.B., Komili, S., Pandolfi, J.R., Mestriner, C.A., Lustrì, W.R., and Valentini, S.R. (2006). eIF5A binds to translational machinery components and affects translation in yeast. *Biochem. Biophys. Res. Commun.* *348*, 1358–1366.
- Zavialov, A. V., Hauryliuk, V. V., and Ehrenberg, M. (2005). Splitting of the Posttermination Ribosome into Subunits by the Concerted Action of RRF and EF-G. *Mol. Cell* *18*, 675–686.
- Zeng, F., and Jin, H. (2016). Peptide release promoted by methylated RF2 and ArfA in nonstop translation is achieved by an induced-fit mechanism. *RNA* *22*, 49–60.
- Zeng, F., Chen, Y., Remis, J., Shekhar, M., Phillips, J.C., Tajkhorshid, E., and Jin, H. (2017). Structural basis of co-translational quality control by ArfA and RF2 bound to ribosome. *Nature* *541*, 554–557.

References

- Zhang, D., Yan, K., Zhang, Y., Liu, G., Cao, X., Song, G., Xie, Q., Gao, N., and Qin, Y. (2015). New insights into the enzymatic role of EF-G in ribosome recycling. *Nucleic Acids Res.* *43*, 10525–10533.
- Zhou, J., Korostelev, A., Lancaster, L., and Noller, H.F. (2012a). Crystal structures of 70S ribosomes bound to release factors RF1, RF2 and RF3. *Curr. Opin. Struct. Biol.* *22*, 733–742.
- Zhou, J., Korostelev, A., Lancaster, L., and Noller, H.F. (2012b). Crystal structures of 70S ribosomes bound to release factors RF1, RF2 and RF3. *Curr. Opin. Struct. Biol.* *22*, 733–742.
- Zhou, J., Lancaster, L., Trakhanov, S., and Noller, H.F. (2012c). Crystal structure of release factor RF3 trapped in the GTP state on a rotated conformation of the ribosome. *RNA* *18*, 230–240.
- Zhou, J., Lancaster, L., Donohue, J.P., and Noller, H.F. (2013). Crystal structures of EF-G-ribosome complexes trapped in intermediate states of translocation. *Science* *340*, 1236086.
- Zhou, J., Lancaster, L., Donohue, J.P., and Noller, H.F. (2014). How the ribosome hands the A-site tRNA to the P site during EF-G-catalyzed translocation. *Science* (80-.). *345*, 1188–1191.
- Zoldák, G., Redecke, L., Svergun, D.I., Konarev, P. V, Voertler, C.S., Dobbek, H., Sedlák, E., and Sprinzl, M. (2007). Release factors 2 from *Escherichia coli* and *Thermus thermophilus*: structural, spectroscopic and microcalorimetric studies. *Nucleic Acids Res.* *35*, 1343–1353.
- Zou, S.B., Hersch, S.J., Roy, H., Wiggers, J.B., Leung, A.S., Buranyi, S., Xie, J.L., Dare, K., Ibba, M., and Navarre, W.W. (2012a). Loss of Elongation Factor P Disrupts Bacterial Outer Membrane Integrity. *J. Bacteriol.* *194*, 413–425.
- Zou, S.B., Hersch, S.J., Roy, H., Wiggers, J.B., Leung, A.S., Buranyi, S., Xie, J.L., Dare, K., Ibba, M., and Navarre, W.W. (2012b). Loss of elongation factor P disrupts bacterial outer membrane integrity. *J. Bacteriol.* *194*, 413–425.

6 Publications

Publication 1

Arenz, S., Juette, M.F., Graf, M., Nguyen, F., **Huter, P.**, Polikanov, Y.S., Blanchard, S.C., and Wilson, D.N. (2016). Structures of the orthosomycin antibiotics avilamycin and evernimicin in complex with the bacterial 70S ribosome. **Proc. Natl. Acad. Sci. U. S. A.** 113.

Publication 2

Graf, M., Arenz, S., **Huter, P.**, Dönhöfer, A., Nováček, J., and Wilson, D.N. (2017). Cryo-EM structure of the spinach chloroplast ribosome reveals the location of plastid-specific ribosomal proteins and extensions. **Nucleic Acids Res.** 45.

Publication 3

Huter, P., Müller, C., Beckert, B., Arenz, S., Berninghausen, O., Beckmann, R., and Wilson, D.N. (2017). Structural basis for ArfA–RF2-mediated translation termination on mRNAs lacking stop codons. **Nature** 541, 546–549.

Publication 4

Huter, P., Müller, C., Arenz, S., Beckert, B., and Wilson, D.N. (2017). Structural Basis for Ribosome Rescue in Bacteria. **Trends Biochem. Sci.** 42, 669–680.

Publication 5

Huter, P., Arenz, S., Bock, L.V., Graf, M., Frister, J.O, Heuer, A., Peil, L., Starosta, A.L., Wohlgemuth, I., Peske, F., et al. (2017). Structural Basis for Polyproline-Mediated Ribosome Stalling and Rescue by the Translation Elongation Factor EF-P. **Mol. Cell** 68, 515–527.e6.

Structures of the orthosomycin antibiotics avilamycin and evernimicin in complex with the bacterial 70S ribosome

Stefan Arenz^a, Manuel F. Juetter^b, Michael Graf^a, Fabian Nguyen^a, Paul Huter^a, Yury S. Polikanov^{c,d,1}, Scott C. Blanchard^{b,1}, and Daniel N. Wilson^{a,e,1}

^aGene Center and Department for Biochemistry, University of Munich, 81377 Munich, Germany; ^bDepartment of Physiology and Biophysics, Weill Medical College, Cornell University, New York, NY 10065; ^cDepartment of Biological Sciences, University of Illinois at Chicago, Chicago, IL 60607; ^dDepartment of Medicinal Chemistry and Pharmacognosy, University of Illinois at Chicago, Chicago, IL 60607; and ^eCenter for Integrated Protein Science Munich, University of Munich, 81377 Munich, Germany

Edited by Gregory A. Petsko, Weill Cornell Medical College, New York, NY, and approved May 18, 2016 (received for review March 23, 2016)

The ribosome is one of the major targets for therapeutic antibiotics; however, the rise in multidrug resistance is a growing threat to the utility of our current arsenal. The orthosomycin antibiotics evernimicin (EVN) and avilamycin (AVI) target the ribosome and do not display cross-resistance with any other classes of antibiotics, suggesting that they bind to a unique site on the ribosome and may therefore represent an avenue for development of new antimicrobial agents. Here we present cryo-EM structures of EVN and AVI in complex with the *Escherichia coli* ribosome at 3.6- to 3.9-Å resolution. The structures reveal that EVN and AVI bind to a single site on the large subunit that is distinct from other known antibiotic binding sites on the ribosome. Both antibiotics adopt an extended conformation spanning the minor grooves of helices 89 and 91 of the 23S rRNA and interacting with arginine residues of ribosomal protein L16. This binding site overlaps with the elbow region of A-site bound tRNA. Consistent with this finding, single-molecule FRET (smFRET) experiments show that both antibiotics interfere with late steps in the accommodation process, wherein aminoacyl-tRNA enters the peptidyltransferase center of the large ribosomal subunit. These data provide a structural and mechanistic rationale for how these antibiotics inhibit the elongation phase of protein synthesis.

antimicrobial | cryo-EM | evernimicin | rRNA | Zircin

Many clinically used antibiotics target the ribosome to inhibit bacterial growth (1). X-ray crystallography structures have revealed that the majority of antibiotics that target the large ribosomal subunit bind at or near the peptidyl-transferase center (PTC), the active site for peptide bond formation (1, 2). The emergence of multidrug resistance in pathogenic bacteria, which has the potential to render our current arsenal of antibiotics obsolete, highlights the need for the development of new antibiotics that target distinct sites on the ribosome. Although structurally uncharacterized, biochemical and resistance studies indicate that one such class of antibiotics is the orthosomycins (3), which includes evernimicin (originally termed evernimicin, and hereafter referred to as EVN) and avilamycin (AVI) (2).

AVI is produced by *Streptomyces viridochromogenes* strain Tü57 (4), whereas EVN was identified and isolated from the producer *Micromonospora carbonacea* (5, 6). EVN and AVI display excellent antimicrobial activity against Gram-positive bacteria (3), including methicillin-resistant *Staphylococcus aureus* (7), as well as some Gram-negative bacteria, such as *Borrelia burgdorferi* (8). Importantly, strains resistant to EVN and AVI do not display cross-resistance to any other known antimicrobial agents, including ribosome-targeting antibiotics, such as chloramphenicol, tetracycline, or erythromycin (9, 10).

EVN/AVI resistance in *Streptococcus pneumoniae* and in the archaeon *Halobacterium halobium* arises via mutations within helix 89 (H89) and H91 of the 23S rRNA (10–12). Resistance to EVN and AVI also occurs via the action of methyltransferases that

modify H89 and H91 (13, 14). Consistently, both EVN/AVI protect nucleotides within H89 and H91 from chemical modification (11, 12), suggesting that these two rRNA helices comprise at least part of the orthosomycin binding site. Additionally, EVN/AVI resistance has been associated with mutations in Arg-51, Ile-52, and Arg-56 of the ribosomal protein L16 in *Enterococcus faecalis*, *E. faecium*, *S. pneumoniae*, and *S. aureus* (15–18). However, it remains unclear whether these effects are direct consequences of EVN/AVI interacting with L16 or are mediated indirectly via changes in the 23S rRNA, as observed for other ribosomal protein-derived resistance mechanisms (2).

As expected based on the locations of the reported resistance mutations, both AVI and EVN bind to the ribosomal 50S subunit (19) and inhibit protein synthesis in vivo and in vitro (19, 20). Subsequent in vitro studies revealed that EVN inhibits IF2-dependent 70S initiation complex formation (11, 21); however, the inhibitory effect of EVN is not restricted to translation initiation because toeprinting assays indicate that EVN also inhibits translation elongation (22). EVN and AVI do not inhibit puromycin reaction (11, 12) and do not compete for binding with antibiotics that target PTC of the ribosome, such as chloramphenicol, linezolid, lincomycin, or

Significance

The ribosome is the protein-synthesizing machine of the cell and is a major target for antibiotics. The increase in multidrug-resistant bacteria has limited the utility of our current arsenal of clinically used antibiotics, highlighting the need for further development of compounds that have distinct binding sites and do not display cross-resistance. Using cryo-electron microscopy, we have visualized the binding site of the orthosomycins evernimicin and avilamycin on the bacterial 70S ribosome. The binding site and mode of interaction of evernimicin and avilamycin are distinct from other ribosome-targeting antibiotics. Together with single-molecule studies, our structures reveal how the orthosomycin antibiotics inhibit protein synthesis by preventing accommodation of the aminoacyl-tRNA at the A site of the ribosome.

Author contributions: S.A., M.F.J., S.C.B., and D.N.W. designed research; S.A., M.F.J., M.G., F.N., P.H., and Y.S.P. performed research; S.A., M.F.J., Y.S.P., S.C.B., and D.N.W. analyzed data; and S.A., S.C.B., and D.N.W. wrote the paper.

The authors declare no conflict of interest.

This article is a PNAS Direct Submission.

Freely available online through the PNAS open access option.

Data deposition: The cryo-EM maps and models for the EVN- and AVI-SRC have been deposited in the EMDataBank (accession nos. EMD-8238 and EMD-8237) and the Protein Data Bank, www.pdb.org (PDB ID codes 5KCS and 5KCR).

¹To whom correspondence may be addressed. Email: wilson@lmb.uni-muenchen.de, yuryp@uic.edu, or scb2005@med.cornell.edu.

This article contains supporting information online at www.pnas.org/lookup/suppl/doi:10.1073/pnas.1604790113/-DCSupplemental.

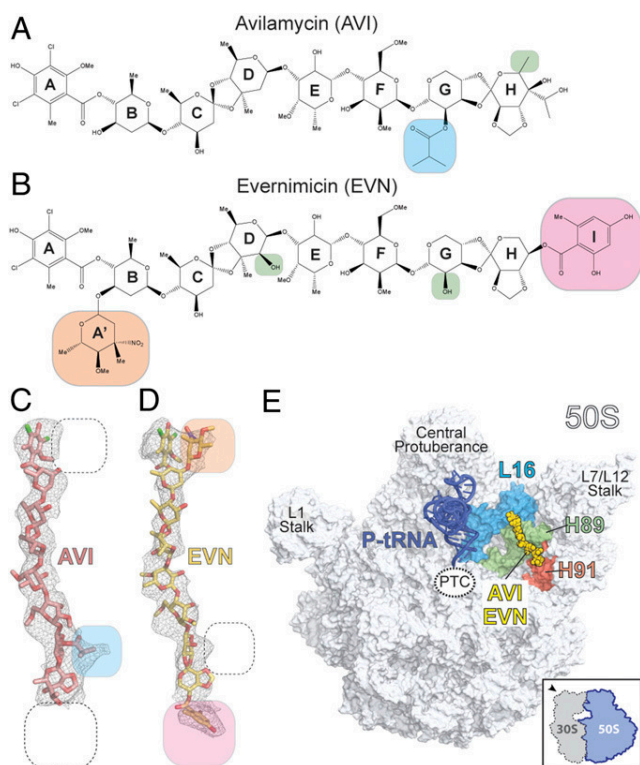


Fig. 1. Cryo-EM reconstructions of EVN- and AVI-SRC. (A and B) Chemical structures of the orthosomycins AVI (A) and EVN (B), with compositional differences highlighted. (C and D) Cryo-EM electron densities (gray mesh) with fitted models for AVI (red; C) and EVN (yellow; D). (E) Overview of EVN/AVI binding site on the 70S ribosome (50S, gray, and 30S subunit omitted for clarity). Binding position of EVN/AVI (yellow) is shown relative to the P-site tRNA (blue), ribosomal protein L16 (cyan), H89 (green), and H91 (red).

clindamycin (19). Moreover, EVN has no inhibitory effect on the ribosome-dependent GTPase activity of EF-G (21). EVN and AVI are hypothesized to inhibit elongation by preventing tRNA binding to the A site (12, 20); however, this model remains to be conclusively demonstrated.

AVI has long been used in animal feed as a growth promoter (Surmax/Maxus; Elanco Animal Health), thereby limiting its clinical usefulness. However, EVN (SCH27899; Ziracin) underwent phase II/III clinical trials before being dropped in 2000 by Schering-Plough because of side effects and poor solubility. Nevertheless, the lack of cross-resistance between AVI/EVN and other clinically used ribosome-targeting antibiotics makes the orthosomycins attractive for further investigation (9, 10). The total chemical synthesis of EVN (23) and the biosynthesis of novel AVI derivatives with improved solubility (24) provide a good basis for further drug development; however, a structural understanding of how these antibiotics interact with the ribosome is necessary to facilitate rational design of improved orthosomycin derivatives.

Here we present two cryo-EM structures of EVN or AVI in complex with the *Escherichia coli* 70S ribosome at 3.6- to 3.9-Å resolution. These structures reveal that the conserved heptasaccharide core of both orthosomycins spans across the minor grooves of H89 and H91 of the 23S rRNA, whereas the terminal dichloro-ring interacts with the arginine residues of ribosomal protein L16. The binding positions of EVN and AVI overlap with the elbow region of a tRNA bound in the A site. Consistently, single-molecule FRET (smFRET) imaging of the tRNA selection process demonstrates that EVN and AVI allow initial

binding of aminoacyl-tRNA (aa-tRNA) at the A site, but prevent complete accommodation of the incoming aa-tRNA, thus providing a structural explanation of how orthosomycin antibiotics inhibit translation elongation.

Results and Discussion

Cryo-EM Structures of EVN and AVI in Complex with the *E. coli* 70S Ribosome.

To determine the structures of EVN and AVI on the ribosome, we prepared Erm-stalled ribosome complexes (SRCs) as reported (25, 26). The SRCs were incubated with either 100 μ M EVN or AVI, and the complexes were then subjected to single-particle cryo-EM analysis (*Materials and Methods*). The resulting cryo-EM reconstructions of the EVN- and AVI-SRC had an average resolution of 3.9 and 3.6 Å, respectively, with local resolution extending to 3.5 Å within the core of the ribosome (Fig. S1). Careful analysis of the cryo-EM maps revealed only a single binding site of EVN on the 50S subunit of the 70S ribosome, consistent with previous biochemical studies showing a 1:1 stoichiometry of EVN with the 50S subunit (19). In contrast to early reports that AVI binds to the 30S subunit (20), we observed only a single AVI binding site on the 50S subunit at the same location as EVN, a result that is consistent with the competition between these two antibiotics for ribosome binding (19).

AVI has a terminal dichloroisoevernic acid moiety (ring A) linked to a linear heptasaccharide chain consisting of D-olivose (rings B and C), 2-deoxy-D-evalose (ring D), 4-O-methyl-D-fucose (ring E), 2,6-di-O-methyl-D-mannose (ring F), the unusual pentose L-lyxose (ring G), and the bicyclic eurekaanate (ring H) (ref. 27; Fig. 1A). Similar to AVI, EVN contains a nearly identical core heptasaccharide chain, but, unlike AVI, EVN is branched by a 2-deoxy- β -glycoside nitrosugar (ring A') attached to ring B, and also contains an additional terminal benzyl moiety (ring I) attached to eurekaanate ring H (28) (Fig. 1B). The presence of distinct electron density corresponding to the additional rings A' and I of EVN in the cryo-EM map of the EVN-SRC, and absence of the same features in the AVI-SRC map, enabled us to unambiguously orient both AVI and EVN on the ribosome (Fig. 1C and D). Despite the good fit of the refined molecular models to the cryo-EM electron density maps, higher resolution will be required to provide an unambiguous description of the hydrogen-bond interactions of the

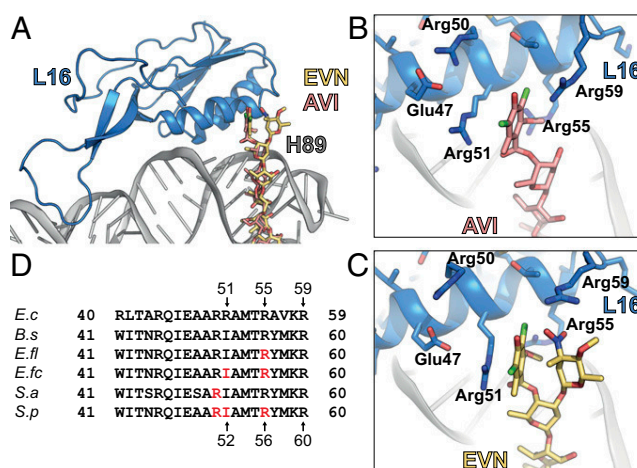


Fig. 2. Interactions of EVN and AVI with the ribosomal protein L16. (A) Overview of L16 (blue) interactions with EVN (gold) and AVI (red). (B and C) Close-up views of showing interactions between Arg-51, -55, and -59 of L16 (blue) and ring A of AVI (B) and rings A and A' of EVN (C). (D) Sequence alignment of the L16 from *E. coli* (*E.c*), *B. subtilis* (*B.s*), *E. faecalis* (*E.fl*), *E. faecium* (*E.fc*), *S. aureus* (*S.a*), and *S. pneumoniae* (*S.p*), with residues conferring resistance to EVN and AVI highlighted in red.

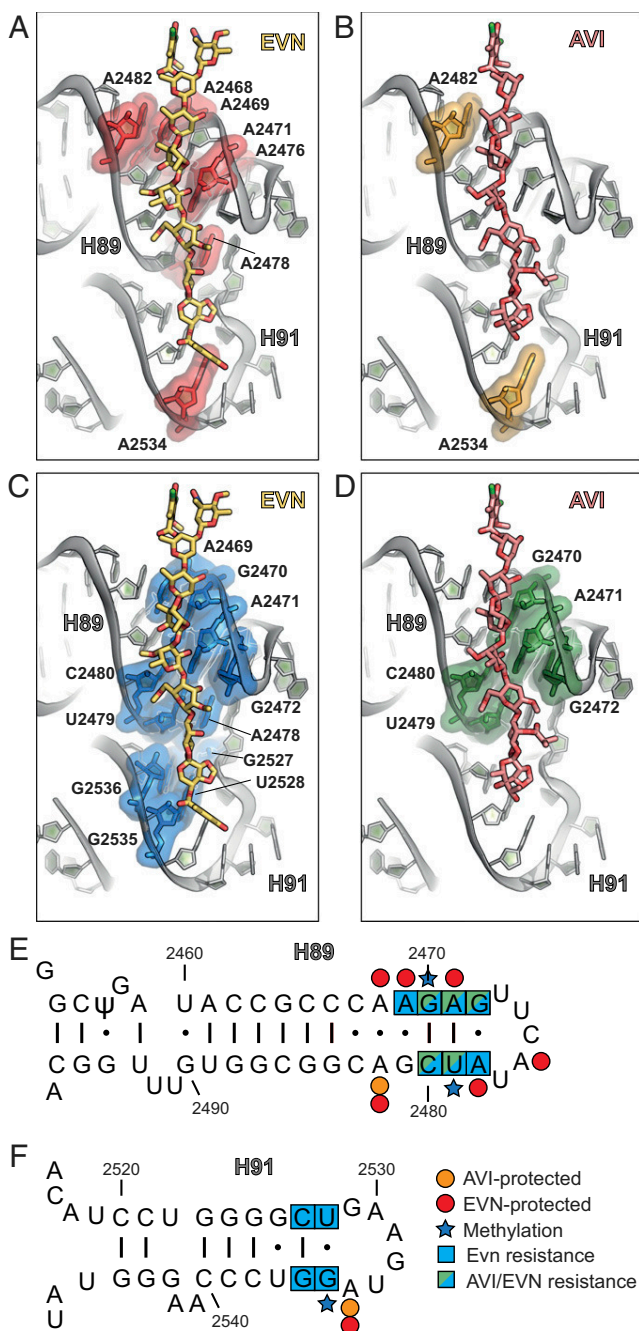


Fig. 3. Interactions of EVN and AVI with H89 and H91 of the 23S rRNA. (A and B) Binding site of EVN (gold) (A) and AVI (red) (B), with nucleotides in H89 and H91 protected from DMS modification highlighted in red and orange, respectively. (C and D) Binding site of EVN (gold) (C) and AVI (red) (D), with resistance mutations in H89 and H91 highlighted in blue and green, respectively. (E and F) Secondary structure of 23S rRNA with zoom on H89 (E) and H91 (F), with nucleotides protected by EVN (red) and AVI (orange), EVN (blue) and AVI (green) resistance mutations and methylations (blue star) as indicated (10–18).

drugs with the ribosome. Nevertheless, these structures reveal that both drugs adopt elongated conformations on the ribosome, with the heptasaccharide rings B–H of both orthosomycins inserting into the minor grooves of H89 and H91 of the 23S rRNA (Fig. 1E and Movie S1) and the terminal ring A interacting with ribosomal protein L16 (Fig. 2A).

Interactions of EVN/AVI with Arginine Residues of L16. The terminal dichloroioevermic acid moiety (ring A) of AVI establishes stacking interactions with the side chain of Arg-51 of L16 (Fig. 2A and B and Movie S1). In addition, the side chains of Arg-55 and -59 also approach ring A of AVI (Fig. 2B); however, the density for these side chains is less well defined. In contrast to AVI, the electron density for the terminal region of EVN is bifurcated (Fig. 1D), consistent with the presence of the additional 2-deoxy- β -glycoside nitrosugar (ring A') (Fig. 1B). Unfortunately, the resolution does not allow unambiguous assignment of ring A and A' to the bifurcated density. Therefore, our current model is based on the rationale that ring A of EVN occupies the same position as ring A of AVI, and the remaining density is then assigned to the ring A' (Fig. 2C). Sequence alignments (Fig. 2D), as well as comparison with the structures of the *B. subtilis* 70S ribosome (29) and *S. aureus* 50S subunit (30) (Fig. S2), reveals that *E. coli* Arg-51 and -55 are equivalent to Ile-52 and Arg-56 in most Gram-positive bacteria. Consistently, mutations of Arg-56–His or Ile-52–Ser/Thr/Asn in L16 render *E. faecalis*, *E. faecium*, and *S. pneumoniae* isolates resistant to EVN and AVI (15–17). Chemical mutagenesis experiments in *S. aureus* led to the identification of strains with Arg-51–Cys or Arg-51–His mutations in L16 that conferred increased resistance to both compounds (18). In our structure, residue Arg-50 (*E. coli*), equivalent to residue Arg-51 in *S. aureus*, does not contact the drug (Fig. 2B and C and Fig. S2). This finding suggests that the Arg-51–Cys/His mutations may indirectly confer EVN/AVI resistance in *S. aureus*, possibly by affecting the neighboring Ile-52 residue. Alternatively, EVN/AVI may interact with *S. aureus* ribosomes using a slightly different binding mode that enables direct interaction between Arg-51 and the drugs. Nevertheless, the finding that both EVN and AVI directly interact with L16 in the region where EVN/AVI resistance mutations occur illustrates the importance of this interaction for drug binding. Moreover, it also reveals that resistance occurs because the mutations directly perturb drug binding, rather than indirectly preventing drug binding by distorting the local rRNA conformation of H89/H91.

Interaction of EVN and AVI with H89 and H91 of the 23S rRNA. Within the limits of the present resolution, we observed no significant difference between the interaction of the conserved heptasaccharide cores of EVN and AVI with H89 and H91 of the 23S rRNA (Fig. 3A–D). The largest interaction surface between the drugs and the ribosome encompasses rings B–F of EVN/AVI and the minor groove of H89, specifically, nucleotides A2468–G2472 and A2478–A2482 (Fig. 3A–D), which base pair to form the stem of H89 (Fig. 3E). Additional interactions were observed between rings G and H of EVN/AVI with the minor groove of H91 (Fig. 3A–D) formed by nucleotides G2527–U2528 and A2534–G2536 (Fig. 3F). This interaction pattern is consistent with footprinting data on *E. coli*, *E. faecium*, and *H. halobium* ribosomes showing that EVN protects multiple nucleotides within H89, including A2468, A2469, A2471, A2476, A2478, and A2482, as well as nucleotide A2534 in H91, from chemical modification by dimethyl sulfate (DMS) (11, 13) (Fig. 3A, E, and F). Similarly, AVI protects A2482 in H89 and A2534 in H91 from chemical modification by DMS on *E. coli* 70S ribosomes (12) (Fig. 3B, E, and F). The terminal benzyl moiety (ring I) of EVN establishes additional interactions with nucleotides within the loop of H91 (Fig. 3A and C), which may contribute to the higher potency of EVN compared with AVI.

Resistance to EVN/AVI via 23S rRNA Mutations. A striking correlation exists between the nucleotides that comprise the EVN/AVI binding site observed here and the reported mutations in 23S rRNA that confer resistance to these two drugs (Fig. 3C–F). In *S. pneumoniae*, selection for EVN resistance led to the identification of 23S rRNA mutations A2469C, C2480U (in H89), G2535A, or G2536C (in H91) (ref. 10; Fig. 3C, E, and F). The G2535A mutation was also subsequently reported to confer EVN resistance in *E. faecalis* (16). The archaeon *H. halobium* has also been used to select for EVN

resistance, producing A2471G/C, A2478C, U2479C, and C2480A/U mutations in H89 and G2527A, U2528A, and G2535A mutations in H91 (11) (Fig. 3 C, E, and F). In contrast, selection for AVI using *H. halobium* only led to the identification of mutations within H89, namely, G2470U, A2471G, G2473U, U2479C, and C2480U (12) (Fig. 3 D and E). The increased frequency of resistance mutations located in H89, as well as the higher resistance conferred by these mutations compared with H91 mutations (11, 12), emphasizes the importance of the extensive interaction surface between rings B-F of EVN/AVI and nucleotides comprising the minor groove of H89. Because all of the reported mutations are expected to alter base-pairing potential, resistance is likely to arise from distortions of the helical geometry of H89 and H91, which thereby reduce the affinity of the drugs for their binding site.

Resistance to EVN/AVI via Methylation of the 23S rRNA. Analysis of the binding site of EVN and AVI reveals a structural basis for the resistance obtained via posttranslational modifications of nucleotides within H89 and H91 (13, 14) (Fig. 4). *S. viridochromogenes* Tü57, the producer of AVI, expresses two methyltransferases, AviRa and AviRb, which confer resistance to EVN/AVI. Whereas AviRb methylates the ribose 2'OH of U2479 within H89 to confer high-level AVI resistance, AviRa methylates the N7 position of G2535 within H91 to confer low-level resistance (14, 31). Inspection of the EVN/AVI binding site reveals that a 2'-O-methylation of U2479 would lead to a direct clash with ring F of the drug (Fig. 4A). In contrast, N7-methylation of G2535 appears to neither interfere with the drug binding (Fig. 4B) nor disrupt base pairing with U2528, suggesting that methylation at this position indirectly confers resistance by inducing local conformational changes, possibly during ribosome assembly. We note that both AviRa and AviRb are required to obtain full protection against the AVI (31), suggesting that they function in a synergistic manner, similar to the methyltransferases that cause resistance to tylosin (32). The EVN methyltransferase EmtA, which was identified on a plasmid-borne insertion element in EVN-resistant *E. faecium* strains (isolated from animals given AVI as a growth promotant), was shown to methylate G2470 of H89 (13). Although the exact site of the modification has not been identified, we note that methylation of the N2 position of G2470 or the ribose 2'OH would lead to a direct clash with rings D and C, respectively, of EVN/AVI (Fig. 4C), whereas an N7-methylation would most likely confer resistance indirectly via conformational changes.

Inhibition of IF2 and A-tRNA Accommodation by EVN and AVI. EVN has been reported to inhibit formation of the IF2-dependent 70S initiation complex (70S-IC) (11, 21). Therefore, we compared the binding sites of EVN/AVI relative to structures of IF2 on the 70S ribosome (33) and 30S subunit (34, 35). No overlap was observed between EVN/AVI and IF2 on the 70S, with the shortest distance between ring E of EVN/AVI being 2–3 Å away from the linker

between domains III and IV of IF2 (Fig. S3). In contrast, alignment of IF2-30S complex to the AVI/EVN-SRC reveals a slight overlap between EVN/AVI and domain IV of IF2 (Fig. S3), suggesting that EVN/AVI may interfere with IF2-dependent 70S-IC formation by blocking a transient intermediate state of IF2 that arises upon subunit binding and transition from the 30S-IC to the 70S-IC.

EVN and AVI have also been suggested to inhibit translation elongation by interfering with the tRNA binding to the A site of the ribosome (12, 20, 22). Therefore, we compared the binding position of EVN/AVI relative to the tRNA in the A/T state observed during decoding when the aa-tRNA is bound to the ribosome but still remains in complex with EF-Tu (36, 37), as well as with the tRNA in the classical A/A state in which the acceptor arm of the aa-tRNA is released from EF-Tu and has accommodated at the PTC on the large ribosomal subunit (38). These comparisons show that the EVN/AVI binding site does not overlap with aa-tRNA within the A/T state, whereas there is direct clash between rings A-C of EVN/AVI and nucleotides 51–53 within the stem region of the T Ψ C-loop (elbow region) of fully accommodated aa-tRNA (Fig. 5A, Fig. S4, and Movie S1).

To investigate the impact of EVN and AVI on the selection and accommodation of aa-tRNA, we used pre-steady-state smFRET measurements that enable real-time visualization of tRNA motion during EF-Tu-catalyzed delivery of aa-tRNA to surface-immobilized ribosomes (39–41) (Fig. 5B). Here, the time evolution of FRET efficiency was monitored at 10 ms per frame time resolution within individual 70S ribosomes bound with (Cy3-s⁴U8)-labeled fMet-tRNA^{Met} in the P site upon stopped-flow injection of ternary complex containing EF-Tu, GTP and (LD650-acp³U47)-labeled Phe-tRNA^{Phe} (Fig. 5B). As expected from previous studies (40, 41), in the absence of the drug, productive FRET events leading to the incorporation of aa-tRNA at the A site evolved from a low (~0.2) to high (~0.63) FRET state via the reversible transit of at least one intermediate (~0.35) FRET configuration, which reflects the A/T state of the A-site tRNA (Fig. 5B and C) (39, 40). Consistent with rapid aa-tRNA progression through the selection process, the time delay between the initial observation of low FRET and formation of the stable, high-FRET state, corresponding to the fully accommodated, classically configured A/A-tRNA position, was ~60 ms (~16 s⁻¹) (Fig. 5B and C and Fig. S5).

In the presence of saturating concentrations (20 μ M) of EVN or AVI, aa-tRNA progression into the ribosome was strongly and specifically blocked during the transition between the A/T state (~0.35 FRET) and the fully accommodated A/A state (~0.63 FRET) (Fig. 5D and E and Fig. S5). To examine the dynamics underlying this inhibition, we visualized the ensemble of observed molecular transitions using transition density plots (42). In this representation, observed transitions appear as peaks in a 2D histogram of initial and final FRET efficiencies (Fig. 5F–H). The peak corresponding to reverse transitions from high to intermediate

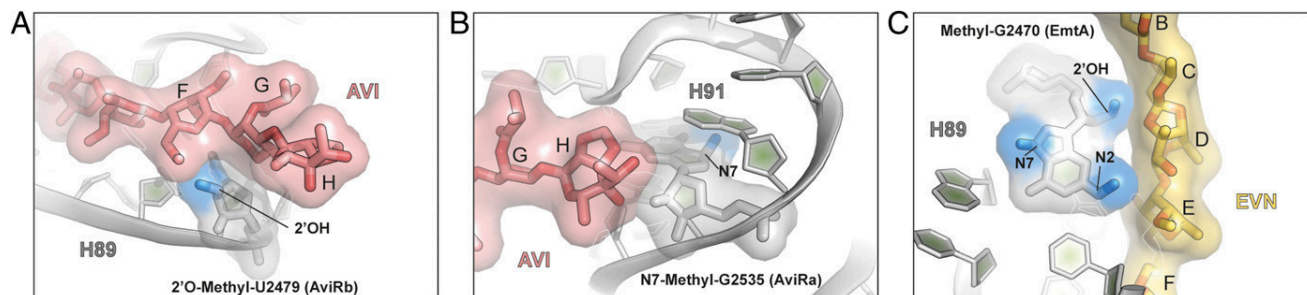


Fig. 4. Structural basis for EVN/AVI resistance via methylation of the 23S rRNA residues. (A) The 2'-O-methylation of U2479 in H89 by AviRb (14) clashes with the ring F of the drug. (B) N7 methylation of G2535 in H91 by AviRa (14) is located distal from the AVI binding site. (C) Methylation of the 2'OH of the ribose or N2 position in the nucleobase of G2470 by EmtA (13) clashes with EVN (gold), whereas the N7 position is distal to the drug-binding site.

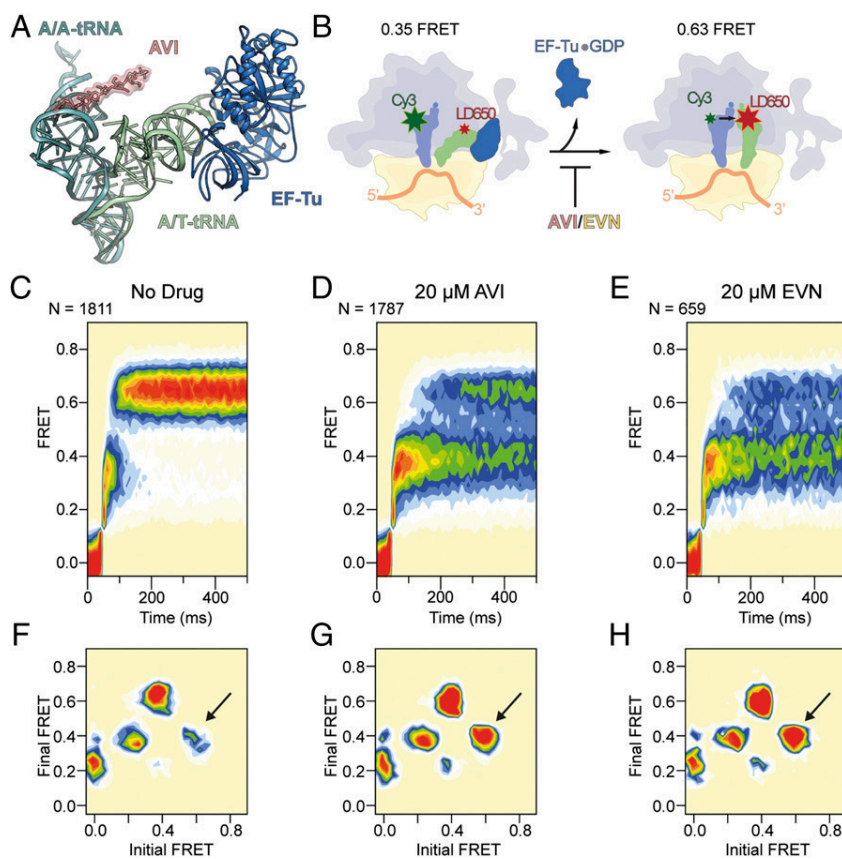


Fig. 5. EVN/AVI inhibit accommodation of tRNA into the A site. (A) Comparison of the relative binding positions on the ribosome of AVI (red), EF-Tu (blue), A/T-tRNA (green) (36, 56), and A/A-tRNA (teal) (38). (B) Schematic diagram of smFRET measurements of tRNA selection. After delivery of EF-Tu-GTP-tRNA ternary complex containing cognate Phe-tRNA^{Phe}(LD650) to the A site of *E. coli* 70S ribosomes containing tRNA^{Met}(Cy3) in the P site, tRNA motion can be tracked through the progression of FRET efficiencies from low (0.2) to intermediate (0.35) FRET during initial steps of selection to high (0.63) FRET upon A-site tRNA accommodation, which is inhibited by AVI/EVN. (C–E) Ensemble smFRET histograms showing the time course of aa-tRNA selection, imaged in the absence of drugs (C) or in the presence of 20 μ M AVI (D) or 20 μ M EVN (E). The histograms were postsynchronized by aligning each observed event to the first appearance of nonzero FRET states. (F–H) Transition density plots for the data shown in C–E, respectively. These 2D histograms juxtapose the FRET efficiencies immediately before and after FRET transitions. As indicated by arrows, EVN and AVI promote reversible transitions between high and intermediate FRET.

FRET is significantly enhanced in the presence of both EVN or AVI (arrows in Fig. 5 F–H), confirming that inhibition was characterized by an exacerbation of the reversible excursions between A/T and accommodated positions that normally accompany proofreading (40) (Fig. S4). These findings are in agreement with toeprinting experiments demonstrating that 70S ribosomes initiated on the AUG start codon of mRNA do not proceed into the elongation phase of translation when increasing concentrations of EVN or AVI are present (Fig. S6). Our findings contrast with a previous report (22) in which Evn did not appear to significantly affect the first elongation cycle, but, rather, allowed successive rounds of elongation before inhibition was observed. One possibility for this discrepancy is that the strength of the inhibition of the orthosomycins depends on the nature of the aa-tRNA that is being accommodated.

Conclusion

The cryo-EM structures of EVN- and AVI-SRC reported here reveal that both orthosomycins bind to a single site on the large subunit that is distinct from other known antibiotic binding sites on the ribosome (Fig. S7), explaining the lack of cross-resistance with other ribosome-targeting antibiotics (9, 10). The orthosomycin binding site comprises the minor grooves of H89 and H91 of the 23S rRNA, as well as arginine residues of L16 (Fig. 1E), consistent with available chemical protection and resistance data (Figs. 2–4) (10–18). The binding position for EVN and AVI provides a structural explanation for how the orthosomycins inhibit IF2-dependent 70S-IC formation (11, 21)—namely, by interfering with the transition from the IF2-30S conformation to the IF2-70S that occurs upon subunit joining (Fig. S3). Additionally, our smFRET data demonstrate that both EVN and AVI interfere with the accommodation of aa-tRNA at the A site of the ribosome (Fig. 5 C–H), consistent with the overlap between EVN/AVI and the elbow region of a fully accommodated A-tRNA (Fig. S4). Overall, our study also demonstrates that cryo-EM can be

used to determine de novo the binding site of antibiotics on the bacterial ribosome, as was also recently demonstrated for the antiprotozoan drug emetine in complex with the *Plasmodium falciparum* 80S ribosome (43).

Materials and Methods

The SRCs were prepared essentially as described (25, 44). Cryo-EM data collection was performed on the Titan Krios (FEI) 300-kV TEM equipped with a Falcon II direct electron detector. Images of individual ribosome particles were aligned by using Motion Correction software (45), and then particles were selected automatically by using SIGNATURE (46). All images were processed by using a frequency-limited refinement protocol that prevents overfitting (47) using the SPIDER software package (48), as described (25, 44). The final maps were subjected to the program EM-BFACTOR (49) to apply an automatically determined negative B factor for sharpening of the map, and local resolution was calculated by using ResMap (50). Molecular models were fitted and adjusted by using COOT (51) and refined in Phenix (52). Model validation was carried out by using the MolProbity server (53), and the final model statistics are presented in Table S1. All figures showing atomic models as well as Movie S1 were generated by using PyMOL (Schrödinger). Fig. S1 was generated by using Chimera (54). The smFRET experiments were performed as described (39–41, 55). Further details can be found in *SI Materials and Methods*. The cryo-EM maps and models for the EVN- and AVI-SRC have been deposited in the EMDatabank (accession nos. EMD-8238 and EMD-8237) and the Protein Data Bank (PDB ID codes 5KCS and 5KCR).

ACKNOWLEDGMENTS. We thank Rishi Matadeen and Sacha DeCarlo for data collection at the NeCEN facility, Leiden, The Netherlands; Charlotte Ungewickell for expert technical assistance; and Shura Mankin and Birte Vester for kindly providing copious amounts of EVN and AVI, respectively. This research was supported by Deutsche Forschungsgemeinschaft Grants FOR1805, WI3285/3-2, and GRK1721 (to D.N.W.); National Institutes of Health Grants GM079238 and GM098859 (to S.C.B.); the Human Frontiers of Science Program (D.N.W. and S.C.B.); and the Illinois State startup funds (Y.S.P.).

- Wilson DN (2014) Ribosome-targeting antibiotics and mechanisms of bacterial resistance. *Nat Rev Microbiol* 12(1):35–48.
- Wilson DN (2009) The A-Z of bacterial translation inhibitors. *Crit Rev Biochem Mol Biol* 44(6):393–433.
- Wright D (1979) The orthosomycins, a new family of antibiotics. *Tetrahedron* 35(10):1209–1327.
- Buzzetti F, et al. (1968) [Avilamycin]. *Experientia* 24(4):320–323.
- Wagman GH, Luedemann GM, Weinstein MJ (1964) Fermentation and isolation of evernimicin. *Antimicrob Agents Chemother (Bethesda)* 10:33–37.
- Weinstein MJ, Luedemann GM, Oden EM, Wagman GH (1964) Evernimicin, a new antibiotic complex from *Micromonospora Carbonacea*. *Antimicrob Agents Chemother (Bethesda)* 10:24–32.
- Boucher HW, Thauvin-Eliopoulos C, Loebenberg D, Eliopoulos GM (2001) In vivo activity of evernimicin (SCH 27899) against methicillin-resistant *Staphylococcus aureus* in experimental infective endocarditis. *Antimicrob Agents Chemother* 45(1):208–211.
- Dever LL, Torigan CV, Barbour AG (1999) In vitro activities of the evernimicin SCH 27899 and other newer antimicrobial agents against *Borrelia burgdorferi*. *Antimicrob Agents Chemother* 43(7):1773–1775.
- Sanders WE, Jr, Sanders CC (1974) Microbiological characterization of evernimicins B and D. *Antimicrob Agents Chemother* 6(3):232–238.
- Adrian PV, et al. (2000) Evernimicin (SCH27899) inhibits a novel ribosome target site: analysis of 23S ribosomal DNA mutants. *Antimicrob Agents Chemother* 44(11):3101–3106.
- Belova L, Tenson T, Xiong L, McNicholas PM, Mankin AS (2001) A novel site of antibiotic action in the ribosome: Interaction of evernimicin with the large ribosomal subunit. *Proc Natl Acad Sci USA* 98(7):3726–3731.
- Kofoed CB, Vester B (2002) Interaction of avilamycin with ribosomes and resistance caused by mutations in 23S rRNA. *Antimicrob Agents Chemother* 46(11):3339–3342.
- Mann PA, et al. (2001) EmtA, a rRNA methyltransferase conferring high-level evernimicin resistance. *Mol Microbiol* 41(6):1349–1356.
- Treede I, et al. (2003) The avilamycin resistance determinants AviRa and AviRb methylate 23S rRNA at the guanosine 2535 base and the uridine 2479 ribose. *Mol Microbiol* 49(2):309–318.
- Aarestrup FM, Jensen LB (2000) Presence of variations in ribosomal protein L16 corresponding to susceptibility of enterococci to oligosaccharides (avilamycin and evernimicin). *Antimicrob Agents Chemother* 44(12):3425–3427.
- Zarazaga M, Tenorio C, Del Campo R, Ruiz-Larrea F, Torres C (2002) Mutations in ribosomal protein L16 and in 23S rRNA in *Enterococcus* strains for which evernimicin MICs differ. *Antimicrob Agents Chemother* 46(11):3657–3659.
- Adrian PV, et al. (2000) Mutations in ribosomal protein L16 conferring reduced susceptibility to evernimicin (SCH27899): Implications for mechanism of action. *Antimicrob Agents Chemother* 44(3):732–738.
- McNicholas PM, et al. (2001) Effects of mutations in ribosomal protein L16 on susceptibility and accumulation of evernimicin. *Antimicrob Agents Chemother* 45(1):79–83.
- McNicholas PM, et al. (2000) Evernimicin binds exclusively to the 50S ribosomal subunit and inhibits translation in cell-free systems derived from both gram-positive and gram-negative bacteria. *Antimicrob Agents Chemother* 44(5):1121–1126.
- Wolf H (1973) Avilamycin, an inhibitor of the 30S ribosomal subunits function. *FEBS Lett* 36(2):181–186.
- Mikolajka A, et al. (2011) Differential effects of thiopeptide and orthosomycin antibiotics on translational GTPases. *Chem Biol* 18(5):589–600.
- Orelle C, et al. (2013) Tools for characterizing bacterial protein synthesis inhibitors. *Antimicrob Agents Chemother* 57(12):5994–6004.
- Nicolaou KC, et al. (2000) Total synthesis of evernimicin 13,384-1-Part 4: Explorations of methodology; stereocontrolled synthesis of 1,1'-disaccharides, 1,2-seleno migrations in carbohydrates, and solution- and solid-phase synthesis of 2-deoxy glycosides and orthoesters. *Chemistry* 6(17):3166–3185.
- Weitnauer G, et al. (2004) Novel avilamycin derivatives with improved polarity generated by targeted gene disruption. *Chem Biol* 11(10):1403–1411.
- Arenz S, et al. (2014) Drug sensing by the ribosome induces translational arrest via active site perturbation. *Mol Cell* 56(3):446–452.
- Arenz S, Nguyen F, Beckmann R, Wilson DN (2015) Cryo-EM structure of the tetracycline resistance protein TetM in complex with a translating ribosome at 3.9-Å resolution. *Proc Natl Acad Sci USA* 112(17):5401–5406.
- Boll R, et al. (2006) The active conformation of avilamycin A is conferred by AviX12, a radical AdoMet enzyme. *J Biol Chem* 281(21):14756–14763.
- Ganguly AK (2000) Ziracin, a novel oligosaccharide antibiotic. *J Antibiot (Tokyo)* 53(10):1038–1044.
- Sohmen D, et al. (2015) Structure of the *Bacillus subtilis* 70S ribosome reveals the basis for species-specific stalling. *Nat Commun* 6:6941.
- Eyal Z, et al. (2015) Structural insights into species-specific features of the ribosome from the pathogen *Staphylococcus aureus*. *Proc Natl Acad Sci USA* 112(43):E5805–E5814.
- Weitnauer G, et al. (2001) An ATP-binding cassette transporter and two rRNA methyltransferases are involved in resistance to avilamycin in the producer organism *Streptomyces viridochromogenes* Tu57. *Antimicrob Agents Chemother* 45(3):690–695.
- Liu M, Douthwaite S (2002) Resistance to the macrolide antibiotic tylosin is conferred by single methylations at 23S rRNA nucleotides G748 and A2058 acting in synergy. *Proc Natl Acad Sci USA* 99(23):14658–14663.
- Sprink T, et al. (2016) Structures of ribosome-bound initiation factor 2 reveal the mechanism of subunit association. *Sci Adv* 2(3):e1501502.
- Simonetti A, et al. (2008) Structure of the 30S translation initiation complex. *Nature* 455(7211):416–420.
- Simonetti A, et al. (2013) Involvement of protein IF2 N domain in ribosomal subunit joining revealed from architecture and function of the full-length initiation factor. *Proc Natl Acad Sci USA* 110(39):15656–15661.
- Schmeing TM, et al. (2009) The crystal structure of the ribosome bound to EF-Tu and aminoacyl-tRNA. *Science* 326(5953):688–694.
- Fischer N, et al. (2015) Structure of the *E. coli* ribosome-EF-Tu complex at <3 Å resolution by C-corrected cryo-EM. *Nature* 520:567–570.
- Selmer M, et al. (2006) Structure of the 70S ribosome complexed with mRNA and tRNA. *Science* 313(5795):1935–1942.
- Blanchard SC, Gonzalez RL, Kim HD, Chu S, Puglisi JD (2004) tRNA selection and kinetic proofreading in translation. *Nat Struct Mol Biol* 11(10):1008–1014.
- Geggie P, et al. (2010) Conformational sampling of aminoacyl-tRNA during selection on the bacterial ribosome. *J Mol Biol* 399(4):576–595.
- Juette MF, et al. (2016) Single-molecule imaging of non-equilibrium molecular ensembles on the millisecond timescale. *Nat Methods* 13(4):341–344.
- McKinney SA, Joo C, Ha T (2006) Analysis of single-molecule FRET trajectories using hidden Markov modeling. *Biophys J* 91(5):1941–1951.
- Wong W, et al. (2014) Cryo-EM structure of the *Plasmodium falciparum* 80S ribosome bound to the anti-protozoan drug emetine. *eLife* 3:3.
- Arenz S, et al. (2014) Molecular basis for erythromycin-dependent ribosome stalling during translation of the ErmBL leader peptide. *Nat Commun* 5:3501.
- Li X, et al. (2013) Electron counting and beam-induced motion correction enable near-atomic-resolution single-particle cryo-EM. *Nat Methods* 10(6):584–590.
- Chen JZ, Grigorieff N (2007) SIGNATURE: A single-particle selection system for molecular electron microscopy. *J Struct Biol* 157(1):168–173.
- Scheres SH, Chen S (2012) Prevention of overfitting in cryo-EM structure determination. *Nat Methods* 9(9):853–854.
- Frank J, et al. (1996) SPIDER and WEB: Processing and visualization of images in 3D electron microscopy and related fields. *J Struct Biol* 116(1):190–199.
- Fernández JJ, Luque D, Castón JR, Carrascosa JL (2008) Sharpening high resolution information in single particle electron cryomicroscopy. *J Struct Biol* 164(1):170–175.
- Kucukelbir A, Sigworth FJ, Tagare HD (2014) Quantifying the local resolution of cryo-EM density maps. *Nat Methods* 11(1):63–65.
- Emsley P, Cowtan K (2004) Coot: Model-building tools for molecular graphics. *Acta Crystallogr D Biol Crystallogr* 60(Pt 12 Pt 1):2126–2132.
- Adams PD, et al. (2010) PHENIX: A comprehensive Python-based system for macromolecular structure solution. *Acta Crystallogr D Biol Crystallogr* 66(Pt 2):213–221.
- Chen VB, et al. (2010) MolProbity: All-atom structure validation for macromolecular crystallography. *Acta Crystallogr D Biol Crystallogr* 66(Pt 1):12–21.
- Pettersen EF, et al. (2004) UCSF Chimera—A visualization system for exploratory research and analysis. *J Comput Chem* 25(13):1605–1612.
- Munro JB, Altman RB, O'Connor N, Blanchard SC (2007) Identification of two distinct hybrid state intermediates on the ribosome. *Mol Cell* 25(4):505–517.
- Schuette JC, et al. (2009) GTPase activation of elongation factor EF-Tu by the ribosome during decoding. *EMBO J* 28(6):755–765.
- Rohou A, Grigorieff N (2015) CTFFIND4: Fast and accurate defocus estimation from electron micrographs. *J Struct Biol* 192(2):216–221.
- Becker T, et al. (2012) Structural basis of highly conserved ribosome recycling in eukaryotes and archaea. *Nature* 482(7386):501–506.
- Loerke J, Giesebrecht J, Spahn CM (2010) Multiparticle cryo-EM of ribosomes. *Methods Enzymol* 483:161–177.
- Noeske J, et al. (2015) High-resolution structure of the *Escherichia coli* ribosome. *Nat Struct Mol Biol* 22(4):336–341.
- Noeske J, et al. (2014) Synergy of streptogramin antibiotics occurs independently of their effects on translation. *Antimicrob Agents Chemother* 58(9):5269–5279.
- Demeshkina N, Jenner L, Westhof E, Yusupov M, Yusupova G (2012) A new understanding of the decoding principle on the ribosome. *Nature* 484(7393):256–259.
- Schüttelkopf AV, van Aalten DM (2004) PRODRG: A tool for high-throughput crystallography of protein-ligand complexes. *Acta Crystallogr D Biol Crystallogr* 60(Pt 8):1355–1363.
- Dave R, Terry DS, Munro JB, Blanchard SC (2009) Mitigating unwanted photophysical processes for improved single-molecule fluorescence imaging. *Biophys J* 96(6):2371–2381.
- Munro JB, Altman RB, Tung CS, Sanbonmatsu KY, Blanchard SC (2010) A fast dynamic mode of the EF-G-bound ribosome. *EMBO J* 29(4):770–781.
- Juette MF, et al. (2014) The bright future of single-molecule fluorescence imaging. *Curr Opin Chem Biol* 20:103–111.
- Zheng Q, et al. (2014) Ultra-stable organic fluorophores for single-molecule research. *Chem Soc Rev* 43(4):1044–1056.
- Akyuz N, et al. (2015) Transport domain unlocking sets the uptake rate of an aspartate transporter. *Nature* 518(7537):68–73.
- Starosta AL, et al. (2014) Translational stalling at polyproline stretches is modulated by the sequence context upstream of the stall site. *Nucleic Acids Res* 42(16):10711–10719.
- Seefeldt AC, et al. (2016) Structure of the mammalian antimicrobial peptide Bac7(1-16) bound within the exit tunnel of a bacterial ribosome. *Nucleic Acids Res* 44(5):2429–2438.

Supporting Information

Arenz et al. 10.1073/pnas.1604790113

SI Materials and Methods

Cryo-EM and Single Particle Reconstruction. The SRCs were prepared essentially as described (25, 44). The AVI- and EVN-SRCs ($4A_{260}/\text{mL}$) were applied to 2-nm precoated Quantifoil R3/3 holey carbon supported grids and vitrified by using a Vitrobot Mark IV (FEI). Data collection was performed at NeCEN on a Titan Krios (FEI) transmission electron microscope equipped with a Falcon II direct electron detector at 300 kV with a magnification of 125,085 \times , a pixel size of 1.108 Å, and a defocus range of 0.8–2.4 μm . The data were provided as a series of seven frames (dose per frame is $4\text{ e}^{-}/\text{Å}^2$), from which we summed frames 1–4 (AVI-SRC) or 1–6 (EVN-SRC) (accumulated dose, including the pre-exposure frame, of 20 and 28 $\text{e}^{-}/\text{Å}^2$, respectively, as described in Table S1) after alignment by using Motion Correction software (45). Images were processed by using a frequency-limited refinement protocol that helps prevent overfitting (47), specifically by truncation of high frequencies (in this case at 7–8 Å using Butterworth filter). Power spectra and defocus values were determined by using CTFFIND4 (57). Data were processed further by using the SPIDER software package (48), in combination with an automated workflow as described (58). After initial, automated particle selection based on the program SIGNATURE (46), initial alignments were performed (102,837 particles for AVI-SRC and 127,205 particles for EVN-SRC) by using *E. coli* 70S ribosome as a reference structure (25). After 3D classification using an incremental K-means-like method of unsupervised 3D sorting (59), the final AVI- and EVN-SRC maps [61,651 (60%) and 78,186 (75%) particles, respectively] could be refined to average resolutions of 3.6 Å (AVI-SRC) and 3.9 Å (EVN-SRC) (Fig. S1). The final refined maps were subjected to the program EM-BFACTOR (49) to apply an automatically determined negative B-factor for sharpening of the map. Local resolution calculations were performed by using ResMap (50), revealing that the majority of the cores of the 30S and 50S subunits extended to 3.5 Å (Fig. S1).

Model Building and Structure Refinement Procedures. The initial atomic model for the *E. coli* 70S ribosome was generated by using the 50S subunit from Protein Data Bank (PDB) ID code 4YBB (60) and the 30S subunit from PDB ID code 4TP9 (61). The initial model for the P-tRNA was based on PDB ID code 3TVF (62), and the model for the P-site mRNA was built de novo. Atomic models for AVI and EVN were generated from their known chemical structures by using PRODRG online software (63), which was also used to generate CIF restraints for the subsequent fitting and refinement. The initial models of the entire 70S ribosome with bound mRNA, P-site tRNA, and either AVI or EVN were fitted into the cryo-EM electron-density maps by real-space rigid-body refinement in PHENIX (52) with the ribosome split into multiple rigid-body domains. Resulting molecular models were further adjusted by using COOT (51) and refined in PHENIX (52). Model validation was carried out by using the MolProbity server (53). The final model statistics are presented in Table S1. All figures showing atomic models, as well as Movie S1, were generated by using PyMOL (Schrodinger). Fig. S1 was generated by using Chimera (54).

smFRET Imaging. Single-molecule experiments were performed in Tris-polymix buffer containing 50 mM Tris-acetate (pH 7.5), 5 mM MgCl_2 , 100 mM KCl, 5 mM $\text{NH}_4(\text{CH}_3\text{COO})$, 0.5 mM CaCl_2 , 0.1 mM EDTA, 5 mM putrescine, 1 mM spermidine, 1.5 mM β -mercaptoethanol, and 1 mM GTP, in the presence of an oxygen-scavenging system consisting of 2 mM protocatechuic acid, 50 mM protocatechuate 3,4-dioxygenase, and photostabilizing compounds

(1 mM Trolox, 1 mM cyclooctatetraene, and 1 mM nitrobenzyl-alcohol) (64). EF-Tu-GTP-Phe-tRNA^{Phe}(LD650-acp³U47) ternary complex was prepared as described (39, 65). LD650 (Lumidyne Technologies) is an intramolecularly photostabilized derivative of Cy5 (66–68). Surface immobilization of ribosome complexes (0.5 nM) programmed with biotinylated mRNA was achieved by brief incubation in PEG-passivated, streptavidin-coated quartz microfluidic devices (55). Complexes lacking ribosomal protein L1 were used to minimize the contribution of hybrid state tRNA configurations after peptide bond formation (55).

smFRET data were acquired on a home-built prism-based total internal reflection microscope as described (41). Briefly, a 532-nm laser (Opus 532; Laser Quantum) was used to excite Cy3 fluorophores attached to tRNA^{Met}. Emitted fluorescence from Cy3 donor and LD650 acceptor fluorophores was collected by using a 1.27-NA 60 \times water immersion objective (Nikon), spectrally separated by using a MultiCam-LS device (Cairn) equipped with a dichroic mirror (T635lpxr-UF2; Chroma), and imaged onto two scientific complementary metal-oxide semiconductor cameras (Orca-Flash 4.0 V2; Hamamatsu Photonics) acquiring at 10-ms integration time. FRET efficiency time courses for individual ribosomes were calculated, selected, and analyzed by using the freely available MATLAB-based software package SPARTAN as described (41).

Toe-Printing Assay. The position of the ribosome on the mRNA was monitored by using a toe-printing assay based on the PURExpress (New England Biolabs) in vitro coupled transcription-translation system, as described (69, 70). Briefly, each translation reaction consisted of 2 μL of solution A, 1.5 μL of solution B, and 1 μL (0.6 pmol) of DNA template (hns40aa): (5'- ATTAATACGACTCACTATA-GGGATATAAGGAGGAAAACATATGAGCGAAGCACTTAA-AATTCTGAACAACATCCGTACTCTTCGTGCGCAGGCAAG-AGAATGTACACTTGAAACGCTGGAAGAAATGCTGGAAA-AATTAGAAGTTGTTGTTAACGAACGTTGGATTTTGTGAAG-TGATAGAATTCTATCGTTAATAAGCAAAATTCATTATA-ACC-3', with the ATG start and TAA stop codon highlighted in bold and the primer-binding site underlined) and 0.5 μL of additional agents (nuclease-free water, Ths, Ede, AVI, or EVN). The template was synthesized via PCR from gDNA (*E. coli* MG1655). Translation was performed at 37 °C for 15 min in 1.5-mL reaction tubes with constant shaking at 500 rpm. After translation, 2 pmol of Alexa 647-labeled NV-1 toe-printing primer (5'-GGTTA-TAATGAATTTTGCTTATTAAC-3') was added to each reaction and incubated at 37 °C for 5 min without shaking. Reverse transcription (RT) was performed with 0.5 μL of AMV reverse transcriptase (NEB), 0.1 μL of dNTP mix (10 mM), and 0.4 μL of Pure System Buffer and incubated at 37 °C for 20 min. The RT reaction was quenched and RNA degraded by addition of 1 μL of 10 M NaOH and incubation for at least 15 min at 37 °C and then was neutralized with 0.7 μL of 25% HCl. Then, 20 μL of toe-printing resuspension buffer and 200 μL of PN1 buffer were added to each reaction before treatment with a QIAquick Nucleotide Removal Kit (Qiagen). The Alexa 647-labeled DNA was then eluted from the QIAquick columns with 80 μL of nuclease-free water. A vacuum concentrator was used to vaporize the solvent, and the Alexa 647-labeled DNA was then dissolved into 3.5 μL of formamide dye. The samples were heated to 95 °C for 5 min before being applied onto a denaturing 6% (vol/vol) polyacrylamide (19:1) sequencing gel containing 7 M urea. Gel electrophoresis was performed at 40 W and 2,000 V for 2 h. The GE Typhoon FLA9500 imaging system was subsequently used to scan the polyacrylamide gel.

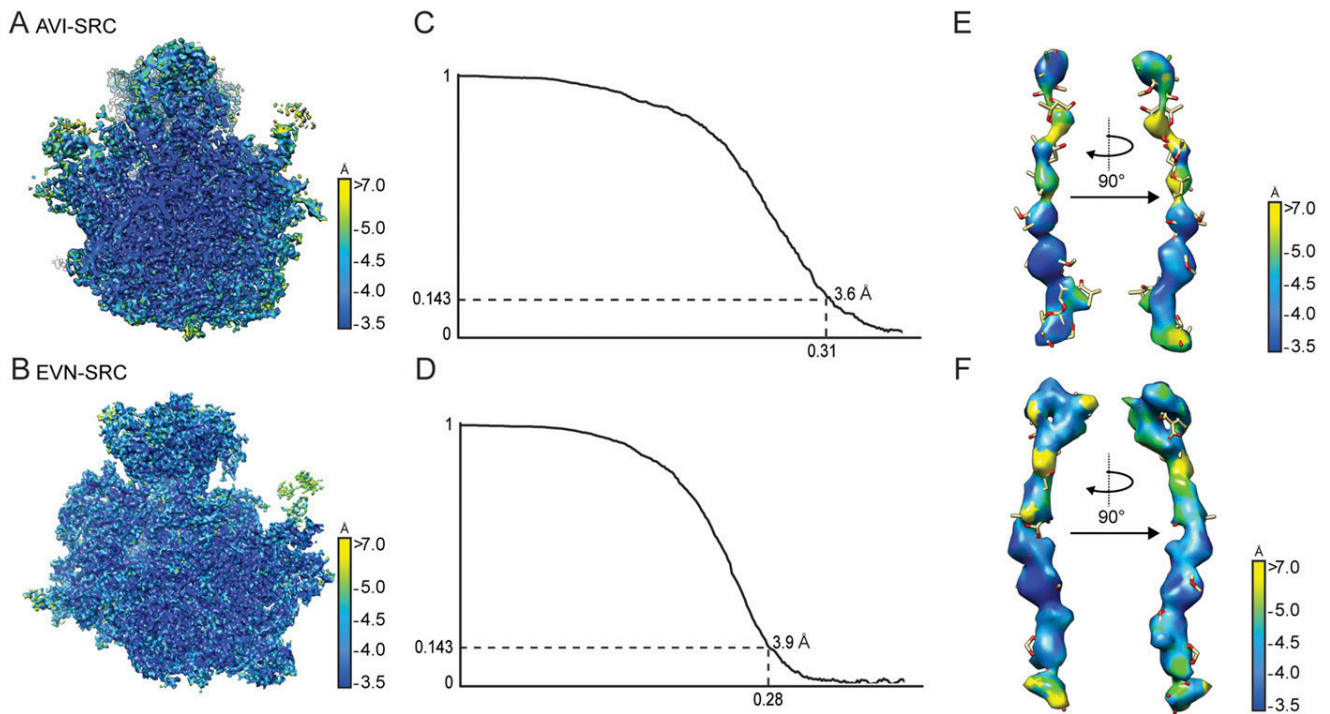


Fig. S1. Average and local resolution determination of AVI- and EVN-SRCs. (A and B) Transverse section of the cryo-EM reconstructions of the AVI-SRC (A) and the EVN-SRC (B) colored according to local resolution. (C and D) Average resolution of the AVI-SRC (C) and EVN-SRC (D) was 3.6 and 3.9 Å using the Fourier shell correlation (FSC) cutoff value of 0.143. Because of image processing with an absence of spatial frequencies >8 Å, the FSC value of 0.143 was used for average resolution determination (47). (E and F) Local resolution of the density for AVI (E) and EVN (F).

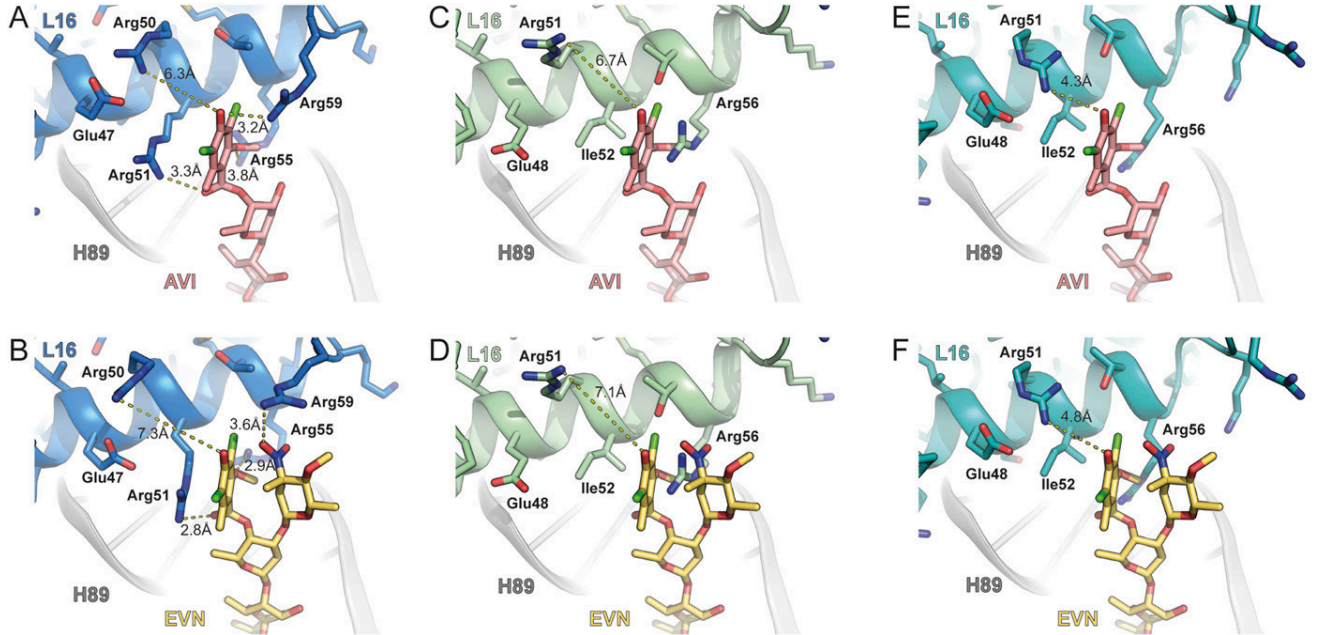


Fig. S2. Comparison of AVI/EVN binding site with respect to *E. coli*, *B. subtilis*, and *S. aureus* L16. Interaction of AVI (red; A) and EVN (gold; B) with *E. coli* L16 (blue) compared with the relative position of *B. subtilis* L16 (green; C and D) (29) and *S. aureus* L16 (cyan; E and F) (30). In *E. coli*, Arg-50 is 6.3–7.3 Å from ring A of AVI/EVN, whereas the equivalent residue Arg-51 is 6.7–7.1 Å and 4.3–4.8 Å when superimposing AVI/EVN with *B. subtilis* L16 (green; C and D) (29) and *S. aureus* L16 (cyan; E and F) (30).

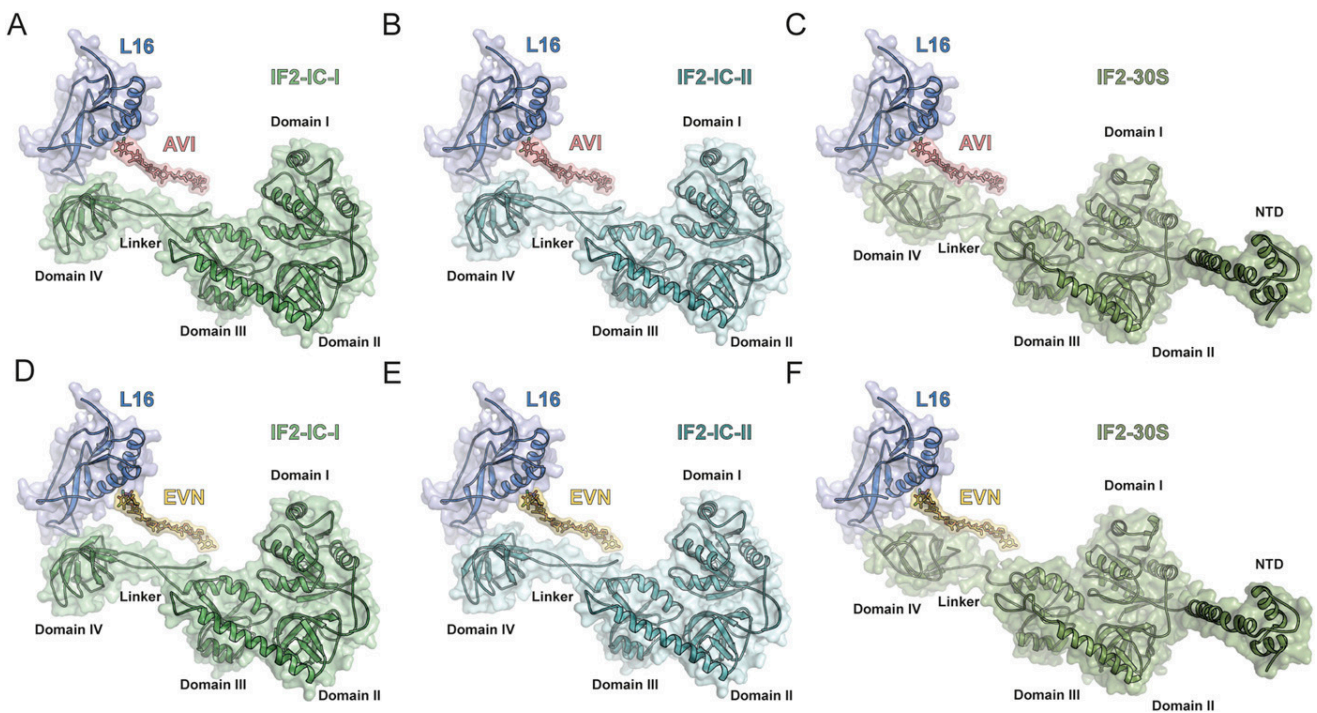


Fig. S3. Comparison of AVI/EVN binding site with respect IF2. Binding position of AVI (red; A–C) and EVN (D–F) on the *E. coli* 70S ribosome relative to IF2-IC conformation I (green; A and D) and IF2-IC conformation II (teal; B and E) on the 70S ribosome (33) and IF2-GTP conformation (olive; C and F) on the 30S subunit (34, 35).

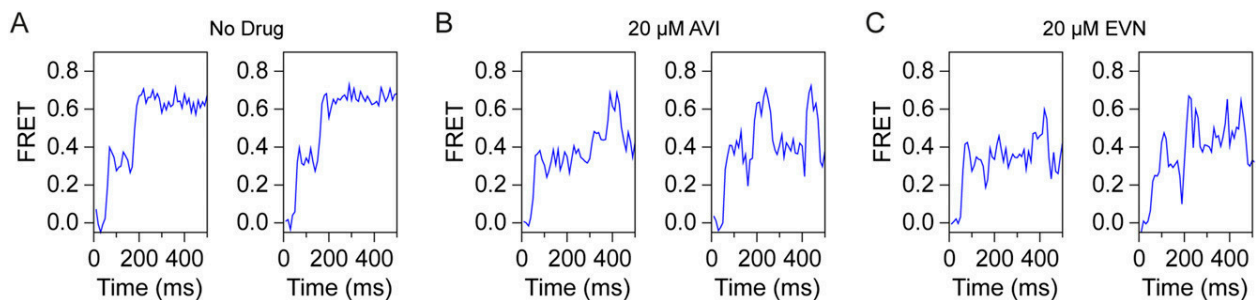


Fig. S4. EVN and AVI specifically block accommodation of A-tRNA into the classical state. Representative smFRET traces exemplifying the processes shown in Fig. 5 C–E are shown. (A) In the absence of drug, aa-tRNA rapidly achieves the fully accommodated A/A state (0.63 FRET) via reversible forward-sampling from the 0.35 FRET A/T state. (B and C) AVI (B) and EVN (C) inhibit formation of the A/A state, leading to repeated, unsuccessful sampling events.

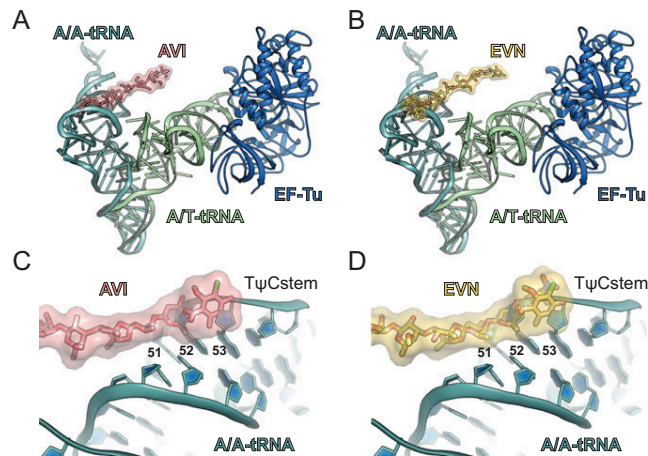


Fig. S5. Relative position of EVN/AVI to A/T- and A/A-tRNA. (A and B) Comparison of the relative binding position on the ribosome of AVI (red; A) and EVN (B), with EF-Tu (blue) and A/T-tRNA (green) (36, 56), as well as with accommodated A/A-tRNA (teal) (38). (C and D) Zoom showing the overlap between AVI (red; C) and EVN (gold; D) with nucleotides 51–53 with the T ψ C stem of the an accommodated A/A-tRNA (teal) (38).

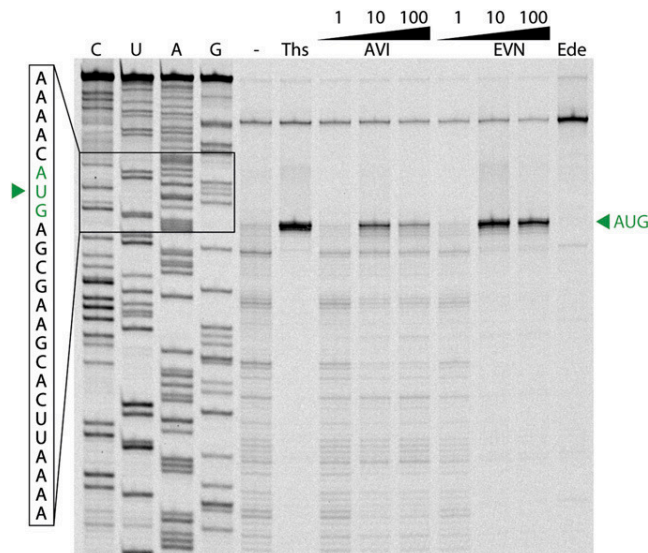


Fig. S6. EVN and AVI block ribosomes at the start codon of the mRNA. Toe-printing assay monitoring translation in the presence of increasing concentrations (1, 10, and 100 μ M) of EVN or AVI is shown. Additionally, control reactions without antibiotic (–) or including thioestrepton (Ths, 100 μ M) or edeine (Ede, 50 μ M) are shown. AUG designates location of the ribosomes stalled at the start codon. C, U, A, and G indicate the sequencing lanes.

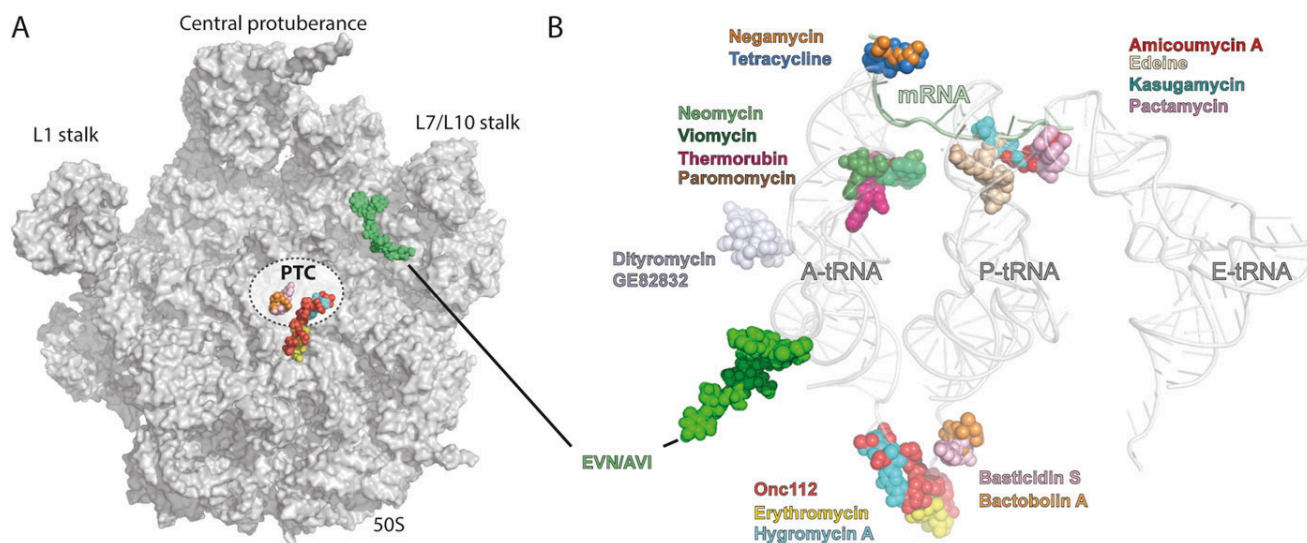
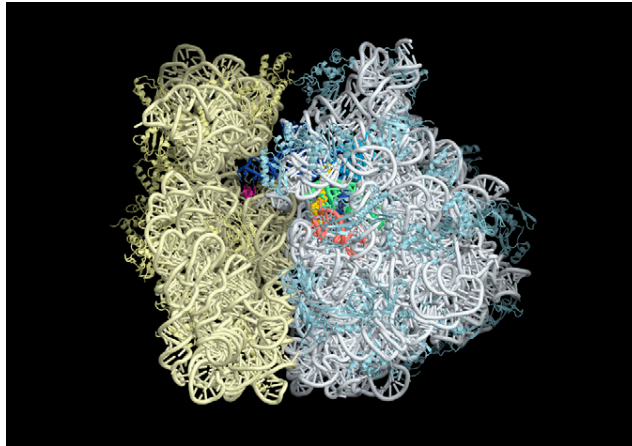


Fig. S7. Relative position of EVN/AVI to other ribosome-targeting antibiotics. (A) Overview of ribosomal 50S subunit (gray) with relative position of EVN/AVI (yellow) compared with known antibiotics that target the PTC. (B) Relative position of EVN/AVI (green) compared with known antibiotics that target the small and large ribosomal subunit, with A-, P-, and E-tRNAs shown for reference.

Table S1. Data collection and refinement statistics

Data collection and refinement	EVN-SRC	AVI-SRC
Particles	78,186	61,651
Pixel size, Å	1.108	1.108
Defocus range, μm	1.0–2.4	0.7–2.4
Voltage, kV	300	300
Electron dose, e ⁻ /Å ²	28	20
Map sharpening B factor, Å ²	-234.20	-126.14
Resolution, Å (0.143 FSC)	3.9	3.6
Model composition		
Nonhydrogen atoms	149,026	145,176
Protein residues	6,664	5,626
RNA bases	4,645	4,696
Validation (proteins)		
Poor rotamers, %	0.00	0.08
Ramachandran outliers, %	2.61	1.68
Ramachandran favored, %	88.98	92.36
Bad backbone bonds, %	0.00	0.12
Bad backbone angles	0.00	0.01
MolProbity score	2.02 (74th percentile)	2.16 (100th percentile)
Validation (nucleic acids)		
Correct sugar puckers, %	97.71	99.46
Bad backbone conformations, %	12.89	13.86
Bad bonds, %	0.05	0.39
Bad angles	0.01	0.01
Clashscore, all atoms	8.29 (80th percentile)	15.25 (97th percentile)



Movie S1. Binding site of AVI on the bacterial 70S ribosome. Overview of AVI (bright yellow) binding site on the 70S ribosome (small subunit, yellow; large subunit, white and blue). The P-tRNA (blue) and mRNA (magenta) are highlighted, as well as 23S rRNA helices H89 (red) and H91 (green) and ribosomal protein L16 (light blue). A morph between A/T-tRNA in complex with EF-Tu and an accommodated A-tRNA demonstrates that AVI allows delivery of the A/T-tRNA, but sterically interferes with the accommodation of the A-tRNA on the large subunit.

[Movie S1](#)

Cryo-EM structure of the spinach chloroplast ribosome reveals the location of plastid-specific ribosomal proteins and extensions

Michael Graf¹, Stefan Arenz¹, Paul Huter¹, Alexandra Dönhöfer¹, Jiří Nováček² and Daniel N. Wilson^{1,3,*}

¹Gene Center, Department for Biochemistry and Center for integrated Protein Science Munich (CiPSM), University of Munich, 81377 Munich, Germany, ²Central European Institute of Technology (CEITEC), Masaryk University, Kamenice 5, 62500 Brno, Czech Republic and ³Department of Biochemistry and Molecular Biology, University of Hamburg, 20146 Hamburg, Germany

Received October 28, 2016; Revised December 01, 2016; Editorial Decision December 05, 2016; Accepted December 06, 2016

ABSTRACT

Ribosomes are the protein synthesizing machines of the cell. Recent advances in cryo-EM have led to the determination of structures from a variety of species, including bacterial 70S and eukaryotic 80S ribosomes as well as mitoribosomes from eukaryotic mitochondria, however, to date high resolution structures of plastid 70S ribosomes have been lacking. Here we present a cryo-EM structure of the spinach chloroplast 70S ribosome, with an average resolution of 5.4 Å for the small 30S subunit and 3.6 Å for the large 50S ribosomal subunit. The structure reveals the location of the plastid-specific ribosomal proteins (RPs) PSRP1, PSRP4, PSRP5 and PSRP6 as well as the numerous plastid-specific extensions of the RPs. We discover many features by which the plastid-specific extensions stabilize the ribosome via establishing additional interactions with surrounding ribosomal RNA and RPs. Moreover, we identify a large conglomerate of plastid-specific protein mass adjacent to the tunnel exit site that could facilitate interaction of the chloroplast ribosome with the thylakoid membrane and the protein-targeting machinery. Comparing the *Escherichia coli* 70S ribosome with that of the spinach chloroplast ribosome provides detailed insight into the co-evolution of RP and rRNA.

INTRODUCTION

Chloroplasts are organelles found in plant and algal cells, which are responsible for carrying out photosynthesis. The origin of chloroplasts is thought to result from an endosymbiotic event where an early eukaryotic cell engulfed a pho-

tosynthetic cyanobacterium (1). As such chloroplasts possess their own genome, as well as the transcription and translation machinery to convert the genetic information into polypeptides or proteins (2,3). Chloroplast ribosomes, or chlororibosomes, are very specialized since they are only involved in synthesizing the limited number of proteins encoded in the chloroplast genome (2,3). For example, the complete genome sequence of the *Spinacea oleracea* (spinach) chloroplast contains 146 genes encoding protein products and structural RNAs (4). The majority of the chloroplast-encoded proteins are targeted to the chloroplast thylakoid membranes and encompass components of the adenosine triphosphate (ATP) synthase, cytochrome b/f and photosystem I and II complexes (4). In addition, chlororibosomes translate NADH dehydrogenase, the large subunit (LSU) of RuBisCO, RNA polymerase subunits and a distinct subset of ribosomal proteins (RPs), 12 from the small subunit (SSU) and 8 from the LSU. Other proteins essential for chloroplast function are nuclear encoded and must therefore be imported into the chloroplast. This includes the remaining 32 chloroplast RPs (cpRPs), which bear N-terminal chloroplast-targeting sequences that are cleaved off upon import (5,6).

Sequence comparisons indicate that the components of the chloroplast translational machinery are similar to those of eubacteria, especially cyanobacteria, but also γ -proteobacteria, such as *Escherichia coli*. The chloroplast 16S rRNA (cp16S) of the SSU contains 1491 nucleotides (nts) and is therefore only slightly smaller than the *E. coli* 16S rRNA (Ec16S), which has 1542 nts. The *E. coli* LSU contains 2 rRNAs, the 5S (120 nts) and 23S (2904 nts) rRNAs, totaling to 3024 nts. While the chloroplast LSU comprises 3 rRNAs, 5S (121 nts), 4.8S (103 nts) and 23S (2810 nts) rRNAs, the total length of 3034 nts is only slightly larger (10 nts) than in *E. coli*. Similarly, chlororibosomes contain a total of 52 cpRPs (25 in the SSU and 33 in the

*To whom correspondence should be addressed. Tel: +49 89 2180 76903; Fax: +49 89 2180 76945; Email: wilson@lmb.uni-muenchen.de

© The Author(s) 2016. Published by Oxford University Press on behalf of Nucleic Acids Research. This is an Open Access article distributed under the terms of the Creative Commons Attribution License (<http://creativecommons.org/licenses/by-nc/4.0/>), which permits non-commercial re-use, distribution, and reproduction in any medium, provided the original work is properly cited. For commercial re-use, please contact journals.permissions@oup.com

LSU) and with the exception of L25 and L30, have orthologs in *E. coli* (5,6). However, the cpRPs are generally larger than their *E. coli* counterparts, predominantly due to N- and C-terminal extensions (NTEs and CTEs) (5,6). Proteomic studies also identified six non-orthologous proteins, termed ‘plastid-specific RPs’ (or PSRPs) (5–7). Four PSRPs (PSRP1–4) were found to be associated with the SSU and two (PSRP5 and PSRP6) with the LSU (5–7). A cryo-EM reconstruction of the spinach chlororibosome at 9.4 Å provided first insights into the localization of the PSRPs and cpRP extensions (8), however, higher resolution is required to accurately assign and describe the interactions of the PSRPs and cpRP extensions within the chlororibosome.

Here we present a cryo-EM structure of the spinach chlororibosome, with an average resolution of 5.4 Å for the SSU and 3.6 Å for the LSU, revealing the binding site of the PSRP1, PSRP4, PSRP5 and PSRP6 as well as the conformation of numerous cpRP extensions. The structure illustrates how cpRP extensions and PSRPs wind their way through the core of the chlororibosome establishing interactions with neighboring rRNA and RPs. In many cases, the cpRP extensions interact with RNA or protein features that are specific to the chlororibosome, thus providing insight into their co-evolution. We also identify a large conglomerate of cpRP mass adjacent to the tunnel exit site that we suggest facilitates interaction of the chlororibosome with the thylakoid membrane and the protein-targeting machinery.

MATERIALS AND METHODS

Isolation of chloroplast 70S ribosomes

Chloroplast ribosome isolation was performed as described previously (9). Briefly, 6 kg of spinach leaves were de-veined and washed thoroughly. The leaves were homogenized (2l/kg of leaves) using 0.7 M Sorbitol in buffer A (10 mM Tris-HCl pH 7.6, 50 mM KCl, 10 mM MgOAc, 7 mM β -mercaptoethanol). The homogenate was filtered through several layers of cheesecloth and one layer of Miracloth (Calbiochem) before centrifugation at $1200 \times g$ for 15 min. The pellet was resuspended in 0.4 M Sorbitol in buffer A and re-centrifuged at $1200 \times g$ for 15 min. The washed chloroplast pellet was resuspended in buffer A supplemented with 2% (v/v) Triton-X100 and incubated on ice for 30 min. The lysed suspension was clarified by centrifugation at $26\,000 \times g$ for 30 min before isolation of crude ribosomes by centrifugation at $50\,000 \times g$ for 24 h through a 1M sucrose (in buffer B: buffer A with 10% glycerol). The greenish pellet was washed and then resuspended in buffer B with gentle agitation. The crude ribosomes were clarified by centrifugation at $26\,000 \times g$ for 15 min before being either snap frozen at -80°C . Alternatively, the clarified supernatant was applied directly onto a 10–30% sucrose gradient (in buffer B) in order to obtain tight-coupled chloroplast 70S ribosomes.

Negative-stain electron microscopy

Ribosomal particles were diluted in buffer A to a final concentration of 5 A_{260}/ml . One drop of each sample was deposited on a carbon-coated grid. After 30 s, grids were

washed with distilled water and then stained with 2% aqueous uranyl acetate for 15 s. The remaining liquid was removed by touching the grid with filter paper. Micrographs were taken using a Morgagni transmission electron microscope (FEI), 80 kV, wide angle 8K CCD at direct magnifications of 110K.

Cryo-electron microscopy and single particle reconstruction

A total of 5 A_{260}/ml chloroplast ribosome sample was applied to 2 nm pre-coated Quantifoil R3/3 holey carbon supported grids and vitrified using a Vitrobot Mark IV (FEI, Eindhoven). Data collection was performed using an FEI Titan Krios transmission electron microscope equipped with a Falcon II direct electron detector (FEI, Eindhoven), using a pixel size of 1.061 Å and an underfocus range of 1.0–2.3 μm resulting in 2031 micrographs. Each micrograph was recorded as a series of 7 frames ($3.9\text{ e}^-/\text{Å}^2$ pre-exposure; $5.2\text{ e}^-/\text{Å}^2$ dose per frame). All seven frames (accumulated dose of $40.3\text{ e}^-/\text{Å}^2$) were motion-corrected using the Unblur program (10) and power-spectra, defocus values, astigmatism and estimation of micrograph resolution were determined using CTFFIND4 (11). Five hundred and forty-five micrographs showing Thon rings beyond 3.2 Å resolution were manually inspected further for good areas and power-spectra quality. Three times decimated data were pre-processed using the SPIDER software package (12), in combination with an automated workflow as described previously (13). After initial, automated particle selection based on the program SIGNATURE (14), initial alignment was performed with 56 475 particles using *E. coli* LSU as a reference structure (15). The dataset could be sorted into 37 626 (66.6%) ribosomal particles and 18 849 (33.3%) non-aligning particles using an incremental K-means-like method of unsupervised 3D sorting (16) (Supplementary Figure S2). Underestimated ribosomal particles were again initially aligned against an *E. coli* LSU and subsequently refined using FREALIGN (17). Since the SSU of the chlororibosome was flexible, focused alignment and refinement was performed by applying masks either on the SSU or LSU. Due to inherent flexibility, the SSU of the chlororibosome could be refined to an average resolution of 5.4 Å (0.143 FSC) and a local resolution extending to 5.0 Å for the core, whereas the LSU of the chlororibosome could be refined to an average resolution of 3.6 Å (0.143 FSC) and a local resolution extending to <3.5 Å for the core. The local resolution of the final maps was computed using ResMap (18) (Supplementary Figure S2). The final maps were sharpened by dividing the maps by the modulation transfer function of the detector and by applying an automatically determined negative B-factor (-86 for the LSU and -130 for the SSU) to the maps using RELION (19).

Molecular modeling and map-docking procedures

The molecular model of the chloroplast LSU was based on the *E. coli*-70S-EF-Tu structure (20). The 23S rRNA secondary structure was initially generated by manual alignment of the chloroplast 23S rRNA sequence and the secondary structure map (21) to the *E. coli* 23S secondary structure map, which shows high structural similarity. The

16S, 5S and 4.8S rRNA sequences of the chloroplast ribosome were aligned accordingly. The resulting rRNA homology models were rigid-body fitted into the respective chloroplast EM-map using Chimera (22). Subsequently, the models were manually adjusted and refined using Coot (23). *E. coli*-based (20) homology models of the cpRPs were built using SwissModel (24) and HHPred (25) and rigid-body fitted into the map. cpRP-specific extensions were modeled in Coot (23). PSRP5 and PSRP6 were modeled *de novo*, using secondary structure predictions generated by PsiPred (26) as a reference. The complete atomic model of the chloroplast LSU was subsequently refined using *phenix.real-space.refine* (27) with secondary structure restraints calculated by PHENIX. In order to reduce the clashscore, the model was additionally refined in reciprocal space using REFMAC (28) in EM mode. Cross-validation against overfitting was performed as described elsewhere (29,30). The statistics of the refined model were obtained using MolProbity (31).

Figure preparation

All figures showing electron densities and atomic models were generated using UCSF Chimera (22) and PyMol Molecular Graphics Systems (version 1.8 Schrödinger).

RESULTS AND DISCUSSION

Cryo-EM structure of the chloroplast 70S ribosome

Chloroplast 70S ribosomes were isolated from *S. oleracea* (spinach) leaves as described previously (8,9) and subjected to single particle cryo-EM analysis. The cryo-EM data was collected on a Titan Krios transmission electron microscope with a Falcon II direct electron detector. From a total of 56,475 ribosomal particles, *in silico* sorting revealed extreme flexibility of the SSU with respect to the LSU (Supplementary Figure S1). To overcome this conformational heterogeneity, focused alignment was performed independently for each ribosomal subunit using FREALIGN (17). Subsequent refinement yielded cryo-EM reconstructions of the chloroplast SSU and LSU (Figure 1A–D), with an average resolution of 5.4 Å and 3.6 Å, respectively (Supplementary Figure S2 and Table S1).

Analysis of the chloroplast SSU

The resolution of the SSU allowed a homology model of the spinach chloroplast SSU to be rigid body fitted based on the high sequence similarity between the *E. coli* and *S. oleracea* rRNA and RPs (8). As already noted (8), the major difference with respect to the 16S rRNA is the shortening of helices h6, h10 and h17 in the chlororibosome rRNA, leading to a truncated spur (Figure 1A and B) when compared to the *E. coli* SSU. In the previous chlororibosome cryo-EM structure, additional protein density was observed, which was tentatively assigned to PSRP2 and PSRP3, and proposed to compensate for the truncated spur rRNA (8). At higher resolution, this extra spur density was not well-resolved (Figure 1A and B), however, filtering at lower resolution indeed revealed extra density within this region (Supplementary Figure S3). The mass of the extra spur density

could not account fully for either PSRP2 or PSRP3, suggesting that if one of these PSRPs is bound there it is highly flexible.

As mentioned, the *S. oleracea* cpRPs are larger than their respective *E. coli* counterparts due to the presence of NTEs and/or CTEs (6). To ascertain the location of the cpRP extensions, homology models for the *S. oleracea* cpRPs were generated based on *E. coli* templates (20,32), which were then fitted to the cryo-EM map of the chloroplast SSU (Figure 1A and B). In many cases, additional density continuous with the N- or C-termini of the cpRPs could be identified, consistent with the presence of predicted *S. oleracea* cpRP-extensions that are absent in the respective *E. coli* RPs (Figure 1A and B). For example, density was observed for the NTE of cpS5, which is 86 aa longer than *E. coli* S5 (EcS5) (6). In addition, density for the NTEs of cpS9, cpS10 and cpS21 and the CTEs of cpS16 and cpS18 were observed, as well as a rearrangement of the N-terminus of cpS4. The extensions of the cpRPs are located exclusively on the back or cytosolic side of the SSU, but nevertheless encroach on two functional regions related to the path of the mRNA. Specifically, the CTE of cpS18 and the NTE of cpS21 are located at the platform region in vicinity of where the Shine-Dalgarno helix forms between the 5' end of the mRNA and the 3' end of the 16S rRNA (Supplementary Figure S3). The N-terminus of cpS4, and particularly the NTE of cpS5, surround the mRNA entry channel (Figure 1A and B; Supplementary Figure S3). Curiously, we also observed extra density in this region that does not originate from any of the neighboring cpRP extensions. The extra density connects the head and body of the 30S subunit, namely, bridging the tip of helix h16 in the body with cpS3 of the head. This connection is often referred to as the 'latch' because it has been observed to open and close during translation initiation (33,34). Mass spectrometry analysis did not detect additional non-orthologous proteins on the spinach chloroplast SSU (5–7), therefore, the additional density may actually be derived from part of PSRP2 or PSRP3, but we cannot exclude that it is derived from unrelated proteins.

Finally, we identified two additional densities that we assigned to PSRP1 and PSRP4 (Supplementary Figure S4A and B). In agreement with the previous localization (8), we allocated the density within the head of the SSU to PSRP4 (Figure 1A and B) based on its similarity in sequence and binding position with Thx, a small RP identified in the *Thermus thermophilus* SSU (35). Similarly, we assigned the additional density located within the decoding site on the inter-subunit side of the SSU to the N-terminal domain (NTD) of PSRP1, as reported previously (8,36). Sequence alignments indicated that PSRP1 is not a *bone fide* cpRP but rather a homolog of a long form hibernation-promoting factor, which is responsible for 100S formation (70S dimerization) (37). The NTD of PSRP1 is homologous with YfiA and the short form HPF, both of which have also been shown to bind analogously to the SSU of bacterial 70S ribosomes (38,39), overlapping the binding site of the mRNA and tRNAs in the A- and P-sites (Supplementary Figure S4C and D). No density was observed for the C-terminal domain of PSRP1, which has been shown to be responsible for 100S formation in some bacteria (40,41).

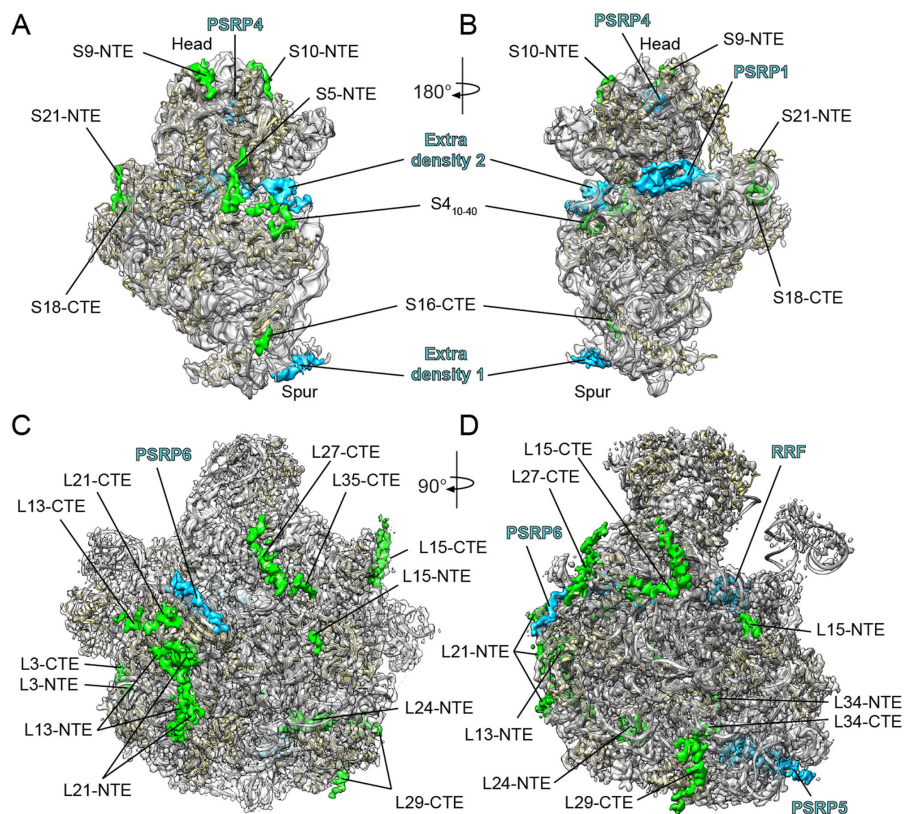


Figure 1. Cryo-EM structure of the chloroplast SSU and LSU. (A–D) Cryo-EM map (transparent gray) of the spinach chloroplast (A and B) SSU and (C and D) LSU, illustrating the additional density for cpRPs (green) and extra density assigned to PSRPs (blue) and the ribosome recycling factor (RRF). The molecular model for the SSU and LSU includes rRNA (gray) and cpRPs (yellow).

Molecular model for the chloroplast LSU

Consistent with the local resolution calculations (Supplementary Figure S2), the electron density was particularly well resolved within the core of the LSU, whereas the periphery of the subunit was less defined. We were able to generate molecular models for 28 of the 33 cpRPs present in the chlororibosome (Figure 2A–C; Supplementary Table S2). cpRPs L1, L10, L11, L7/L12 and L31 were not modeled due to poor density. The density for cpL5, cpL6 and cpL18 allowed only a rigid body fit of a homology model based on EcL5 and EcL6, and only the NTD of cpL9 was included in the final model. As observed previously (8), density was not observed for L25 and L30, consistent with the absence of genes encoding these cpRPs in plant and chloroplast genomes (4). We could also model domain I of the chloroplast ribosome recycling factor (cpRRF) (Supplementary Figure S4), which was bound analogously to that reported previously on the chlororibosome at lower resolution (8) as well as on bacterial ribosomes (42,43). Together with cpEF-G, cpRRF has been demonstrated to dissociate PSRP1 from the chlororibosome (36). In addition, molecular models are presented for the complete 5S and 2843 (97.6%) of the 2913 nucleotides that comprise the 4.8S and 23S rRNAs (Figure 3A and B; Supplementary Figure S5).

Features of the chloroplast LSU rRNAs

Unlike the mammalian mitoribosome where a tRNA molecule substitutes for the lack of a 5S rRNA (44,45), the chlororibosome contains a 5S rRNA (Figure 3A and B) that is highly similar in sequence and structure to the bacterial 5S rRNA. As mentioned, the chloroplast 23S rRNA is present in the chlororibosome as two pieces, a 5' fragment representing H1–H97 of domains I–VI (hereafter referred to as cp23S rRNA) and a 3' fragment comprising H99–H101 of domain VII (termed 4.8S rRNA) (Figure 3A and Supplementary Figure S5). This results in the loss of H98 ($\Delta 16$ nts) that links domains VI and VII within the *E. coli* 23S (Ec23S) rRNA (Figure 3C). Together with reductions in helices H9 ($\Delta 14$ nts), H45, ($\Delta 6$ nts), H63 ($\Delta 27$ nts) (Figure 3A and B), the cp23S rRNA has a total of 75 nts missing relative to the Ec23S rRNA. While the reductions lead to a shortening in the length of H9 and H45 (Figure 3D and E), the effect on H98 and H63 results in the complete absence of these helices in the chlororibosome (Figure 3C and F). Nevertheless, the combined length of the chloroplast LSU rRNA (3034 nts) is similar to that for *E. coli* (3024 nts) because the four rRNA reductions in the cp23S rRNA are compensated by five rRNA additions (8). This includes additional nucleotides within H15 (+30 nts), H38 (+20 nts), H58 (+23 nts) and H68 (+4 nts) of the cp23S rRNA, as well as +8

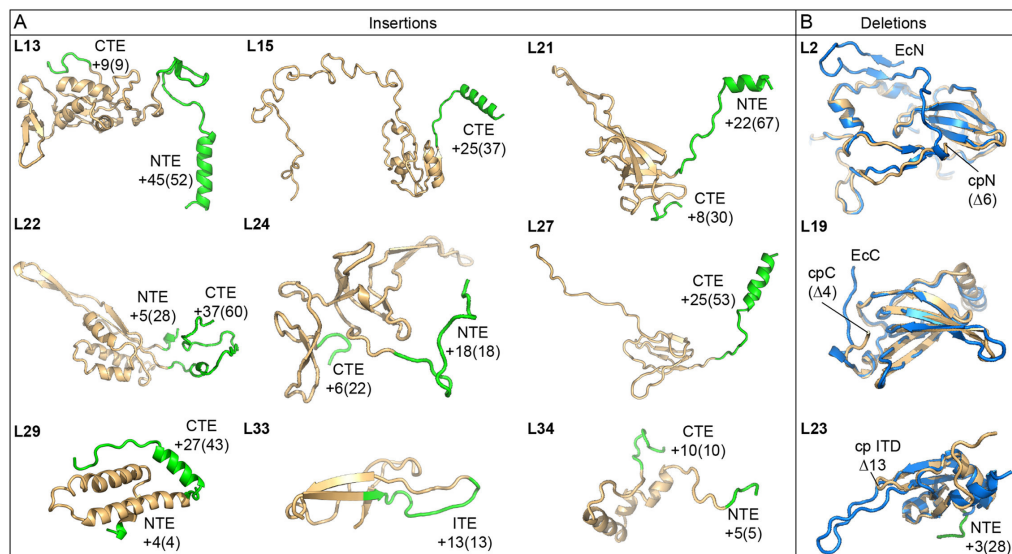


Figure 4. Molecular models indicating cpRP extensions and deletions. (A) Structures of cpRPs showing the core region equivalent to the respective EcRPs (gold) with N-terminal extensions (NTEs), C-terminal extensions (CTEs) or the internal expansion (ITE) highlighted (green). The numbers indicate the modeled residues with the total expansion length indicated in parentheses. (B) Structures of cpRPs (gold) compared with the respective EcRPs (blue) highlighting amino acid deletions (in parentheses) in cpRPs relative to EcRPs.

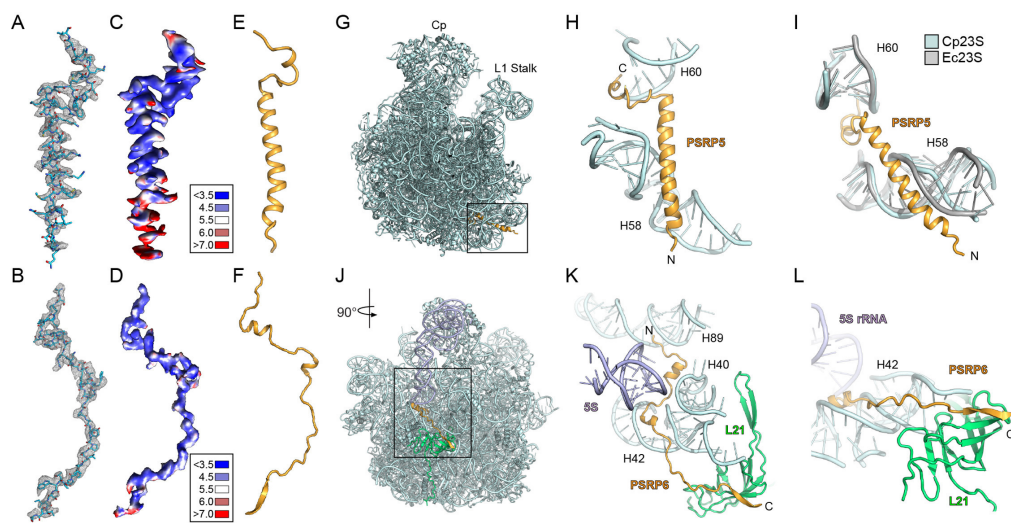


Figure 5. Localization of PSRP5 and PSRP6 on the chlororibosome. (A and B) Cryo-EM electron density (mesh) with molecular models for (A) PSRP5 and (B) PSRP6. (C and D) Cryo-EM electron density for (C) PSRP5 and (D) PSRP6 colored according to local resolution. (E and F) Molecular models showing secondary structure for (E) PSRP5 and (F) PSRP6. (G) Binding site of PSRP5 (gold) on the LSU (cyan). (H and I) Interaction between PSRP5 (gold) and H58 and H60 of the cp23S rRNA (cyan), with (I) comparison of different conformation of H58 from the Ec23S rRNA (gray). (J) Binding site of PSRP6 (gold) on the LSU (cyan). (K and L) Interaction between the N-terminus of PSRP6 (gold) and H40, H42 and H89 of the cp23S rRNA (cyan), and (L) the C-terminus of PSRP6 (gold) with the cpL21 (green).

B), in agreement with local resolution calculations (Figure 5C and D), enabling unambiguous models for both PSRP5 and PSRP6 to be generated (Figure 5E and F; Supplementary Figure S4). Consistent with secondary structure predictions, PSRP5 consists of a short C-terminal α -helix connected by a linker to a long central α -helix (Figure 5E). The binding site of PSRP5 is located at the base of the LSU directly under the L1 stalk, with the N-terminus extending to-

ward the intersubunit interface (Figure 5G). We note that 38 aa are missing from the N-terminus in our model, presumably due to flexibility outside of the ribosome. The surface of the buried regions of PSRP5 is highly positively charged (Supplementary Figure S4F and G), as would be expected from the surrounding negatively charged rRNA environment. The short C-terminal α -helix of PSRP5 inserts into the minor groove of H60, whereas the central α -helix es-

establishes interactions with H58 (Figure 5H). The specificity of PSRP5 for the chlororibosome may be due to the interaction with H58, since there are significant differences in both the sequence and structural conformation of H58 when comparing with the *E. coli* 70S ribosome (Figure 5I). We note that the position of PSRP5 was mis-assigned in the previous structure of *S. oleracea* chloroplast 70S ribosome (8), probably due to the small size of the protein and the limited resolution of the reconstruction.

PSRP6 adopts a very extended conformation (Figure 5F) that winds its way through the ribosome (Figure 5J–L). The N-terminal half of PSRP6 is predominantly positively charged (Supplementary Figure S4I–K), consistent with the extensive interaction with the negatively charged rRNA (Figure 5K). The N-terminus of PSRP6 interacts with the minor grooves of H89, H40 and H42 as it winds its way out of the ribosomal core (Figure 5K). The two short central α -helices of PSRP6 are positioned within the minor grooves of H40 and H42 and are separated by a linker region that passes near to the 5S rRNA (Figure 5K). The C-terminal half of PSRP6 is less charged (Supplementary Figure S4I), consistent with an interaction with the globular domain of cpL21, rather than with rRNA. The C-terminus of PSRP6 donates a β -strand to augment the β -sheet of cpL21 (Figure 5L) before extending into the solvent where the C-terminal 22 aa are not visualised. The conservation of this region between *S. oleracea* chloroplast and *E. coli* 70S ribosomes suggests that PSRP6 could in principal bind analogously to the *E. coli* 70S ribosome.

cpRP extensions and rRNA stabilization

Generally, the NTE and CTE of cpRPs contain positively charged amino acids that establish additional interactions with the surrounding rRNA, predominantly with the phosphate-oxygens of the backbone. For example, the 10 aa CTE of cpL34 interacts with the loop of helix H8 of the 23S rRNA and forms a potential hydrogen bond from Lys148 with the backbone of U1638 within H51 (Figure 6A). In many cases, the cpRP extensions interact with the minor groove of rRNA helices. Such an interaction is illustrated by the 25 aa CTE of cpL15, which inserts into the minor groove of a helix formed from the loops of H22 and H88 (Figure 6B). Lys243 comes within hydrogen bonding distance of the ribose of A427 and Tyr241 stacks upon A213 that makes an A-minor interaction within the H22/H88 helix (Figure 6B). Similarly, the 18 aa NTE of cpL24 that penetrates deeper into the ribosomal core, approaches the minor groove of an rRNA helix formed from the loops of H6 and H7, before the N-terminus emerges within the tunnel lumen (see later).

We also observed that the cpRP extensions often reinforce interactions with rRNA elements that are already contacted by the core of the cpRP, as illustrated by cpRPs L35 and L13 (Figure 6C and D). Arg140 in the core of cpL35 contacts the phosphate-oxygen of G966 in H38, an interaction also observed for EcL35 (Figure 6C). This contact is reinforced in the chlororibosome by a potential hydrogen bond from Arg157 within the 7 aa CTE of cpL35 to the backbone of C966 within H38 (Figure 6C). Similarly, the interaction from Arg126 in the core of cpL13 with A1170 in H41 is reinforced in the chlororibosome by an additional

hydrogen bond from Arg245 within the NTE of cpL13 to the backbone of A1170 within H41 (Figure 6D).

Three of the cpRP extensions contain α -helical secondary structure, namely within the NTE of cpL13 and the CTEs of cpL15 and cpL27 (Figure 4A). The α -helix within the CTE of cpL15 interacts with H68, which as mentioned is extended in the chlororibosome compared to the *E. coli* 70S (Figure 3H). In the chlororibosome, the NTE of cpL13 forms an α -helix that interacts with the junction where the 5' end of the 4.8S rRNA meets the 3' end of the cp23S rRNA (Figure 6E). Comparison with the *E. coli* 70S ribosome revealed that the N-terminal α -helix of cpL13 occupies the position of H10 of the Ec23S rRNA (Figure 6F), which is absent in the chlororibosome (Figure 6E). The α -helix within the CTE of cpL27 appears to stabilize a three-way junction formed by the insertion of 20 nts within H38 of the cp23S rRNA (Figure 6G), which is lacking in the Ec23S rRNA (Figure 6H). The site of insertion in H38 in the cp23S rRNA correlates with the position of expansion segment 12 (ES12L) in eukaryotic 80S ribosomes (47,48). In the *E. coli* ribosome, EcL30 contacts H38 in the vicinity of the insertion site (Figure 6H). Such an L30-H38 interaction would not be possible in the chlororibosome due to the presence of the additional rRNA helix in H38, thus providing a possible explanation as to why L30 is missing in plant chloroplasts.

Intertwining of cpRP extensions at the tunnel exit

A number of differences with the *E. coli* 70S ribosome were evident when examining the back or cytosolic side of the LSU of the chlororibosome, in particular, the region surrounding the tunnel exit site. As mentioned, the β -hairpin of cpL23 is shorter than EcL23 leading to an enlarged luminal space near the exit site of the chlororibosome (Figure 7A–C). In contrast, the opposite side of the tunnel from cpL23 has extra mass due to the presence of the NTE of cpL24 that penetrates into the ribosomal core from the surface located globular domain (Figure 7B). The 27 aa CTE of cpL29 intertwines with the NTE of cpL23 (Figure 7B), which together occupy the space where 23S rRNA helix H10 is situated in the *E. coli* 70S ribosome (Figure 7C). Comparison with the binding site of *E. coli* SRP on the ribosome (49,50), suggests that the CTE of cpL29 could play a role in recruitment of cpSRP54 to the chlororibosome (Figure 7D).

By far the largest conglomerate of cpRP extensions is located at the back of the LSU adjacent to the tunnel exit site (Figure 7E). This conglomerate comprises the 45 aa (of 52 aa) NTE of cpL13, 22 aa (of 67 aa) from the NTE of cpL21 and 37 aa (of 60 aa) CTE of cpL22, which reach out from the respective globular domains to form multiple protein–protein interactions with each other (Figure 7F). The high flexibility of the extensions, and the poor quality of the density at the periphery of the ribosome, enabled only the backbone of the protein extensions to be traced. Moreover, the N-terminal 45 aa of the NTE of cpL21 could not be modeled, although density was observed at lower thresholds suggesting that these residues establish additional interactions with the CTE of cpL22. Collectively, these cpRP extensions expand the area of the LSU and could facilitate interaction with the thylakoid membrane (Figure 7E).

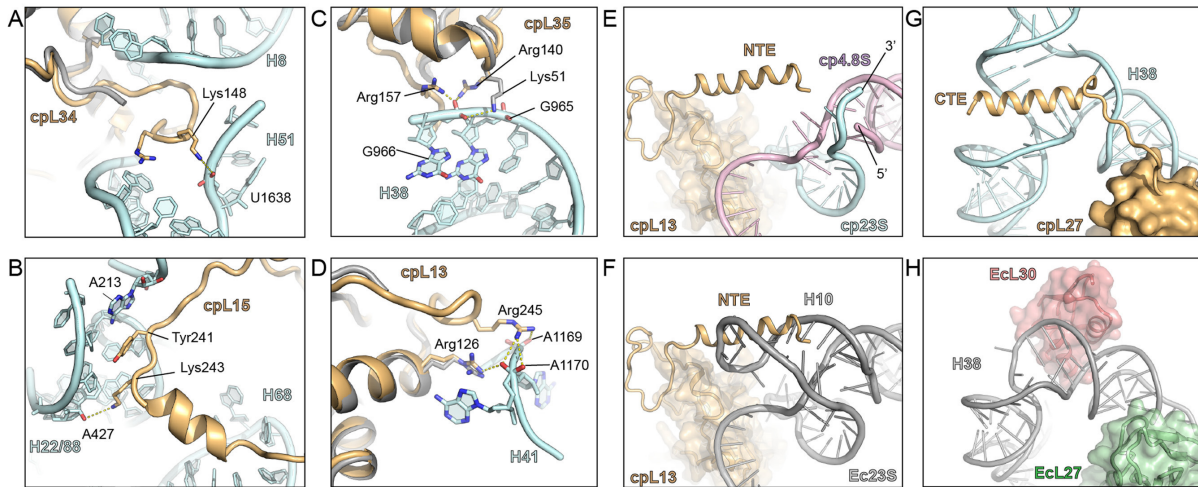


Figure 6. Interaction of cpRP extensions with rRNA. (A–D) Examples of interaction of cpRP extensions (gold) with cp23S rRNA (cyan) include the (A) CTE of cpL34 with H51, (B) CTE of cpL15 with H22/H88, (C) CTE of cpL35 with H38 and (D) NTE of cpL13 with H41. (E) Interaction of NTE of cpL13 (gold) with the 3' end of the cp23S (cyan) and the 5' end of the 4.8S (pink) in the chlororibosome, superimposed with the (F) *Escherichia coli* 70S ribosome showing that H10 of the Ec23S (gray) overlaps with the NTE of cpL13 (gold). (G) Interaction of CTE of cpL27 (gold) with the three-way junction of H38 (cyan) of the chlororibosome, whereas in the (H) *E. coli* 70S ribosome, Ecl27 (green) has no extension and H38 (gray) is bound by Ecl30 (red).

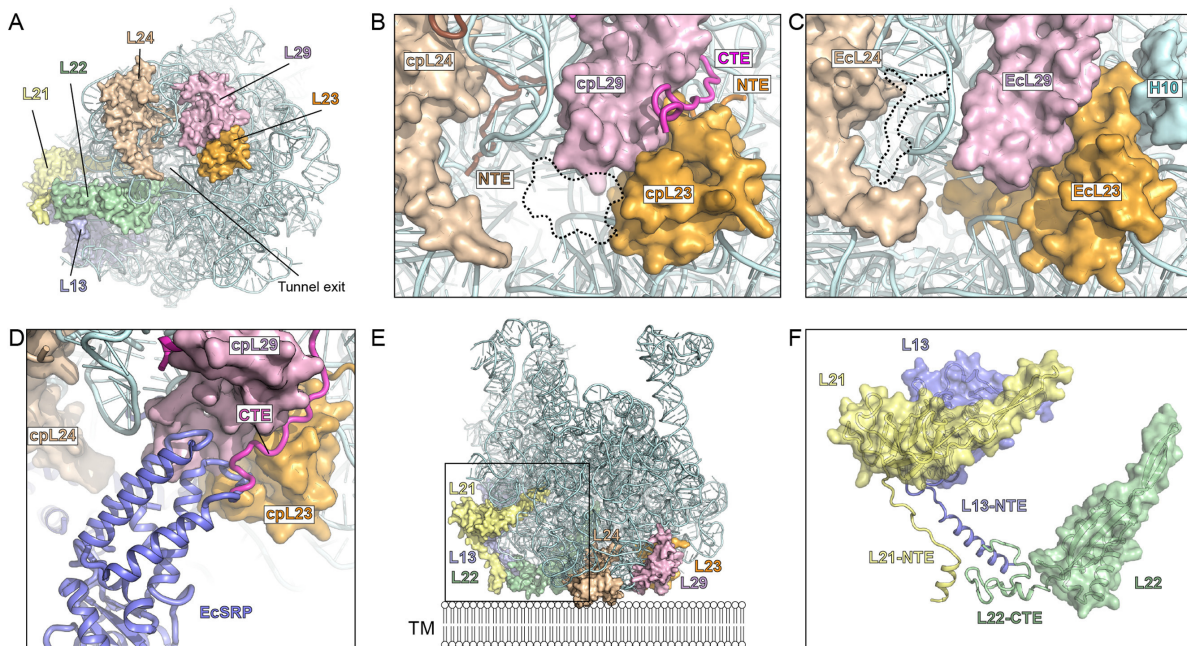


Figure 7. Interaction of cpRP extensions with rRNA. (A) View onto the tunnel exit site of the chloroplast LSU with rRNA (cyan) and highlighting cpRPs L23 (orange), L29 (purple), L24 (tan), L22 (green), L13 (blue) and L21 (yellow). (B) Zoom of (A) highlighting the NTE of cpL24 and cpL23, and the CTE of cpL29 as well as the shorter β -hairpin of cpL23. (C) Equivalent view of (B) but for *Escherichia coli* 70S ribosome, highlighting the absence of Ecl24-NTE and the presence of the β -hairpin of Ecl23 in the tunnel lumen, as well as H10 of Ec23S rRNA. (D) Superimposition of EcSRP (blue) on chlororibosome illustrating overlap with the CTE of cpL29. (E) Chloroplast LSU, colored as in (A), illustrating additional cpRP protein mass that expands the potential surface area of the LSU and facilitates its possible interaction with the thylakoid membrane (TM). (F) Zoom of boxed region in (E) without rRNA to illustrate the contribution of the cpRP extensions (NTE/CTE) of L21 (yellow), L13 (blue) and L22 (green) to the thylakoid membrane interaction surface.

CONCLUSION

Here we present a near-complete molecular model for the spinach chloroplast LSU, revealing the location of rRNA insertions and deletions, cpRP extensions as well as the binding site of two plastid-specific RPs, PSRP5 and PSRP6. Prior to submission, a cryo-EM structure of the spinach chloroplast 50S subunit was reported by Ahmed and coworkers (51). Generally, the results appear to be in good agreement with our structure, although a careful comparison cannot be undertaken as the cryo-EM map and model were not yet available at the time of submission, nor during the review process. In general, the differences of the chlororibosome with respect to the eubacterial *E. coli* 70S ribosome are localized to peripheral regions of the ribosome and not within core functional regions that would be expected to influence translational activity, such as the subunit interface, peptidyl-transferase center or translation factor binding site. One major exception is related to the ribosomal tunnel through which the nascent polypeptide chain passes as it is synthesized. In the chlororibosome, we observed that the lower region of the tunnel differs from bacteria due to a shorter β -hairpin of cpL23 and the additional presence of the NTE of cpL24. Formation of α -helical secondary structure within nascent polypeptides chains has been observed in this region of the ribosomal tunnel (52). Structural changes within this region of the chlororibosome may facilitate targeting and insertion of transmembrane-containing proteins into the thylakoid membrane. In this respect, we also note that the CTE of cpL29 could play a role in recruitment of cpSRP54 to the chlororibosome. Unlike bacterial SRPs, the cpSRP lacks the 4.5S RNA (termed, SRP RNA) and comprises only the SRP54 protein, and therefore the CTE of cpL29 may contribute to stabilization of SRP54 interaction with the chlororibosome. Finally, we observed a large conglomerate of cpRP extensions that expand the surface area at the back of the LSU. We suggest that this may facilitate interaction of the chlororibosome directly with the thylakoid membrane and/or membrane-bound components of the targeting machinery, and thereby increase the efficiency of membrane protein insertion. As mentioned, the majority of the chloroplast-encoded proteins is targeted to the thylakoid membranes, including components of the ATP synthase, cytochrome b/f and especially photosystem I and II complexes (4).

ACCESSION NUMBERS

The coordinates and cryo-EM map for the chlororibosome have been deposited in the Protein Data Bank and EM DataBank under accession codes PDB ID 5MLC and EMD-3525/EMD-3526, respectively.

SUPPLEMENTARY DATA

Supplementary Data are available at NAR Online.

ACKNOWLEDGEMENTS

We would like to thank Heidmarie Sieber, Susi Rieder and Charlotte Ungewickell for expert technical assistance and Sarah Schlaak for help with data analysis. CIISB research

infrastructure project LM2015043 funded by MEYS CR is gratefully acknowledged for the financial support of the measurements at the CF Cryo-electron Microscopy and Tomography CEITEC MU.

FUNDING

Deutsche Forschungsgemeinschaft (DFG) [FOR-1805, SPP-1879, GRK-1721 to D.N.W.]; iNEXT project [653706]; Horizon 2020 program of the European Union; MEYS CR (CIISB research infrastructure project LM2015043. Funding for open access charge: DFG.

Conflict of interest statement. None declared.

REFERENCES

- Reyes-Prieto, A., Weber, A.P. and Bhattacharya, D. (2007) The origin and establishment of the plastid in algae and plants. *Annu. Rev. Genet.*, **41**, 147–168.
- Tiller, N. and Bock, R. (2014) The translational apparatus of plastids and its role in plant development. *Mol. Plant*, **7**, 1105–1120.
- Sun, Y. and Zerges, W. (2015) Translational regulation in chloroplasts for development and homeostasis. *Biochim. Biophys. Acta*, **1847**, 809–820.
- Schmitz-Linneweber, C., Maier, R.M., Alcaraz, J.P., Cottet, A., Herrmann, R.G. and Mache, R. (2001) The plastid chromosome of spinach (*Spinacia oleracea*): complete nucleotide sequence and gene organization. *Plant Mol. Biol.*, **45**, 307–315.
- Yamaguchi, K. and Subramanian, A.R. (2000) The plastid ribosomal proteins. Identification of all the proteins in the 50S subunit of an organelle ribosome (chloroplast). *J. Biol. Chem.*, **275**, 28466–28482.
- Yamaguchi, K., von Knoblauch, K. and Subramanian, A.R. (2000) The plastid ribosomal proteins. Identification of all the proteins in the 30S subunit of an organelle ribosome (chloroplast). *J. Biol. Chem.*, **275**, 28455–28465.
- Yamaguchi, K. and Subramanian, A.R. (2003) Proteomic identification of all plastid-specific ribosomal proteins in higher plant chloroplast 30S ribosomal subunit. *Eur. J. Biochem.*, **270**, 190–205.
- Sharma, M.R., Wilson, D.N., Datta, P.P., Barat, C., Schluenzen, F., Fucini, P. and Agrawal, R.K. (2007) Cryo-EM study of the spinach chloroplast ribosome reveals the structural and functional roles of plastid-specific ribosomal proteins. *Proc. Natl. Acad. Sci. U.S.A.*, **104**, 19315–19320.
- Bartsch, M., Kimura, M. and Subramanian, A.R. (1982) Purification, primary structure, and homology relationships of a chloroplast ribosomal protein. *Proc. Natl. Acad. Sci. U.S.A.*, **79**, 6871–6875.
- Grant, T. and Grigorieff, N. (2015) Measuring the optimal exposure for single particle cryo-EM using a 2.6 Å reconstruction of rotavirus VP6. *Elife*, **4**, e06980.
- Rohou, A. and Grigorieff, N. (2015) CTFFIND4: fast and accurate defocus estimation from electron micrographs. *J. Struct. Biol.*, **192**, 216–221.
- Frank, J., Radermacher, M., Penczek, P., Zhu, J., Li, Y., Ladjadj, M. and Leith, A. (1996) SPIDER and WEB: processing and visualization of images in 3D electron microscopy and related fields. *J. Struct. Biol.*, **116**, 190–199.
- Becker, T., Franckenberg, S., Wickles, S., Shoemaker, C.J., Anger, A.M., Armache, J.P., Sieber, H., Ungewickell, C., Berninghausen, O., Daberkow, I. et al. (2012) Structural basis of highly conserved ribosome recycling in eukaryotes and archaea. *Nature*, **482**, 501–506.
- Chen, J.Z. and Grigorieff, N. (2007) SIGNATURE: a single-particle selection system for molecular electron microscopy. *J. Struct. Biol.*, **157**, 168–173.
- Arenz, S., Meydan, S., Starosta, A.L., Berninghausen, O., Beckmann, R., Vazquez-Laslop, N. and Wilson, D.N. (2014) Drug sensing by the ribosome induces translational arrest via active site perturbation. *Mol. Cell*, **56**, 446–452.
- Loerke, J., Giesebrecht, J. and Spahn, C.M. (2010) Multiparticle cryo-EM of ribosomes. *Methods Enzymol.*, **483**, 161–177.
- Grigorieff, N. (2007) FREALIGN: high-resolution refinement of single particle structures. *J. Struct. Biol.*, **157**, 117–125.

18. Kucukelbir, A., Sigworth, F.J. and Tagare, H.D. (2014) Quantifying the local resolution of cryo-EM density maps. *Nat. Methods*, **11**, 63–65.
19. Scheres, S.H. (2012) RELION: implementation of a Bayesian approach to cryo-EM structure determination. *J. Struct. Biol.*, **180**, 519–530.
20. Fischer, N., Neumann, P., Konevega, A.L., Bock, L.V., Ficner, R., Rodnina, M.V. and Stark, H. (2015) Structure of the E. coli ribosome-EF-Tu complex at <3 Å resolution by C-corrected cryo-EM. *Nature*, **520**, 567–570.
21. Cannone, J.J., Subramanian, S., Schnare, M.N., Collett, J.R., D'Souza, L.M., Du, Y., Feng, B., Lin, N., Madabusi, L.V., Muller, K.M. *et al.* (2002) The comparative RNA web (CRW) site: an online database of comparative sequence and structure information for ribosomal, intron, and other RNAs. *Biomed Central Bioinformatics*, **3**, 2.
22. Pettersen, E.F., Goddard, T.D., Huang, C.C., Couch, G.S., Greenblatt, D.M., Meng, E.C. and Ferrin, T.E. (2004) UCSF chimera—a visualization system for exploratory research and analysis. *J. Comput. Chem.*, **25**, 1605–1612.
23. Emsley, P. and Cowtan, K. (2004) Coot: model-building tools for molecular graphics. *Acta Crystallogr. D Biol. Crystallogr.*, **60**, 2126–2132.
24. Guex, N. and Peitsch, M.C. (1997) SWISS-MODEL and the Swiss-PdbViewer: an environment for comparative protein modeling. *Electrophoresis*, **18**, 2714–2723.
25. Soding, J., Biegert, A. and Lupas, A.N. (2005) The HHpred interactive server for protein homology detection and structure prediction. *Nucleic Acids Res.*, **33**, W244–W248.
26. Buchan, D., Minnici, F., Nugent, T., Bryson, K. and Jones, D. (2013) Scalable web services for the PSIPRED Protein Analysis Workbench. *Nucleic Acids Res.*, **41**, W340–W348.
27. Adams, P.D., Afonine, P.V., Bunkoczi, G., Chen, V.B., Davis, I.W., Echols, N., Headd, J.J., Hung, L.W., Kapral, G.J., Grosse-Kunstleve, R.W. *et al.* (2010) PHENIX: a comprehensive Python-based system for macromolecular structure solution. *Acta Crystallogr. D Biol. Crystallogr.*, **66**, 213–221.
28. Vagin, A.A., Steiner, R.A., Lebedev, A.A., Potterton, L., McNicholas, S., Long, F. and Murshudov, G.N. (2004) REFMAC5 dictionary: organization of prior chemical knowledge and guidelines for its use. *Acta Crystallogr. D Biol. Crystallogr.*, **60**, 2184–2195.
29. Brown, A., Long, F., Nicholls, R.A., Toots, J., Emsley, P. and Murshudov, G. (2015) Tools for macromolecular model building and refinement into electron cryo-microscopy reconstructions. *Acta Crystallogr. D Biol. Crystallogr.*, **71**, 136–153.
30. Amunts, A., Brown, A., Bai, X.C., Llacer, J.L., Hussain, T., Emsley, P., Long, F., Murshudov, G., Scheres, S.H. and Ramakrishnan, V. (2014) Structure of the yeast mitochondrial large ribosomal subunit. *Science*, **343**, 1485–1489.
31. Chen, V.B., Arendall, W.B. 3rd, Headd, J.J., Keedy, D.A., Immormino, R.M., Kapral, G.J., Murray, L.W., Richardson, J.S. and Richardson, D.C. (2010) MolProbity: all-atom structure validation for macromolecular crystallography. *Acta Crystallogr. D Biol. Crystallogr.*, **66**, 12–21.
32. Noeske, J., Wasserman, M.R., Terry, D.S., Altman, R.B., Blanchard, S.C. and Cate, J.H. (2015) High-resolution structure of the Escherichia coli ribosome. *Nat. Struct. Mol. Biol.*, **22**, 336–341.
33. Llacer, J.L., Hussain, T., Marler, L., Aitken, C.E., Thakur, A., Lorsch, J.R., Hinnebusch, A.G. and Ramakrishnan, V. (2015) Conformational differences between open and closed states of the eukaryotic translation initiation complex. *Mol. Cell*, **59**, 399–412.
34. Hussain, T., Llacer, J.L., Wimberly, B.T., Kieft, J.S. and Ramakrishnan, V. (2016) Large-scale movements of IF3 and tRNA during bacterial translation initiation. *Cell*, **167**, 133–144.
35. Wimberly, B.T., Brodersen, D.E., Clemons, W.M., Morgan-Warren, R.J., Carter, A.P., Vonnrhein, C., Hartsch, T. and Ramakrishnan, V. (2000) Structure of the 30S ribosomal subunit. *Nature*, **407**, 327–339.
36. Sharma, M.R., Donhofer, A., Barat, C., Marquez, V., Datta, P.P., Fucini, P., Wilson, D.N. and Agrawal, R.K. (2010) PSRP1 is not a ribosomal protein, but a ribosome-binding factor that is recycled by the ribosome-recycling factor (RRF) and elongation factor G (EF-G). *J. Biol. Chem.*, **285**, 4006–4014.
37. Yoshida, H. and Wada, A. (2014) The 100S ribosome: ribosomal hibernation induced by stress. *Wiley Interdisciplin. Rev. RNA*, **5**, 723–732.
38. Vila-Sanjurjo, A., Schuwirth, B.S., Hau, C.W. and Cate, J.H.D. (2004) Structural basis for the control of translational initiation during stress. *Nat. Struct. Mol. Biol.*, **11**, 1054–1059.
39. Polikanov, Y.S., Blaha, G.M. and Steitz, T.A. (2012) How hibernation factors RMF, HPF, and YfiA turn off protein synthesis. *Science*, **336**, 915–918.
40. Puri, P., Eckhardt, T.H., Franken, L.E., Fusetti, F., Stuart, M.C., Boekema, E.J., Kuipers, O.P., Kok, J. and Poolman, B. (2014) Lactococcus lactis YfiA is necessary and sufficient for ribosome dimerization. *Mol. Microbiol.*, **91**, 394–407.
41. Basu, A. and Yap, M.N. (2016) Ribosome hibernation factor promotes Staphylococcal survival and differentially represses translation. *Nucleic Acids Res.*, **44**, 4881–4893.
42. Wilson, D.N., Schluenzen, F., Harms, J.M., Yoshida, T., Ohkubo, T., Albrecht, R., Buerger, J., Kobayashi, Y. and Fucini, P. (2005) X-ray crystallography study on ribosome recycling: the mechanism of binding and action of RRF on the 50S ribosomal subunit. *EMBO J.*, **24**, 251–260.
43. Weixlbaumer, A., Petry, S., Dunham, C.M., Selmer, M., Kelley, A.C. and Ramakrishnan, V. (2007) Crystal structure of the ribosome recycling factor bound to the ribosome. *Nat. Struct. Mol. Biol.*, **14**, 733–737.
44. Amunts, A., Brown, A., Toots, J., Scheres, S.H. and Ramakrishnan, V. (2015) Ribosome. The structure of the human mitochondrial ribosome. *Science*, **348**, 95–98.
45. Greber, B.J., Bieri, P., Leibundgut, M., Leitner, A., Aebersold, R., Boehringer, D. and Ban, N. (2015) Ribosome. The complete structure of the 55S mammalian mitochondrial ribosome. *Science*, **348**, 303–308.
46. Ban, N., Nissen, P., Hansen, J., Moore, P.B. and Steitz, T.A. (2000) The complete atomic structure of the large ribosomal subunit at 2.4 Å resolution. *Science*, **289**, 905–920.
47. Ben-Shem, A., Garreau de Loubresse, N., Melnikov, S., Jenner, L., Yusupova, G. and Yusupov, M. (2011) The structure of the eukaryotic ribosome at 3.0 Å resolution. *Science*, **334**, 1524–1529.
48. Anger, A.M., Armache, J.P., Berninghausen, O., Habeck, M., Subklewe, M., Wilson, D.N. and Beckmann, R. (2013) Structures of the human and Drosophila 80S ribosome. *Nature*, **497**, 80–85.
49. Halic, M., Blau, M., Becker, T., Mielke, T., Pool, M.R., Wild, K., Sinning, I. and Beckmann, R. (2006) Following the signal sequence from ribosomal tunnel exit to signal recognition particle. *Nature*, **444**, 507–511.
50. Jomaa, A., Boehringer, D., Leibundgut, M. and Ban, N. (2016) Structures of the E. coli translating ribosome with SRP and its receptor and with the translocon. *Nat. Commun.*, **7**, 10471.
51. Ahmed, T., Yin, Z. and Bhushan, S. (2016) Cryo-EM structure of the large subunit of the spinach chloroplast ribosome. *Sci. Rep.*, **6**, 35793.
52. Wilson, D.N. and Beckmann, R. (2011) The ribosomal tunnel as a functional environment for nascent polypeptide folding and translational stalling. *Curr. Opin. Struct. Biol.*, **21**, 1–10.

SUPPLEMENTARY ONLINE MATERIALS

for

Cryo-EM structure of the spinach chloroplast ribosome reveals the location of plastid-specific ribosomal proteins and extensions

Michael Graf¹, Stefan Arenz¹, Paul Huter¹, Alexandra Dönhöfer¹, Jiří Nováček², Daniel N. Wilson^{1,3,*}

¹ Gene Center, Department for Biochemistry and Center for integrated Protein Science Munich (CiPSM), University of Munich, 81377 Munich, Germany

² Central European Institute of Technology (CEITEC), Masaryk University, Kamenice 5, 62500 Brno, Czech Republic.

³ Department of Biochemistry and Molecular Biology, University of Hamburg, 20146 Hamburg, Germany.

* To whom correspondence should be addressed. Tel: +49 89 2180 76903; Fax: +49 89 2180 76945; Email: wilson@lmb.uni-muenchen.de.

SUPPLEMENTARY FIGURES

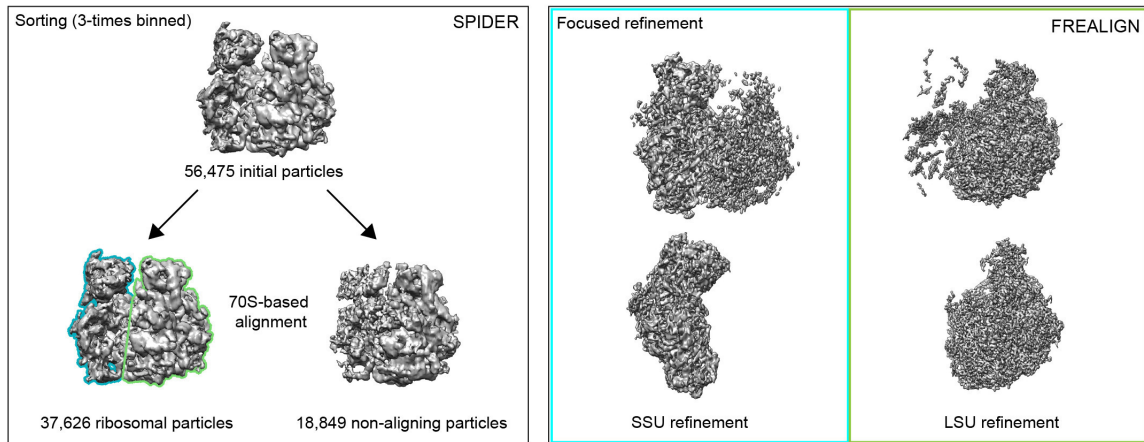


Figure S1: *In silico* sorting and refinement of the chloroplast SSU and LSU. (A) *In silico* sorting was performed using SPIDER (2), starting with an initial 56,475 particles that yielded after removal of non-aligning particles (18,849), a dataset of 37,626 ribosomal particles. **(B)** Subsequently, focused alignment and refinement of the SSU and LSU was performed in FREALIGN (3).

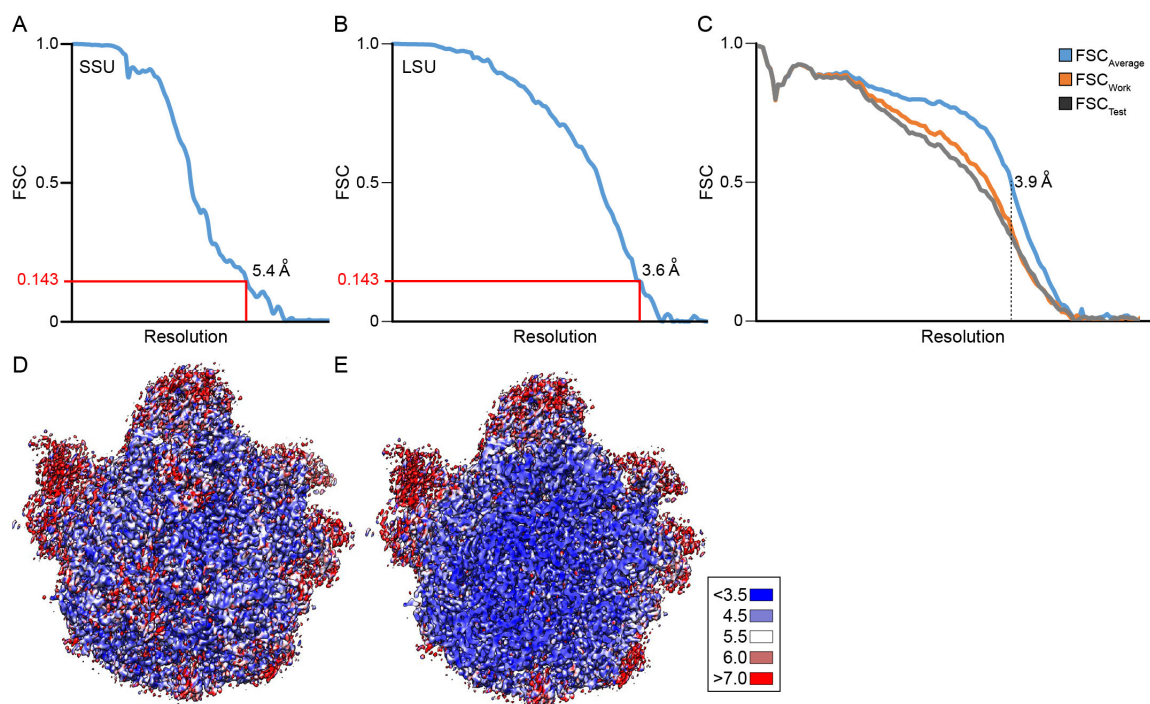


Figure S2: Resolution of the cryo-EM reconstruction of the chloroplast SSU and LSU. (A,B) Fourier-shell correlation curve (FSC) of the refined final map of the chloroplast (A) SSU and (B) LSU, indicating the average resolution is 5.4 Å and 3.6 Å, respectively. (C) Fit of models to maps. FSC curves calculated between the refined model and the final map (blue), with the self- and cross-validated correlations in orange and black, respectively. Information beyond 3.6 Å was not used during refinement and preserved for validation. (D) Overview and (E) transverse section through the chloroplast LSU colored according to the local resolution as calculated using ResMap (1).

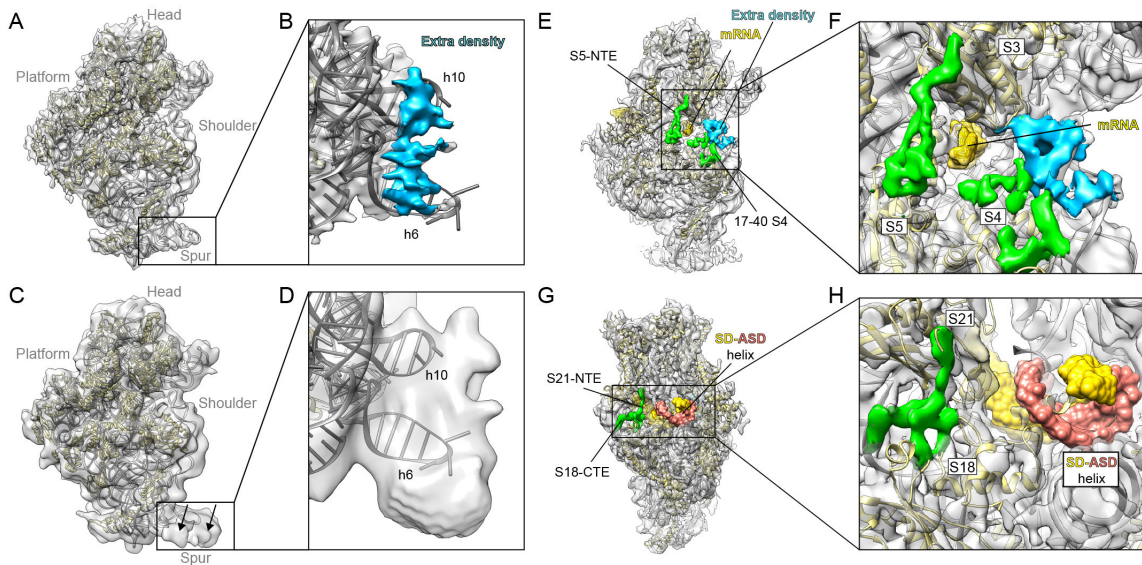


Figure S3: Localization of extra density on the SSU. (A) Overview of the back of the cryo-EM map (grey) of the chloroplast SSU with molecular model (rRNA, grey; RPs, yellow), and with (B) zoom onto the spur region, showing extra density (blue). (C) Overview of the back of the cryo-EM map (grey) of the chloroplast SSU from Sharma and coworkers (4) with molecular model (rRNA, grey; RPs, yellow), and with (D) zoom onto the spur region, showing additional density that was assigned to PSRP2/3. (E) Overview and (F) zoom onto the back of the cryo-EM map (grey) of the chloroplast SSU with molecular model (rRNA, grey; RPs, yellow), with cpRP densities (green) and unassigned extra density (blue) shown relative to the position of mRNA (yellow; superimposed from PDB ID 318G (5)). (G) Overview and (H) zoom onto the platform of the cryo-EM map (grey) of the chloroplast SSU with molecular model (rRNA, grey; RPs, yellow) and cpRP densities (green) shown relative to the position of SD-aSD helix (yellow/red; superimposed from PDB ID 318G (5)).

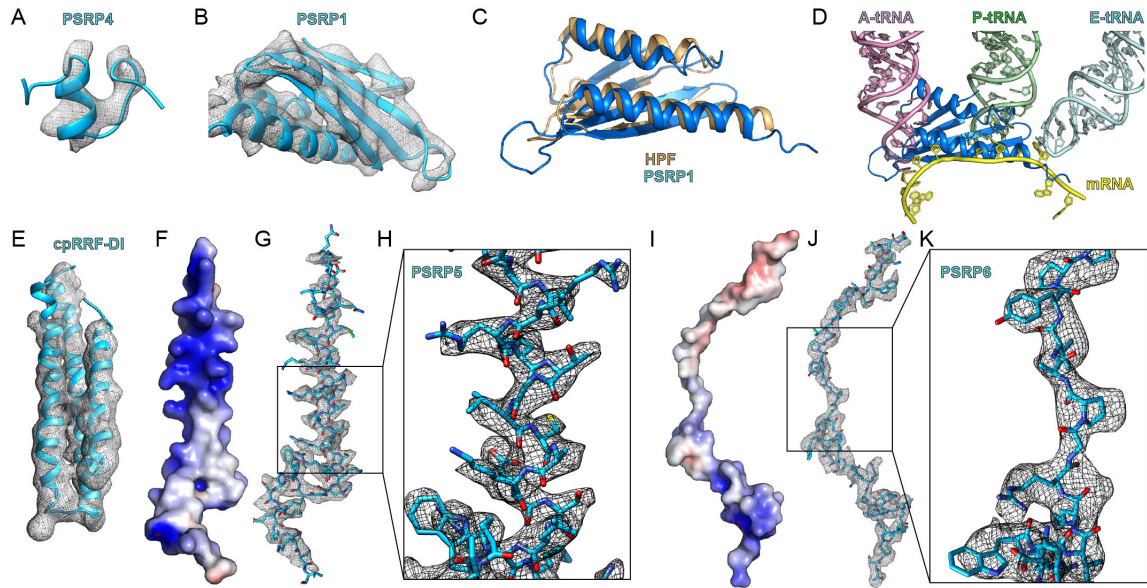


Figure S4: Localization of PSRPs on the chlororibosome. (A,B) Cryo-EM electron density (grey mesh) for (A) PSRP4 and (B) PSRP1. (C,D) Superimposition of the binding site of PSRP1 (blue) on the chlororibosome relative to (C) *E. coli* HPF (orange) bound to the *Thermus thermophilus* 70S ribosome (PDB ID 4V8H, (6)) and (D) mRNA (yellow) and A-site (pink), P-site (green) and E-site (cyan) tRNAs (PDB ID 3I8G, (5)). (E) Cryo-EM electron density (grey mesh) for domain I of the cpRRF (blue, cpRRF-DI). (F-H) Molecular model for PSRP5 shown as (F) surface charge (blue, positive) and (G) with electron density (grey mesh) and (H) zoom of the boxed region in (G). (I-K) Molecular model for PSRP6 shown as (I) surface charge (blue, positive, white neutral, red, negative) and (J) with electron density (grey mesh) and (K) zoom of the boxed region in (J).

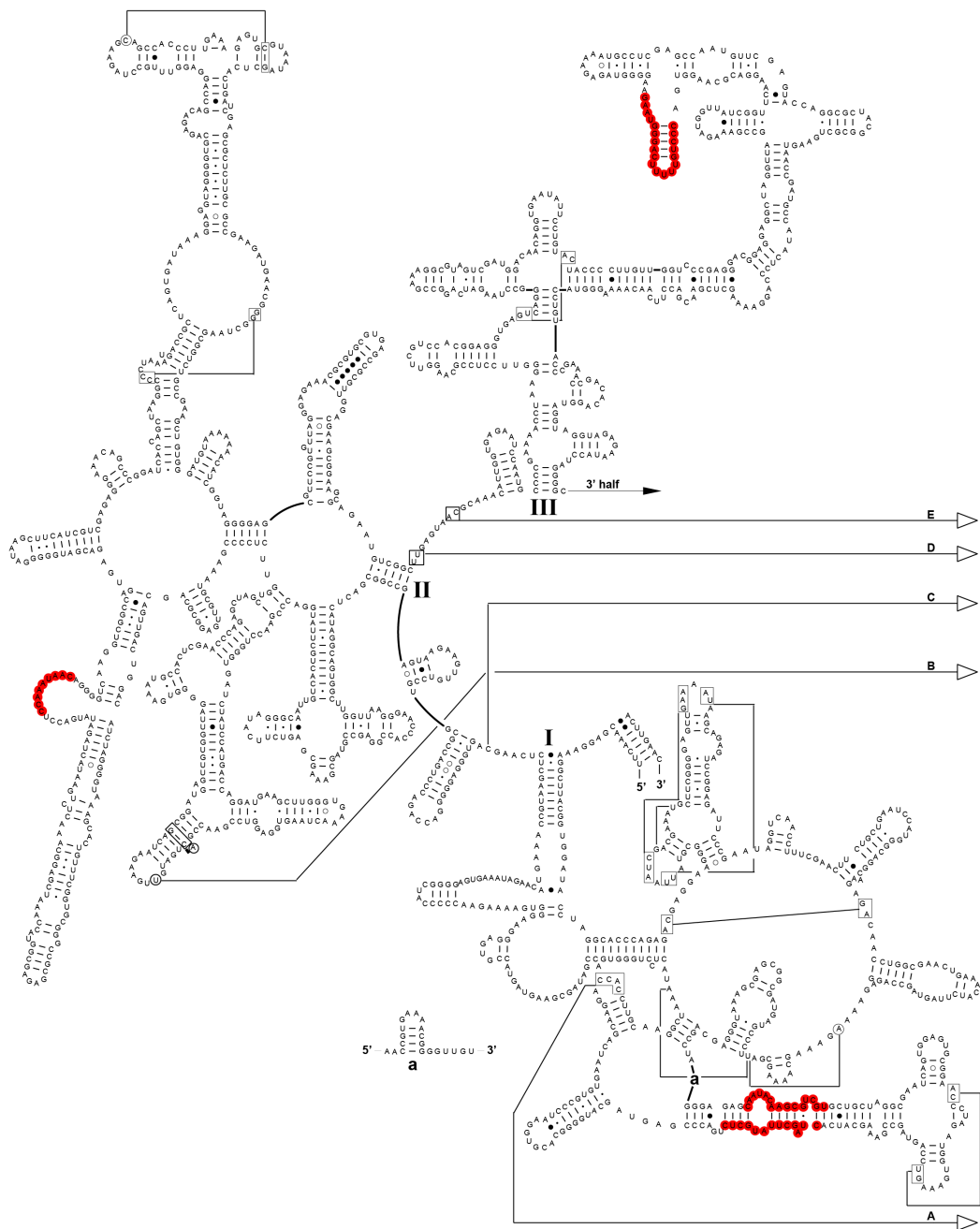


Figure S5: Modelled nucleotides of the chloroplast 4.8S and 23S rRNAs. (A) Secondary structure of the 5' portion of the cp23S rRNA, with nucleotides highlighted in red that were not modelled. The secondary structure diagram was taken from the Comparative RNA Web (CRW) Site (www.rna.ccbb.utexas.edu) (7).

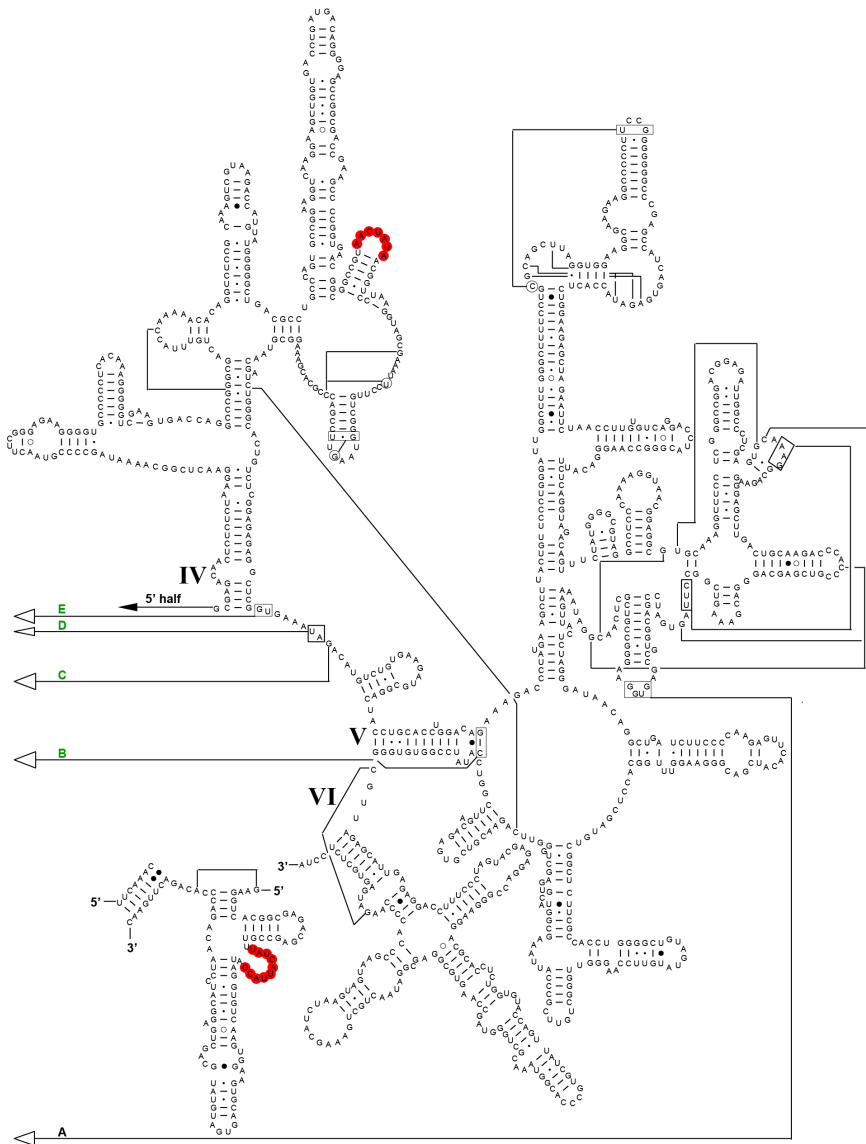


Figure S5: Modelled nucleotides of the chloroplast 4.8S and 23S rRNAs. (B) Secondary structure of the 3' portion of the cp23S rRNA and 4.8S rRNA, with nucleotides highlighted in red that were not modelled. The secondary structure diagram was taken from the Comparative RNA Web (CRW) Site (www.rna.ccbb.utexas.edu) (7).

SUPPLEMENTARY TABLES

Supplementary Table S1. Data collection and refinement statistics

Data Collection and Refinement	Cp50S
Particles	37,636
Pixel size (Å)	1.061
Defocus range (µm)	-1.0-2.3
Voltage (kV)	300
Electron dose (e ⁻ /Å ⁻²)	40.3
Map sharpening B factor (Å ²)	-84.98
Resolution (Å, 0.143 FSC)	3.6
FSC _{Average}	0.88
Model Composition	
Protein residues	3,392
RNA bases	2,963
Validation (proteins)	
Poor rotamers (%)	7.11
Ramachandran outliers (%)	2.94
Ramachandran favored (%)	85.51
Bad backbone bonds (%)	0.04
Bad backbone angles	0.01
MolProbity score	2.48 (99 th percentile)
Validation (nucleic acids)	
Correct sugar puckers (%)	96.39
Good backbone conformations (%)	69.83
Bad bonds (%)	0.01
Bad angles	0.21
Clash score, all atoms	3.96 (100th percentile)

Supplementary Table S2 Modeled proteins of the chloroplast LSU

Protein	UniProtKB	Preprotein	Mature Length	Modeled Residues
uL01c	Q9LE95	1-352	73-352	
uL02c	P06509		2-272	26-271
uL03c	A0A0K9QEC7	1-305	85-305	85-303
uL04c	O49937	1-293	51-293	56-260
uL05c	P82192		1-220	16-194
uL06c	A0A0K9R4N9	1-220	39-220	40-217
bL09c	A0A0K9RQ91	1-196	42-196	43-87
uL10c	A0A0K9R3N5	1-232	53-232	
uL11c	P31164	1-224	67-224	
bL12c	P02398	1-189	57-189	
uL13c	P12629	1-250	48-250	55-250
uL14c	P09596		1-121	1-120
uL15c	A0A0K9QHT0	1-271	61-271	78-259
uL16c	P17353		1-135	1-135
bL17c	A0A0K9RLJ4	1-126	11-126	11-126
uL18c	A0A0K9QQ60	1-166	45-166	49-166
bL19c	P82413	1-233	78-233	117-230
bL20c	P28803		2-128	2-117
bL21c	P24613	1-256	56-256	101-234
uL22c	P09594		2-199	25-176
uL23c	Q9LWB5	1-198	77-198	104-194
uL24c	P27683	1-191	47-191	47-175
bL27c	A0A0K9R4I2	1-194	57-194	59-166
bL28c	A0A0K9RD02	1-148	72-148	72-146
uL29c	A0A0K9R7W8	1-168	59-168	59-152
bL31c	A0A0K9R0R6	1-130	37-130	
bL32c	P28804	1-57	2-57	2-43
bL33c	P28805		1-66	6-65
bL34c	P82244	1-152	92-152	92-152
bL35c	P23326	1-159	87-159	90-159
bL36c	P12230		1-37	1-37
PSRP5	P27684	1-142	59-142	97-142
PSRP6	P82411	1-116	48-116	48-94
RRF	P82231		1-271	89-114;191-271

SUPPLEMENTARY REFERENCES

1. Kucukelbir, A., Sigworth, F.J. and Tagare, H.D. (2014) Quantifying the local resolution of cryo-EM density maps. *Nat. Methods*, **11**, 63-65.
2. Frank, J., Radermacher, M., Penczek, P., Zhu, J., Li, Y., Ladjadj, M. and Leith, A. (1996) SPIDER and WEB: processing and visualization of images in 3D electron microscopy and related fields. *J. Struct. Biol.*, **116**, 190-199.
3. Grigorieff, N. (2007) FREALIGN: high-resolution refinement of single particle structures. *J. Struct. Biol.*, **157**, 117-125.
4. Sharma, M.R., Wilson, D.N., Datta, P.P., Barat, C., Schluenzen, F., Fucini, P. and Agrawal, R.K. (2007) Cryo-EM study of the spinach chloroplast ribosome reveals the structural and functional roles of plastid-specific ribosomal proteins. *Proc. Natl. Acad. Sci. USA*, **104**, 19315-19320.
5. Jenner, L.B., Demeshkina, N., Yusupova, G. and Yusupov, M. (2010) Structural aspects of messenger RNA reading frame maintenance by the ribosome. *Nat. Struct. Mol. Biol.*, **17**, 555-560.
6. Polikanov, Y.S., Blaha, G.M. and Steitz, T.A. (2012) How hibernation factors RMF, HPF, and YfiA turn off protein synthesis. *Science*, **336**, 915-918.
7. Cannone, J.J., Subramanian, S., Schnare, M.N., Collett, J.R., D'Souza, L.M., Du, Y., Feng, B., Lin, N., Madabusi, L.V., Muller, K.M. *et al.* (2002) The comparative RNA web (CRW) site: an online database of comparative sequence and structure information for ribosomal, intron, and other RNAs. *BioMed Central Bioinformatics*, **3**, 2.

Structural basis for ArfA–RF2–mediated translation termination on mRNAs lacking stop codons

Paul Huter^{1*}, Claudia Müller^{1*}, Bertrand Beckert^{1,2}, Stefan Arenz¹, Otto Berninghausen¹, Roland Beckmann¹ & Daniel N. Wilson^{1,2}

In bacteria, ribosomes stalled on truncated mRNAs that lack a stop codon are rescued by the transfer-messenger RNA (tmRNA), alternative rescue factor A (ArfA) or ArfB systems¹. Although tmRNA–ribosome and ArfB–ribosome structures have been determined^{2–7}, how ArfA recognizes the presence of truncated mRNAs and recruits the canonical termination release factor RF2 to rescue the stalled ribosomes is unclear. Here we present a cryo-electron microscopy reconstruction of the *Escherichia coli* 70S ribosome stalled on a truncated mRNA in the presence of ArfA and RF2. The structure shows that the C terminus of ArfA binds within the mRNA entry channel on the small ribosomal subunit, and explains how ArfA distinguishes between ribosomes that bear truncated or full-length mRNAs. The N terminus of ArfA establishes several interactions with the decoding domain of RF2, and this finding illustrates how ArfA recruits RF2 to the stalled ribosome. Furthermore, ArfA is shown to stabilize a unique conformation of the switch loop of RF2, which mimics the canonical translation termination state by directing the catalytically important GGQ motif within domain 3 of RF2 towards the peptidyl-transferase centre of the ribosome. Thus, our structure reveals not only how ArfA recruits RF2 to the ribosome but also how it promotes an active conformation of RF2 to enable translation termination in the absence of a stop codon.

Premature transcription termination or truncation of a full-length mRNA can lead to mRNAs lacking a stop codon. Ribosomes translating these truncated mRNAs become trapped at the 3' end of the mRNA because translation elongation or termination cannot occur. In bacteria, these stalled ribosomes are recognized and recycled by the tmRNA rescue system (reviewed in ref. 1). A subset of bacteria, such as *E. coli*, can survive without the tmRNA system owing to the presence of ArfA⁸. The synthetic lethality arising from inactivation of both the tmRNA and ArfA rescue systems can be alleviated by overexpression of ArfB⁹. Collectively, these studies illustrate the physiological importance that the rescue of stalled ribosomes has for cell viability. Structural studies have revealed how ribosomes stalled on truncated mRNA are recognized and recycled by the tmRNA–SmpB complex^{6,7} or ArfB⁵. In the case of ArfB, the empty mRNA channel of the ribosome is probed by the C-terminal helix, positioning the N-terminal catalytic GGQ-containing domain at the peptidyl-transferase centre (PTC) to trigger peptidyl-tRNA hydrolysis⁵. Similarly, in the tmRNA–SmpB complex, the C-terminal helix of SmpB recognizes the empty mRNA channel and positions the tRNA-like domain of tmRNA at the PTC to enable peptidyltransfer^{6,7}. Translation then continues on the mRNA-like domain of tmRNA, which encodes a short peptide targeting the incompletely translated nascent polypeptide chain for degradation¹. Biochemical studies have demonstrated that ArfA represents a back-up system for tmRNA^{10,11}. The *arfA* mRNA contains a stem-loop that acts as a transcription terminator as well as a substrate for RNase III

cleavage^{10–12}. In the presence of tmRNA, the short ArfA product produced from the truncated *arfA* mRNA is tagged by tmRNA and targeted for degradation. However, in the absence of tmRNA, the short ArfA product is not degraded and assumes the role of recycling ribosomes stalled on truncated mRNAs^{10,11}. The full-length *E. coli* ArfA protein is 72 amino acids long and contains a C-terminal hydrophobic region that leads to aggregation of the protein *in vivo*¹⁰. Shorter forms of ArfA that result from truncated *arfA* mRNAs and lack the terminal 17–18 amino acids retain full recycling activity^{10,11}. ArfA alone is insufficient to recycle ribosomes stalled on truncated mRNAs and requires the assistance of the canonical termination release factor RF2 to hydrolyse the peptidyl-tRNA on the ribosome^{13,14} (Fig. 1a–c). A mechanistic understanding of how ArfA recognizes ribosomes stalled on truncated mRNAs, recruits RF2 and stabilizes the active conformation of RF2 has so far been hampered by the lack of an ArfA–RF2–ribosome structure.

To generate a suitable complex for structural analysis, *in vitro* translation reactions were performed with a truncated mRNA in the presence and absence of ArfA Δ 17 (lacking residues 56–72) and/or RF2. As reported previously^{13,14}, the presence of both ArfA and RF2 was required for efficient recycling of the peptidyl-tRNA (Extended Data Fig. 1). By contrast, replacing wild-type RF2 with the catalytically inactive RF2-GAQ mutant (in which the tripeptide Gly-Gly-Gln is converted to Gly-Ala-Gln) prevented peptidyl-tRNA hydrolysis and recycling (Extended Data Fig. 1), as described previously¹⁵. Cryo-electron microscopy (cryo-EM) analysis of the ArfA Δ 17–RF2–GAQ-stalled ribosomal complex (hereafter referred to as ArfA–RF2–SRC) and *in silico* sorting of this dataset yielded a major subpopulation of ribosomal particles that contained stoichiometric occupancy of P-tRNA, ArfA and RF2 (Extended Data Fig. 2). Subsequent refinement resulted in a final reconstruction of ArfA–RF2–SRC (Fig. 1d) with an average resolution of 3.1 Å (Extended Data Fig. 3 and Extended Data Table 1). The electron density for most of ArfA was well-resolved with local resolution mostly within the range of 3.0 to 3.5 Å (Fig. 1e), enabling a molecular model to be built *de novo* for residues 2–46 of ArfA (Fig. 1f, g). The lack of density for the C-terminal 9 amino acids of ArfA prevented these residues from being included in the final model.

The ArfA-binding site is located on the 30S subunit within the decoding A-site, where it is sandwiched between helices 18 (h18), h34 and h44 of the 16S rRNA and ribosomal protein S12 (Fig. 2a). ArfA establishes two contact sites with the β -hairpin of S12, namely, from the N terminus in which potential hydrogen bonds are possible between Thr38 of S12 and the backbone of Arg3 of ArfA, and between two highly conserved arginines (Arg26 and Arg28) of ArfA and Lys43 and Ser46 of S12 (Fig. 2b and Extended Data Fig. 3f). The large interaction surface that ArfA establishes with the 30S subunit may explain how ArfA can interact with the ribosome in the absence of RF2 (ref. 15). The C terminus of

¹Gene Center, Department of Biochemistry and Center for integrated Protein Science Munich (CIPSM), Ludwig-Maximilians-Universität München, Feodor-Lynen-Strasse 25, 81377 Munich, Germany. ²Institute for Biochemistry and Molecular Biology, University of Hamburg, Martin-Luther-King-Pl. 6, 20146 Hamburg, Germany.

*These authors contributed equally to this work.

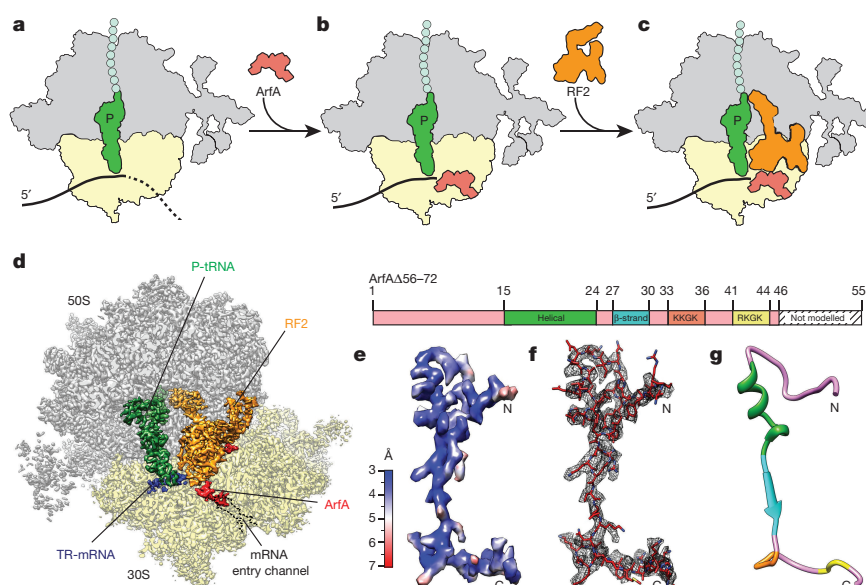


Figure 1 | Cryo-EM structure of ArfA-RF2-SRC. **a–c**, Schematic representation of ArfA-RF2-mediated rescue of ribosomes stalled on truncated mRNA (TR-mRNA). **d**, Transverse section of the cryo-EM map of ArfA-RF2-SRC, highlighting the 30S (yellow) and 50S (grey) subunits, P-tRNA (green), TR-mRNA (blue), RF2 (orange) and ArfA

(red). **e**, Electron density for ArfA, coloured according to local resolution. **f**, Electron density (mesh) with molecular model for ArfA (red). **g**, Model for ArfA with features highlighted corresponding to the schematic of the ArfA protein, including helical region (green), β -strand (blue) and KKGK (orange) and RKGK (yellow) motifs.

ArfA extends from the decoding A-site into the mRNA entry channel, where it occupies the space that would normally house the 3' end of a full-length mRNA (Fig. 2c). The lack of density for the C-terminal residues of ArfA suggests that they are less important for binding, which is consistent with their poor conservation across ArfA from different species^{8,12}. By contrast, two positively charged motifs, KKGK (residues 33–36) and RKGK (residues 41–44), are highly conserved and provide multiple interaction opportunities with the surrounding negatively charged rRNA forming the mRNA channel (Fig. 2d). We note that mutation of any single residue in ArfA, including within the K(R)KGK motifs, to cysteine is reported to have little effect on the recycling activity of ArfA¹⁵, suggesting a redundancy in the importance of the interactions of ArfA with the ribosome. Biochemical studies have demonstrated that the efficiency of ArfA-RF2-mediated ribosome recycling decreases with increasing length of the 3' end of the mRNA extending into the A-site^{14–16}. Specifically, recycling occurred,

albeit with reduced efficiency, when the mRNA was extended by up to 3–4 A-site nucleotides, whereas almost no recycling was observed on artificially stalled ribosomes with mRNAs extended by six or more A-site nucleotides^{14–16}. Consistently, superimposition of a full-length mRNA and the ArfA binding position suggests that only three nucleotides can be accommodated in the A-site without notable clashes with ArfA (Fig. 2e).

The location of the C terminus of ArfA within the mRNA channel of the 30S subunit observed in the Arf-RF2-SRC structure is also compatible with hydroxyl-radical probing experiments performed in the absence of RF2 (ref. 15; Extended Data Fig. 4), suggesting that ArfA initially uses a similar conformation to monitor the vacant mRNA channel. By contrast, 16S rRNA cleavages indicate that the N terminus of ArfA is flexible and only adopts a defined conformation contacting h18 upon binding of RF2 (ref. 15), as observed in the Arf-RF2-SRC structure (Extended Data Fig. 4). The ArfA-RF2-SRC structure also

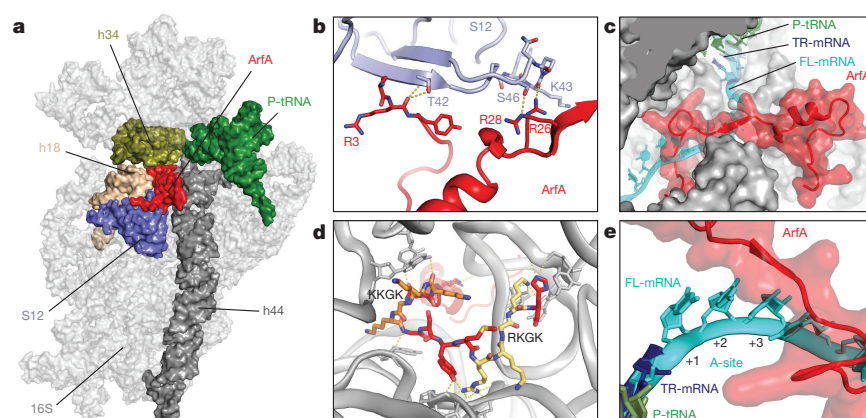


Figure 2 | Interaction of ArfA with the small subunit. **a**, Overview of ArfA (red) and 30S (16S rRNA, grey) interaction partners; h18 (tan), h34 (olive), h44 (dark grey), S12 (blue) and P-tRNA (green). **b**, Contacts between ArfA (red) and S12 (blue). **c**, Superimposition of ArfA (red) and truncated mRNA (TR-mRNA, blue), with full-length mRNA (FL-mRNA;

cyan, PDB code 4V6F)²⁵ within the mRNA entry channel (grey). **d**, Interaction of the KKGK (orange) and RKGK (yellow) motifs of ArfA with surrounding rRNA (grey ribbons). **e**, As in c, but highlighting the relative position of ArfA (red) with the A-site codon of the FL-mRNA (cyan).

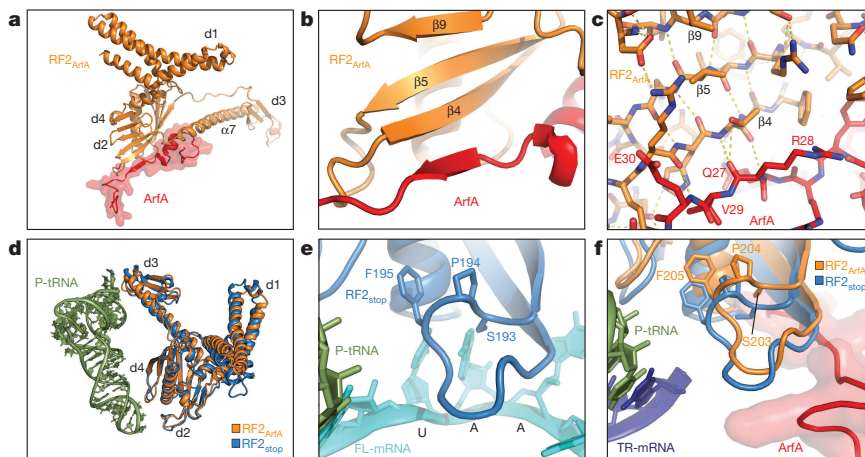


Figure 3 | Interaction of ArfA with RF2 on the ribosome. **a**, Overview of the interaction surface of ArfA (red) with RF2 (orange). **d**, domain. **b**, **c**, ArfA (red) donates a β -strand to augment the β -sheet of RF2 (orange). In **c**, potential hydrogen bonds are shown with dashed yellow lines. **d**, Superimposition of the relative positions of the RF2 on the ribosome when decoding a stop codon (RF2_{stop}; blue, PDB code 4V5E)¹⁸ or interacting

with ArfA (RF2_{ArfA}, orange), with P-tRNA (green) shown for reference. **e**, Interaction of the SPF motif of RF2_{stop} with the UAA stop codon of the full-length mRNA (cyan) in the A-site¹⁸. **f**, Superimposition of RF2_{stop} from **e** with ArfA (red) and RF2 (RF2_{ArfA}, orange) from the ArfA-RF2-SRC structure.

provides insight into how ArfA recruits RF2 despite the absence of a stop codon in the mRNA. ArfA has a large interaction interface with RF2, encompassing the central portion (residues 15–31) of ArfA that contacts the distal end of α -helix α 7 of domain 3 as well as the β 4– β 5 strands of domain 2 of RF2 (Fig. 3a, b and Extended Data Fig. 3g). The nature of the backbone interactions between ArfA and RF2 suggest that residues 27–30 of ArfA donate a small β -strand to the β -sheet of domain 2/4 (Fig. 3b, c). The overall position of RF2 in ArfA-RF2-SRC is similar to that observed during canonical translation termination^{17,18} (Fig. 3d), although a slight shift in the position of the decoding domain 2/4 is observed. The shift affects the loop between the β 4– β 5 strands of domain 2 bearing the SPF (*E. coli* 205-Ser-Pro-Phe-207) motif, which is involved in the specificity of recognition of the first and second positions of the UGA/UAA stop codons^{17,18,19} (Fig. 3e, f). Importantly, the structure illustrates that ArfA does not interact with the SPF motif and therefore does not directly mimic the presence of a stop codon (Fig. 3f).

This observation is consistent with a previous report that demonstrates that mutations in the SPF motif impairing RF2 termination activity do not affect ArfA–RF2-mediated recycling activity¹³. Furthermore, RF1 mutants bearing the SPF instead of PAT motif, conferring termination activity at UGA, are inactive in the ArfA-mediated recycling system¹³. An analysis of the ArfA–RF2 interaction network, together with *E. coli* RF1/RF2 sequence alignments (Extended Data Fig. 5) and models for *E. coli* RF1–ArfA on the ribosome (Extended Data Fig. 6), identified several regions in domain 2 of RF2 (Q133, V198 and G210–F221) and within the switch loop (K307–S321) that could potentially explain the specificity of ArfA for RF2.

During canonical termination, recognition of the stop codon by RF1 and RF2 is proposed to stabilize a rearranged conformation of the switch loop, which directs domain 3 into the PTC^{20,21}. The switch loop conformation is stabilized by specific interactions with A1492 and A1493, which, in the case of RF2, involves stacking interactions

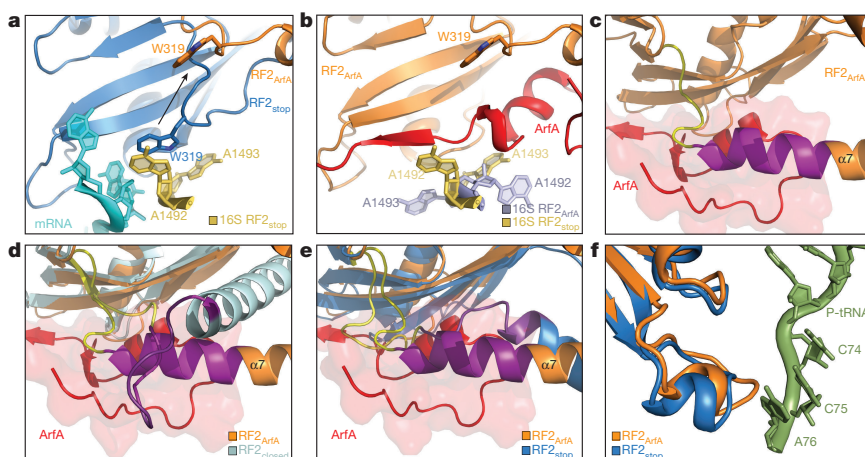


Figure 4 | ArfA stabilizes a unique conformation of the RF2 switch loop. **a**, Interaction between W319 (W307 in *Thermus thermophilus* RF2) of the switch region of RF2_{stop} and A1492 of the 16S rRNA (yellow) during decoding of the UAA stop codon of the mRNA (cyan; PDB code 4V5E)¹⁸. The switch loop conformation of RF2 (RF2_{ArfA}, orange) observed upon ArfA binding is superimposed and arrowed. **b**, Same view as in **a**, showing the distinct conformation of the switch loop of *E. coli* RF2 (orange) and A1492/A1493 (pale blue) when ArfA (red) is present. **c**, ArfA

(red) induces conformational changes within the switch loop (yellow) of RF2 (orange), leading to an extension (purple) of α -helix α 7 of the RF2 domain 3 by 2–3 helical turns. **d**, **e**, Superimposition of **c** with the switch loop and α -helix α 7 conformation in the crystal structure of the closed form of RF2 (RF2_{closed}; cyan, PDB code 1GQE)²² (**d**) and during canonical termination¹⁸ (**e**). **f**, Superimposition of domain 3 of RF2_{stop} (blue)¹⁸ and RF2_{ArfA} (orange), with P-tRNA (green) shown for reference.

of W319 (*E. coli* numbering) of RF2 with A1492 of the 16S rRNA^{17,18} (Fig. 4a). In the ArfA–RF2–SRC structure, the conformation of A1492 and A1493 are distinct from those observed during canonical translation termination, and the presence of ArfA precludes the interaction between the switch loop and A1492 (Fig. 4a, b). Instead, ArfA itself appears to stabilize a distinct conformation of the switch loop in RF2 that extends the α -helix α 7 of domain 3 of RF2 by three helical turns when compared to the crystal structure of the free (closed) form of RF2 (ref. 22) (Fig. 4c, d, Supplementary Video 1). The extension of helix α 7 is analogous to that observed during canonical translation termination with RF2 (refs 17, 18) (Fig. 4e, Supplementary Video 2). As observed for canonical termination^{17,18}, the open conformation of RF2 on the ribosome in the presence of ArfA also directs the GGQ motif of domain 3 into the PTC (Fig. 4f), although the density for the GAQ motif is poorly resolved, possibly owing to the inactivity of the mutation. The A18T mutation that led to the discovery of ArfA does not interfere with ribosome binding⁸ or RF2 recruitment, but prevents peptidyl-tRNA hydrolysis¹⁴. This can be rationalized on the basis of the ArfA–RF2–SRC structure since the A18T mutation is not located at the ArfA–ribosome or ArfA–RF2 interfaces, but would rather perturb the conformation of the N terminus of ArfA and thereby interfere indirectly with the correct placement of domain 3 of RF2 at the PTC (Extended Data Fig. 7).

In conclusion, our findings indicate that ArfA not only provides an interface to recruit RF2 to the ribosome in the absence of a stop codon, but also, by interacting with the switch loop of RF2, induces conformational changes that lead to the accurate placement of domain 3 at the PTC. Structurally, the bacterial recycling systems are similar in that they use tmRNA–SmpB^{6,7}, ArfB⁵ or ArfA (Extended Data Fig. 8) to monitor the mRNA channel and release the nascent polypeptide before ribosome splitting. This contrasts with the eukaryotic recycling of ribosomes stalled on truncated mRNAs, in which ribosome splitting by Dom34–Hbs1 and ABCE1 occurs before nascent polypeptide chain release^{23,24}.

Online Content Methods, along with any additional Extended Data display items and Source Data, are available in the online version of the paper; references unique to these sections appear only in the online paper.

Received 26 September; accepted 25 November 2016.

Published online 1 December 2016.

- Keiler, K. C. Mechanisms of ribosome rescue in bacteria. *Nat. Rev. Microbiol.* **13**, 285–297 (2015).
- Valle, M. *et al.* Visualizing tmRNA entry into a stalled ribosome. *Science* **300**, 127–130 (2003).
- Fu, J. *et al.* Visualizing the transfer-messenger RNA as the ribosome resumes translation. *EMBO J.* **29**, 3819–3825 (2010).
- Weis, F. *et al.* tmRNA–SmpB: a journey to the centre of the bacterial ribosome. *EMBO J.* **29**, 3810–3818 (2010).
- Gagnon, M. G., Seetharaman, S. V., Bulkley, D. & Steitz, T. A. Structural basis for the rescue of stalled ribosomes: structure of YaeJ bound to the ribosome. *Science* **335**, 1370–1372 (2012).
- Neubauer, C., Gillet, R., Kelley, A. C. & Ramakrishnan, V. Decoding in the absence of a codon by tmRNA and SmpB in the ribosome. *Science* **335**, 1366–1369 (2012).
- Ramrath, D. J. *et al.* The complex of tmRNA–SmpB and EF-G on translocating ribosomes. *Nature* **485**, 526–529 (2012).
- Chadani, Y. *et al.* Ribosome rescue by *Escherichia coli* ArfA (YhdL) in the absence of trans-translation system. *Mol. Microbiol.* **78**, 796–808 (2010).

- Chadani, Y., Ono, K., Kutsukake, K. & Abo, T. *Escherichia coli* YaeJ protein mediates a novel ribosome-rescue pathway distinct from SsrA- and ArfA-mediated pathways. *Mol. Microbiol.* **80**, 772–785 (2011).
- Chadani, Y. *et al.* trans-translation-mediated tight regulation of the expression of the alternative ribosome-rescue factor ArfA in *Escherichia coli*. *Genes Genet. Syst.* **86**, 151–163 (2011).
- Garza-Sánchez, F., Schaub, R. E., Janssen, B. D. & Hayes, C. S. tmRNA regulates synthesis of the ArfA ribosome rescue factor. *Mol. Microbiol.* **80**, 1204–1219 (2011).
- Schaub, R. E., Poole, S. J., Garza-Sánchez, F., Benbow, S. & Hayes, C. S. Proteobacterial ArfA peptides are synthesized from non-stop messenger RNAs. *J. Biol. Chem.* **287**, 29765–29775 (2012).
- Chadani, Y., Ito, K., Kutsukake, K. & Abo, T. ArfA recruits release factor 2 to rescue stalled ribosomes by peptidyl-tRNA hydrolysis in *Escherichia coli*. *Mol. Microbiol.* **86**, 37–50 (2012).
- Shimizu, Y. ArfA recruits RF2 into stalled ribosomes. *J. Mol. Biol.* **423**, 624–631 (2012).
- Kurita, D., Chadani, Y., Muto, A., Abo, T. & Himeno, H. ArfA recognizes the lack of mRNA in the mRNA channel after RF2 binding for ribosome rescue. *Nucleic Acids Res.* **42**, 13339–13352 (2014).
- Zeng, F. & Jin, H. Peptide release promoted by methylated RF2 and ArfA in nonstop translation is achieved by an induced-fit mechanism. *RNA* **22**, 49–60 (2016).
- Korostelev, A. *et al.* Crystal structure of a translation termination complex formed with release factor RF2. *Proc. Natl Acad. Sci. USA* **105**, 19684–19689 (2008).
- Weixlbaumer, A. *et al.* Insights into translational termination from the structure of RF2 bound to the ribosome. *Science* **322**, 953–956 (2008).
- Ito, K., Uno, M. & Nakamura, Y. A tripeptide ‘anticodon’ deciphers stop codons in messenger RNA. *Nature* **403**, 680–684 (2000).
- Youngman, E. M., McDonald, M. E. & Green, R. Peptide release on the ribosome: mechanism and implications for translational control. *Annu. Rev. Microbiol.* **62**, 353–373 (2008).
- Zhou, J., Korostelev, A., Lancaster, L. & Noller, H. F. Crystal structures of 70S ribosomes bound to release factors RF1, RF2 and RF3. *Curr. Opin. Struct. Biol.* **22**, 733–742 (2012).
- Vestergaard, B. *et al.* Bacterial polypeptide release factor RF2 is structurally distinct from eukaryotic eRF1. *Mol. Cell* **8**, 1375–1382 (2001).
- Franckenberg, S., Becker, T. & Beckmann, R. Structural view on recycling of archaeal and eukaryotic ribosomes after canonical termination and ribosome rescue. *Curr. Opin. Struct. Biol.* **22**, 786–796 (2012).
- Simms, C. L., Thomas, E. N. & Zaher, H. S. Ribosome-based quality control of mRNA and nascent peptides. *Wiley Interdiscip. Rev. RNA* <http://dx.doi.org/10.1002/wrna.1366> (2016).
- Jenner, L. B., Demeshkina, N., Yusupova, G. & Yusupov, M. Structural aspects of messenger RNA reading frame maintenance by the ribosome. *Nat. Struct. Mol. Biol.* **17**, 555–560 (2010).

Supplementary Information is available in the online version of the paper.

Acknowledgements We thank H. Sieber, S. Rieder and C. Ungewickell for technical assistance and L. Bischoff and R. Green for providing expression plasmids for *E. coli* ArfA Δ 17 and RF2, respectively. This research was supported by grants from the Deutsche Forschungsgemeinschaft W13285/4-1, SPP-1879 (to D.N.W.), GRK 1721 and FOR1805 (to R.B. and D.N.W.).

Author Contributions D.N.W. designed the study. C.M. and P.H. prepared the cryo-EM sample. P.H., C.M. and B.B. processed the cryo-EM data. P.H., S.A. and D.N.W. built and refined the molecular models. O.B. collected the cryo-EM data. P.H., C.M., R.B. and D.N.W. interpreted the results and D.N.W. wrote the paper.

Author Information Reprints and permissions information is available at www.nature.com/reprints. The authors declare no competing financial interests. Readers are welcome to comment on the online version of the paper. Correspondence and requests for materials should be addressed to D.N.W. (daniel.wilson@chemie.uni-hamburg.de).

Reviewer Information *Nature* thanks T. Abo, Y. Hashem, K. Keiler and the other anonymous reviewer(s) for their contribution to the peer review of this work.

METHODS

No statistical methods were used to predetermine sample size. The experiments were not randomized and investigators were not blinded to allocation during experiments and outcome assessment.

Protein expression and purification. *Escherichia coli* RF2 was expressed from a pET11a vector incorporating a C-terminal hexa-histidine tag (His₆) for purification and detection purposes. An inactive RF2-GAQ mutant was generated by site-directed mutagenesis. *E. coli* ArfA without 17 C-terminal amino acids (ArfAΔ17) was cloned into pBAD vector with a N-terminal His₆ and 3C protease cleavage site. The wild-type RF2, RF2-GAQ and ArfAΔ17 proteins were over-expressed in *E. coli* BL21 (DE3) at 37 °C for 1.5 h after induction with 1 mM IPTG or 0.2% arabinose as required. Cells were collected and the pellet was re-suspended in lysis buffer (50 mM NaH₂PO₄·2H₂O, 300 mM NaCl, 5 mM imidazole, pH 7.5). Lysis was performed using a microfluidizer (Microfluidics M-110L) by passing cells three times at 18,000 p.s.i. The cell debris was removed upon centrifugation and the proteins were purified from the supernatant by His-tag affinity chromatography using Ni-NTA agarose beads (Clontech). The bound proteins were washed with lysis buffer containing 10 mM imidazole and then eluted with lysis buffer containing 250 mM imidazole. The proteins were purified by size-exclusion chromatography using HiLoad 16/600 Superdex 75 (GE Life Sciences) in gel filtration buffer (50 mM HEPES, pH 7.4, 50 mM KCl, 100 mM NaCl, 2% glycerol, 5 mM β-mercaptoethanol). The proteins were concentrated using Amicon Ultra-4 Centrifugal Filter Units (Merck Millipore), Ultracel-3 for ArfAΔ17 and Ultracel-30 for wild-type RF2 and RF2-GAQ.

Template preparation for in vitro translation. Truncated *nlpD* template containing an N-terminal His₆ and a HA tag was amplified from pET21b-R1*nlpD*²⁶ using primers binding to pET21b upstream of the T7-promotor (GATCGAGA TCTCGATCCCGCG) and to nucleotides 133–159 of *nlpD* (AATCAACA TACCAGAATTAGTATTGTC). PCR products were purified via spin columns (Qiagen).

ArfA peptidyl-tRNA recycling assays. The recycling activity of the purified ArfAΔ17 and RF2 (wild-type and GAQ mutant) was monitored by independent triplicate experiments using PURExpress ΔRF123 *In Vitro* Protein Synthesis Kit (NEB E6850S) (Extended Data Fig. 1). Reactions of 6 μl were performed according to the manual protocol by mixing 250 ng of truncated *nlpD* PCR template, 5 μM of anti-ssrA oligo, 2 μM of ArfAΔ17 and/or wild-type RF2 or RF2-GAQ. The reactions were incubated at 37 °C for 15 min with shaking at 1,000 r.p.m. The translation reactions were stopped by adding 6 μl of tricine sample buffer (200 mM Tris-HCl pH 6.8, 40% glycerol, 2% SDS, 0.04% Coomassie Blue G-250) and then applied to 16.5% tricine-SDS-PAGE gels. The products were detected by western blotting using anti-haemagglutinin-peroxidase (Roche 11667475001) at 1:1,000 in 2.5% milk/TBS (2.5% (w/v) skim milk powder, 20 mM Tris, pH 7.5, 150 mM NaCl).

Generation of ArfA-RF2-SRC. *In vitro* translation was carried out using PURExpress *In Vitro* Protein Synthesis Kit (NEB 6800). The translation reaction (750 μl in total) was prepared according to the protocol of the PURExpress *In Vitro* Protein Synthesis Kit supplemented with 5 μM anti-ssrA oligo. Translation was started by adding the truncated *nlpD* PCR product at 37 °C for 20 min, shaking at 1,000 r.p.m. The ribosomes were first isolated from the *in vitro* reaction mix by centrifugation through a sucrose cushion (50 mM HEPES KOH pH 7.2, 250 mM potassium acetate, 25 mM magnesium acetate, 750 mM sucrose, 0.1% DDM) for 180 min at 72,000g using a TLA120.2 rotor (Beckman Coulter). The pellet was resuspended in buffer B250 (50 mM HEPES KOH pH 7.2, 250 mM potassium acetate, 25 mM magnesium acetate, 0.1% DDM) and the stalled ribosomal complexes (SRC) were isolated using Talon cobalt-chelate affinity resin (Clontech). SRCs bound to the Talon matrix by the N-terminal His₆ tag of NlpD were washed with buffer B500 (50 mM HEPES KOH pH 7.2, 500 mM potassium acetate, 25 mM magnesium acetate, 0.1% DDM) and eluted using buffer B250i (50 mM HEPES KOH pH 7.2, 250 mM potassium acetate, 25 mM magnesium acetate, 250 mM imidazole, 0.1% DDM). The eluted SRC was loaded onto a linear sucrose gradient (10–40% (w/v) sucrose in B250 buffer) for 18 h at 43,000g in a SW28 rotor (Beckman Coulter). The isolated 70S peak was pelleted by centrifugation for 3 h at 139,000g using a Ti70.1 rotor (Beckman Coulter). The pellet was re-suspended in SRC buffer (50 mM HEPES pH 7.2, 250 mM potassium acetate, 10 mM magnesium acetate, 0.05% DDM). The purified SRC was then incubated together with a 2.5× excess of ArfAΔ17 and RF2-GAQ mutant for 5 min at 37 °C before being applied to EM grids.

Cryo-electron microscopy and single particle reconstruction. Five microlitres (4.5 OD) of *E. coli* ArfA-RF2-SRC at OD_{260 nm} was applied to 2 nm pre-coated Quantifoil R3/3 holey carbon supported grids and vitrified using the Vitrobot Mark IV (FEI, Holland). Data collection was performed using EM-TOOLS (TVIPS GmbH) on a Titan Krios transmission electron microscope equipped with a Falcon II direct electron detector (FEI, Holland) at 302 kV at a pixel size of 1.084 Å and a

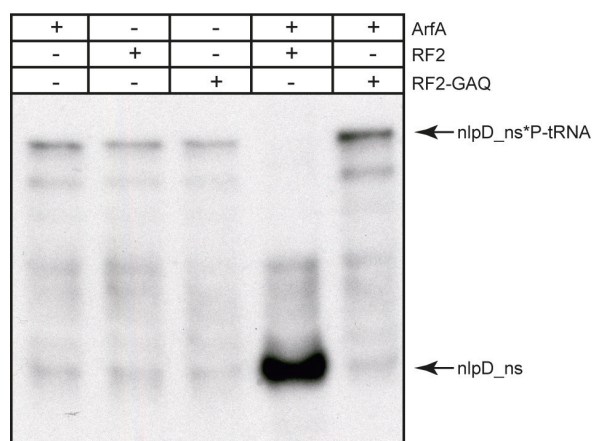
defocus range of 0.7–2.2 μm. Ten frames (dose per frame of 2.5 e⁻ Å⁻²) were aligned using Motion Correction Software²⁷. Power-spectra, defocus values and astigmatism were determined with CTFIND4 software²⁸. Micrographs showing Thon rings beyond 3.5 Å were manually inspected for good areas and power-spectra quality. Automatic particle picking was performed using SIGNATURE²⁹ and single particles were processed using RELION 1.4 (ref. 30). 227,608 particles were first subjected to 3D refinement using *E. coli* 70S ribosome as reference structure³¹ and movie particle extraction was performed as described before³⁰ (Extended Data Fig. 2). The 227,608 polished particles were finally subjected to 3D classification and refinement using FREALIGN resulting in a final reconstruction of 3.11 Å (0.143 FSC) average resolution containing 69,089 particles (Extended Data Figs 2 and 3). Local resolution was finally calculated using ResMap³².

Molecular modelling and refinement of the ArfA-RF2-SRC. The molecular model for the ribosomal proteins and rRNA of the 70S ribosome of the ArfA-RF2-SRC was based on the molecular model from the recent cryo-EM reconstruction of the *E. coli* 70S ribosome (PDB code 5AF1)³³. The molecular model was initially fitted as a rigid body into the cryo-EM density map of the corresponding stalled complex using UCSF Chimera³⁴. Owing to flexibility and poor density, the L1, L10, L11 protein and the L7/L12 stalk were not included in the final model. For *E. coli* RF2, a homology model was generated using HHPred³⁵ based on a template from *T. thermophilus* RF2 (PDB code 4V5E)¹⁸. Owing to flexibility and poor density, the GAQ motif, domain I, and the linker between domains 3 and 4 of RF2 were based on PDB code 2WH1. Residues 2–46 of ArfAΔ17 were built *de novo* using an HHPred model as an initial starting point in terms of placement of the central helical region. The complete atomic model of the ArfA-RF2-SRC was manually adjusted using Coot³⁶ and refined using phenix.real_space_refine³⁷, with restraints obtained by phenix.secondary_structure_restraints³⁷. The model and refinement statistics are presented in Extended Data Table 1. To reduce the clash score the model was refined using REFMAC³⁸. The statistics of the refined model were calculated using Molprobity³⁹ and the validation of the model was performed as previously described⁴⁰.

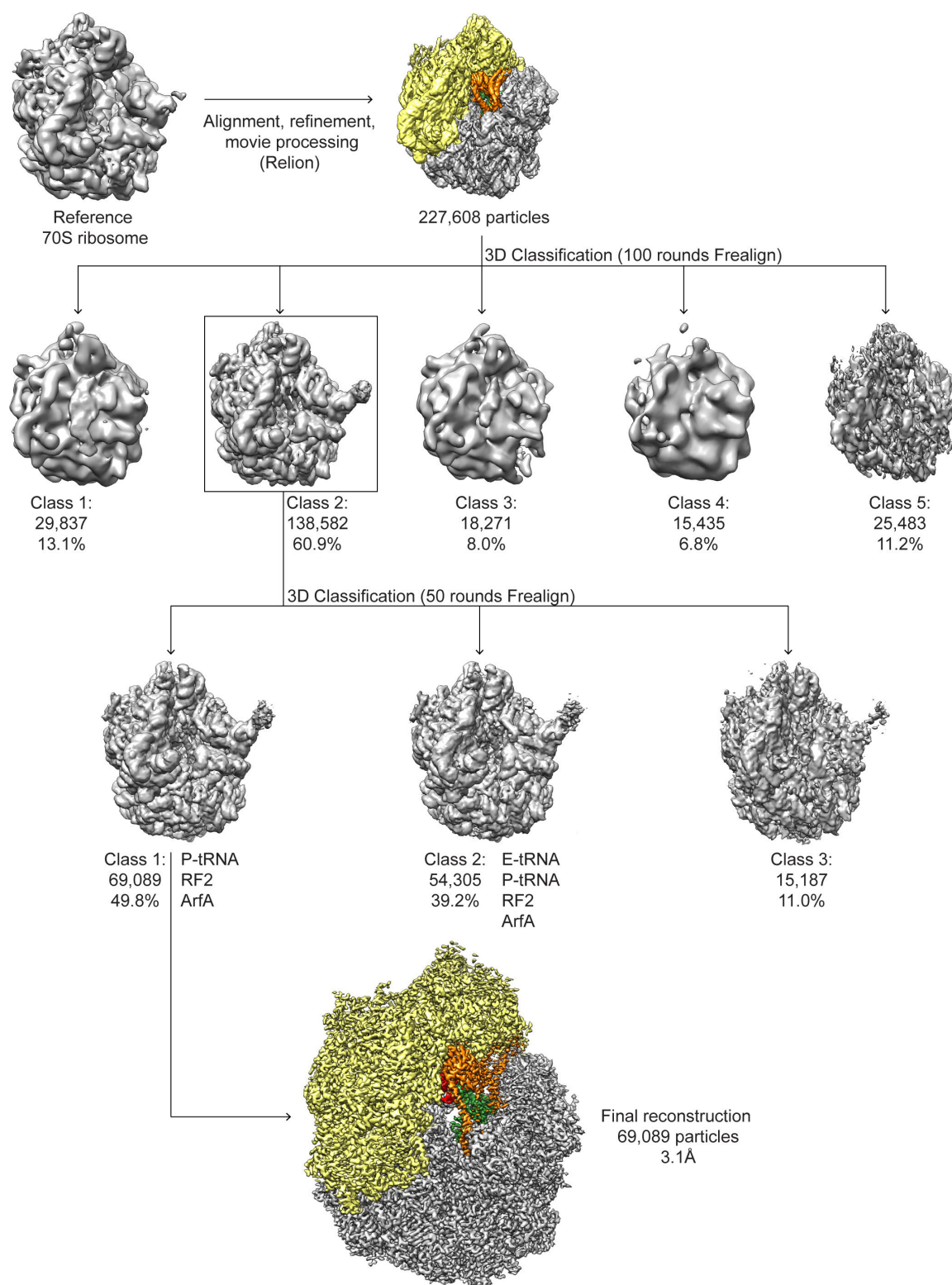
Figure preparation. Figures showing electron densities and atomic models were generated using either UCSF Chimera³⁴ or PyMol Molecular Graphic Systems (version 1.8 Schrödinger).

Data availability. The cryo-electron microscopy map for the ArfA-RF2-SRC has been deposited in the Electron Microscopy Data Bank (EMDB) with the accession code EMD-3508. The respective coordinates for electron-microscopy-based model of the ArfA-RF2-SRC are deposited in the Protein Data Bank (PDB) under the accession code 5MGP. All other data are available from the corresponding author upon reasonable request.

- Starosta, A. L. *et al.* Translational stalling at polyproline stretches is modulated by the sequence context upstream of the stall site. *Nucleic Acids Res.* **42**, 10711–10719 (2014).
- Li, X. *et al.* Electron counting and beam-induced motion correction enable near-atomic-resolution single-particle cryo-EM. *Nat. Methods* **10**, 584–590 (2013).
- Rohou, A. & Grigorieff, N. CTFIND4: Fast and accurate defocus estimation from electron micrographs. *J. Struct. Biol.* **192**, 216–221 (2015).
- Chen, J. Z. & Grigorieff, N. SIGNATURE: a single-particle selection system for molecular electron microscopy. *J. Struct. Biol.* **157**, 168–173 (2007).
- Scheres, S. H. RELION: implementation of a Bayesian approach to cryo-EM structure determination. *J. Struct. Biol.* **180**, 519–530 (2012).
- Arenz, S. *et al.* The stringent factor RelA adopts an open conformation on the ribosome to stimulate ppGpp synthesis. *Nucleic Acids Res.* **44**, 6471–6481 (2016).
- Kucukelbir, A., Sigworth, F. J. & Tagare, H. D. Quantifying the local resolution of cryo-EM density maps. *Nat. Methods* **11**, 63–65 (2014).
- Fischer, N. *et al.* Structure of the *E. coli* ribosome-EF-Tu complex at <3 Å resolution by Cs-corrected cryo-EM. *Nature* **520**, 567–570 (2015).
- Pettersen, E. F. *et al.* UCSF Chimera—a visualization system for exploratory research and analysis. *J. Comput. Chem.* **25**, 1605–1612 (2004).
- Söding, J., Biegert, A. & Lupas, A. N. The HHPred interactive server for protein homology detection and structure prediction. *Nucleic Acids Res.* **33**, W244–W248 (2005).
- Emsley, P. & Cowtan, K. Coot: model-building tools for molecular graphics. *Acta Crystallogr. D* **60**, 2126–2132 (2004).
- Adams, P. D. *et al.* PHENIX: a comprehensive Python-based system for macromolecular structure solution. *Acta Crystallogr. D* **66**, 213–221 (2010).
- Vagin, A. A. *et al.* REFMAC5 dictionary: organization of prior chemical knowledge and guidelines for its use. *Acta Crystallogr. D* **60**, 2184–2195 (2004).
- Chen, V. B. *et al.* MolProbity: all-atom structure validation for macromolecular crystallography. *Acta Crystallogr. D* **66**, 12–21 (2010).
- Brown, A. *et al.* Tools for macromolecular model building and refinement into electron cryo-microscopy reconstructions. *Acta Crystallogr. D* **71**, 136–153 (2015).

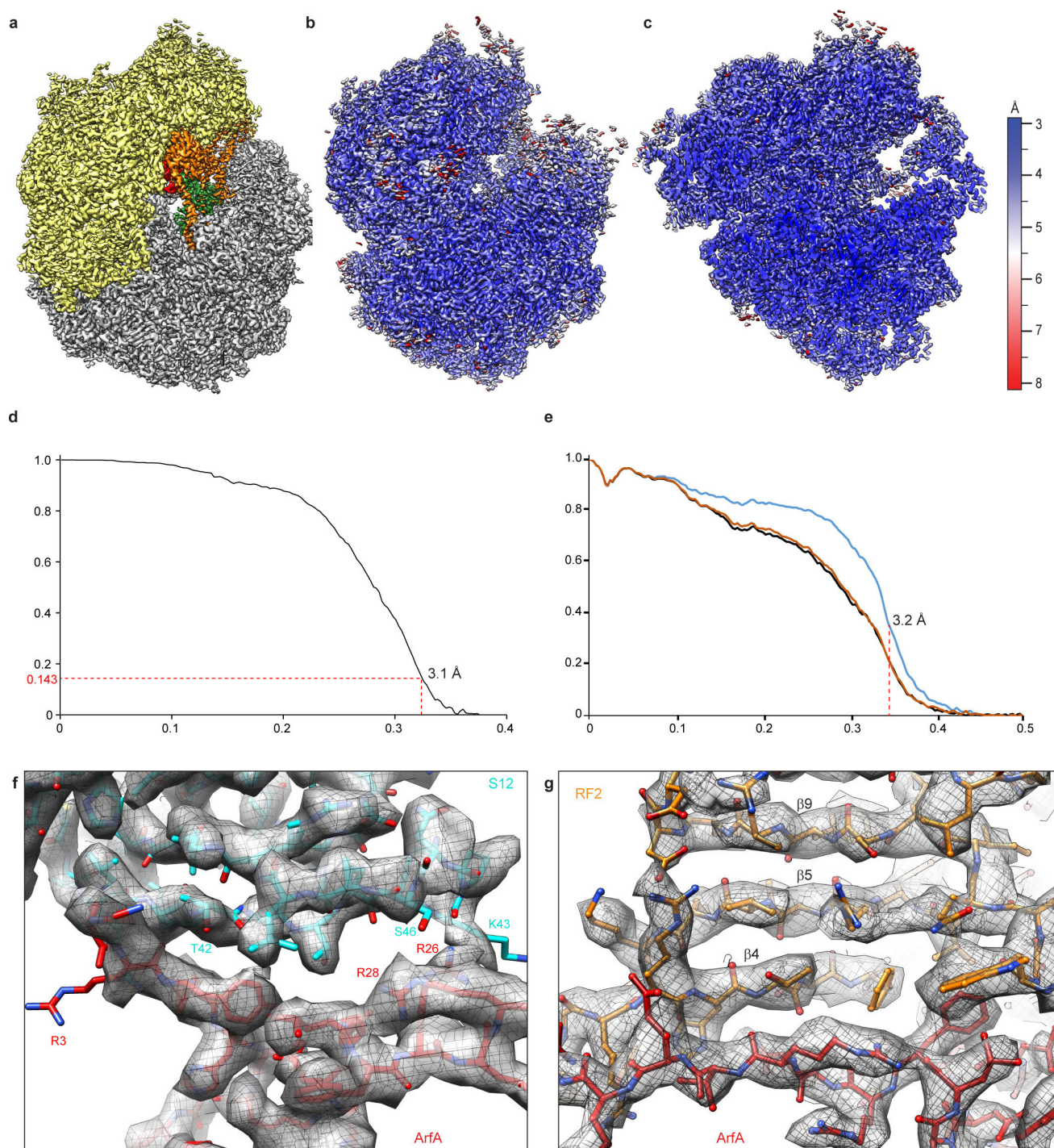


Extended Data Figure 1 | Recycling of ribosomes stalled on truncated mRNA by ArfA and RF2. *In vitro* translation assay of the truncated *nlpD* template was performed in the presence of ArfA, RF2 or RF2-GAQ, revealing a peptidyl-tRNA band (nlpD_{ns}*P-tRNA), whereas the peptidyl-tRNA was absent and free *nlpD* peptide (nlpD_{ns}) was observed when the reaction was performed with ArfA and RF2. Replacing wild-type RF2 with the inactive RF2-GAQ mutant led to the reappearance of the peptidyl-tRNA band and loss of the free *nlpD* peptide.



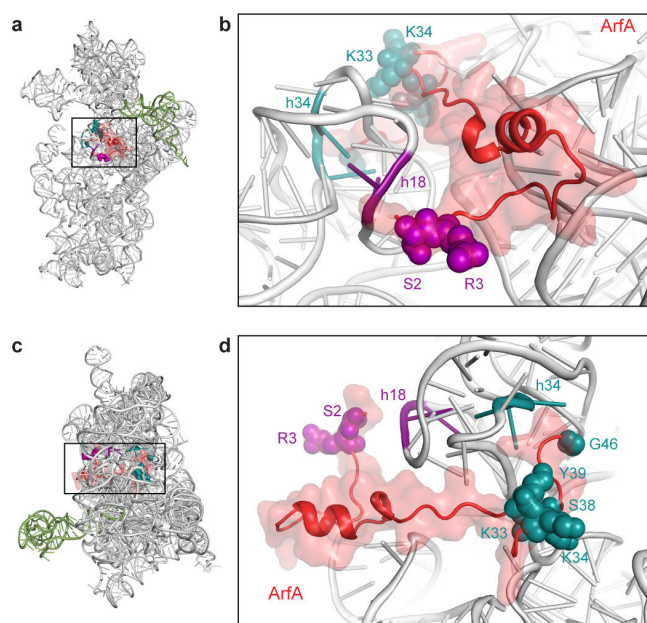
Extended Data Figure 2 | Classification of the ArfA-RF2-SRC. The complete dataset of 227,608 particles was initially aligned against a vacant *E. coli* 70S ribosome, refined with RELION using 3D auto-refine and the movie particles were extracted. The polished particles were then subjected to a 3D refinement and 3D classification using FREALIGN. The class 2 (138,582 particles) resulting from the 100 rounds of 3D classification

with 3× binned images using a ribosomal mask was then further refined and classified with 2× binned images. The remaining 69,089 particles containing ArfA-RF2-SRC were then 3D-refined, resulting in a final reconstruction of 3.1 Å (0.143 Fourier shell correlation (FSC)) average resolution.

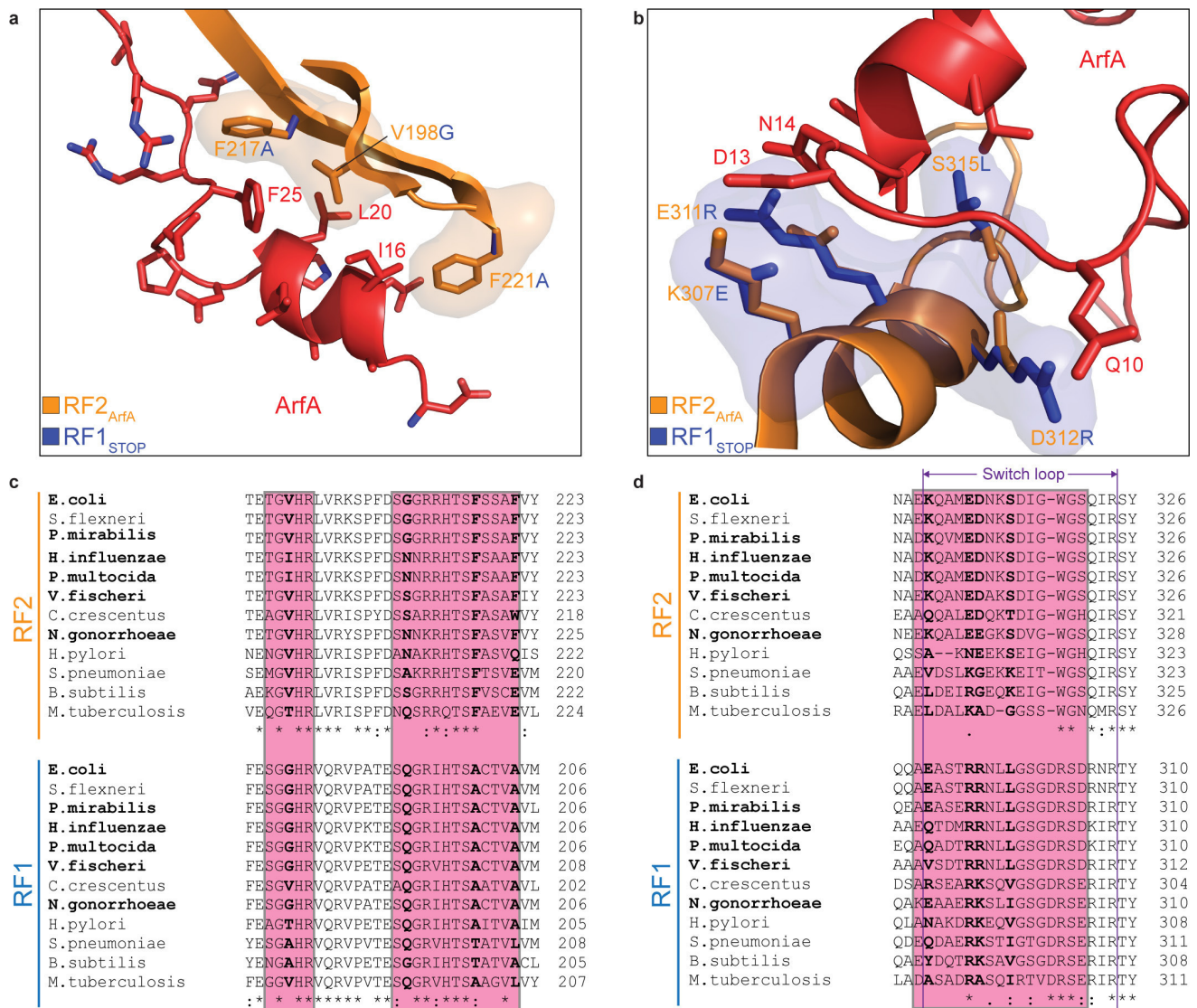


Extended Data Figure 3 | Resolution of the ArfA-RF2-SRC. **a**, Overview of the final refined cryo-EM map of the ArfA-RF2-SRC with separated densities for small (yellow) and large (grey) ribosomal subunit, as well as ArfA (red), RF2 (orange) and P-tRNA (green). **b**, Same view as in **a** but coloured according to local resolution. **c**, Transverse section of **b** showing local resolution in the core of the ribosomal subunits. **d**, FSC curve of the refined final map, indicating that the average resolution of the ArfA-RF2-SRC is 3.1 Å (at 0.143). **e**, Fit of models to maps. FSC curves calculated between

the refined model and the final map (blue), with the self- and cross-validated correlations in orange and black, respectively. Information beyond 3.2 Å was not used during refinement and preserved for validation. **f**, **g**, Selected examples illustrating the quality of fit of the molecular models to the unsegmented cryo-EM map (grey mesh) for the ArfA (red) interaction with S12 (blue), related to Fig. 2b (f), and with RF2 (orange), related to Fig. 3c (g).

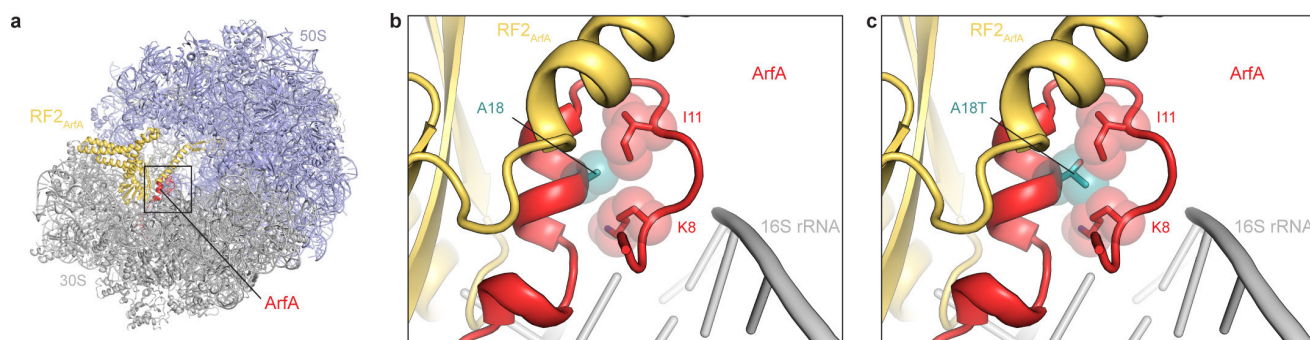


Extended Data Figure 4 | Hydroxyl radical probing of ArfA on the ribosome. a–d, Hydroxyl-radical probing data¹⁵ of ArfA in complex with RF2 on the ribosome reveal that tethers linked to the N-terminal region of ArfA, for example, residues S2 and R3 (magenta), cleave the 16S rRNA within the vicinity of helices h18, whereas tethers linked to the C-terminal region of ArfA, such as residues 33–34/38–39 and 46 (teal), cleave the 16S rRNA within the vicinity of helices h34 (ref. 15). These findings are in excellent agreement with the position of ArfA (red) within the ArfA-RF2-SRC structure reported here. In the overview panels a and c, P-tRNA (green) is shown for reference.

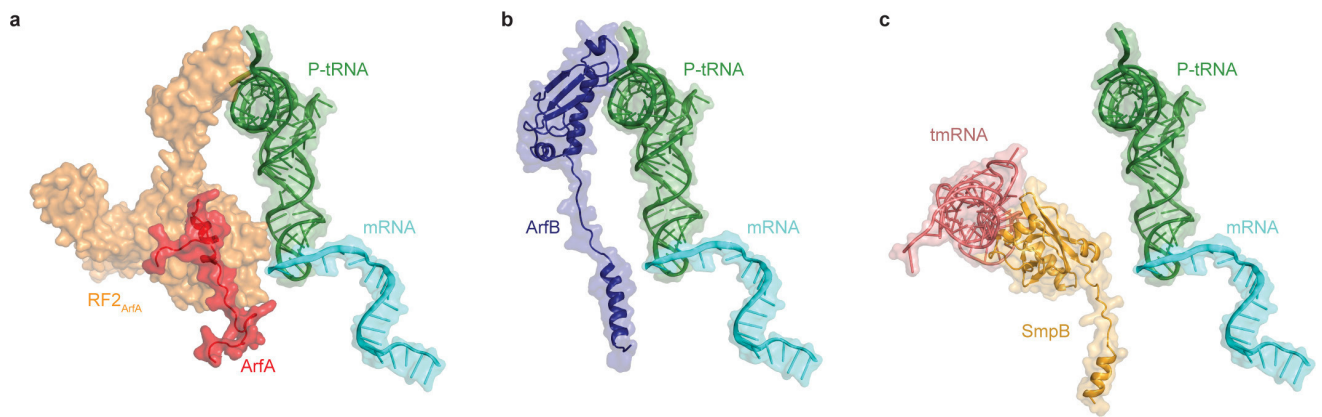


Extended Data Figure 6 | Potential specificity determinants for ArfA-mediated ribosome recycling. **a, b,** ArfA (red) and *E. coli* RF2 (orange) compared to homology model of *E. coli* RF1 (blue) aligned to RF2 in the ArfA-RF2-SRC. **a,** The ArfA interface with $\beta 4$ and $\beta 5$ strands of *E. coli* RF2 (orange) consists of hydrophobic residues V198, F217 and F221, which are mutated to Gly, Ala and Ala, respectively, in RF1 (blue). **b,** The ArfA interface with α -helix $\alpha 7$ of RF2 (orange). Replacing negatively charged residues such as E311 and D312 in RF2 with Arg in RF1 is also likely to disrupt the interaction with ArfA. **c, d,** Sequence alignments for the

regions of RF1 and RF2 corresponding to **a** and **b**, respectively. The pink boxes indicate regions of RF2 that form an interface with ArfA, including residues in bold predicted to prevent interaction of RF1 with ArfA and therefore could provide the basis for RF2-specificity of ArfA action. Organisms in bold contain ArfA, whereas others have no detectable ArfA homologue. Asterisk (*), colon (:), or full stop (.) indicate a single, fully conserved residue or residues with strong (>0.5 in the Gonnet PAM 250 matrix) and weakly (>0.5) similar properties, respectively.



Extended Data Figure 7 | Location of the ArfA-A18T mutation relative to RF2. **a**, Overview of ArfA (red) and RF2 (gold) on the ribosome (30S, grey; 50S, slate). **b**, **c**, Zoom of boxed region in **a** showing the environment of A18 (teal) of ArfA in close proximity to I11 and K8 in the N terminus of ArfA (red) (**b**), and A18T (teal) of ArfA in sterically clashing with I11 and K8 in the N terminus of ArfA (red) (**c**).



Extended Data Figure 8 | Comparison of ArfA with other ribosome rescue systems. a–c, Relative orientation on the ribosome with truncated mRNAs and ArfA (red) and RF2 (orange) (a), ArfB (purple, PDB code 4V95)⁵ (b) or tmRNA (brown) and SmpB (yellow) (PDB code 4V8Q)⁶ (c). In all cases, the mRNA and P-tRNA are coloured cyan and green, respectively.

Extended Data Table 1 | Data collection and refinement statistics

ArfA-RF2-SRC	
Data collection	
Particles	69,089
Pixel size (Å)	1.084
Defocus range (µm)	0.7-2.2
Voltage (kV)	302
Electron dose (e ⁻ /Å ²)	24
Model composition	
Protein residues	6,480
RNA nucleotides	4,642
Refinement	
Resolution (Å)	3.11
Map sharpening B factor (Å ²)	-60.34
FSC _{Average}	0.85
Validation proteins	
Poor rotamers (%)	4.67
Ramachandran outliers (%)	2.45
Ramachandran favored (%)	88.09
Bad backbone bonds (%)	0.02
Bad backbone angles (%)	0.02
Validation RNA	
Correct sugar puckers (%)	98.91
Good backbone conformations (%)	78.72
Bad bonds (%)	0.00
Bad angles (%)	0.14
Scores	
MolProbity	2.20 (99 th percentile)
Clash score, all atoms	3.04 (100 th percentile)

Special Issue: Ribosomes and Translation

Review

Structural Basis for Ribosome Rescue in Bacteria

Paul Huter,¹ Claudia Müller,¹ Stefan Arenz,¹ Bertrand Beckert,^{1,2} and Daniel N. Wilson^{1,2,*}

Ribosomes that translate mRNAs lacking stop codons become stalled at the 3' end of the mRNA. Recycling of these stalled ribosomes is essential for cell viability. In bacteria three ribosome rescue systems have been identified so far, with the most ubiquitous and best characterized being the trans-translation system mediated by transfer-messenger RNA (tmRNA) and small protein B (SmpB). The two additional rescue systems present in some bacteria employ alternative rescue factor (Arf) A and release factor (RF) 2 or ArfB. Recent structures have revealed how ArfA mediates ribosome rescue by recruiting the canonical termination factor RF2 to ribosomes stalled on truncated mRNAs. This now provides us with the opportunity to compare and contrast the available structures of all three bacterial ribosome rescue systems.

Bacterial Ribosome Rescue Systems

Ribosome rescue systems are necessary to recycle ribosomes that have become stalled at the 3' end of mRNAs, so-called non-stop ribosome complexes [1,2]. Translation on these non-stop mRNAs is blocked due to the absence of a sense or stop **codon** (see [Glossary](#)) in the ribosomal **A site**, which is crucial for elongation or termination to continue. These truncated or non-stop mRNAs can arise in the cell due to premature transcription termination or mRNA damage; for example, by the action of **RNases**. Additionally, non-programmed frameshifting events or nonsense suppression (readthrough of a stop codon) can also lead to accumulation of non-stop complexes. Ribosome rescue systems that deal with non-stop complexes are present in all species of life. In archaea and eukaryotes, non-stop complexes are rescued by the combined action of Dom34 and Hbs1, which are homologs of eukaryotic RF (eRF) 1 and eRF3 [2]. Bacteria have evolved completely unrelated pathways to deal with rescue of non-stop complexes (reviewed in [2–7]). These include the trans-translation system mediated by the tmRNA and SmpB as well as two more recently identified Arf systems involving ArfA and ArfB (formerly known in *Escherichia coli* as YhdL and YaeJ, respectively). The occurrence of non-stop complexes appears to be a frequent event in bacteria. Experiments in *E. coli* indicate that 0.4% of all transcripts undergo trans-translation [8] and that 2–4% of **peptidyl-tRNAs** remain non-hydrolyzed when ribosome rescue pathways are inactivated [9]. This explains why the presence of at least one of the bacterial ribosome rescue pathways is essential for cell viability [10]. While structural studies have provided much insight into the mechanism of tmRNA-SmpB- and ArfB-mediated rescue of non-stop ribosome complexes, structural insight into ArfA-mediated ribosome rescue has been lacking. Recently, five cryoelectron microscopy (cryo-EM) structures of ArfA-RF2-non-stop ribosome complexes were reported [11–15], providing the opportunity to not only compare the similarities and differences of the structures with one another, but also to contrast the findings with the structures of the other bacterial ribosome rescue systems.

Trends

Bacterial ribosome rescue systems are ubiquitous in bacteria and essential for cell viability. Homologs of some rescue factors are also found in eukaryotic mitochondria and plant chloroplasts.

Bacterial ribosome rescue factors such as small protein B (SmpB), alternative rescue factor (Arf) A, and ArfB recognize ribosomes stalled on truncated mRNAs by using their positively charged C-terminal tails to probe whether the mRNA channel is vacant.

ArfA induces conformational changes within the 'switch' loop of release factor 2 (RF2) that promotes transition from a closed to an open conformation, placing the catalytically important glycine-glycine-glutamine (GGQ) motif of RF2 at the peptidyltransferase center of the ribosome.

The distinct pathways used to rescue bacterial and eukaryotic cytoplasmic non-stop ribosome complexes suggest that bacterial ribosome rescue may be a potential target for the development of new antimicrobial agents.

¹Gene Center, Department of Biochemistry and Center for Integrated Protein Science Munich (CiPSM), Feodor-Lynenstr. 25, 81377 München, Germany
²Institute for Biochemistry and Molecular Biology, University of Hamburg, Martin-Luther-King-Platz 6, 20146 Hamburg, Germany

*Correspondence: Daniel.wilson@chemie.uni-hamburg.de (D.N. Wilson).

Trans-translation Mediated by tmRNA and SmpB

Genes encoding tmRNA (*ssrA*) and SmpB have been found in most if not all sequenced bacterial genomes, including the smallest genomes of *Mycoplasma* species as well as endosymbionts such as *Carsonella rudii* [16]. Moreover, tmRNA is essential in many bacteria, including many pathogenic bacteria such as *Neisseria gonorrhoeae*, *Mycobacterium tuberculosis*, and *Legionella pneumophila* [6,17]. ArfB, and particularly ArfA, have more limited phylogenetic distributions, with ArfB being present in 34% of representatively sequenced bacterial genomes and ArfA limited to a subset of β - and γ -proteobacteria [18,19]. In many bacteria trans-translation is not essential, presumably due to the presence of redundant alternative rescue pathways. Nevertheless, the loss of trans-translation usually leads to reduction in fitness, particularly under various stress conditions, such as high or low temperature, ethanol or acid treatment, or nutrient deprivation, or in the presence of antibiotics [6,17]. Such stress conditions can lead to an increase in truncated mRNAs and stalled ribosomes, explaining the higher levels and importance of trans-translation under these circumstances. These findings also highlight that, although the presence of alternative rescue pathways is sufficient to maintain cell viability, they appear to be insufficient to optimally cope with the cellular demands for ribosome rescue in the absence of trans-translation.

In most bacteria, tmRNA comprises a single RNA molecule containing a tRNA-like domain (TLD), which resembles the acceptor stem of an alanyl-tRNA, and a messenger-like domain (MLD) encoding a short, 8–35-aa peptide [20]. The TLD and MLD are linked together by a series of **pseudoknots** (see inset in Figure 1) [20]. The TLD of tmRNAs can be charged with alanine by the canonical alanine tRNA synthetase (AlaRS), a reaction that is enhanced by the presence of SmpB, which interacts with AlaRS and stabilizes the tmRNA structure [20]. The alanine-charged TLD of the tmRNA is recognized by elongation factor (EF)-Tu, which delivers tmRNA to the A site of a non-stop ribosome (Figure 1A,B) [20]. The structure of the TLD of a tmRNA in complex with SmpB and EF-Tu-GDP stabilized on a 70S ribosome using the antibiotic **kirromycin** [21] (Figure 1C) reveals that the TLD of tmRNA interacts with EF-Tu on the ribosome, analogous to the acceptor arm of an **aminoacyl-tRNA (aa-tRNA)** being delivered to the ribosome by EF-Tu [22]. During canonical translation the complementarity between the codon in the A site and the **anticodon** stem-loop (ASL) of the aa-tRNA dictates which aa-tRNA is delivered by EF-Tu [23,24]. On non-stop ribosomes there is no codon in the A site, explaining why the TLD of tmRNA does not require an ASL. Instead, the globular domain of SmpB mimics the ASL of a tRNA and occupies the decoding site of the ribosome [21] (Figure 1B,C), as predicted based on previous X-ray [25,26] and cryo-EM [27,28] studies. The C-terminal tail of SmpB, which is unstructured in solution, adopts an α -helical conformation on the ribosome that probes the mRNA channel (Figure 1B,C) [21], explaining how the tmRNA-SmpB complex can distinguish actively translating ribosomes with mRNA in the channel from ribosomes stalled on truncated mRNAs with a vacant channel [29]. Accommodation of the TLD at the A site of the **peptidyltransferase center (PTC)** of the large ribosomal subunit allows peptide bond formation between the truncated nascent polypeptide chain and the alanine of the TLD of the tmRNA (Figure 1D). Binding of EF-G translocates the TLD of the tmRNA from the A site to the **P site**, which together with SmpB places the first (resume) codon of the MLD into the A site ready to be decoded by the next aa-tRNA (Figure 1E,F) [30]. A cryo-EM structure of the translocated state reveals that the TLD and SmpB occupy a **hybrid A/P site** of the ribosome and the linking pseudoknots wrap around the swiveled head of the small subunit to facilitate positioning of the MLD for decoding (Figure 1E) [31]. Translation then continues on the MLD of the tmRNA incorporating a degradation tag into the C terminus of the truncated polypeptide, which targets it for proteolysis by Clp and other proteases (Figure 1G). Importantly, the MLD of the tmRNA contains a stop codon, such as UAA, which allows canonical translation termination via recruitment of RF1 or RF2 (Figure 1G). The **glycine-glycine-glutamine (GGQ) motif** of RF1 or RF2 then catalyzes the hydrolysis of the tagged polypeptide chain, allowing the

Glossary

Aminoacyl-tRNA (aa-tRNA): tRNA charged at the 3' end with an amino acid.

Anticodon: the region of the tRNA that is complementary to the codon of the mRNA.

Anti conformation: nucleotide conformation where the ring of the nucleobase is nearly perpendicular to the furanose ring but projecting away from the furanose; contrasts with the *syn* conformation where the nucleobase ring is rotated around the glycosidic bond.

A site: the tRNA-binding site on the ribosome where aa-tRNAs are delivered by EF-Tu during translation.

Codon: a sequence of three RNA (or DNA) nucleotides that corresponds to a specific amino acid (or stop signal) during protein synthesis.

Deacylated tRNA: tRNA that is not charged with an amino acid.

E site: the tRNA-binding site on the ribosome where uncharged or deacylated tRNAs exit from the ribosome during translation.

Glycine-glycine-glutamine (GGQ) motif: conserved motif found in protein factors that catalyze PTH on the ribosome.

Hybrid A/P site: when the tRNA is in the A site on the small subunit and in the P site on the large subunit.

Hydroxyl radical probing: chemical probing method that relies on the cleavage of RNA (or DNA) molecules by hydroxyl radicals, which can be generated from site-specific tethers located on neighboring proteins or factors.

Kirromycin: an antibiotic that binds and traps EF-Tu on the ribosome.

Peptidyltransferase center (PTC): the highly conserved region in the large subunit of the ribosome where peptide bond formation occurs.

Peptidyl-tRNA: a tRNA bearing the growing nascent polypeptide chain.

Peptidyl-tRNA hydrolysis (PTH): the activity of hydrolyzing and thereby breaking the ester linkage between the polypeptide chain and the tRNA to which it is attached.

Proline-alanine-threonine (PAT) motif: motif in *Escherichia coli* RF1 that is involved in recognition of the stop codon of the mRNA.

Pseudoknot: a nucleic acid secondary structure containing at least two stem-loop structures in which half of one stem is intercalated

ribosome to be subsequently recycled for the next round of translation. It has been demonstrated that it is the recycling of the stalled ribosomes, rather than tagging of the truncated polypeptide chains for degradation, that makes trans-translation essential for bacterial survival [20,32]. This is consistent with the observation that inactivation of trans-translation in bacteria such as *E. coli* is not lethal, due to the presence of back-up systems such as ArfA [33].

Interplay between the Trans-translation, ArfA, and ArfB Rescue Systems

While the deletion of either the *ssrA* or the *arfA* gene in *E. coli* does not significantly affect viability, deletion of both genes ($\Delta ssrA\Delta arfA$) is synthetic lethal [33], illustrating the importance of having at least one ribosome rescue for bacterial survival [5,10]. Biochemical studies have demonstrated that ArfA represents a back-up system for trans-translation [34,35]. The *arfA* mRNA contains a stem-loop structure that acts as a transcription terminator and/or a substrate for RNase III cleavage [18,34,35] (Figure 2A). In the presence of tmRNA, the short ArfA protein produced from the truncated *arfA* mRNA is tagged by tmRNA and targeted for degradation (Figure 2A). However, in the absence of tmRNA the short ArfA protein product is not degraded and assumes the role of recycling ribosomes stalled on truncated mRNAs [34,35] (Figure 2B). The full-length *E. coli* ArfA protein is 72 aa in length and contains a C-terminal hydrophobic region that leads to aggregation of the protein *in vivo* [34] (Figure 2A). By contrast, shorter forms

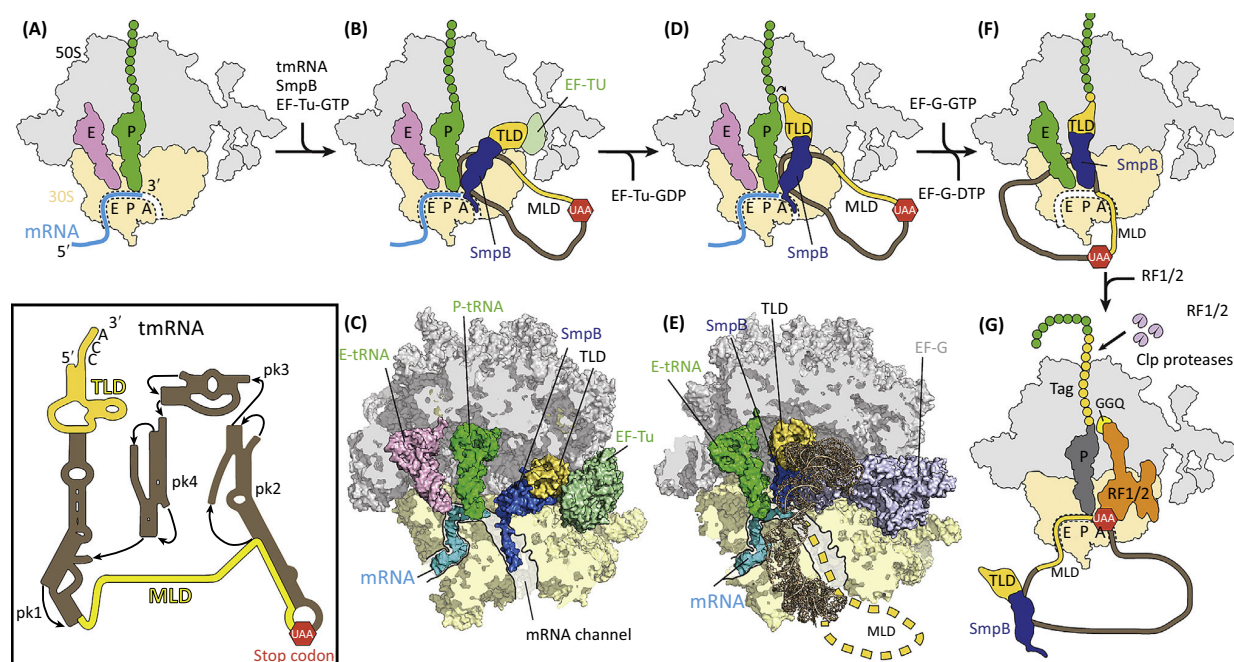
between the two halves of another stem.

P site: the tRNA-binding site for the peptidyl-tRNA on the ribosome.

RNase: a type of nuclease that catalyzes the degradation of RNA; for example, RNase III is an endonuclease that cleaves dsRNA.

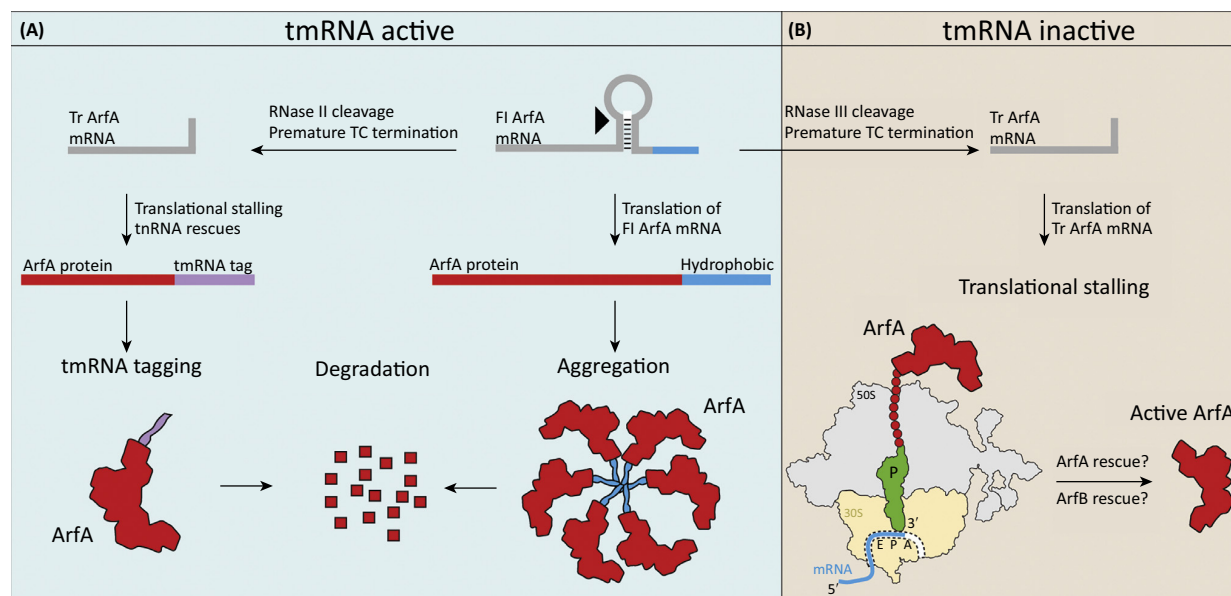
Serine-proline-phenylalanine (SPF) motif: motif in *E. coli* RF2 that is involved in recognition of the stop codon of the mRNA.

Translocation: the process of moving the A and P site tRNAs as well as the associated mRNA through the ribosome into the P and E sites, respectively. This reaction is catalyzed by EF-G in bacteria.



Trends in Biochemical Sciences

Figure 1. Rescue of Non-stop Ribosomal Complexes by Trans-translation. (A) Ribosomes stall on truncated mRNAs (cyan) with vacant A sites. (B) The tRNA-like domain (TLD) (yellow) of transfer-messenger RNA (tmRNA) (brown) is recognized by elongation factor (EF)-Tu (pale green) and delivered together with small protein B (SmpB) (blue) to the ribosomal A site. The globular domain of SmpB occupies the decoding site, while the C-terminal tail of SmpB probes the vacant mRNA channel of the small (30S) subunit. (C) Overview of the structure of the TLD of tmRNA (yellow), with SmpB and EF-Tu bound to the ribosome (PDB ID: 4V8Q) [70]. (D) Accommodation of the TLD at the A site of the large (50S) subunit allows peptide bond formation between the TLD and the nascent polypeptide chain, resulting in transfer from P-tRNA (green) to the TLD. (E) Cryoelectron microscopy (cryo-EM) structure of a translocated state of tmRNA-SmpB with bound EF-G (light blue; PDB ID: 4V6T) [31]. (F) After translocation of TLD by EF-G, the first codon of the mRNA-like domain (MLD) (yellow) is positioned at the A site. (G) Canonical translation termination mediated by release factor (RF) 1 or RF2 (orange) on encountering the UAA stop codon of the MLD at the A site. The translated degradation tag (yellow) is recognized by Clp proteases, leading to degradation of the incompletely translated nascent chain (green). Inset shows the secondary structure of tmRNA, with the TLD and MLD highlighted in yellow.



Trends in Biochemical Sciences

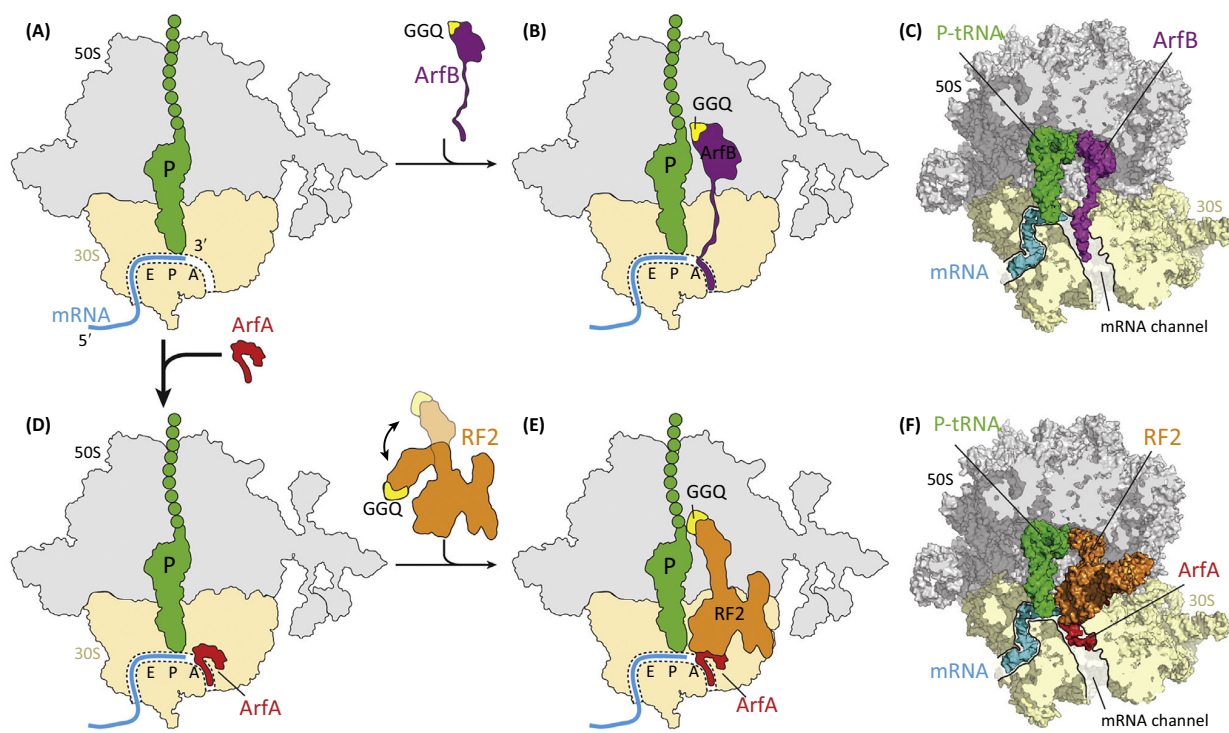
Figure 2. Alternative Rescue Factor A (ArfA) Is a Back-Up System for Trans-translation. (A) Full-length (FI) ArfA mRNA (gray) forms a stem-loop structure that acts as a transcription terminator and/or is recognized and cleaved by RNase III, generating a truncated (Tr) mRNA. Ribosomes stall on the truncated mRNAs, inducing trans-translation, leading to tmRNA tagging (purple) and degradation of the ArfA protein (red). In the case that full-length ArfA protein is translated, the C-terminal region contains a hydrophobic stretch (cyan) that leads to aggregation and degradation of the full-length ArfA. (B) If trans-translation is impaired (or overwhelmed), the short ArfA protein is not tagged or degraded and the active ArfA assumes the role of rescuing non-stop ribosome complexes.

of ArfA resulting from truncated *arfA* mRNA lack the terminal 17–18 aa but retain full rescue activity [34,35].

Curiously, *ssrA* is essential in *Neisseria gonorrhoeae*, despite the presence of an *arfA* gene [32], although *N. gonorrhoeae* ArfA is active when expressed in *E. coli* [18]. By contrast, tmRNA is not essential in *Bacillus subtilis* [36] despite the apparent absence of both the ArfA and ArfB systems, raising the question of additional alternative rescue systems existing in some bacteria [10]. The synthetic lethality of *E. coli* due to the $\Delta ssrA\Delta arfA$ double deletion occurs despite the presence of *arfB*, but overexpression of ArfB can rescue the lethality of the $\Delta ssrA\Delta arfA$ strain [37]. This finding indicates that endogenous levels of ArfB are insufficient to cope with the level of ribosome rescue needed when tmRNA and ArfA are both absent [7]. It also raises the question of whether there are specific growth or stress conditions where ArfB is more important or whether ArfB is simply less important in *E. coli* than in other species due to the additional presence of ArfA.

Ribosome Rescue by ArfB

The globular N-terminal domain (NTD) of ArfB is evolutionarily related to domain 3 of RF1 and RF2 [38,39], which contain a conserved GGQ motif that is critical for **peptidyl-tRNA hydrolysis (PTH)** activity [40]. In contrast to RF1 and RF2, ArfB lacks the domain 2/4 responsible for stop codon recognition and instead has an extended C-terminal tail (Figure 3A–C). In agreement with the finding that overexpression of ArfB can rescue *E. coli* lacking tmRNA and ArfA rescue systems [37], ArfB can efficiently catalyze PTH on ribosomes stalled at the 3' ends of non-stop mRNAs *in vivo* [19,37,41,42] (Figure 3A,B). The crystal structure of ArfB on the ribosome reveals that the NTD interacts with the large subunit such that the GGQ motif is positioned at the PTC (Figure 3C) [43], consistent with the reports that mutations of the GGQ



Trends in Biochemical Sciences

Figure 3. Rescue of Non-stop Ribosomal Complexes by Alternative Rescue Factor (Arf) B and ArfA. (A) Ribosomes stall on truncated mRNAs (cyan) resulting in vacant A sites. (B) These non-stop ribosomes are recognized by the C-terminal tail of ArfB (purple), which probes the vacant mRNA channel. The N-terminal domain of ArfB containing the glycine-glycine-glutamine (GGQ) motif (yellow) catalyzes the hydrolysis of polypeptide from the P-tRNA (green). (C) Overview of the structure of ArfB (purple) bound to the ribosome (PDB ID: 4V95) [43]. (D) Non-stop ribosomes are also recognized by the C-terminal tail of ArfA (red), which also probes the vacant mRNA channel. (E) ArfA recruits release factor 2 (RF2) (orange) to the non-stop ribosome to catalyze peptidyl-tRNA (green) hydrolysis. (F) Overview of the structure of ArfA (red) and RF2 (orange) bound to a non-stop ribosome (PDB ID: 5MGP) [12].

motif of ArfB impair the rescue activity of ArfB both *in vitro* [19,37] and *in vivo* [37]. The C-terminal tail of ArfB, which was disordered in previous unbound ArfB structures [38,39,44], adopts a α -helical conformation that reaches into the mRNA channel of the small subunit (Figure 3B,C) [43]. This suggests that, like SmpB, ArfB also utilizes the C-terminal tail to distinguish actively translating ribosomes from those stalled on truncated mRNAs. Truncation of ten residues or more from the C terminus of ArfB leads to a severe reduction in ribosome binding and PTH activity as well as the ability to rescue the Δ ssrA Δ arfA strain [19,37,39]. The NTD and C-terminal helix are connected by a flexible linker of \sim 12 aa that adopts an extended conformation on the ribosome (Figure 3B,C). Deletion of one or two residues within the linker of ArfB led to progressive loss of PTH activity although the ribosome interaction remained unaffected [39], suggesting that the linker is important for positioning of the NTD at the PTC of the ribosome.

While ArfB rescue is most efficient on non-stop ribosomes, it maintains some rescue activity on longer mRNAs that extend into the A site [19,42]. The ArfB rescue activity decreases with increasing length of the 3' end, such that little activity is observed when the 3' end extends $>$ 14 nucleotides from the P site [42]. This suggests that the C-terminal tail of ArfB can efficiently compete and may even displace short mRNA 3' ends from the channel and that longer mRNAs encompassing the entire mRNA channel are resilient to displacement by ArfB, explaining why ArfB does not interfere with canonical translation elongation.

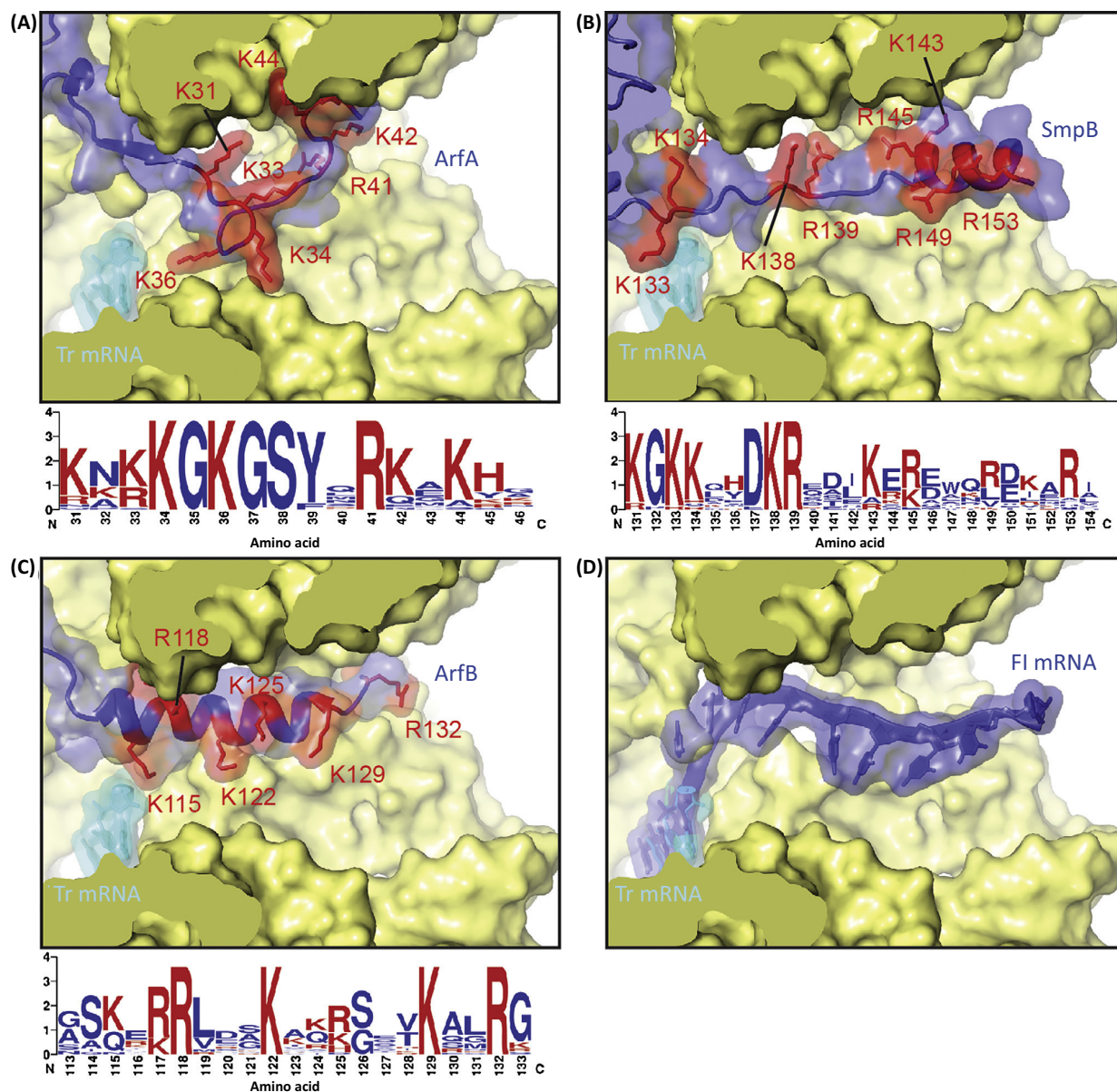
ArfB homologs are present in most, if not all, eukaryotes, where they are targeted to mitochondria [45]. In addition, some plants also encode ArfB homologs with chloroplast-targeting signals. By contrast, there is no evidence for ArfA genes in eukaryotes and tmRNA/SmpB genes are found only in some protist mitochondria [46]. The best-characterized organellar ArfB homolog is the human mitochondrial immature colon carcinoma transcript-1 (ICT1) (reviewed in [47]). Like other ArfB homologs, ICT1 displays excellent rescue activity on non-stop ribosomal complexes from either *E. coli* [39,42,48] or mammalian mitochondria [49]. The rescue activity is dependent on an intact GGQ motif and the presence of a C-terminal tail [39,48,49]. Loss or knockdown of ICT1 leads to a loss of cell viability [38,48], which can be rescued by the expression of a bacterial ArfB homolog [42]. Likewise, ICT1 supported the viability of a bacterial Δ ssrA Δ arfA strain, suggesting that ICT1 and ArfB are functionally interchangeable [42]. However, unlike bacterial ArfB, ICT1 was shown to be an integral component of the mitochondrial large subunit [48], where it is located at the base of the central protuberance [50]. Subsequent *in vitro* experiments demonstrated that the integrated ICT1 does not appear to display any rescue activity on non-stop complexes, but rather exogenous ICT1 is required [49]. So far, ribosome-free ICT1 has not been detected in mitochondria [48], raising the question of whether ICT1 is released from the mitoribosome to rescue stalled ribosomes or whether ICT1 expression is upregulated under specific stress conditions.

Ribosome Rescue by ArfA and RF2

ArfA was originally identified in a screen for factors that are essential for viability of *E. coli* when the *ssrA* gene is disabled [33]. The loss-of-function mutation identified had an Ala-to-Thr substitution at position 18 (A18T) in ArfA [33]. ArfA, as well as the ArfA-A18T mutant, were both shown to co-localize with ribosomes *in vivo*, but only the wild-type ArfA could rescue non-stop ribosomes [33]. Interestingly, recombinant ArfA was effective at rescuing non-stop ribosomes *in vitro* when an *E. coli*-extract-based system was used [33] but displayed no rescue activity with purified non-stop ribosome complexes [37]. This indicated that ArfA requires an additional cellular factor present in the *E. coli* extract to mediate ribosome rescue [37]. Subsequent *in vitro* studies using a reconstituted cell-free translation system revealed that RF2, but not RF1, cooperates with ArfA to hydrolyze the peptidyl-tRNA and rescue non-stop ribosomes [41,51] (Figure 3D,E). ArfA does not interact with RF2 in solution [51,52] but rather interacts with non-stop ribosomes [52] (Figure 3D) before recruiting RF2 to the complex (Figure 3E). Initial binding assays observed interaction of ArfA with the large ribosomal subunit [33], whereas subsequent **hydroxyl radical probing** experiments indicated a binding site located on the 30S subunit in the vicinity of the mRNA channel [52]. The five cryo-EM structures of ArfA-RF2-non-stop ribosome complexes [11–15] (Figure 3F) revealed that ArfA interacts almost exclusively with the small subunit. Overall, the structures are in excellent agreement with each other and enable most of the available biochemical data to be rationalized. The structures provide much-needed structural insight into the mechanisms of action of ArfA and RF2 in rescuing non-stop ribosome complexes, which are discussed in detail in the following sections.

Monitoring the mRNA Channel of the Non-stop Ribosome

Full-length *E. coli* ArfA is 72 aa in length but is aggregation prone; therefore, C-terminally truncated ArfA variants were used for the structural analysis that lacked either 12 [11,15] or 17 residues [12–14]. In each case, however, the flexibility of the C terminus permitted only 46–48 of the 55–60 aa of ArfA to be modeled. The absence of electron density for the very-C terminus of ArfA suggests that these residues are less important for binding, which is consistent with their poor conservation across ArfA from different species [18,33]. In all five cryo-EM structures [11–15], the C-terminal part of ArfA extends from the decoding A site into the mRNA entry channel (Figure 4A), analogous to the C-terminal tails of SmpB [21] (Figure 4B) and ArfB [43] (Figure 4C) as well as the 3' end of a full-length mRNA [53] (Figure 4D). The location of the C terminus of ArfA within the mRNA channel is also compatible with hydroxyl radical probing experiments



Trends in Biochemical Sciences

Figure 4. Monitoring of the mRNA Channel by Ribosome Rescue Factors. The mRNA channel of the ribosome is probed by the C-terminal tail of (A) alternative rescue factor (Arf) A (PDB ID: 5MGP) [12], (B) small protein B (SmpB) (PDB ID: 4V8Q) [70], or (C) ArfB (PDB ID: 4V95) [43]. The interaction is mediated via positively charged amino acids (red), the conservation of which is presented as a WebLogo [71] below the respective panels. (D) For comparison, the path of a full-length (FI) mRNA is indicated (PDB ID: 4V6F) [53].

performed in the absence of RF2 [52], suggesting that ArfA initially uses a similar conformation to monitor the vacant mRNA channel.

Like SmpB and ArfB, the C terminus of ArfA also contains several highly conserved positively charged arginine and lysine residues that establish interactions with the negatively charged 16S rRNA comprising the walls of the mRNA channel [11–15] (Figure 4A–C). There appears to be

some redundancy in the interaction of these conserved residues of ArfA, since individual point mutations had little to no effect on the recycling activity of ArfA [13,52], although some reduction was reported for K34C and R41C mutations in a recent study [14]. The C-terminal tail of SmpB is also rich in positively charged residues and includes several highly conserved stretches, such as $_{131}\text{KGKK}_{134}$ and $_{137}\text{DKR}_{139}$ (Figure 4B). Although single mutations within the $_{137}\text{DKR}_{139}$ motif had little effect, a triple alanine substitution abolished SmpB's ability to support tmRNA activity *in vivo* [54,55]. Similar loss of activity was observed when the C-terminal helix of SmpB was truncated [56]. Single mutations within the C-terminal tail of *E. coli* ArfB, such as K122A, K129A, and R132A, as well as the equivalent residues in ICT1, dramatically decreased the rescue activity of the respective factors [39] (Figure 4C). Similar to ArfB [19,37,39], C-terminal truncations in human ICT1 that remove these residues also abolished rescue activity [39,49].

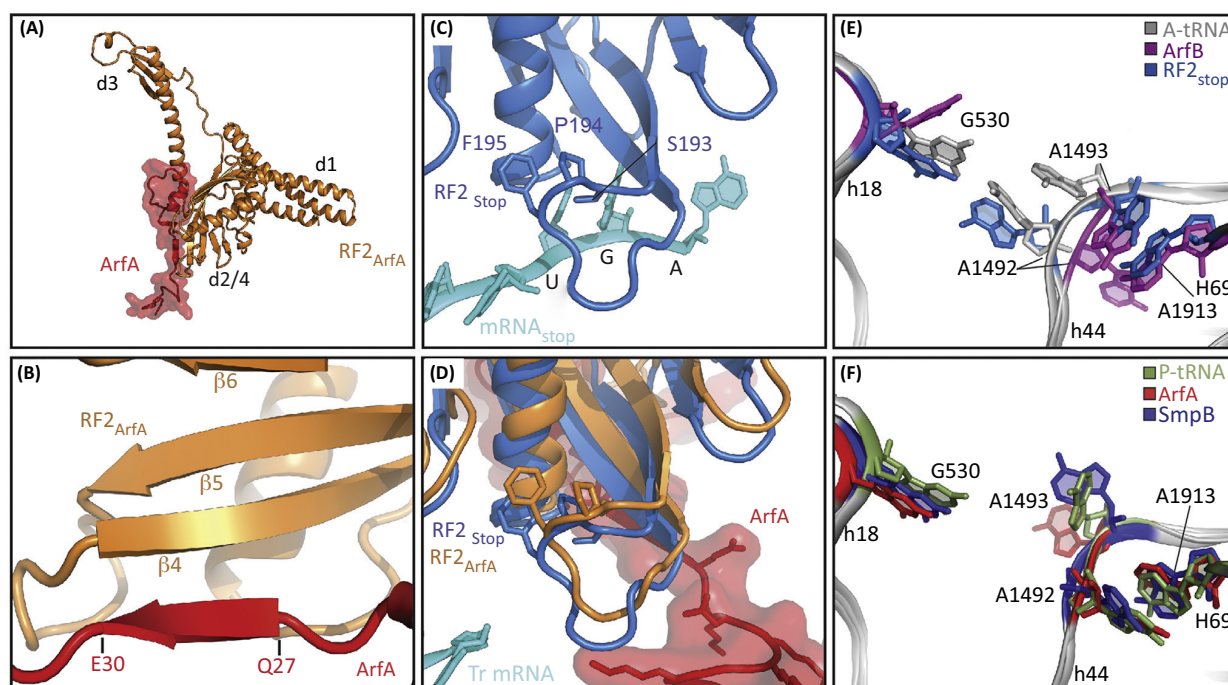
Biochemical studies have demonstrated that the efficiency of ArfA–RF2-mediated ribosome rescue decreases with increasing length of the 3' end of the mRNA that extends into the A site [41,57]. Specifically, rescue was observed, although with reduced efficiency, when mRNA extended by up to three or four A-site nucleotides was used [41,57]. Almost no rescue occurred on artificially stalled ribosomes with mRNAs extended by six or more A-site nucleotides [41,57]. This is consistent with the overlap in the binding position of ArfA [11–15] (Figure 4A) and a full-length mRNA (Figure 4D), which indicates that three nucleotides (but not more) can be accommodated in the A site without significant clashes with ArfA. By contrast, the tmRNA–SmpB trans-translation system is less sensitive to mRNA length, with the most dramatic reductions in trans-translation activity being observed when mRNAs with 12 or more A-site nucleotides were used [29,58,59]. mRNA length dependence for the rescue activity of ArfB has also been reported and appears to be intermediate to the ArfA and trans-translation systems [41]. It remains to be determined whether the length dependencies of the different rescue systems correlate with the ability of C-terminal extensions of the respective rescue factors to displace the 3' portion of the mRNA from the mRNA channel, or whether the factors utilize different binding modes when the mRNA channel is occupied.

Recruitment of RF2 to the Ribosome by ArfA

The recent cryo-EM structures also provide insight into how ArfA recruits RF2 to the ribosome despite the absence of a stop codon in the mRNA [11–15]. ArfA establishes a large interaction interface with RF2 encompassing the central portion (residues 15–31) of ArfA and the distal end of α helix $\alpha 7$ of domain 3 as well as the $\beta 4$ – $\beta 5$ strands of domain 2 of RF2 (Figure 5A). Residues 27–30 of ArfA form a small β strand that complements the β sheet of RF2 domain 2/4 (Figure 5B). The overall position of RF2 in the ArfA–RF2–non-stop complex is similar to that observed during canonical translation termination [60,61], although the decoding domain 2/4 is slightly shifted. The shift affects the loop between the $\beta 4$ – $\beta 5$ strand of domain 2 of RF2 bearing the **serine–proline–phenylalanine (SPF) motif** (*E. coli* Ser205–Pro206–Phe207), which is involved in the specificity of recognition of the first and second positions of the UGA and UAA stop codons [60–62] (Figure 5C,D). Importantly, the structures illustrate that ArfA does not interact with the SPF motif and therefore does not directly mimic the presence of a stop codon (Figure 5D). Consistently, mutations in the SPF motif that impair RF2 termination activity do not affect ArfA–RF2-mediated rescue activity [51] whereas RF1 mutants bearing the SPF motif instead of the **proline–alanine–threonine (PAT) motif** (which confers termination activity at UGA) remain inactive in the ArfA-mediated rescue system [51].

Distinct Conformations of the Decoding Site during Ribosome Rescue

During canonical termination G530 of the 16S rRNA adopts an **anti conformation** that stacks on the A3 nucleotide of a stop codon [40]. The same flipped *anti* conformation of G530 is also stabilized during ribosome rescue via interaction with E30 of ArfA [11–15] or by stacking interactions with Y126 of SmpB [21] and Arg118 of ArfB [43]. G530, together with A1492 and



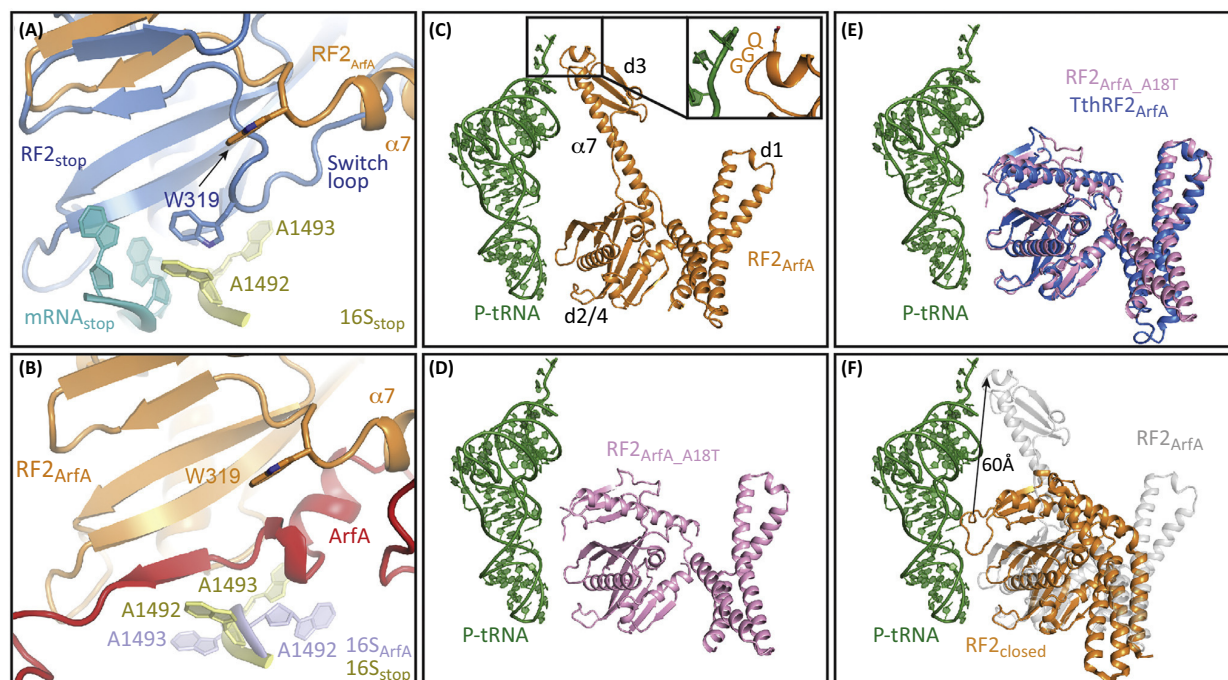
Trends in Biochemical Sciences

Figure 5. Recruitment of Release Factor 2 (RF2) to Non-stop Ribosomes by Alternative Rescue Factor A (ArfA). (A) Interaction surface between ArfA (red) and RF2 (orange). (B) ArfA donates a β strand to the β sheet of domain 2/4 of RF2 (orange). (C) Interaction of the serine-proline-phenylalanine (SPF) motif of RF2 with the A-site UGA stop codon of an mRNA ($mRNA_{stop}$, cyan; PDB ID: 4V5E) [60]. (D) Same view as (C) but superimposed with the ArfA-RF2-non-stop ribosome complex containing ArfA (red), RF2 (orange), and the truncated (Tr) mRNA (cyan; PDB ID: 5MGP) [12]. (E,F) Superimposition of decoding center showing 16S rRNA nucleotides G530, A1492, and A1493 as well as the 23S rRNA nucleotide A1913 from ribosomes bound with (E) A-tRNA (grey; PDB ID: 4V6F) [53], RF2_{stop} with a UGA codon (marine blue; PDB ID: 4V5E) [60], ArfB (purple; PDB ID: 4V95) [43], (F) P-tRNA (green; PDB ID: 4V9B) [64], ArfA (red; PDB ID: 5MGP) [12], or small protein B (SmpB) (blue; PDB ID: 4V8Q) [70].

A1493, is critical for monitoring the interaction between the codon of the mRNA and the anticodon of the A-site tRNA [23,63]. While both A1492 and A1493 are flipped out of helix 44 (h44) during decoding of sense codons [23,63], only A1492 is flipped during termination by RFs while A1493 stacks on A1913 in H69 of the 23S rRNA (Figure 5E) [40]. In the presence of ArfB, A1492 is only partially flipped out and A1493 is stacked with A1913 (Figure 5E) and Pro110 of ArfB [43]. The opposite occurs with ArfA or SmpB; namely, A1493 is flipped out of h44 whereas A1492 stacks on A1913 [11–15,21] (Figure 5F). This is similar to the conformation observed when tRNA is bound at the P site but the A site is vacant [64] (Figure 5F). Thus, the flexibility of the decoding site is manipulated in various ways to accommodate binding of the rescue factors on the ribosome. While mutations with the decoding center of the ribosome (G530A, A1492G, or A1493G) have a dramatic effect (1000-fold reduction) on aa-tRNA accommodation at the PTC, only a twofold reduction was observed on peptidyl-transfer to Ala-tmRNA [55]. It remains to be determined to what extent such mutants influence factor binding and accommodation at the PTC during ArfA- and ArfB-mediated ribosome rescue.

ArfA Induces the Active Open Conformation of RF2 on the Ribosome

During canonical termination, recognition of the stop codon by RF1 and RF2 stabilizes a rearranged conformation of the switch loop that directs domain 3 into the PTC [40,65]. The switch loop conformation is stabilized via specific interactions with A1492 and A1493 that, in the case of RF2, involve stacking interactions of W319 of RF2 with A1492 [60,61] (Figure 6A). In



Trends in Biochemical Sciences

Figure 6. Alternative Rescue Factor A (ArfA) Induces a Closed-to-Open Transition in Release Factor 2 (RF2). (A) Interaction between Trp319 (W307 in *Thermus thermophilus* RF2) of the switch region of RF2_{stop} (sky blue) and A1492 of the 16S rRNA (yellow) during decoding of the UGA stop codon (cyan; PDB ID: 4V5E) [60]. The switch loop conformation of RF2 (RF2_{ArfA}, orange) observed on ArfA binding is superimposed and arrowed. (B) Same view as (A) showing the distinct conformation of the switch loop of *Escherichia coli* RF2 (orange) and A1492/A1493 (pale blue) when ArfA (red) is present. (C) The open conformation of RF2 (orange) in the non-stop complex with ArfA (PDB ID: 5MGF) [12] compared with the closed RF2 conformations observed when using (D) RF2 (pink) in the presence of ArfA A18T (PDB ID: 5MDW) [11], (E) *T. thermophilus* RF2 (blue; PDB ID: 5MDY) [11], or (F) the free RF2 structure (orange; PDB ID: 1GQE) [66], which was aligned with the ribosome-bound RF2 (gray) on the basis of domain 2/4 (d2/4). In (C–F) the P-tRNA (green) is shown for reference.

the cryo-EM structures, ArfA precludes the interaction between the switch loop and A1492 [11–15] (Figure 6B). Instead, ArfA itself appears to stabilize a distinct conformation of the switch loop in RF2 that extends the α helix $\alpha 7$ of domain 3 of RF2 by two to three helical turns, analogous to that observed during canonical translation termination with RF2 [60,61]. As observed for canonical termination [60,61], the open conformation of RF2 on the ribosome in the presence of ArfA also directs the GGQ motif of domain 3 into the PTC (Figure 6C). The A18T mutation that led to the discovery of ArfA does not interfere with ribosome binding [33] or with RF2 recruitment, but prevents PTH [41]. Consistently, the cryo-EM structure of the ArfA–A18T non-stop complex reveals that RF2 is recruited to the ribosome but adopts a closed rather than an open conformation [11] (Figure 6D). The A18T mutation appears to destabilize the interaction of the N terminus of ArfA and the switch loop of RF2, preventing the transition from the closed to the open conformation [11]. A closed conformation of RF2 was also observed when *Thermus thermophilus* RF2 replaced *E. coli* RF2 [11] (Figure 6E), suggesting an incompatibility between *T. thermophilus* RF2 and *E. coli* ArfA (note: *T. thermophilus* does not have an ArfA homolog). The ribosome-bound closed conformations resemble the closed conformation observed previously in the structures of the unbound form of RF2 [66,67] (Figure 6F). The closed conformation may reflect a *bona fide* intermediate during ribosome rescue, since this state represented a major population in the cryo-EM analysis of Demo *et al.* [15], where wild-type RF2 was employed. The open conformation and positioning of domain 3 of RF2 at the PTC observed in the different cryo-EM structures are very similar despite two of

the structures reflecting pre-hydrolysis states (obtained using either a GAQ mutant or a non-hydrolyzable P-tRNA) [11,12] and the other three representing post-hydrolysis states (assembled with **deacylated tRNA** in the P site) [13–15].

Concluding Remarks

The availability of structures of ArfA and RF2 on the non-stop ribosome has provided much needed mechanistic insight into this bacterial ribosome rescue system and enabled comparisons with the tmRNA/SmpB and ArfB systems to be made. The structures have also provided initial insights into specificity determinants in ArfA and RF2 that allow ArfA to cooperate with RF2 but not RF1; however, this needs to be validated biochemically (see Outstanding Questions). Similarly, the species specificity of ArfA–RF2 action has so far not been addressed systematically. The apparent absence of Arfs in some species where trans-translation is not essential raises the possibility of other novel, unidentified Arf systems. Will novel ArfA or ArfA-like systems emerge in bacteria where RF1, rather than RF2, is recruited to the stalled ribosomes? Perhaps bacteria exist where entirely different GGQ-containing factors (ArfB-like?) or even non-GGQ factors are recruited to non-stop ribosomes to mediate PTH. The wider distribution of ArfB/ICT1 compared with ArfA suggests that it may play a more important role in other bacteria and organelles than it does in *E. coli*. Distinguishing the division of labor of alternative rescue systems in different bacteria will provide much needed insight into their importance under different environmental and stress conditions. The importance of ribosome rescue in bacteria, coupled with the distinct pathways used by eukaryotic ribosomes, suggests that ribosome rescue may be a possible target for the development of novel antimicrobial agents. Small molecules have already been discovered that specifically target trans-translation [68,69]. Can similar approaches be used to identify lead compounds that selectively target the Arf systems?

Acknowledgments

The work from the Wilson laboratory described in this review is funded by grants from the Deutsche Forschungsgemeinschaft (DFG).

References

1. Harigaya, Y. and Parker, R. (2010) No-go decay: a quality control mechanism for RNA in translation. *Wiley Interdiscip. Rev. RNA* 1, 132–141
2. Buskirk, A.R. and Green, R. (2017) Ribosome pausing, arrest and rescue in bacteria and eukaryotes. *Philos. Trans. R. Soc. Lond. B Biol. Sci.* Published online January 30, 2017. <http://dx.doi.org/10.1098/rstb.2016.0183>
3. Giudice, E. and Gillet, R. (2013) The task force that rescues stalled ribosomes in bacteria. *Trends Biochem. Sci.* 38, 403–411
4. Shimizu, Y. (2014) Biochemical aspects of bacterial strategies for handling the incomplete translation processes. *Front. Microbiol.* 5, 170
5. Keiler, K.C. (2015) Mechanisms of ribosome rescue in bacteria. *Nat. Rev. Microbiol.* 13, 285–297
6. Himeno, H. *et al.* (2015) Ribosome rescue systems in bacteria. *Biochimie* 114, 102–112
7. Abo, T. and Chadani, Y. (2014) The fail-safe system to rescue the stalled ribosomes in *Escherichia coli*. *Front. Microbiol.* 5, 156
8. Moore, S.D. and Sauer, R.T. (2005) Ribosome rescue: tmRNA tagging activity and capacity in *Escherichia coli*. *Mol. Microbiol.* 58, 456–466
9. Ito, K. *et al.* (2011) Nascentome analysis uncovers futile protein synthesis in *Escherichia coli*. *PLoS One* 6, e28413
10. Keiler, K.C. and Feaga, H.A. (2014) Resolving nonstop translation complexes is a matter of life or death. *J. Bacteriol.* 196, 2123–2130
11. James, N.R. *et al.* (2016) Translational termination without a stop codon. *Science* 354, 1437–1440
12. Huter, P. *et al.* (2017) Structural basis for ArfA–RF2-mediated translation termination on mRNAs lacking stop codons. *Nature* 541, 546–549
13. Zeng, F. *et al.* (2017) Structural basis of co-translational quality control by ArfA and RF2 bound to ribosome. *Nature* 541, 554–557
14. Ma, C. *et al.* (2017) Mechanistic insights into the alternative translation termination by ArfA and RF2. *Nature* 541, 550–553
15. Demo, G. *et al.* (2017) Mechanism of ribosome rescue by ArfA and RF2. *Elife* 6, e23687
16. Gueneau de Novoa, P. and Williams, K.P. (2004) The tmRNA website: reductive evolution of tmRNA in plastids and other endosymbionts. *Nucleic Acids Res.* 32, D104–D108
17. Brunel, R. and Charpentier, X. (2016) Trans-translation is essential in the human pathogen *Legionella pneumophila*. *Sci. Rep.* 6, 37935
18. Schaub, R.E. *et al.* (2012) Proteobacterial ArfA peptides are synthesized from non-stop messenger RNAs. *J. Biol. Chem.* 287, 29765–29775
19. Handa, Y. *et al.* (2011) YaeJ is a novel ribosome-associated protein in *Escherichia coli* that can hydrolyze peptidyl-tRNA on stalled ribosomes. *Nucleic Acids Res.* 39, 1739–1748
20. Moore, S.D. and Sauer, R.T. (2007) The tmRNA system for translational surveillance and ribosome rescue. *Annu. Rev. Biochem.* 76, 101–124
21. Neubauer, C. *et al.* (2012) Decoding in the absence of a codon by tmRNA and SmpB in the ribosome. *Science* 335, 1366–1369
22. Schmeing, T.M. *et al.* (2009) The crystal structure of the ribosome bound to EF-Tu and aminoacyl-tRNA. *Science* 326, 688–694

Outstanding Questions

What are the specificity determinants in ArfA and RF2 that allow only RF2, and not RF1, to be recruited by ArfA to non-stop ribosomes?

Are there other, as-yet-unidentified alternative rescue factor systems in bacteria, particularly in those bacteria where tmRNA does not appear to be essential?

Will ArfA or ArfA-like systems emerge in bacteria where RF1, and not RF2, is recruited to non-stop ribosomes?

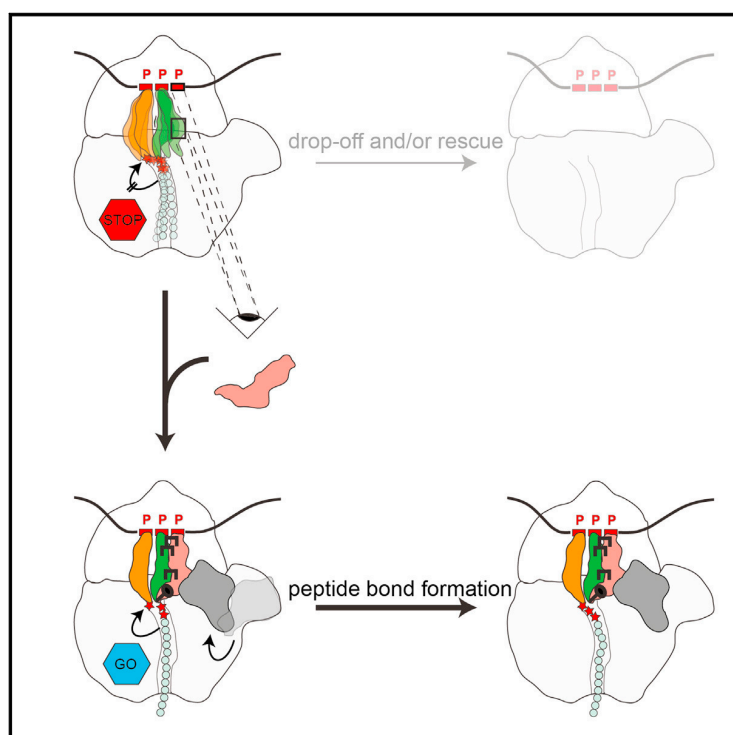
What is the role of ArfB? When is ArfB expressed? Is ArfB action more important under specific stress or growth conditions or in different bacterial species?

Is it possible to develop specific antibiotics that selectively target the alternative rescue factor systems?

23. Ogle, J.M. and Ramakrishnan, V. (2005) Structural insights into translational fidelity. *Annu. Rev. Biochem.* 74, 129–177
24. Rozov, A. *et al.* (2016) New structural insights into translational miscoding. *Trends Biochem. Sci.* 41, 798–814
25. Gutmann, S. *et al.* (2003) Crystal structure of the transfer-RNA domain of transfer-messenger RNA in complex with SmpB. *Nature* 424, 699–703
26. Bessho, Y. *et al.* (2007) Structural basis for functional mimicry of long-variable-arm tRNA by transfer-messenger RNA. *Proc. Natl. Acad. Sci. U. S. A.* 104, 8293–8298
27. Cheng, K. *et al.* (2010) tmRNA-SmpB complex mimics native aminoacyl-tRNAs in the A site of stalled ribosomes. *J. Struct. Biol.* 169, 342–348
28. Weis, F. *et al.* (2010) Accommodation of tmRNA-SmpB into stalled ribosomes: a cryo-EM study. *RNA* 16, 299–306
29. Kurita, D. *et al.* (2014) Rejection of tmRNA-SmpB after GTP hydrolysis by EF-Tu on ribosomes stalled on intact mRNA. *RNA* 20, 1706–1714
30. Weis, F. *et al.* (2010) tmRNA-SmpB: a journey to the centre of the bacterial ribosome. *EMBO J.* 29, 3810–3818
31. Ramrath, D.J. *et al.* (2012) The complex of tmRNA-SmpB and EF-G on translocating ribosomes. *Nature* 485, 526–529
32. Huang, C. *et al.* (2000) Charged tmRNA but not tmRNA-mediated proteolysis is essential for *Neisseria gonorrhoeae* viability. *EMBO J.* 19, 1098–1107
33. Chadani, Y. *et al.* (2010) Ribosome rescue by *Escherichia coli* ArfA (YhdL) in the absence of trans-translation system. *Mol. Microbiol.* 78, 796–808
34. Chadani, Y. *et al.* (2011) Trans-translation-mediated tight regulation of the expression of the alternative ribosome-rescue factor ArfA in *Escherichia coli*. *Genes Genet. Syst.* 86, 151–163
35. Garza-Sanchez, F. *et al.* (2011) tmRNA regulates synthesis of the ArfA ribosome rescue factor. *Mol. Microbiol.* 80, 1204–1219
36. Wiegert, T. and Schumann, W. (2001) SsrA-mediated tagging in *Bacillus subtilis*. *J. Bacteriol.* 183, 3885–3889
37. Chadani, Y. *et al.* (2011) *Escherichia coli* YaeJ protein mediates a novel ribosome-rescue pathway distinct from SsrA- and ArfA-mediated pathways. *Mol. Microbiol.* 80, 772–785
38. Handa, Y. *et al.* (2010) Solution structure of the catalytic domain of the mitochondrial protein ICT1 that is essential for cell vitality. *J. Mol. Biol.* 404, 260–273
39. Kogure, H. *et al.* (2014) Identification of residues required for stalled-ribosome rescue in the codon-independent release factor YaeJ. *Nucleic Acids Res.* 42, 3152–3163
40. Zhou, J. *et al.* (2012) Crystal structures of 70S ribosomes bound to release factors RF1, RF2 and RF3. *Curr. Opin. Struct. Biol.* 22, 733–742
41. Shimizu, Y. (2012) ArfA recruits RF2 into stalled ribosomes. *J. Mol. Biol.* 423, 624–631
42. Feaga, H.A. *et al.* (2016) Human cells require non-stop ribosome rescue activity in mitochondria. *PLoS Genet.* 12, e1005964
43. Gagnon, M.G. *et al.* (2012) Structural basis for the rescue of stalled ribosomes: structure of YaeJ bound to the ribosome. *Science* 335, 1370–1372
44. Singarapu, K.K. *et al.* (2008) NMR structure of the peptidyl-tRNA hydrolase domain from *Pseudomonas syringae* expands the structural coverage of the hydrolysis domains of class 1 peptide chain release factors. *Proteins* 71, 1027–1031
45. Duarte, I. *et al.* (2012) Evolution and diversification of the organellar release factor family. *Mol. Biol. Evol.* 29, 3497–3512
46. Hudson, C.M. *et al.* (2015) Islander: a database of precisely mapped genomic islands in tRNA and tmRNA genes. *Nucleic Acids Res.* 43, D48–D53
47. Wesolowska, M.T. *et al.* (2014) Overcoming stalled translation in human mitochondria. *Front. Microbiol.* 5, 374
48. Richter, R. *et al.* (2010) A functional peptidyl-tRNA hydrolase, ICT1, has been recruited into the human mitochondrial ribosome. *EMBO J.* 29, 1116–1125
49. Akabane, S. *et al.* (2014) Ribosome rescue and translation termination at non-standard stop codons by ICT1 in mammalian mitochondria. *PLoS Genet.* 10, e1004616
50. Brown, A. *et al.* (2014) Structure of the large ribosomal subunit from human mitochondria. *Science* 346, 718–722
51. Chadani, Y. *et al.* (2012) ArfA recruits release factor 2 to rescue stalled ribosomes by peptidyl-tRNA hydrolysis in *Escherichia coli*. *Mol. Microbiol.* 86, 37–50
52. Kurita, D. *et al.* (2014) ArfA recognizes the lack of mRNA in the mRNA channel after RF2 binding for ribosome rescue. *Nucleic Acids Res.* 42, 13339–13352
53. Jenner, L.B. *et al.* (2010) Structural aspects of messenger RNA reading frame maintenance by the ribosome. *Nat. Struct. Mol. Biol.* 17, 555–560
54. Sundermeier, T.R. *et al.* (2005) A previously uncharacterized role for small protein B (SmpB) in transfer messenger RNA-mediated trans-translation. *Proc. Natl. Acad. Sci. U. S. A.* 102, 2316–2321
55. Miller, M.R. *et al.* (2011) The role of SmpB and the ribosomal decoding center in licensing tmRNA entry into stalled ribosomes. *RNA* 17, 1727–1736
56. Jacob, Y. *et al.* (2005) Function of the SmpB tail in transfer-messenger RNA translation revealed by a nucleus-encoded form. *J. Biol. Chem.* 280, 5503–5509
57. Zeng, F. and Jin, H. (2016) Peptide release promoted by methylated RF2 and ArfA in nonstop translation is achieved by an induced-fit mechanism. *RNA* 22, 49–60
58. Ivanova, N. *et al.* (2004) Ribosome rescue by tmRNA requires truncated mRNAs. *J. Mol. Biol.* 338, 33–41
59. Asano, K. *et al.* (2005) Competition between trans-translation and termination or elongation of translation. *Nucleic Acids Res.* 33, 5544–5552
60. Weixlbaumer, A. *et al.* (2008) Insights into translational termination from the structure of RF2 bound to the ribosome. *Science* 322, 953–956
61. Korostelev, A. *et al.* (2008) Crystal structure of a translation termination complex formed with release factor RF2. *Proc. Natl. Acad. Sci. U. S. A.* 105, 19684–19689
62. Ito, K. *et al.* (2000) A tripeptide ‘anticodon’ deciphers stop codons in messenger RNA. *Nature* 403, 680–684
63. Rozov, A. *et al.* (2015) Structural insights into the translational infidelity mechanism. *Nat. Commun.* 6, 7251
64. Jenner, L. *et al.* (2013) Structural basis for potent inhibitory activity of the antibiotic tigecycline during protein synthesis. *Proc. Natl. Acad. Sci. U. S. A.* 110, 3812–3816
65. Youngman, E.M. *et al.* (2008) Peptide release on the ribosome: mechanism and implications for translational control. *Annu. Rev. Microbiol.* 62, 353–373
66. Vestergaard, B. *et al.* (2001) Bacterial polypeptide release factor RF2 is structurally distinct from eukaryotic eRF1. *Mol. Cell.* 8, 1375–1382
67. Zoldák, G. *et al.* (2007) Release factors 2 from *Escherichia coli* and *Thermus thermophilus*: structural, spectroscopic and microcalorimetric studies. *Nucleic Acids Res.* 35, 1343–1353
68. Ramadoss, N.S. *et al.* (2013) Small molecule inhibitors of trans-translation have broad-spectrum antibiotic activity. *Proc. Natl. Acad. Sci. U. S. A.* 110, 10282–10287
69. Alumasa, J.N. and Keller, K.C. (2015) Clicking on trans-translation drug targets. *Front. Microbiol.* 6, 498
70. Neubauer, C. *et al.* (2009) The structural basis for mRNA recognition and cleavage by the ribosome-dependent endonuclease RelE. *Cell* 139, 1084–1095
71. Crooks, G.E. *et al.* (2004) WebLogo: a sequence logo generator. *Genome Res.* 14, 1188–1190

Structural Basis for Polyproline-Mediated Ribosome Stalling and Rescue by the Translation Elongation Factor EF-P

Graphical Abstract



Authors

Paul Huter, Stefan Arenz,
Lars V. Bock, ..., Marina V. Rodnina,
Andrea C. Vaiana, Daniel N. Wilson

Correspondence

daniel.wilson@chemie.uni-hamburg.de

In Brief

Huter et al. present cryo-EM structures of polyproline-stalled ribosomes in the presence and absence of translation elongation factor EF-P. The structures reveal that polyproline sequences arrest translation by destabilizing the P-site tRNA, whereas binding of EF-P stabilizes the P-site tRNA and promotes a favorable geometry for peptide bond formation.

Highlights

- Polyproline-containing peptides stall translation by destabilizing the P-site tRNA
- Elongation factor EF-P recognizes the P-site tRNA and E-site mRNA codon
- The lysine modification of EF-P stabilizes the CCA end of the P-site tRNA
- EF-P promotes a favorable geometry of the P-site for peptide bond formation



Structural Basis for Polyproline-Mediated Ribosome Stalling and Rescue by the Translation Elongation Factor EF-P

Paul Huter,¹ Stefan Arenz,¹ Lars V. Bock,² Michael Graf,¹ Jan Ole Frister,³ Andre Heuer,¹ Lauri Peil,⁴ Agata L. Starosta,^{1,7} Ingo Wohlgemuth,³ Frank Peske,³ Jiří Nováček,⁵ Otto Berninghausen,¹ Helmut Grubmüller,² Tanel Tenson,⁴ Roland Beckmann,¹ Marina V. Rodnina,³ Andrea C. Vaiana,² and Daniel N. Wilson^{1,6,8,*}

¹Gene Center, Department for Biochemistry and Center for integrated Protein Science Munich (CiPSM), University of Munich, Feodor-Lynenstr. 25, 81377 Munich, Germany

²Department of Theoretical and Computational Biophysics, Max Planck Institute for Biophysical Chemistry, Am Fassberg 11, Göttingen 37077, Germany

³Department of Physical Biochemistry, Max Planck Institute for Biophysical Chemistry, Am Fassberg 11, 37077 Göttingen, Germany

⁴University of Tartu, Institute of Technology, Nooruse 1, 50411 Tartu, Estonia

⁵Central European Institute of Technology (CEITEC), Masaryk University, Kamenice 5, 62500 Brno, Czech Republic

⁶Institute for Biochemistry and Molecular Biology, University of Hamburg, Martin-Luther-King-Platz 6, 20146 Hamburg, Germany

⁷Present address: Centre for Bacterial Cell Biology, Institute for Cell and Molecular Biosciences, University of Newcastle, Newcastle upon Tyne NE2 4AX, UK

⁸Lead Contact

*Correspondence: daniel.wilson@chemie.uni-hamburg.de

<https://doi.org/10.1016/j.molcel.2017.10.014>

SUMMARY

Ribosomes synthesizing proteins containing consecutive proline residues become stalled and require rescue via the action of uniquely modified translation elongation factors, EF-P in bacteria, or archaeal/eukaryotic eIF5A. To date, no structures exist of EF-P or eIF5A in complex with translating ribosomes stalled at polyproline stretches, and thus structural insight into how EF-P/eIF5A rescue these arrested ribosomes has been lacking. Here we present cryo-EM structures of ribosomes stalled on proline stretches, without and with modified EF-P. The structures suggest that the favored conformation of the polyproline-containing nascent chain is incompatible with the peptide exit tunnel of the ribosome and leads to destabilization of the peptidyl-tRNA. Binding of EF-P stabilizes the P-site tRNA, particularly via interactions between its modification and the CCA end, thereby enforcing an alternative conformation of the polyproline-containing nascent chain, which allows a favorable substrate geometry for peptide bond formation.

INTRODUCTION

Ribosomes catalyze the synthesis of proteins in cells by providing a platform for the binding of tRNAs. There are three tRNA binding sites on the ribosome, the A, P, and E sites. During translation elongation, aminoacyl-tRNAs (aa-tRNAs) binding at the A site undergo peptide bond formation with the peptidyl-

tRNA located at the P site. The rate of peptide bond formation is influenced by the chemical nature of the amino acid substrates in both the A and P sites. Among other amino acids, proline is a particularly poor substrate both as donor and acceptor during peptide bond formation (Pavlov et al., 2009; Johansson et al., 2011; Muto and Ito, 2008; Wohlgemuth et al., 2008; Doerfel et al., 2013, 2015). In fact, ribosomes become stalled when synthesizing proteins containing consecutive proline residues (Doerfel et al., 2013; Ude et al., 2013; Woolstenhulme et al., 2013). To alleviate the ribosome stalling and allow translation to continue, a specialized translation factor is required, elongation factor P (EF-P) in bacteria or initiation factor 5A (IF5A) in archaea and eukaryotes (Doerfel et al., 2013; Ude et al., 2013; Gutierrez et al., 2013). IF5A has been shown to be essential in eukaryotes (Dever et al., 2014), and deletion of *efp* in some bacteria leads to growth defects and avirulence (Lassak et al., 2016).

Both EF-P and IF5A bear post-translational modifications that are essential for their rescue activity (Doerfel et al., 2013; Ude et al., 2013; Gutierrez et al., 2013; Peil et al., 2013). In *Escherichia coli*, lysine 34 (K34) of EF-P is post-translationally modified by the combined action of EpmA (YjeA), EpmB (YjeK), and EpmC (YfcM). EpmB converts (S)- α -lysine to (R)- β -lysine (Behshad et al., 2006), and EpmA ligates the (R)- β -lysine to the ϵ -amino group of K34 (Yanagisawa et al., 2010; Navarre et al., 2010). EpmC recognizes the modified form of EF-P and hydroxylates the C5(δ) of K34 (Peil et al., 2012); however, the hydroxylation is not required for the rescue activity of EF-P (Doerfel et al., 2013; Ude et al., 2013). Surprisingly, the resulting ϵ (R)- β -lysyl-hydroxylysine modification of *E. coli* EF-P and the enzymes associated with this modification are not conserved across all bacteria (Bailly and de Crécy-Lagard, 2010; Lassak et al., 2015). Instead, unrelated enzymes and/or modifications have been identified in other bacteria. In *Pseudomonas aeruginosa* and *Shewanella oneidensis*, EarP catalyzes the addition of

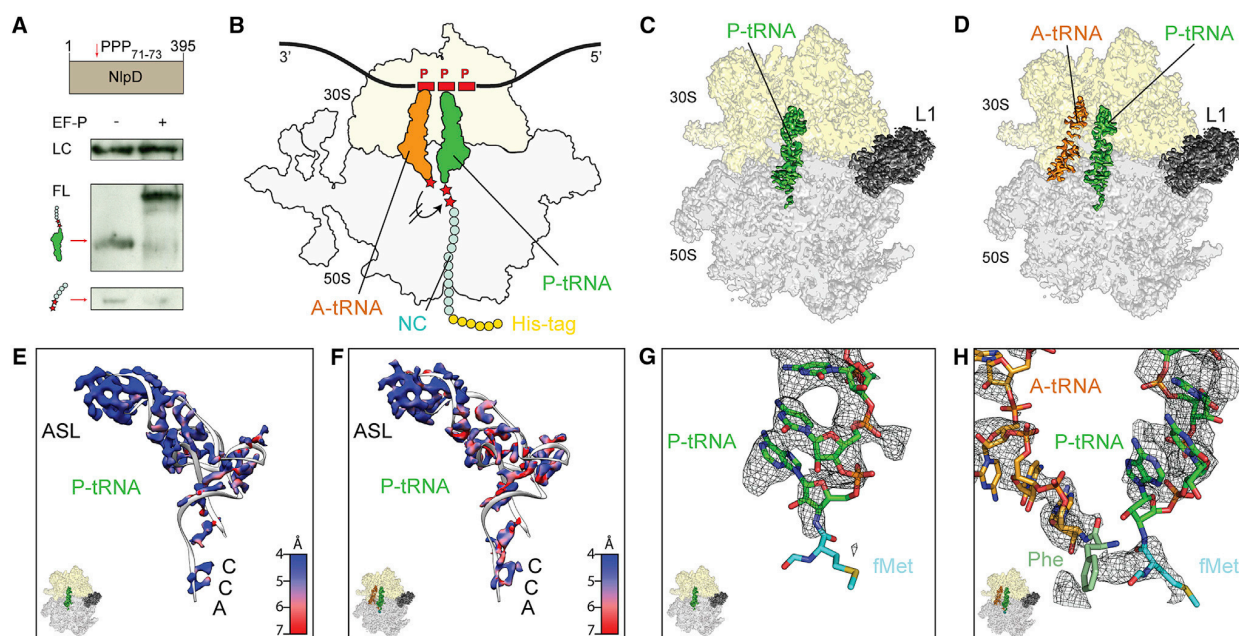


Figure 1. Cryo-EM Structures of Polyproline-Stalled Ribosomes in the Absence of EF-P

(A) Schematic representation of NlpD-PPP reporter protein (brown) with the site of the PPP-motif indicated. Western blot using an anti-HA-tag antibody of *in vitro* translation reactions of NlpD-PPP reporter in the absence (–) and presence (+) of EF-P. Full-length (FL), peptidyl-tRNA, and free peptide, as well as loading control (LC), are indicated.

(B–D) Schematic representation (B) and cryo-EM reconstructions (C and D) of PPP-stalled ribosome complexes formed in the absence of EF-P containing P-tRNA (C) or A- and P-tRNAs (D). The nascent chain (NC) has an N-terminal histidine tag (His-tag).

(E and F) Cryo-EM density at high threshold (7σ), colored according to the local resolution, for the P-site tRNA (gray ribbon) from cryo-EM maps in (C) containing P-tRNA (E) and in (D) containing A- and P-tRNAs (F), respectively.

(G) Cryo-EM density (mesh) of the CCA end of the P-site tRNA (green) from (C), with aligned fMet (cyan, PDB: 1VY4) (Polikanov et al., 2014) illustrating lack of density for nascent chain even at low thresholds (4σ).

(H) Cryo-EM density (mesh) of the CCA end of the A-site tRNA (orange) and P-site tRNA (green) from (D), with aligned Phe (green) and fMet (cyan, PDB: 1VY4) (Polikanov et al., 2014).

See also Figures S1 and S2.

rhamnose to arginine 32 (R32) of EF-P (Lassak et al., 2015; Rajkovic et al., 2015), whereas *Bacillus subtilis* is reported to bear a 5-aminopentanol moiety attached to K32 (Rajkovic et al., 2016). In eukaryotes, a conserved lysine residue is post-translationally modified to hypusine by the action of deoxyhypusine synthase (DHS) and deoxyhypusine hydroxylase (DOHH) (Dever et al., 2014; Lassak et al., 2016).

The structure of bacterial EF-P revealed a three-domain architecture, with the modified residue located at the tip of domain 1 (Hanawa-Suetsugu et al., 2004). eIF5A and aIF5A are homologous to bacterial EF-P domains 1 and 2 but lack the bacterial-specific domain 3 (Dever et al., 2014; Lassak et al., 2016). The X-ray structure of unmodified *Thermus thermophilus* EF-P in complex with *T. thermophilus* 70S ribosome bearing a deacylated tRNA^{fMet} at the P site revealed that EF-P binds within the E site of the ribosome with the unmodified arginine 32 (R32) of EF-P interacting with the CCA end of the P-site tRNA (Blaha et al., 2009). Similarly, structures of modified eIF5A on the yeast ribosome also visualized the hypusine modification extending into the peptidyltransferase center (PTC) of the ribosome (Melnikov et al., 2016b; Schmidt et al., 2016), where it interacts with the

CCA end of the P-site tRNA (Schmidt et al., 2016). However, to date, no structures exist of EF-P or eIF5A in complex with polyproline-stalled ribosomes; therefore, it remains unclear how the proline residues stall translation and how EF-P/eIF5A alleviates these stalled ribosomes.

RESULTS

Structure of a Polyproline-Stalled Ribosome Complex

To investigate how polyproline stretches cause translational arrest, we employed a previously used reporter mRNA coding for NlpD-PPP protein bearing three consecutive proline (₇₁PPP₇₃) residues (Starosta et al., 2014) (Figure 1A), which was translated in an *E. coli* lysate-based translation system derived from an *E. coli* *efp* deletion strain (see STAR Methods). As expected (Starosta et al., 2014), ribosomes with peptidyl-tRNA stalled at the PPP stretch could be alleviated by the exogenous addition of purified modified EF-P protein (Figure 1A). Previous biochemical studies (Doerfel et al., 2013; Ude et al., 2013; Woolstenhulme et al., 2013), as well as toeprinting assays using the same NlpD-PPP template (Starosta et al., 2014), indicate that

Table 1. Cryo-EM Data Collection, Refinement, and Validation Statistics

	#1 P-site tRNA only (EMDB: 3898, PDB: 6ENF)	#2 A- and P-site tRNA + EF-P (EMDB: 3899, PDB: 6ENJ)	#3 P-site tRNA + EF-P (EMDB: 3903, PDB: 6ENU)
Data Collection			
Microscope	FEI Titan Krios	FEI Titan Krios	FEI Titan Krios
Camera	Falcon II	Falcon II	Falcon II
Magnification	129,151	129,151	129,151
Voltage (kV)	300	300	300
Electron dose (e ⁻ /Å ²)	28	28	28
Defocus range (μm)	-0.8 to -2.5	-0.8 to -2.5	-0.8 to -2.5
Pixel size (Å)	1.084	1.084	1.084
Initial particles (no.)	229,613	229,613	229,455
Final particles (no.)	75,089	21,655	69,761
Model Composition			
Protein residues	5,531	5,951	5,944
RNA bases	4,547	4,693	4,613
Refinement			
Resolution range (Å)	3.3	3.9	3.2
Map CC (around atoms)	0.78	0.72	0.80
Map CC (whole unit cell)	0.76	0.75	0.75
FSC _{average}	0.85	0.85	0.85
Map sharpening B factor (Å ²)	-62,88	-66,61	-60,10
RMS Deviations			
Bond lengths (Å)	0.011	0.003	0.007
Bond angles (°)	0.729	0.594	0.932
Validation			
MolProbity score	1.77	1.64	1.77
Clashscore	4.29	3.44	4.11
Poor rotamers (%)	0	0.04	0.41
Ramachandran Plot			
Favored (%)	92.06	91.33	88.83
Allowed (%)	7.76	8.37	10.74
Disallowed (%)	0.18	0.31	0.43

ribosomes stall in the absence of EF-P because of slow peptide bond formation between the peptidyl-Pro-Pro-tRNA in the P site and the incoming Pro-tRNA in the A site (Figure 1B). These PPP-stalled ribosomes were purified using the 6x-Histidine tag located at the N terminus of the nascent peptide (Figure 1B) and subjected to cryo-electron microscopy (cryo-EM) analysis (see STAR Methods). *In silico* sorting of the cryo-EM images yielded two subpopulations of non-rotated ribosomes bearing a P-site tRNA but differing by the absence or presence of A-site tRNA (44% and 17%, respectively; Figure S1A). The cryo-EM structures were refined to yield average resolutions of 3.6 Å and 3.9 Å, respectively (Figures 1C and 1D; Figures S1B–S1E; Table 1). In addition, a large population (30%) of vacant ribosomes was observed, as well as a small population (9%) of 70S ribosomes in a rotated state lacking EF-P but containing hybrid A/P-site and P/E-site tRNAs (Figure S1A), the latter presumably representing a post-peptide bond formation state.

The density quality and resolution for the A-site and P-site tRNAs were generally poorer and less uniform than observed

in previous ribosomal complexes (Arenz et al., 2014a, 2014b, 2016a). In particular, the density was well resolved for the anticodon stem loop (ASL) of the tRNA on the 30S subunit and progressively deteriorated toward the elbow and acceptor arm of the tRNAs on the 50S subunit (Figures 1E and 1F; Figures S2A–S2G). In fact, density for the CCA end of the P- and A-site tRNAs at the PTC was only present at low thresholds (Figures 1G and 1H). Local resolution calculations also confirmed the flexible nature of the CCA end, particularly with respect to the terminal A76 nucleotide (Figures S2H–S2J). In the structure containing only P-site tRNA, no significant density was observed for the nascent polypeptide chain (Figure 1G), whereas in the structure with both A- and P-site tRNAs, the density attributable to the nascent chain was fragmented and disconnected from the tRNAs (Figure 1H). The density for the CCA end of the A-site tRNA was worse than the one of the P-site tRNA (Figure 1D; Figures S2D–S2G), suggesting that the Pro-tRNA had severe problems to accommodate at the A site of the PTC. Consistent with this notion, the N terminus of ribosomal protein L27, which

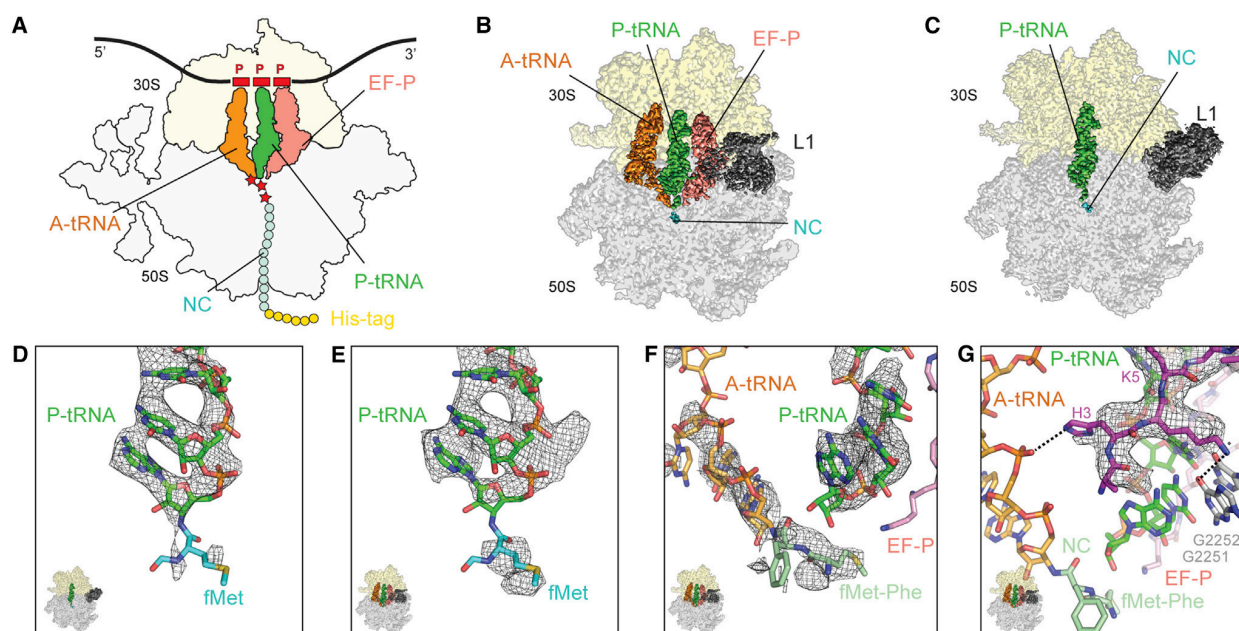


Figure 2. Cryo-EM Structures of Polyproline-Stalled Ribosomes in the Presence of EF-P

(A–C) Schematic representation (A) and cryo-EM reconstructions (B and C) of PPP-stalled ribosome complexes with (B) or without (C) of EF-P (salmon) bound in the E site.

(D and E) Cryo-EM density (mesh) of the CCA end of the P-site tRNA (green) from cryo-EM maps in (C) without EF-P (D) and in (B) with EF-P (E), respectively, with aligned fMet (cyan, PDB: 1VY4) (Polikanov et al., 2014).

(F) Cryo-EM density (mesh) of the CCA end of the A-site tRNA (orange) and P-site tRNA (green) from (B), with aligned fMet-Phe dipeptide (green, PDB: 1VY5) (Polikanov et al., 2014).

(G) Cryo-EM density (mesh) for the N-terminal residues of L27 (purple) showing possible interactions with residues G2251 and G2252 of the P loop (gray) and A-site tRNA (orange).

See also Figure S1.

becomes stabilized upon A-site tRNA accommodation (Polikanov et al., 2014; Voorhees et al., 2009), remained disordered (Figure S2K). Collectively, our findings suggest that the presence of the polyproline stretch within the nascent polypeptide chain leads to destabilization of the peptidyl-tRNA and prevents accommodation of the aa-tRNA at the A site, thereby causing translational stalling.

EF-P in Complex with PPP-Stalled Ribosomes

To investigate structurally how EF-P relieves the translation arrest caused by polyproline stretches, we incubated PPP-stalled ribosomes with fully modified *E. coli* EF-P (Figure 2A) and analyzed the resulting complexes by cryo-EM. *In silico* sorting of the cryo-EM data yielded two major subpopulations of ribosomes bearing P-site tRNA, distinguished by the presence (30%) or absence (33%) of EF-P (Figure S1F). The EF-P-containing subpopulation was extremely heterogeneous, and only a stable subpopulation containing A- and P-site tRNAs with EF-P bound in the E site (Figure 2B) could be refined further, yielding an average resolution of 3.7 Å (Figures S1G and S1H; Table 1). Despite multiple attempts, we were unable to obtain a clean subpopulation containing P-site tRNA and EF-P but lacking A-site tRNA. For completeness, we also refined the major P-site tRNA subpopulation lacking EF-P (Figure 2C) to an average

resolution of 3.2 Å (Figures S1I and S1J; Table 1). As before (Figure 1G), little density was observed for the nascent polypeptide chain attached to the P-site tRNA in the EF-P-lacking structure (Figure 2D) despite the improved quality of the density for the CCA end of the P-site tRNA. By contrast, additional nascent chain density was observed when EF-P was present (Figure 2E); however, this density fused directly to the A-site tRNA rather than the P-site tRNA (Figure 2F). Therefore, we concluded that the EF-P-containing subpopulation represents a post-peptide bond formation state with deacylated tRNA in the P site and peptidyl-tRNA in the A site. We also observe that the N terminus of L27 was ordered (Figure 2G), which, as mentioned, is diagnostic for accommodation of the aa-tRNA at the A site (Polikanov et al., 2014; Voorhees et al., 2009).

EF-P in Complex with PP-Stalled Ribosomes without the A-Site tRNA

In order to capture EF-P bound to polyproline-stalled ribosomes in a pre-peptide bond formation state, we employed a modified version of the NlpD-PPP mRNA that was truncated directly after the codon for the second proline of the PPP motif (Figure 3A). Ribosomes translating the truncated NlpD-PP mRNA become stalled after the PP motif because the absence of an A-site codon precludes binding of the next aa-tRNA; thus, the

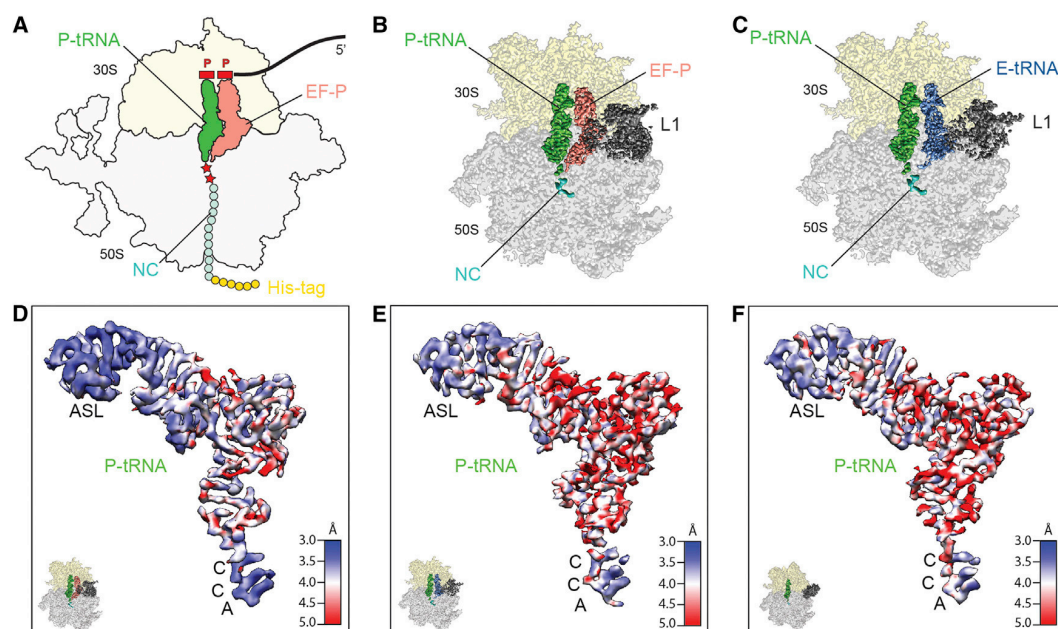


Figure 3. Stabilization of the P-Site Peptidyl-tRNA by EF-P

(A–C) Schematic representation (A) and cryo-EM reconstructions (B and C) of truncated NlpD-PP-stalled ribosomes in the presence (B) or absence (C) of EF-P (salmon).

(D–F) Cryo-EM densities colored according to local resolution for the P-site tRNAs from reconstructions illustrated in (B) and (C), respectively, (D and E) as well as from the reconstruction from Figure 2C (F).

See also Figure S1.

ribosomes cannot catalyze peptide bond formation even when EF-P is present (Figure 3A). The purified truncated NlpD-PP-stalled ribosomes were then incubated with active modified *E. coli* EF-P (Figure 3A), and the resulting complexes were analyzed by cryo-EM. *In silico* sorting of the cryo-EM data yielded two major subpopulations of ribosomes bearing either P- and E-site tRNAs (22%) or P-site tRNA with EF-P bound in the E site (74%) (Figure S1K). The EF-P-containing subpopulation could be further segregated into ribosome populations that differed with respect to the L1 stalk adopting an “in” (30%) or “out” (44%) conformation. The “in” position of the L1 stalk significantly improved the quality of the EF-P density, and therefore this population was further refined, yielding a final cryo-EM structure (Figure 3B) with an average resolution of 3.1 Å (Figures S1L and S1M; Table 1). Similarly, we could also refine the major P- and E-site tRNA-containing ribosome subpopulation that lacked EF-P (Figure 3C) to a final average resolution of 3.2 Å (Figures S1N and S1O). Local resolution calculations indicate less flexibility of the P-site tRNA in the presence of EF-P (Figure 3D) when compared to ribosomes bound with E-site tRNA (Figure 3E) or having a vacant E site (Figure 3F), thus supporting the hypothesis that EF-P stabilizes the P-site peptidyl-tRNA on the ribosome.

EF-P Residues Critical for P-Site tRNA Interaction

The well-resolved density for *E. coli* EF-P bound to the ribosome population with the L1 “in” conformation enabled a complete

molecular model to be generated (Figure 4A; Figure S3A). The overall conformation of *E. coli* EF-P on a polyproline-stalled ribosome is very similar to that observed by X-ray crystallography for *T. thermophilus* EF-P bound to a *T. thermophilus* 70S ribosome with a deacylated-tRNA^{Met} in the P site (Blaha et al., 2009), whereas it deviates more significantly from the binding position observed for the yeast homolog eIF5A bound to the 80S ribosome (Schmidt et al., 2016; Melnikov et al., 2016b) (Figures S3B and S3C). We observe that the backbone of Asp69 of *E. coli* EF-P is within hydrogen bonding distance of U17a within the D-loop of the peptidyl-tRNA^{Pro} in the P site (Figure S13D). This interaction is also observed in the *T. thermophilus* EF-P-ribosome structure (Blaha et al., 2009) (Figure S3E) but is not possible for tRNAs containing shorter D-loops (Figure S3F), thus providing a specificity determinant for EF-P to recognize tRNA^{Met} and tRNA^{Pro} (Katoh et al., 2016) (Figures S3D and S3E). By contrast, such a specific interaction between yeast eIF5A and the P-site tRNA was not observed (Schmidt et al., 2016; Melnikov et al., 2016b), consistent with the diverse range of non-proline-containing stalling motifs that are recognized and rescued by eIF5A (Schuller et al., 2017; Pelechano and Alepuz, 2017).

Unlike eIF5A, bacterial EF-P has an additional domain 3 that contacts the small ribosomal subunit and the ASL of the P-site tRNA (Figure 4B). In particular, two conserved residues Tyr183 and Arg186 are within hydrogen bonding distance of A42 of the P-site tRNA and G1338 within helix h29 of the 16S rRNA

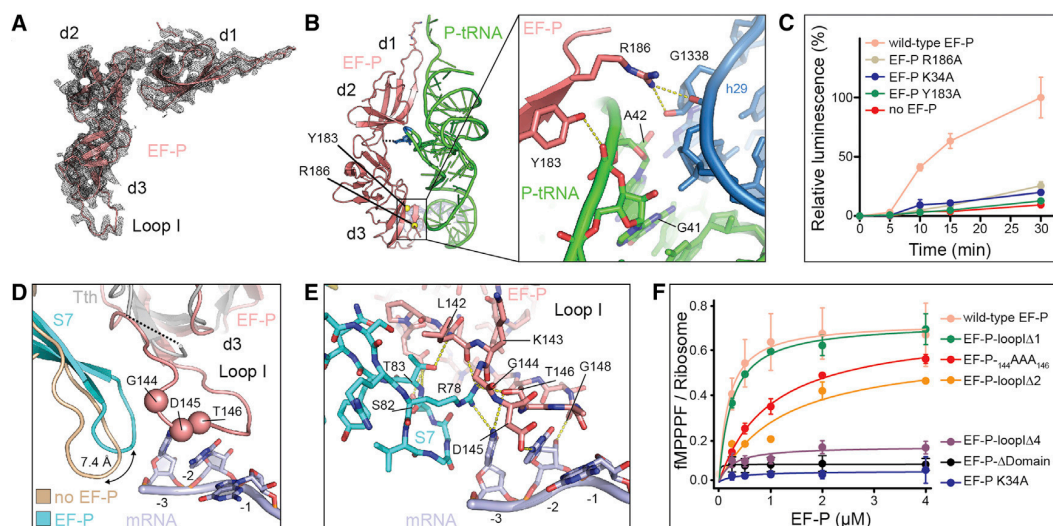


Figure 4. Interaction of EF-P with the P-Site tRNA

(A) Cryo-EM density (mesh) with molecular model for EF-P (salmon ribbon) with domains 1–3 (d1–d3) indicated.

(B) Overview of EF-P relative to P-site-bound tRNA^{Pro} (green) with a zoom on the interactions between Y183 and R186 of EF-P and their respective interaction partners of tRNA^{Pro} and h29 (blue) of the 30S subunit.

(C) Luminescence resulting from *in vitro* translated Fluc-3xPro was monitored over time and quantified in the absence of EF-P (red) or in the presence of wild-type EF-P (pink) or indicated EF-P variants. 100% luminescence is defined as the luminescence produced by Fluc-3xPro after a 30-min incubation in the presence of wild-type EF-P. Error bars represent the standard deviation of three independent experiments.

(D) Location of EF-P d3 loop I relative to peptidyl-tRNA^{Pro} (green) in the P site, mRNA (light blue), and ribosomal protein S7 (cyan), with the position of the loop of S7 in the absence of EF-P (tan) indicated for reference. The relative position of *T. thermophilus* EF-P (Blaha et al., 2009) (gray) is shown with the disordered region of d3 loop of EF-P indicated (dashed line). The positions of the conserved residues within the ₁₄₄GDT₁₄₆ motif within loop I of EF-P are indicated by spheres.

(E) Potential hydrogen-bond interactions (dashed yellow lines) between Loop I of EF-P (salmon), the E-site codon (blue), and S7 (cyan).

(F) Synthesis of the fMPPPF peptide as a function of EF-P concentration in the presence of wild-type EF-P (pink) or various EF-P variants. In the absence of EF-P, 0.06 ± 0.01 fMPPPF peptide were formed per ribosome. Error bars represent the standard deviation of three independent experiments. See also Figures S3–S5.

(Blaha et al., 2009) (Figure 4B). To investigate the importance of these interactions, we generated modified EF-P variants bearing Y183A or R186A substitutions and monitored their ability to promote translation of a polyproline-containing firefly luciferase (Fluc) reporter protein (Ude et al., 2013) (Figure 4C). In the absence of EF-P, ribosomes stall at the polyproline motif and little or no luminescence is observed because translation of full-length Fluc is prevented. As expected, addition of modified wild-type EF-P rescues the polyproline-stalled ribosomes, leading to production of full-length Fluc and a corresponding increase in luminescence (Figure 4C). By contrast, the EF-P-Y183A and EF-P-R186A variants were both completely inactive, as was the previously reported inactive EF-P-K34A variant (Ude et al., 2013). These findings demonstrate that the Tyr183 and Arg186 residues are critical for the rescue activity of EF-P and explain their high conservation among bacterial EF-P proteins.

Interaction of EF-P with the mRNA Codon in the E Site

In the X-ray structure of *T. thermophilus* EF-P-ribosome structure, loop I of domain 3 of EF-P is disordered (Blaha et al., 2009) (Figure 4D). By contrast, loop I is well resolved in the cryo-EM structure of *E. coli* EF-P in complex with the PP-stalled ribosome (Figure 4A; Figures S4A and S4B), where it interacts with the ribosomal protein S7 and E-site codon of the mRNA

(Figures 4D and 4E). Binding of EF-P to the ribosome leads to a shift in conformation of the β -hairpin of S7 by 7.4 Å (Figure 4D), which is stabilized via potential hydrogen bond interactions between the sidechain of Arg78 of S7 and the backbone of Gly144 as well as the sidechain of T146 of EF-P (Figure 4E). Additional interactions are formed between S7 (Thr83 and Ser82) and EF-P (the backbone of Leu142 and the side chain of Asp139) (Figure 4E; Figures S4C and S4D). Loop I of domain 3 of EF-P contains a highly conserved Gly144-Asp145-Thr146 (GDT) motif, which establishes contact with the nucleobase of the first and second positions of the E-site codon of the mRNA (Figures 4D and 4E; Figures S4E and S4F). To assess the importance of the GDT motif for EF-P activity, we generated modified EF-P bearing a triple substitution of GDT to AAA (EF-P-₁₄₄AAA₁₄₆). Since most of the interactions involve the backbone of the GDT motif, we also generated EF-P variants where 1, 2, or 4 residues within loop I were deleted (EF-P-loopI Δ 1, -loopI Δ 2, and -loopI Δ 4, respectively). The activity of the EF-P variants was assessed by monitoring the formation of fMPPPF peptide on the ribosome, as described previously (Doerfel et al., 2013, 2015). As seen in Figure 4F, no fMPPPF peptide was synthesized when the inactive EF-P-K34A variant was used (or when EF-P was absent, see legend to Figure 4), whereas the presence of wild-type EF-P led to efficient fMPPPF peptide formation.

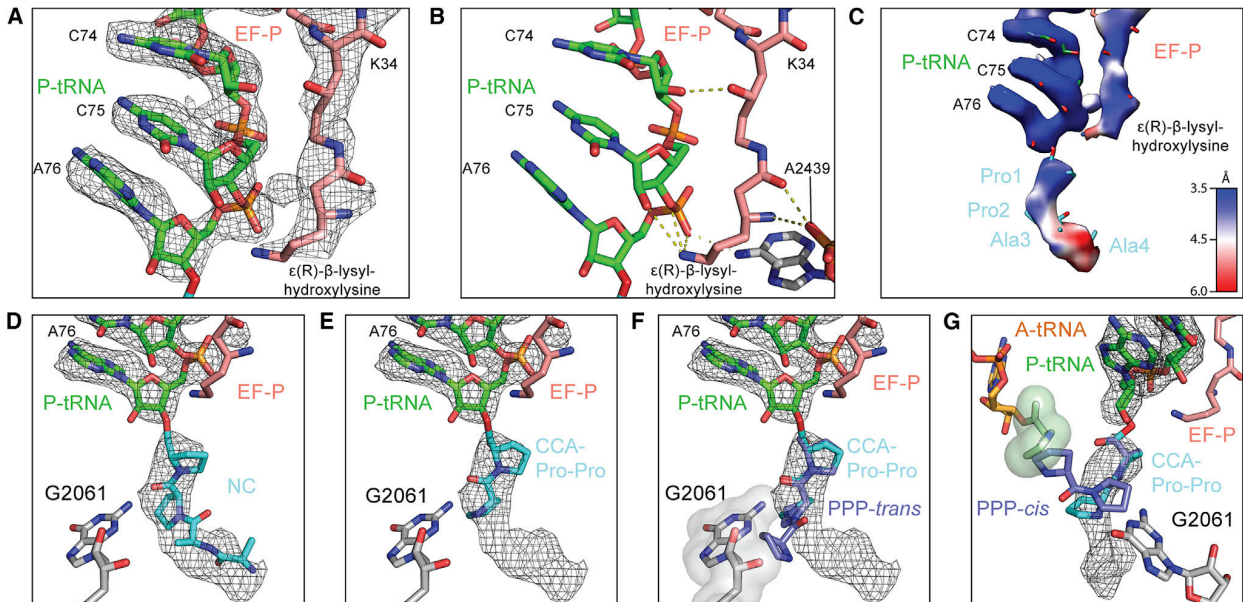


Figure 5. EF-P Stabilizes the PP-Containing Nascent Chain

(A) Cryo-EM density (gray mesh) for the CCA end of the P-site tRNA (green) and $\epsilon(\text{R})$ - β -lysyl-hydroxylysine modification of EF-P (salmon).

(B) Same as (A), but without cryo-EM density, and potential hydrogen bond interactions (dashed lines) between the $\epsilon(\text{R})$ - β -lysyl-hydroxylysine modification, P-site tRNA (green), and A2439 (gray) are indicated.

(C) Cryo-EM density colored according to the local resolution for the CCA end of the P-site tRNA, $\epsilon(\text{R})$ - β -lysyl-hydroxylysine modification of EF-P, and the modeled nascent chain (Pro1-Pro2-Ala3-Ala4).

(D–G) Cryo-EM density (mesh) for the P-site tRNA with the first four residues of the modeled nascent chain (NC) Pro1-Pro2-Ala3-Ala4 (cyan) (D), all-*trans* Pro-Pro conformation of CCA-Pro-Pro tRNA mimic in complex with yeast 80S ribosome (PDB: 5DGV) (Melnikov et al., 2016a) (E), three prolines of a polyproline type II (P_{II}) helix (PP-*trans*) modeled onto the CCA end of the P-site tRNA, with G2061 shown as a surface to better illustrate the steric clash with the PP-*trans* nascent chain (F), and three prolines of a polyproline type I (P_I) helix (PP-*cis*) modeled onto CCA end of the P-site tRNA (G), showing a potential clash with a Pro residue (light green surface) attached to the A-site tRNA (orange).

See also Figure S6.

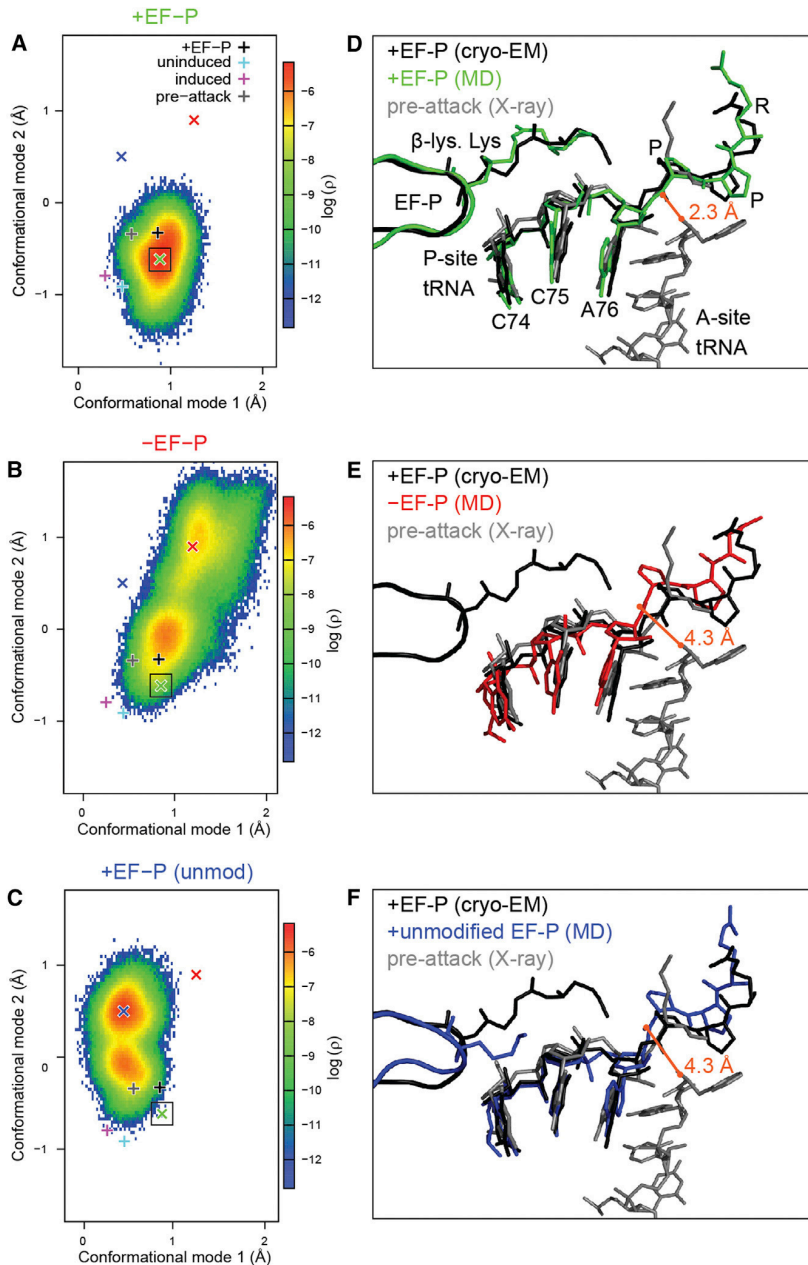
While the EF-P-loopI Δ 1 retained wild-type-like activity, the EF-P-₁₄₄AAA₁₄₆ and EF-P-loopI Δ 2 variants displayed reduced activity, and the EF-P-loopI Δ 4 variant was completely inactive (Figure 4F). Furthermore, an EF-P variant with the complete domain 3 deleted (EF-P- Δ Domain 3) was also inactive (Figure 4F).

These results suggest that the conserved loop I of domain 3 of EF-P is critical for the rescue activity of EF-P and raises the possibility that EF-P recognizes the nature of the E-site codon, analogous to stop codon recognition by the SPF and PXT containing loops of termination factors RF2 and RF1, respectively (Zhou et al., 2012). Modeling on the basis of our structure suggests that purines in the first and second position, such as AAA or GGG codons, in the E site lead to clashes with EF-P, whereas UUU could be accommodated but in a less stable manner (Figures S5A–S5D). In the X-ray structure of *T. thermophilus* EF-P-ribosome structure, the E-site codon was AAA (Blaha et al., 2009) (Figures S5E and S5F), possibly explaining why loop I of domain 3 of EF-P was disordered. Moreover, the –3 nucleotide was also not visualized, supporting the suggestion that EF-P is critical for positioning and stabilization of the E-site codon (Figures S5E and S5F). Further biochemical experiments will be necessary to assess whether loop I of EF-P can really distinguish

CCN proline codons in the E site from other sense codons. The absence of domain 3 in eIF5A does, however, preclude recognition of the nature of the E-site codon, which may contribute to the relaxed specificity of eIF5A, allowing eIF5A to also act on a diverse range of non-proline containing stalling motifs (Schuller et al., 2017; Pelechano and Alepuz, 2017).

Stabilization of the CCA End of the P-Site tRNA by the EF-P Modification

Clear electron density is observed at the tip of domain 1 of EF-P that corresponds to the $\epsilon(\text{R})$ - β -lysylhydroxylysine located at position K34 of EF-P (Figures 5A and 5B). The post-translational modification extends into a crevice located adjacent to the CCA end of the P-site tRNA (Figures 5A and 5B), similar but distinct from that observed previously for the unmodified R32 residues of *T. thermophilus* EF-P (Blaha et al., 2009), and the hypusine modification located at position K51 of yeast eIF5A (Schmidt et al., 2016; Melnikov et al., 2016b) (Figures S3G–S3I). The structure reveals how the EF-P modification can stabilize the P-site tRNA (Figure 5C) by forming interactions with the backbone of the CCA end (Figure 5B). Specifically, hydrogen bonds are possible between the ϵ -amino group of the (R)-lysyl moiety of EF-P and the 2' OH of the ribose of C75 and the bridging oxygen



of A76 (Figure 5B). Furthermore, the hydroxyl group that is post-translationally added to K34 of EF-P by EpmC (Peil et al., 2012) comes within hydrogen binding distance of the 2' OH of C74, but this interaction is unlikely to be critical since EF-P lacking the hydroxylation retains rescue activity (Doerfel et al., 2013; Ude et al., 2013; Peil et al., 2013). In addition, the EF-P modification can form hydrogen bonds with the conserved nucleotide A2439 of the 23S rRNA (Figure 5B), analogous to those formed between eIF5A and A2808 (Schmidt et al., 2016; Melnikov et al., 2016b), the equivalent residue in the yeast 28S rRNA (Figure S3I).

tentatively modeled into the density (Figure 5D). To compare the C-terminal Pro-Pro residues in our structure to other conformations of Pro-Pro peptides, we initially aligned the X-ray structure of a short CCA-Pro-Pro tRNA mimic bound to the yeast 80S ribosome (Melnikov et al., 2016a) (Figure 5E). These two proline residues adopt an all-*trans* conformation, which is present in type II polyproline helices (Figure 5F) and also observed in other diprolyl-containing proteins, such as ribosomal proteins S11 and L11 (Fischer et al., 2015), and the ribosome-bound antimicrobial peptide Onc112 (Seefeldt et al., 2015; Roy et al., 2015)

Figure 6. MD Simulations of Polyproline-Stalled Ribosomes in the Presence and Absence of EF-P

(A–C) Conformational landscape explored by MD simulations with EF-P (A), without EF-P (B), or with unmodified EF-P (C). The logarithm of the probability density ρ is shown along the two most dominant conformational modes of the CCA end and the C-terminal proline backbone atoms. Probability density maxima are indicated by crosses, green (simulations with EF-P, additionally marked with a square), red (without EF-P), and blue (unmodified EF-P). For comparison, plus signs (+) indicate the projections of our cryo-EM derived structure (black), the pre-attack state (Polikanov et al., 2014) (gray), and the uninduced and the induced states (Schmeing et al., 2005) (cyan and magenta, respectively).

(D–F) Conformations of P-site tRNA with peptide and EF-P corresponding to the density maxima obtained from MD simulations with EF-P (D; green), without EF-P (E; red) and with unmodified EF-P (F; blue). The cryo-EM structure with EF-P (black) and the pre-attack (Polikanov et al., 2014) (gray) conformation are shown for comparison. Distance between the ester carbonyl carbon of the peptidyl-tRNA and the α -amino group of the aa-tRNA is indicated in orange. See also Figure S7.

By contrast, the overall position and interactions of the modified K34 residue of *E. coli* EF-P differs dramatically from that of the unmodified R32 residues of *T. thermophilus* EF-P (Blaha et al., 2009), which is significantly shorter and interacts only with the nucleobase of C75 of the P-site tRNA (Figure S3H).

The Conformation of the Nascent Chain in the Presence of EF-P

The presence of additional density for the nascent polypeptide chain attached to the P-site tRNA (Figures 5C and 5D) suggests that by stabilizing the P-site tRNA, EF-P also indirectly stabilizes the nascent chain. Nevertheless, local resolution calculations indicate that the nascent chain is still relatively flexible (Figure 5C), permitting only the four C-terminal residues to be

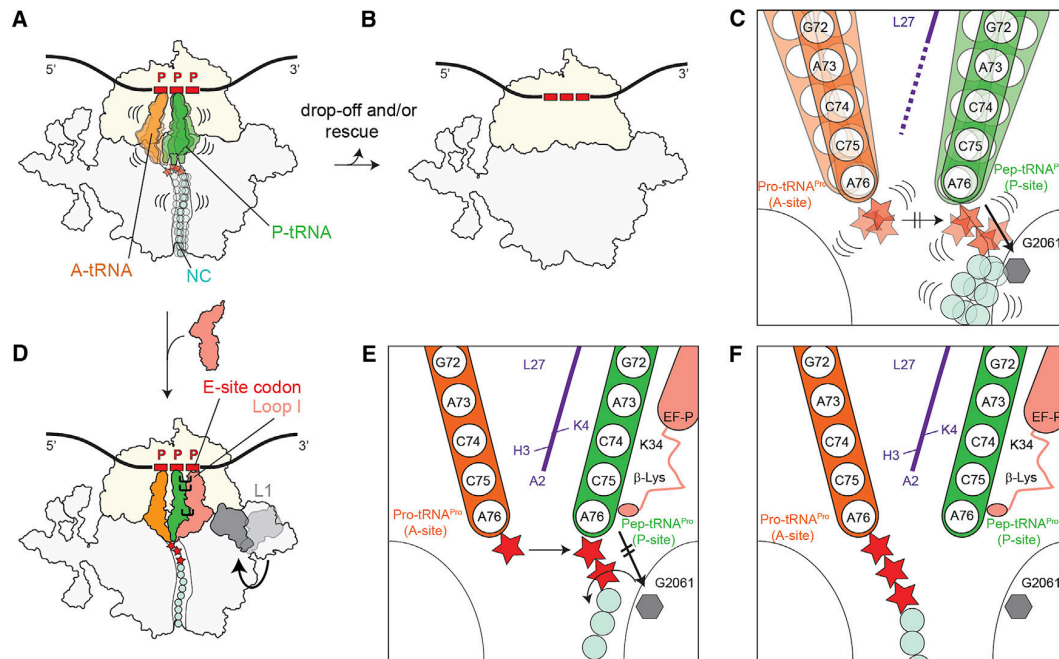


Figure 7. Mechanism of Action of EF-P on Polyproline-Stalled Ribosomes

(A and B) Ribosomes stall during translation of proteins containing three consecutive prolines (Doerfel et al., 2013; Ude et al., 2013) leading to destabilization of the peptidyl-tRNA in the P site (A), which leads to peptidyl-tRNA drop-off, particular with short peptidyl-tRNAs (Doerfel et al., 2013) (B).

(C) The all-*trans* or all-*cis* conformation of polyprolines (red stars) of the nascent chain is not possible because of a steric clash with G2061 (gray) within the tunnel wall, leading to peptidyl-tRNA destabilization and thus preventing accommodation of the A-site tRNA and peptide bond formation.

(D) Ribosomes stalled on polyproline stretches are recognized by EF-P, which binds within the E-site region and stabilizes the peptidyl-tRNA. EF-P binding is facilitated via contacts with the L1 stalk (Blaha et al., 2009) and the P-site tRNA (Katoh et al., 2016) as well as E-site codon.

(E) Interaction of the ϵ (R)- β -lyl-hydroxylysine with the CCA end of P-site tRNA^{Pro} stabilizes the P-site tRNA, as well as the nascent chain, by forcing the prolines to adopt an alternative conformation that passes into the ribosomal exit tunnel.

(F) Thus, an optimal geometry between the nascent chain and the aminoacyl-tRNA in the A site is achieved and peptide bond formation can occur.

(Figures S6A–S6C). However, this conformation cannot occur on the ribosome because it would produce a steric clash between the –2 residue of the nascent chain and nucleotide G2061 of the 23S rRNA that comprises part of the ribosomal exit tunnel (Figure 5F; Figures S6A–S6C). Similarly, an all-*cis* conformation of the two prolyl residues is compatible neither with the density nor with translation, since it directs the nascent chain into the ribosomal A site (Figure 5G). Instead, the diprolyl moiety appears to adopt an alternative *trans*-conformation, allowing the –2 residue of the nascent chain to bypass G2061 and extend into the lumen of the ribosomal exit tunnel (Figure 5D). Although higher resolution will be required to accurately describe the *trans*-conformation in detail, our model suggests that the backbone Psi angle of $\sim 120^\circ$ is identical with the all-*trans* conformation, but the Phi angle of approximately -90° differs by $\sim 30^\circ$ from the all-*trans* Phi angle (-60°). Although the structure represents a “rescued state,” the alternative conformation appears to be similar to that observed on a ribosome stalled by the diprolyl-containing, CMV-stalling peptidyl-tRNA (Matheisel et al., 2015) (Figure S6D), and the overall path of the nascent chain is similar to that observed for other stalling nascent polypeptide chains observed on the ribosome, such as TnaC (Bischoff et al., 2014), VemP (Su et al., 2017), MifM (Sohmen et al., 2015), and SecM (Zhang et al., 2015) (Figures S6E and S6F).

We note that when the rigid five-membered proline ring is replaced with a more flexible four-membered ring, such as in azetidine-2-carboxylic, ribosome stalling was reduced (Doerfel et al., 2015; Shin et al., 2017), possibly indicating that the additional freedom of the azetidine-2-carboxylic allows alternative conformations to be adopted more easily that do not sterically clash with G2061. In summary, we suggest that the incompatibility between the preferred diprolyl conformation of the nascent chain and the ribosome induces a strained conformation that can be relieved either by (1) destabilization of the P-site peptidyl-tRNA and therefore ribosomal stalling ensues or (2) binding of EF-P that stabilizes the P-site peptidyl-tRNA and forces the nascent chain to adopt an alternative conformation, with the outcome that peptide bond formation can occur.

EF-P Stabilizes the P-Site tRNA in a Pre-attack Conformation

To assess the dynamics of the region surrounding the PTC in the presence of modified EF-P or unmodified EF-P or the absence of EF-P, we carried out all-atom explicit-solvent molecular dynamics (MD) simulations. The first MD simulation was initiated using the model of the cryo-EM structure of the NlpD-PP-EF-P-ribosome, and two subsequent simulations were performed

where either the β -lysine part of modification on K34 or the entire EF-P protein were computationally removed. A total of 15 simulations, 2 μ s each, accumulating to a total simulation run time of 30 μ s were performed using a reduced system encompassing a 35 Å radius from the PTC. Principal-component analysis (PCA) (Amadei et al., 1993) was used to extract the two most dominant conformational modes of motion. As shown in Figure 6A, in the presence of modified EF-P, the major conformations are stable and remain close to the cryo-EM structure, which is similar to that observed in the X-ray structures of the *T. thermophilus* pre-attack conformation (Polikanov et al., 2014) as well as uninduced and induced conformations from *H. marismortui* (Schmeing et al., 2005). By contrast, after the β -lysine modification of EF-P or the complete EF-P protein was removed from the simulation, the system explored new conformations, moving away from the conformations observed in presence of EF-P, particularly with respect to conformational mode 2 (Figure 6C). Since conformational mode 2 reflects the relative distance between the α -amino group of an aminoacyl-tRNA in the A site and the carbonyl-carbon of the aminoacyl ester linkage in the peptidyl-Pro-Pro-tRNA (Figure S7), the MD simulations suggest that when the EF-P modification or the entire EF-P protein was absent, the peptidyl-tRNA moved away from the A-site tRNA, generating a geometry that is incompatible with peptide bond formation (Figures 6E and 6F). By contrast, the presence of the EF-P modification stabilized the pre-attack conformation of the P-site tRNA, thus promoting peptide bond formation (Figure 6D).

DISCUSSION

Collectively, our biochemical and structural findings, together with the available literature, lead us to propose a model for polyproline-mediated translational stalling and rescue by EF-P (Figure 7). Ribosomes translating proteins containing polyproline-stretches become stalled because of slow peptide bond formation between the peptidyl-Pro-Pro-tRNA in the P site and the incoming Pro-tRNA in the A site (Doerfel et al., 2013) (Figure 7A). The favorable all-*trans* conformation of the Pro-Pro peptide is not possible within the context of the ribosomal tunnel, which leads to destabilization of the P-site tRNA and nascent chain (Figure 7B). For short oligo-peptidyl-tRNAs, this results in high levels of peptidyl-tRNA drop-off (Doerfel et al., 2013, 2015). For longer peptidyl-tRNAs that are more refractory to drop-off, the destabilized peptidyl-tRNA results in suboptimal positioning for peptide bond formation and may also disfavor accommodation of the aminoacyl-tRNA at the A site (Figure 7B). Additionally, the destabilized peptidyl-tRNAs may be more susceptible to peptide release and/or ribosome rescue systems (Figures 7A and 7B), which may explain the unusually high proportion (30%) of vacant 70S ribosomes that were present in the PPP-stalled ribosome sample following purification (Figure S1A). Polyproline-stalled ribosomes are recognized by EF-P, which utilizes features of the E site codon of the mRNA, as well as specific interactions with D-loop of the P-site Pro-tRNA (Kato et al., 2016), the L1 stalk, and the 30S subunit to promote binding (Blaha et al., 2009) (Figure 7C). While the presence of EF-P generally stabilizes the binding of the P-site tRNA, the ϵ (R)- β -lysylhydroxylysine is necessary to specifically interact and stabilize the CCA end at

the PTC (Figure 7D). Stabilization of the CCA end by the ϵ (R)- β -lysylhydroxylysine modification of EF-P also positions the nascent polypeptide chain such that it extends into the lumen of the tunnel (Figure 7E), thus allowing the CCA ends of the tRNAs to adopt the conformation that favors peptide bond formation (Figure 7F). These findings provide a structural rationale for the entropic steering effect of EF-P on peptide bond formation (Doerfel et al., 2015). It will be interesting to see how the distinct modifications found on EF-P in other bacteria, such as the rhamnosylation found in *P. aeruginosa* EF-P (Lassak et al., 2015; Rajkovic et al., 2015) or the 5-aminopentanol moiety of *B. subtilis* EF-P (Rajkovic et al., 2016), stabilize the CCA end of the P-site tRNA to promote an optimal geometry for peptide bond formation. Moreover, although it remains to be determined as to what promotes EF-P dissociation from the ribosome following peptide bond formation, our structure suggests that subunit rotation and opening of the L1 stalk are good candidates for destabilization of EF-P binding.

STAR★METHODS

Detailed methods are provided in the online version of this paper and include the following:

- KEY RESOURCES TABLE
- CONTACT FOR REAGENT AND RESOURCE SHARING
- EXPERIMENTAL MODEL AND SUBJECT DETAILS
 - *E. coli* Strain and Growth Conditions
- METHODS DETAILS
 - Preparation of the *E. coli* Δ efp S12 Translation Extract
 - PCR and *In Vitro* Transcription
 - Preparation of Full-Length NlpD-PPP-SRC and Truncated NlpD-PP-SRC
 - Purification of the NlpD-PPP-SRC and Truncated NlpD-PP-SRC
 - Cryogrid Preparation for the NlpD-PPP-SRC and NlpD-PP-SRC
 - Generation and Purification of Modified EF-P and Mutants
 - Luminescence Determination of Firefly Luciferase
 - Ribosome Complexes for Kinetic Experiments
 - *In Vitro* Translation of fMPPPF Model Peptide
 - Molecular Dynamics Simulations
 - Conformational Landscape of CCA End and C-Terminal Proline
 - Cryo-electron Microscopy and Single Particle Reconstruction
 - Molecular Modeling and Map-Docking Procedures
 - Figure Preparation
- QUANTIFICATION AND STATISTICAL ANALYSIS
 - Cryo-EM Data Analysis
- DATA AND SOFTWARE AVAILABILITY
 - Accession Numbers

SUPPLEMENTAL INFORMATION

Supplemental Information includes seven figures and can be found with this article online at <https://doi.org/10.1016/j.molcel.2017.10.014>.

AUTHOR CONTRIBUTIONS

D.N.W. designed the study. P.H. prepared the cryo-EM samples. O.B., R.B., and J.N. collected the cryo-EM data. P.H., S.A., M.G., and A.H. processed the cryo-EM data. P.H. and S.A. built and refined the molecular models. P.H. performed Fluc assays. M.G., P.H., L.P., A.L.S., and T.T. prepared active EF-P proteins. J.O.F., I.W., F.P., and M.V.R. performed peptide synthesis assays. L.V.B., H.G., and A.C.V. performed and analyzed molecular dynamic simulations. P.H., S.A., R.B., and D.N.W. analyzed the cryo-EM data. P.H. and D.N.W. prepared the figures and wrote the paper with help from I.W., L.V.B., A.C.V., and M.V.R.

ACKNOWLEDGMENTS

We thank Susanne Rieder and Olaf Geintzer for expert technical assistance and Bertrand Beckert for helpful comments. The proteomics facility at University of Tartu is supported by the European Regional Development Fund through the Centre of Excellence for Molecular Cell Engineering. This work has been supported by iNEXT, project number 1503, funded by the Horizon 2020 programme of the European Union. This article reflects only the author's view and the European Commission is not responsible for any use that may be made of the information it contains. CIISB research infrastructure project LM2015043 funded by MEYS CR is gratefully acknowledged for the financial support of the measurements at the CF Cryo-electron Microscopy and Tomography CEITEC MU. This research was supported by grants of the Forschergruppe FOR1805 (to A.C.V., D.N.W., H.G., I.W., L.V.B., M.V.R., and R.B.), WI3285/4-1 (to D.N.W.), and GRK1721 from the Deutsche Forschungsgemeinschaft (DFG).

Received: August 23, 2017
 Revised: September 29, 2017
 Accepted: October 11, 2017
 Published: November 2, 2017

REFERENCES

- Adams, P.D., Afonine, P.V., Bunkóczy, G., Chen, V.B., Davis, I.W., Echols, N., Headd, J.J., Hung, L.W., Kapral, G.J., Grosse-Kunstleve, R.W., et al. (2010). PHENIX: a comprehensive Python-based system for macromolecular structure solution. *Acta Crystallogr. D Biol. Crystallogr.* **66**, 213–221.
- Aduří, R., Psiciuk, B.T., Saro, P., Taniga, H., Schlegel, H.B., and SantaLucia, J. (2007). AMBER force field parameters for the naturally occurring modified nucleosides in RNA. *J. Chem. Theory Comput.* **3**, 1464–1475.
- Amadei, A., Linssen, A.B., and Berendsen, H.J. (1993). Essential dynamics of proteins. *Proteins* **17**, 412–425.
- Arenz, S., Meydan, S., Starosta, A.L., Berninghausen, O., Beckmann, R., Vázquez-Laslop, N., and Wilson, D.N. (2014a). Drug sensing by the ribosome induces translational arrest via active site perturbation. *Mol. Cell* **56**, 446–452.
- Arenz, S., Ramu, H., Gupta, P., Berninghausen, O., Beckmann, R., Vázquez-Laslop, N., Mankin, A.S., and Wilson, D.N. (2014b). Molecular basis for erythromycin-dependent ribosome stalling during translation of the ErmBL leader peptide. *Nat. Commun.* **5**, 3501.
- Arenz, S., Bock, L.V., Graf, M., Innis, C.A., Beckmann, R., Grubmüller, H., Vaiana, A.C., and Wilson, D.N. (2016a). A combined cryo-EM and molecular dynamics approach reveals the mechanism of ErmBL-mediated translation arrest. *Nat. Commun.* **7**, 12026.
- Arenz, S., Juette, M.F., Graf, M., Nguyen, F., Huter, P., Polikanov, Y.S., Blanchard, S.C., and Wilson, D.N. (2016b). Structures of the orthosomycin antibiotics avilamycin and evermicin in complex with the bacterial 70S ribosome. *Proc. Natl. Acad. Sci. USA* **113**, 7527–7532.
- Bailly, M., and de Crécy-Lagard, V. (2010). Predicting the pathway involved in post-translational modification of elongation factor P in a subset of bacterial species. *Biol. Direct* **5**, 3.
- Behshad, E., Ruzicka, F.J., Mansoorabadi, S.O., Chen, D., Reed, G.H., and Frey, P.A. (2006). Enantiomeric free radicals and enzymatic control of stereochemistry in a radical mechanism: the case of lysine 2,3-aminomutases. *Biochemistry* **45**, 12639–12646.
- Berendsen, H.J.C., Postma, J.P.M., Van Gunsteren, W.F., Dinola, A., and Haak, J.R. (1984). Molecular dynamics with coupling to an external bath. *J. Chem. Phys.* **81**, 3684.
- Berendsen, H.J.C., Grigera, J.R., and Straatsma, T.P. (1987). The missing term in effective pair potentials. *J. Phys. Chem.* **91**, 6269–6271.
- Bischoff, L., Berninghausen, O., and Beckmann, R. (2014). Molecular basis for the ribosome functioning as an L-tryptophan sensor. *Cell Rep.* **9**, 469–475.
- Blaha, G., Stanley, R.E., and Steitz, T.A. (2009). Formation of the first peptide bond: the structure of EF-P bound to the 70S ribosome. *Science* **325**, 966–970.
- Bock, L.V., Blau, C., Schröder, G.F., Davydov, I.I., Fischer, N., Stark, H., Rodnina, M.V., Vaiana, A.C., and Grubmüller, H. (2013). Energy barriers and driving forces in tRNA translocation through the ribosome. *Nat. Struct. Mol. Biol.* **20**, 1390–1396.
- Brown, A., Long, F., Nicholls, R.A., Toots, J., Emsley, P., and Murshudov, G. (2015). Tools for macromolecular model building and refinement into electron cryo-microscopy reconstructions. *Acta Crystallogr. D Biol. Crystallogr.* **71**, 136–153.
- Bussi, G., Donadio, D., and Parrinello, M. (2007). Canonical sampling through velocity rescaling. *J. Chem. Phys.* **126**, 014101.
- Chen, J.Z., and Grigorieff, N. (2007). SIGNATURE: a single-particle selection system for molecular electron microscopy. *J. Struct. Biol.* **157**, 168–173.
- Chen, V.B., Arendall, W.B., 3rd, Headd, J.J., Keedy, D.A., Immormino, R.M., Kapral, G.J., Murray, L.W., Richardson, J.S., and Richardson, D.C. (2010). MolProbity: all-atom structure validation for macromolecular crystallography. *Acta Crystallogr. D Biol. Crystallogr.* **66**, 12–21.
- Dever, T.E., Gutierrez, E., and Shin, B.S. (2014). The hypusine-containing translation factor eIF5A. *Crit. Rev. Biochem. Mol. Biol.* **49**, 413–425.
- Doerfel, L.K., Wohlgemuth, I., Kothe, C., Peske, F., Urlaub, H., and Rodnina, M.V. (2013). EF-P is essential for rapid synthesis of proteins containing consecutive proline residues. *Science* **339**, 85–88.
- Doerfel, L.K., Wohlgemuth, I., Kubyshekin, V., Starosta, A.L., Wilson, D.N., Budisa, N., and Rodnina, M.V. (2015). Entropic contribution of elongation factor P to proline positioning at the catalytic center of the ribosome. *J. Am. Chem. Soc.* **137**, 12997–13006.
- Emsley, P., and Cowtan, K. (2004). Coot: model-building tools for molecular graphics. *Acta Crystallogr. D Biol. Crystallogr.* **60**, 2126–2132.
- Essmann, U., Perera, L., Berkowitz, M.L., Darden, T., Lee, H., and Pedersen, L.G. (1995). A smooth particle mesh ewald method. *J. Chem. Phys.* **103**, 8577–8593.
- Feenstra, K.A., Hess, B., and Berendsen, H.J.C. (1999). Improving efficiency of large time-scale molecular dynamics simulations of hydrogen-rich systems. *J. Comput. Chem.* **20**, 786–798.
- Fischer, N., Neumann, P., Konevega, A.L., Bock, L.V., Ficner, R., Rodnina, M.V., and Stark, H. (2015). Structure of the *E. coli* ribosome-EF-Tu complex at 3 \AA resolution by Cs-corrected cryo-EM. *Nature* **520**, 567–570.
- Gutierrez, E., Shin, B.S., Woolstenhulme, C.J., Kim, J.R., Saini, P., Buskirk, A.R., and Dever, T.E. (2013). eIF5A promotes translation of polypyrroline motifs. *Mol. Cell* **51**, 35–45.
- Hanawa-Suetsugu, K., Sekine, S., Sakai, H., Hori-Takemoto, C., Terada, T., Unzai, S., Tame, J.R., Kuramitsu, S., Shirouzu, M., and Yokoyama, S. (2004). Crystal structure of elongation factor P from *Thermus thermophilus* HB8. *Proc. Natl. Acad. Sci. USA* **101**, 9595–9600.
- Hess, B. (2008). P-LINCS:cA parallel linear constraint solver for molecular simulation. *J. Chem. Theory Comput.* **4**, 116–122.
- Hildebrand, A., Rimmert, M., Biegert, A., and Söding, J. (2009). Fast and accurate automatic structure prediction with HHpred. *Proteins* **77** (Suppl 9), 128–132.
- Johansson, M., Jeong, K.W., Trobro, S., Strazewski, P., Åqvist, J., Pavlov, M.Y., and Ehrenberg, M. (2011). pH-sensitivity of the ribosomal peptidyl

- transfer reaction dependent on the identity of the A-site aminoacyl-tRNA. *Proc. Natl. Acad. Sci. USA* **108**, 79–84.
- Joung, I.S., and Cheatham, T.E., 3rd (2008). Determination of alkali and halide monovalent ion parameters for use in explicitly solvated biomolecular simulations. *J. Phys. Chem. B* **112**, 9020–9041.
- Katoh, T., Wohlgemuth, I., Nagano, M., Rodnina, M.V., and Suga, H. (2016). Essential structural elements in tRNA(Pro) for EF-P-mediated alleviation of translation stalling. *Nat. Commun.* **7**, 11657.
- Lassak, J., Keilhauer, E.C., Fürst, M., Wuichet, K., Gödeke, J., Starosta, A.L., Chen, J.M., Søgaard-Andersen, L., Rohr, J., Wilson, D.N., et al. (2015). Arginine-rhamnosylation as new strategy to activate translation elongation factor P. *Nat. Chem. Biol.* **11**, 266–270.
- Lassak, J., Wilson, D.N., and Jung, K. (2016). Stall no more at polyproline stretches with the translation elongation factors EF-P and IF-5A. *Mol. Microbiol.* **99**, 219–235.
- Lindorff-Larsen, K., Piana, S., Palmo, K., Maragakis, P., Klepeis, J.L., Dror, R.O., and Shaw, D.E. (2010). Improved side-chain torsion potentials for the Amber ff99SB protein force field. *Proteins* **78**, 1950–1958.
- Matheisl, S., Berninghausen, O., Becker, T., and Beckmann, R. (2015). Structure of a human translation termination complex. *Nucleic Acids Res.* **43**, 8615–8626.
- Melnikov, S., Mailliot, J., Rigger, L., Neuner, S., Shin, B.S., Yusupova, G., Dever, T.E., Micura, R., and Yusupov, M. (2016a). Molecular insights into protein synthesis with proline residues. *EMBO Rep.* **17**, 1776–1784.
- Melnikov, S., Mailliot, J., Shin, B.S., Rigger, L., Yusupova, G., Micura, R., Dever, T.E., and Yusupov, M. (2016b). Crystal structure of hypusine-containing translation factor eIF5A bound to a rotated eukaryotic ribosome. *J. Mol. Biol.* **428**, 3570–3576.
- Muto, H., and Ito, K. (2008). Peptidyl-prolyl-tRNA at the ribosomal P-site reacts poorly with puromycin. *Biochem. Biophys. Res. Commun.* **366**, 1043–1047.
- Navarre, W.W., Zou, S.B., Roy, H., Xie, J.L., Savchenko, A., Singer, A., Edvokimova, E., Prost, L.R., Kumar, R., Ibba, M., and Fang, F.C. (2010). PoxA, yjeK, and elongation factor P coordinately modulate virulence and drug resistance in *Salmonella enterica*. *Mol. Cell* **39**, 209–221.
- Parrinello, M., and Rahman, A. (1981). Polymorphic transitions in single crystals: a new molecular dynamics method. *J. Appl. Phys.* **52**, 7182.
- Pavlov, M.Y., Watts, R.E., Tan, Z., Cornish, V.W., Ehrenberg, M., and Forster, A.C. (2009). Slow peptide bond formation by proline and other N-alkylamino acids in translation. *Proc. Natl. Acad. Sci. USA* **106**, 50–54.
- Peil, L., Starosta, A.L., Virumäe, K., Atkinson, G.C., Tenson, T., Remme, J., and Wilson, D.N. (2012). Lys34 of translation elongation factor EF-P is hydroxylated by YfcM. *Nat. Chem. Biol.* **8**, 695–697.
- Peil, L., Starosta, A.L., Lassak, J., Atkinson, G.C., Virumäe, K., Spitzer, M., Tenson, T., Jung, K., Remme, J., and Wilson, D.N. (2013). Distinct XPPX sequence motifs induce ribosome stalling, which is rescued by the translation elongation factor EF-P. *Proc. Natl. Acad. Sci. USA* **110**, 15265–15270.
- Pelechano, V., and Alepuz, P. (2017). eIF5A facilitates translation termination globally and promotes the elongation of many non polyproline-specific tripeptide sequences. *Nucleic Acids Res.* **45**, 7326–7338.
- Pettersen, E.F., Goddard, T.D., Huang, C.C., Couch, G.S., Greenblatt, D.M., Meng, E.C., and Ferrin, T.E. (2004). UCSF Chimera—a visualization system for exploratory research and analysis. *J. Comput. Chem.* **25**, 1605–1612.
- Polikanov, Y.S., Steitz, T.A., and Innis, C.A. (2014). A proton wire to couple aminoacyl-tRNA accommodation and peptide-bond formation on the ribosome. *Nat. Struct. Mol. Biol.* **21**, 787–793.
- Pronk, S., Páll, S., Schulz, R., Larsson, P., Bjelkmar, P., Apostolov, R., Shirts, M.R., Smith, J.C., Kasson, P.M., van der Spoel, D., et al. (2013). GROMACS 4.5: a high-throughput and highly parallel open source molecular simulation toolkit. *Bioinformatics* **29**, 845–854.
- Rajkovic, A., Erickson, S., Witzky, A., Branson, O.E., Seo, J., Gafken, P.R., Frietas, M.A., Whitelegge, J.P., Faull, K.F., Navarre, W., et al. (2015). Cyclic rhamnosylated elongation factor P establishes antibiotic resistance in *Pseudomonas aeruginosa*. *MBio* **6**, e00823.
- Rajkovic, A., Hummels, K.R., Witzky, A., Erickson, S., Gafken, P.R., Whitelegge, J.P., Faull, K.F., Kearns, D.B., and Ibba, M. (2016). Translation control of swarming proficiency in *Bacillus subtilis* by 5-amino-pentanolyated elongation factor P. *J. Biol. Chem.* **291**, 10976–10985.
- Rohou, A., and Grigorieff, N. (2015). CTFIND4: fast and accurate defocus estimation from electron micrographs. *J. Struct. Biol.* **192**, 216–221.
- Roy, R.N., Lomakin, I.B., Gagnon, M.G., and Steitz, T.A. (2015). The mechanism of inhibition of protein synthesis by the proline-rich peptide oncocin. *Nat. Struct. Mol. Biol.* **22**, 466–469.
- Scheres, S.H. (2012). RELION: implementation of a Bayesian approach to cryo-EM structure determination. *J. Struct. Biol.* **180**, 519–530.
- Schmeing, T.M., Huang, K.S., Strobel, S.A., and Steitz, T.A. (2005). An induced-fit mechanism to promote peptide bond formation and exclude hydrolysis of peptidyl-tRNA. *Nature* **438**, 520–524.
- Schmidt, C., Becker, T., Heuer, A., Braunger, K., Shanmuganathan, V., Pech, M., Berninghausen, O., Wilson, D.N., and Beckmann, R. (2016). Structure of the hypusinylated eukaryotic translation factor eIF-5A bound to the ribosome. *Nucleic Acids Res.* **44**, 1944–1951.
- Schuller, A.P., Wu, C.C., Dever, T.E., Buskirk, A.R., and Green, R. (2017). eIF5A functions globally in translation elongation and termination. *Mol. Cell* **66**, 194–205.e5.
- Seefeldt, A.C., Nguyen, F., Antunes, S., Pérébasquine, N., Graf, M., Arenz, S., Inampudi, K.K., Douat, C., Guichard, G., Wilson, D.N., and Innis, C.A. (2015). The proline-rich antimicrobial peptide Onc112 inhibits translation by blocking and destabilizing the initiation complex. *Nat. Struct. Mol. Biol.* **22**, 470–475.
- Shin, B.S., Katoh, T., Gutierrez, E., Kim, J.R., Suga, H., and Dever, T.E. (2017). Amino acid substrates impose polyamine, eIF5A, or hypusine requirement for peptide synthesis. *Nucleic Acids Res.* **45**, 8392–8402.
- Sohmen, D., Chiba, S., Shimokawa-Chiba, N., Innis, C.A., Berninghausen, O., Beckmann, R., Ito, K., and Wilson, D.N. (2015). Structure of the *Bacillus subtilis* 70S ribosome reveals the basis for species-specific stalling. *Nat. Commun.* **6**, 6941.
- Starosta, A.L., Lassak, J., Peil, L., Atkinson, G.C., Virumäe, K., Tenson, T., Remme, J., Jung, K., and Wilson, D.N. (2014). Translational stalling at polyproline stretches is modulated by the sequence context upstream of the stall site. *Nucleic Acids Res.* **42**, 10711–10719.
- Su, T., Cheng, J., Sohmen, D., Hedman, R., Berninghausen, O., von Heijne, G., Wilson, D.N., and Beckmann, R. (2017). The force-sensing peptide VemP employs extreme compaction and secondary structure formation to induce ribosomal stalling. *eLife* **6**, 6.
- Ude, S., Lassak, J., Starosta, A.L., Kraxenberger, T., Wilson, D.N., and Jung, K. (2013). Translation elongation factor EF-P alleviates ribosome stalling at polyproline stretches. *Science* **339**, 82–85.
- Voorhees, R.M., Weixlbaumer, A., Loakes, D., Kelley, A.C., and Ramakrishnan, V. (2009). Insights into substrate stabilization from snapshots of the peptidyl transferase center of the intact 70S ribosome. *Nat. Struct. Mol. Biol.* **16**, 528–533.
- Vriend, G. (1990). WHAT IF: a molecular modeling and drug design program. *J. Mol. Graph.* **8**, 52–56, 29.
- Wang, J., Wang, W., Kollman, P.A., and Case, D.A. (2006). Automatic atom type and bond type perception in molecular mechanical calculations. *J. Mol. Graph. Model.* **25**, 247–260.
- Wohlgemuth, I., Brenner, S., Beringer, M., and Rodnina, M.V. (2008). Modulation of the rate of peptidyl transfer on the ribosome by the nature of substrates. *J. Biol. Chem.* **283**, 32229–32235.
- Woolstenhulme, C.J., Parajuli, S., Healey, D.W., Valverde, D.P., Petersen, E.N., Starosta, A.L., Guydosh, N.R., Johnson, W.E., Wilson, D.N., and Buskirk, A.R. (2013). Nascent peptides that block protein synthesis in bacteria. *Proc. Natl. Acad. Sci. USA* **110**, E878–E887.

Yanagisawa, T., Sumida, T., Ishii, R., Takemoto, C., and Yokoyama, S. (2010). A paralog of lysyl-tRNA synthetase aminoacylates a conserved lysine residue in translation elongation factor P. *Nat. Struct. Mol. Biol.* *17*, 1136–1143.

Zhang, J., Pan, X., Yan, K., Sun, S., Gao, N., and Sui, S.-F. (2015). Mechanisms of ribosome stalling by SecM at multiple elongation steps. *eLife* *4*, 4.

Zheng, S.Q., Palovcak, E., Armache, J.P., Verba, K.A., Cheng, Y., and Agard, D.A. (2017). MotionCor2: anisotropic correction of beam-induced motion for improved cryo-electron microscopy. *Nat. Methods* *14*, 331–332.

Zhou, J., Korostelev, A., Lancaster, L., and Noller, H.F. (2012). Crystal structures of 70S ribosomes bound to release factors RF1, RF2 and RF3. *Curr. Opin. Struct. Biol.* *22*, 733–742.

STAR★METHODS

KEY RESOURCES TABLE

REAGENT or RESOURCE	SOURCE	IDENTIFIER
Bacterial and Virus Strains		
<i>E. coli</i> BL21(DE3)pLysS	Merck	69450
<i>E. coli</i> Δ efp	KEIO Collection	BW25113
Biological Samples		
tRNA from <i>E. coli</i> MRE600	Roche	10109550001
Chemicals, Peptides, and Recombinant Proteins		
Ampicillin	Sigma	A9518
Complete, EDTA-free	Roche	05056489001
Dpn 1	NEB	R0176S
GTP	Sigma	G8877
Isopropyl- β -D-1-thiogalactopyranoside	Roth	2316
Kanamycin	Sigma	60615
KOD Xtreme Hot Start Polymerase	Merck	71975
LiCl precipitation solution	Thermo Fisher Scientific	AM9480
n-Dodecyl b-D-maltoside (DDM)	Sigma	D4641
PEG-8000	Sigma	1546605
Phosphoenol pyruvate	Sigma	10108294001
Pyruvate kinase (PK)	Sigma	10109045001
Rnasin	Promega	N2511
rNTPs	Sigma	27-2025-01
Triton X-100	Sigma	T8787
Critical Commercial Assays		
Luciferase Assay System	Promega	E1500
PURExpress <i>In Vitro</i> Protein Synthesis Kit	New England Biolabs	E6800
Talon Purification kit	Clontech	635501
Deposited Data		
Dataset 1: Cryo-EM map of PPP stalled 70S with P-site tRNA	This paper	EMDB: 3900
Dataset 1: Cryo-EM map of PPP-stalled 70S with A+P-site tRNA	This paper	EMDB: 3901
Dataset 2: Cryo-EM map of EF-P/PPP-stalled 70S with P-site tRNA (no EF-P bound) and associated structural model	This paper	EMDB: 3898; PDB: 6ENF
Dataset 2: Cryo-EM map of EF-P/PPP-stalled 70S with A+P-site tRNA and EF-P and associated structural model	This paper	EMDB: 3899; PDB: 6ENJ
Dataset 3: Cryo-EM map of EF-P/PP stalled 70S with P-site tRNA and EF-P and associated structural model	This paper	EMDB: 3903; PDB: 6ENU
Dataset 3: Cryo-EM map of EF-P/PP stalled 70S with P+E-site tRNA (no EF-P bound)	This paper	EMDB: 3902
Oligonucleotides		
EF-P-R186A_FOR: 5'-GGTGAATACGTCTCTGCGGTGAAGTAATGGATC-3'	Eurofins Genomics	N/A
EF-P-R186A_REV: 5'-GATCCATTACTTCACCGCAGAGACGTATTCACC-3'	Eurofins Genomics	N/A
EF-P-Y183A_FOR: 5'-CCCCTCTGGTGAAGCGGTCTCTCGCGTGAAG-3'	Eurofins Genomics	N/A
EF-P-Y183A_REV: 5'-CTTACGCGAGAGACCGCTTACCCAGAGCGGG-3'	Eurofins Genomics	N/A
EF-P-loopID1_FOR: 5'-CTGAAAGGTGATACCGCAACTGGCGGCAAACCGGC-3'	Eurofins Genomics	N/A
EF-P-loopID1_REV: 5'-GCCGGTTTGCCGCCAGTTGCGGTATCACCTTTCAG-3'	Eurofins Genomics	N/A
EF-P-loopID2_FOR: 5'-GGCCTGAAAGGTGATACCGCAACTGGCGGCAAACCGGC-3'	Eurofins Genomics	N/A
EF-P-loopID2_REV: 5'-GCCGGTTTGCCGCCAGTTGCGGTATCACCTTTCAGGC-3'	Eurofins Genomics	N/A

(Continued on next page)

Continued

REAGENT or RESOURCE	SOURCE	IDENTIFIER
EF-P-loopID3_FOR: 5'-CCGGGCCTGAAAGGTGATGGCGGCAAACCGGCTACC-3'	Eurofins Genomics	N/A
EF-P-loopID3_REV: 5'-GGTAGCCGGTTTGCCGCCATCACCTTTCAGGCCCGG-3'	Eurofins Genomics	N/A
EF-P-144AAA146_FOR: 5'-GATCCGGGCCTGAAAGCGGCGGCGGCAGGTACTG GCGGC-3'	Eurofins Genomics	N/A
EF-P-144AAA146_REV: 5'-GCCGCCAGTACCTGCCGCCCGCCTTTCAGGC CCGGATC-3'	Eurofins Genomics	N/A
EF-P-K34A_FOR: 5'-CGTAAAACCGGGTGC GGCCAGGCATTTG-3'	Eurofins Genomics	N/A
EF-P-K34A_REV: 5'-CAAATGCCTGGCCGCACCCGGTTTTACG-3'	Eurofins Genomics	N/A
EF-P-DDomain3_FOR: 5'-GTTACTCCGCCGAAC TAAGTTGAACTGGAAATC-3'	Eurofins Genomics	N/A
EF-P-DDomain3_REV: 5'-GATTTCCAGTTCAACTTAGTTCGGCGGAGTAAC-3'	Eurofins Genomics	N/A
Recombinant DNA		
Plasmid pET21b-R1NlpD	Starosta et al., 2014	N/A
pET46LIC_Ec_efp	Starosta et al., 2014	N/A
pRSFDuet_Ec_yjeK/Ec_yjeA	Starosta et al., 2014	N/A
Software and Algorithms		
WHATIF	Vriend, 1990	N/A
Gromacs 5, Solvate and GENION	Pronk et al., 2013	N/A
LINCS	Hess, 2008	N/A
SIGNATURE	Chen and Grigorieff, 2007	N/A
RELION-2	Scheres, 2012	N/A
CTFFIND4	Rohou and Grigorieff, 2015	N/A
MotionCor2	Zheng et al., 2017	N/A
Chimera	Pettersen et al., 2004	N/A
Coot	Emsley and Cowtan, 2004	N/A
Chem3Dpro	PerkinElmer	N/A
MolProbity	Chen et al., 2010	N/A
HHPred	Hildebrand et al., 2009	N/A
PyMol Molecular Graphic Systems Version 1.8	Schrödinger; https://pymol.org/2/	N/A
Other		
Protino Ni-NTA agarose beads	Macherey-Nagel	745400
Superdex HiLoad S75 16/600	GE Healthcare	28989333

CONTACT FOR REAGENT AND RESOURCE SHARING

Please direct any requests for further information or reagents to the Lead Contact, Daniel N. Wilson (daniel.wilson@chemie.uni-hamburg.de).

EXPERIMENTAL MODEL AND SUBJECT DETAILS***E. coli* Strain and Growth Conditions**

The *E. coli* Δ efp strain (Keio collection BW25113) was grown to $OD_{600} = 5.8$ in an 'INFORCE HT minifors' bench-top fermenter in 2xYPTG (16 g/l peptone, 10 g/l yeast extract, 5 g/l NaCl, 22 mM NaH_2PO_4 , 40 mM Na_2HPO_4 , 19.8 g/l glucose) at 37°C while maintaining pH 7.0 and oxygen level (60%).

METHODS DETAILS**Preparation of the *E. coli* Δ efp S12 Translation Extract**

The *E. coli* Δ efp S12 translation extract was prepared as described for *B. subtilis* S12 translation extract ([Sohmen et al., 2015](#)) with some minor modifications. *E. coli* Δ efp cells (Keio collection BW25113) were grown to $OD_{600} = 5.8$ in an 'INFORCE HT minifors' bench-top fermenter in 2xYPTG (16 g/l peptone, 10 g/l yeast extract, 5 g/l NaCl, 22 mM NaH_2PO_4 , 40 mM Na_2HPO_4 , 19.8 g/l glucose) at 37°C while maintaining pH 7.0 and oxygen level (60%). Cells were collected at 5,000 x g at 4°C for 15 min. 22 g of cells were

resuspended in 14.6 mL of Buffer A (10 mM Tris-acetate, pH 8.2, 14 mM magnesium acetate, 60 mM potassium glutamate, 1 mM dithiothreitol and 6 mM 2-mercaptoethanol) and broken open in an 'microfluidics model 110I lab homogenizer', 3x at 15,000 psi. Subsequently, the lysate was cleared at 12,000 \times g and incubated for 30 min at 37°C in a water bath. The cell extract was aliquoted, snap frozen and stored at -80°C.

PCR and *In Vitro* Transcription

Full-length *nlpD*-PPP construct with a N-terminal 6 x His- and HA-tag was amplified from pET-21b_{-R1}*nlpD* (Starosta et al., 2014) using T7 forward (5'-TAATACGACTCACTATAGGG-3') and T7 terminator (5'-GCTAGTTATTGCTCAGCGG-3') primer. Truncated *nlpD*-PP construct was amplified from *nlpD*-PPP PCR product using T7 forward and revPP (5'-CGGCGGTCTAATCAACATAC-3') primer. To avoid contamination with remaining full-length *nlpD*-PPP product, *nlpD*-PP was excised from the agarose gel and a second PCR was performed using the excised product as a template with T7 forward and revPP as primers. PCR products were purified and *in vitro* transcription reaction was performed using 2 μ g of PCR product and 4 μ l of homemade T7 polymerase per 100 μ l reaction volume (40 mM Tris pH 7.9, 25 mM Spermidine, 26 mM MgCl₂, 0,01% Triton X-100, 5mM DTT and 6.25 mM rNTPs (Sigma)) (Sohmen et al., 2015). The RNA was purified by LiCl/ethanol precipitation.

Preparation of Full-Length NlpD-PPP-SRC and Truncated NlpD-PP-SRC

Full-length NlpD-PPP-SRC was prepared using *E. coli* Δ *efp* S12 translation extract following the procedure described for the *B. subtilis* MifM-SRC (Sohmen et al., 2015). In summary the translation reaction contained 240 mM HEPES pH 8.2, 1.5 mM glucose, 2% PEG-8000, 2 mM DTT, 90 mM potassium glutamate, 80 mM ammonium acetate, 7.5 mM MgAc, 20 mM KH₂PO₄, 35 mM of each amino acid and 6.75 μ l/25 μ l of the S12 cell extract as well as 1.5 μ l/25 μ l reaction of *in vitro* transcribed mRNA. For the purifications of the SRCs the reaction was scaled up to 2500 μ l. *In vitro* translation was carried out for 20 min. Translation reaction was stopped by adding ice cold Buffer B (50 mM HEPES pH 7.2 at 4°C, 250 mM KOAc, 10 mM MgOAc, 0,1% DDM, 1/1,000 complete protease inhibitor (Roche), 0.2 U/ml RNasin). For the truncated NlpD-PP-SRC, the *in vitro* reaction was carried out using PURExpress *In vitro* Protein Synthesis Kit (NEB). The translation reaction (750 μ l in total) was prepared according to the protocol of the PURExpress *In vitro* Protein Synthesis Kit but was supplemented with 5 μ M anti-ssrA oligo (5' TTAAGCTGCTAAAGCGTAGTTTTCG TCGTTTGGCGACTA-3'). Translation was started by adding the truncated *nlpD*-PP PCR product and then the reaction was incubated at 37°C for 20 min with shaking at 1,000 rpm.

Purification of the NlpD-PPP-SRC and Truncated NlpD-PP-SRC

Translation reactions were loaded onto 500 mL sucrose cushion (750 mM sucrose) in Buffer B and pelleted at a speed of 45.000 rpm for 150 min in a TLA 120.2 rotor (Sohmen et al., 2015). The SRCs were resuspended in Buffer B and bound via its N-terminal 6x His-tag to a Talon metal affinity chromatography column (Clontech) which was pre-equilibrated with Buffer B containing 10 mg/ml bulk tRNA. The column was washed with Buffer C (same as Buffer B, but with 500 mM KOAc). The SRCs were eluted by using Buffer B supplemented with 150 mM Imidazole. The eluates were loaded onto 10%–40% sucrose gradients (in Buffer B) and centrifuged for 13h in a Beckman coulter SW40 swinging bucket rotor at 20.000 rpm. 70S peaks were collected, pelleted for 3h in a TLA 120.2 rotor (45.000 rpm) and pellets were resuspended in Buffer B. Purification of the SRCs were confirmed by SDS-Page and western blotting using an anti-HA-tag antibody.

Cryogrid Preparation for the NlpD-PPP-SRC and NlpD-PP-SRC

Dataset 1: For grid preparation 4.5 OD A₂₆₀/ml monosomes of the full-length NlpD-PPP-SRC were used. Dataset 2: For grid preparation 5.0 OD A₂₆₀/ml monosomes of the full length NlpD-PPP-SRC were used and a 3x excess of modified EF-P over 70S was added and incubated for 20 min at 37°C. Dataset 3 For grid preparation 4.5 OD A₂₆₀/ml monosomes of the truncated NlpD-PP SRC were used. A 5x excess of modified EF-P over 70S as well as 100 μ M evernimicin (to ensure absence of A-site tRNA) (Arenz et al., 2016b) were added and incubated for 5 min at 37°C. All samples were applied to 2 nm precoated Quantifoil R3/3 holey carbon supported grids and vitrified using a Vitrobot Mark IV (FEI company).

Generation and Purification of Modified EF-P and Mutants

All EF-P variants were generated by site-directed mutagenesis PCR using the whole plasmid PCR method with pET46LIC_EC_*efp* as a template (primers and plasmids are listed in the Key Resources Table). For the PCR reaction the KOD Xtreme Hot Start Polymerase (Merck) was used with the following conditions: 94°C 2 min; 20x (98°C 10 s, 63°C 30 s, 68°C 2 min); 68°C 7 min. The product was digested with Dpn1 (NEB) for 1h at 37°C and purified using a PCR Purification Kit (Qiaagen). The EF-P variants were coexpressed together with EpmA and EpmB from pRSFDuet vector (to ensure modification of EF-P) in *E. coli* BL21 cells grown at 37°C from overnight culture in lysogeny broth (LB) medium and in the presence of 100 μ g/mL ampicillin and 50 μ g/ml kanamycin. Protein expression was induced at an OD₆₀₀ of 0.4 with a final concentration of 1 mM isopropyl- β -D-1-thiogalactopyranoside (IPTG) (Roth). After 1 hour of expression cells were lysed using a microfluidizer. The cell lysate was cleared using a SS34 rotor at 4°C and 44,100 \times g for 30 minutes. Purification of His-tagged proteins was done with Protino Ni-NTA agarose beads (Macherey-Nagel). The final eluate was applied onto a Superdex HiLoad S75 16/600 column (GE Healthcare) to yield the final concentrated protein in gel filtration buffer

(50 mM HEPES pH 7.4, 50 mM KCl, 100 mM NaCl and 5 mM 2-mercaptoethanol). The post-translational modification of wild-type EF-P and EF-P variants was confirmed by mass spectrometry as performed previously for EF-P (Peil et al., 2012).

Luminescence Determination of Firefly Luciferase

In vitro translation of the firefly luciferase was performed using the PURExpress *in vitro* translation kit. For template generation Fluc3xPro was amplified via PCR using T7 forward and T7 reverse primer from plasmid pVEX-Fluc3xPro (Ude et al., 2013). Samples have been incubated at 37°C for defined time periods. 1 μ l of each reaction were added on to white 96-well chimney flat bottom microtiter plates. 40 μ l of luminol substrate (Promega) was added, immediately before luminescence was detected using a Tecan Infinite M1000.

Ribosome Complexes for Kinetic Experiments

The mRNA (GGGCAAGGAGGUAUUAAUGCCGCGCGUUCUU) coding for fMPPPF was synthesized by IBA Lifescience. Initiation complexes were formed by incubating 70S ribosomes (1 μ M) with IF 1, IF2, IF3 (1.5 μ M each), [³H]Met-tRNA^{Met} (3 μ M) and GTP (1 mM) in buffer D (50 mM Tris-HCl, pH 7.5 at 37°C, 70 mM NH₄Cl, 30 mM KCl and 7 mM MgCl₂) for 30 min (Doerfel et al., 2013). Initiation complexes were purified by centrifugation through a 400 μ l sucrose cushion (40% sucrose in buffer D) at 260,000 g for 2 h at 4°C. Pellets were dissolved in buffer D, flash frozen and stored at -80°C. [¹⁴C]Phe-tRNA^{Phe} was prepared from total tRNA as described. tRNA^{Pro} *in-vitro* transcripts were prepared and aminoacylated as described (Doerfel et al., 2013). Ternary complexes EF-Tu-GTP-aminoacyl-tRNA were prepared by incubating aminoacyl-tRNA (Pro-tRNA^{Pro} and Phe-tRNA^{Phe}) with a 2.5-fold excess of EF-Tu, GTP (1 mM), pyruvate kinase (0.1 μ g/ μ l) and phosphoenolpyruvate (3 mM) for 15 min at 37°C.

In Vitro Translation of fMPPPF Model Peptide

Initiation complexes (0.2 μ M), ternary complexes Pro and Phe (each 2 μ M), EF-G (1 μ M) and EF-P (varying concentrations) were mixed in buffer E (50 mM Tris-HCl, pH 7.5 at 37°C, 70 mM NH₄Cl, 30 mM KCl, 3.5 mM MgCl₂, 0.5 mM spermidine, 8 mM putrescine and 2 mM DTT) at 37°C. The reaction was quenched after 20 s with KOH (0.5 M), hydrolyzed for 30 min at 37°C and neutralized with glacial acetic acid. Amino acids and peptides were separated by reversed-phase HPLC (Chromolith Performance RP8e 100-4.6 column, Merck) using a 0%–65% acetonitrile gradient in 0.1% TFA. Products and educts were quantified by double-label scintillation counting (Doerfel et al., 2013).

Molecular Dynamics Simulations

To obtain the dynamics of the region surrounding the PTC in presence of EF-P, unmodified EF-P or without EF-P, we carried out all-atom explicit-solvent molecular dynamics (MD) simulations. The simulations were started (i) from the cryo-EM structure, (ii) from the cryo-EM structure after removal of the β -lysine modification of Lys34 (EF-P), and (iii) after removal of EF-P. Since the structural differences between the cryo-EM structures with and without EF-P are only found in the vicinity of the PTC, we used a reduced simulation system that allowed us to increase the achievable simulation time. The simulation system (+EF-P) includes all residues of the cryo-EM structure located within 35 Å of any atom of the P-site tRNA CCA tail, of the attached peptide, or of the β -lysine modified Lys34 of EF-P. Nucleotides (amino acids) that are not within this radius, but whose 5'- and 3'- (n- and c-) neighbors are within the radius, are also included in the simulation system. Nucleotides whose 5' (3') bound nucleotide neighbor is not in the simulation system were treated as 5' (3') terminal nucleotides. Any amino acid *i* whose *i*-1 neighbor (*i*+1 neighbor) is not in the simulation system was capped by an uncharged N-terminal acetyl (C-terminal amide). Positions of residues in a 25 Å radius were not restrained (inner layer), while heavy atom positions of the remaining residues (outer layer) were restrained by a harmonic potential. The harmonic force constant *k* of each restrained atom was chosen as $k = 8RT \pi \cdot \text{rmsf}^2$ where rmsf is the root mean square fluctuation of the corresponding atom obtained from a 2 μ s-simulations of the full ribosome in complex with A- and P-site tRNAs and the ErmBL peptide (Arenz et al., 2016a). For those heavy atoms without corresponding atoms in the full-ribosome simulations, the average of all other force constants was used. Two more simulation systems were used, one after removal of the modification of EF-P Lys34 (+EF-P (unmod)) and the other after removal of all EF-P atoms (-EF-P). To place initial Mg²⁺ ions, a cryo-EM structure of the ribosome (Fischer et al., 2015) was aligned to each simulation system. Then, Mg²⁺ ions resolved in the cryo-EM structure that are located within 5 Å of the atoms of the simulation system were extracted from the aligned structure and included in the simulations system. WHATIF (Vriend, 1990) was used to determine the protonation states of the histidines. Each simulation systems was then solvated in a dodecahedron box of water molecules with a minimum distance of 1.5 nm between the atoms of the simulation system and the box boundaries using the program solvate (Pronk et al., 2013). To neutralize the overall charge of each system, first the Coulomb potential at the positions of all water oxygen atoms was calculated based on the charges and positions of all other atoms. Iteratively, the water molecule with the lowest Coulomb potential was replaced by a K⁺ ion and the Coulomb potential at all other water oxygens was updated until the overall charge was neutral. Using the program GENION (Pronk et al., 2013), subsequently 7 mM MgCl₂ and 150 mM KCl were added. All simulations were carried out with Gromacs 5 (Pronk et al., 2013) using the amberff12sb force field (Lindorff-Larsen et al., 2010) and the SPC/E water model (Berendsen et al., 1987). Force field parameters for modified nucleotides were taken from (Aduri et al., 2007). Potassium and chloride ion parameters were taken from (Joung and Cheatham, 2008). Atom types for β -lysine modified Lys were obtained with ANTECHAMBER (Wang et al., 2006) and partial charges were determined using DFT-B3LYP with a 6-31/G* basis set. The ester bond between the C-terminal proline and A76 of the P-site tRNA was treated as described earlier (Bock et al.,

2013). Lennard-Jones and short-range Coulomb interactions were calculated within a distance of 1 nm, while long-range Coulomb interactions were calculated using particle-mesh Ewald summation (Essmann et al., 1995). The LINCS algorithm was used to constrain bond lengths (Hess, 2008) and virtual site constraints (Feenstra et al., 1999) were used for hydrogens, allowing an integration time step of 4 fs. Solute and solvent temperatures were controlled independently at 300 K using velocity rescaling (Bussi et al., 2007) with a coupling time constant of 0.1 ps. For each of the three simulation systems, the system was equilibrated in four steps. First, the potential energy was minimized using steepest descent while restraining the positions of all solute heavy atoms ($k = 1000 \text{ kJ mol}^{-1} \text{ nm}^{-2}$). Second, for the first 50 ns, the pressure was coupled to a Berendsen barostat (1 ps coupling time) (Berendsen et al., 1984) and position restraints were applied. Third, during the next 20 ns, the position restraint force constant was linearly decreased to the values obtained from the full-ribosome simulations for the outer-layer atoms and to zero for the remaining atoms. Finally, for production runs starting at 70 ns, the Parrinello-Rahman barostat was used (Parrinello and Rahman, 1981). At simulation times 170, 270, 370, and 470 ns coordinates were extracted from the trajectory, new velocities were assigned according to a Boltzmann distribution, and subsequently new simulations were started, resulting in a total of 15 simulations, 2 μs each, accumulating to a total production run simulation time of 30 μs .

Conformational Landscape of CCA End and C-Terminal Proline

To investigate how either the removal of the modification of EF-P or the removal of EF-P entirely changes the conformation of the P-site CCA end and the C-terminal proline of the peptide, we carried out a Principal Component Analysis (PCA) (Amadei et al., 1993). A PCA is used to extract the dominant modes of motion, here the first two eigenvectors. To that aim, we first aligned all the trajectories using all 23S P atoms and, second, extracted backbone atoms of the CCA end (O3', C3', C4', C5', O5', and P atoms) and of the peptide (N, CA, C, and O atoms). The extracted trajectories were then concatenated and the atomic displacement covariance matrix was calculated. The eigenvectors of this covariance matrix were sorted according to their eigenvalues. The eigenvectors corresponding to the largest eigenvalues represent the most dominant conformational modes. To describe the structural ensembles obtained from the three sets of simulations, first, the projection of all the frames onto the first two eigenvectors was calculated. For each set of simulations, the projections were then sorted into 2-dimensional bins and the logarithm of the probability $\rho = c_{i,j}/c_{\text{total}}$ of each bin i,j was calculated, where $c_{i,j}$ is the number of the projections in the bin, c_{total} is the total number of frames (Figures 6A–6C). For comparison, our cryo-EM structure with EF-P as well as the X-ray structures of the pre-attack conformation (Polikanov et al., 2014) and the uninduced and induced conformations (Schmeing et al., 2005) were projected onto the two conformational modes (Figures 6A–6C). For each set of simulations, all the structures sorted into the bin marked with a cross in the conformational landscape (Figures 6A–6C) were extracted. For each set, from the extracted structures the one with the median peptide bond distance was chosen and is shown in (Figures 6D–6F).

Cryo-electron Microscopy and Single Particle Reconstruction

Data collections were performed on FEI Titan Krios transmission electron microscopes equipped with a Falcon II direct electron detector (FEI) at 300 kV at a pixel size of 1.064 Å (Dataset 1) or 1.084 Å (Dataset 2 and 3). Dataset 1: Defocus range was from -1.0 to $-2.5 \mu\text{m}$ (underfocus) resulting in 1156 Micrographs after manual inspection and discarding micrographs with resolution worse than 4 Å. Each micrograph contained 16 frames ($2.68 \text{ e}^-/\text{Å}^2$). Original image stacks were motion-corrected and dose weighted using MotionCor2 (Zheng et al., 2017). Dataset 2 and 3: Defocus range was from -0.8 to $-2.5 \mu\text{m}$ (underfocus) resulting in 2109 micrographs for Dataset 2 and 1957 micrographs for Dataset 3 after manual inspection and discarding micrographs showing a resolution worse than 3.3 Å (Dataset 2) and 3.4 Å (Dataset 3), respectively. Each micrograph contained 17 frames in total ($2.4 \text{ e}^-/\text{Å}^2 + 4 \text{ e}^-/\text{Å}^2$ pre exposure) and frames 0–9 were used resulting in a total dose of $28 \text{ e}^-/\text{Å}^2$. Original image stacks were motion-corrected using MotionCor2 (Zheng et al., 2017). Power-spectra, defocus values, astigmatism and estimation of resolution were determined using CTFFIND4 software (Rohou and Grigorieff, 2015). After automated particle picking using SIGNATURE (Chen and Grigorieff, 2007) single particles were processed using RELION-2 (Scheres, 2012). All particles from the three datasets (Dataset 1: 121,704 particles, Dataset 2: 229,613 particles, Dataset 3: 229,458 particles) were first subjected to 3D refinement using an *E. coli* 70S ribosome as reference structure and subsequently a 3D classification was performed (Figure S1). Dataset 1 was classified into four classes and dataset 2 and 3 into eight classes. For dataset 3 classes 2 and 3 were joined and a second classification was performed with a mask focusing on EF-P. Final structures of all datasets were refined, corrected for the modulation transfer function of the Falcon 2 detector and sharpened by applying a negative B-factor automatically estimated by RELION-2 (Figure S1). Resolution was estimated using the “gold standard” criterion (FSC = 0.143).

Molecular Modeling and Map-Docking Procedures

The molecular model for the ribosomal proteins and rRNA of either the PPP or PP stalled complexes is based on the molecular model for the 70S subunit from the cryo-EM reconstruction of the *E. coli* 70S ribosome (PDB: 5AFI) (Fischer et al., 2015) and obtained by performing a rigid body fit into the cryo-EM density map of the corresponding stalled complex using UCSF Chimera (Pettersen et al., 2004) (fit in map function). For *E. coli* EF-P, a homology model was generated using HHPred (Hildebrand et al., 2009) based on a template from *T. thermophilus* (PDB: 3HUW) (Blaha et al., 2009). The model was fitted to the density using Chimera (Pettersen et al., 2004) and refined in Coot (Emsley and Cowtan, 2004). The post-translational modification of $\epsilon(\text{R})-\beta$ -lysylhydroxylysine that is positioned at K34 of EF-P was designed using Chem3DPro (PerkinElmer), manually placed into the cryo-EM density map at

position 34 of EF-P and refined in Coot. P-site tRNA of the *E. coli* 70S ribosome (PDB: 5AFI) (Fischer et al., 2015) was manually mutated to tRNA^{Pro(CCG)}. In the case of the truncated PP-SRC in the presence of EF-P, the L1 stalk and L1 protein were taken from the crystal structure of *T. thermophilus* (PDB: 3HUW), manually mutated and refined using Coot. Nucleotides of the PTC that differ from the cryo-EM *E. coli* 70S ribosome (PDB: 5AFI) (Fischer et al., 2015) were manually refined into density using Coot. Atomic coordinates were refined using *phenix.real_space_refine* (Adams et al., 2010), with restraints obtained by *phenix.secondary_structure_restraints* (Adams et al., 2010). Cross-validation against overfitting was performed as described elsewhere (Brown et al., 2015). Statistics of the refined models were obtained using MolProbity (Chen et al., 2010) and are presented in Table 1.

Figure Preparation

Figures showing electron densities and atomic models were generated using either UCSF Chimera (Pettersen et al., 2004) or PyMol Molecular Graphic Systems (Version 1.8 Schrödinger). Figure panels were assembled using Adobe Illustrator.

QUANTIFICATION AND STATISTICAL ANALYSIS

Cryo-EM Data Analysis

Bayesian selection using RELION software package was used to choose the cryo-EM data package (Scheres, 2012). Resolutions were calculated according to gold standard and the estimation of variation within each group of data was performed using Bayesian calculation within RELION (Scheres, 2012).

DATA AND SOFTWARE AVAILABILITY

Accession Numbers

The atomic coordinates and/or the associated maps have been deposited in the PDB and/or EMDB with the accession codes EMD: 3900 (Dataset 1, P-tRNA only), EMD: 3901 (Dataset 1, A+P-tRNA), EMD: 3898/PDB: 6ENF (Dataset 2, P-tRNA only), EMD: 3899/PDB: 6ENJ (Dataset 2, A+P-tRNA+EF-P), EMD: 3903/PDB: 6ENU (Dataset 3, P-tRNA+EF-P) and EMD: 3902 (Dataset 3, P+E-tRNA).

Molecular Cell, Volume 68

Supplemental Information

Structural Basis for Polyproline-Mediated

Ribosome Stalling and Rescue

by the Translation Elongation Factor EF-P

Paul Huter, Stefan Arenz, Lars V. Bock, Michael Graf, Jan Ole Frister, Andre Heuer, Lauri Peil, Agata L. Starosta, Ingo Wohlgemuth, Frank Peske, Jiří Nováček, Otto Berninghausen, Helmut Grubmüller, Tanel Tenson, Roland Beckmann, Marina V. Rodnina, Andrea C. Vaiana, and Daniel N. Wilson

SUPPLEMENTAL FIGURES

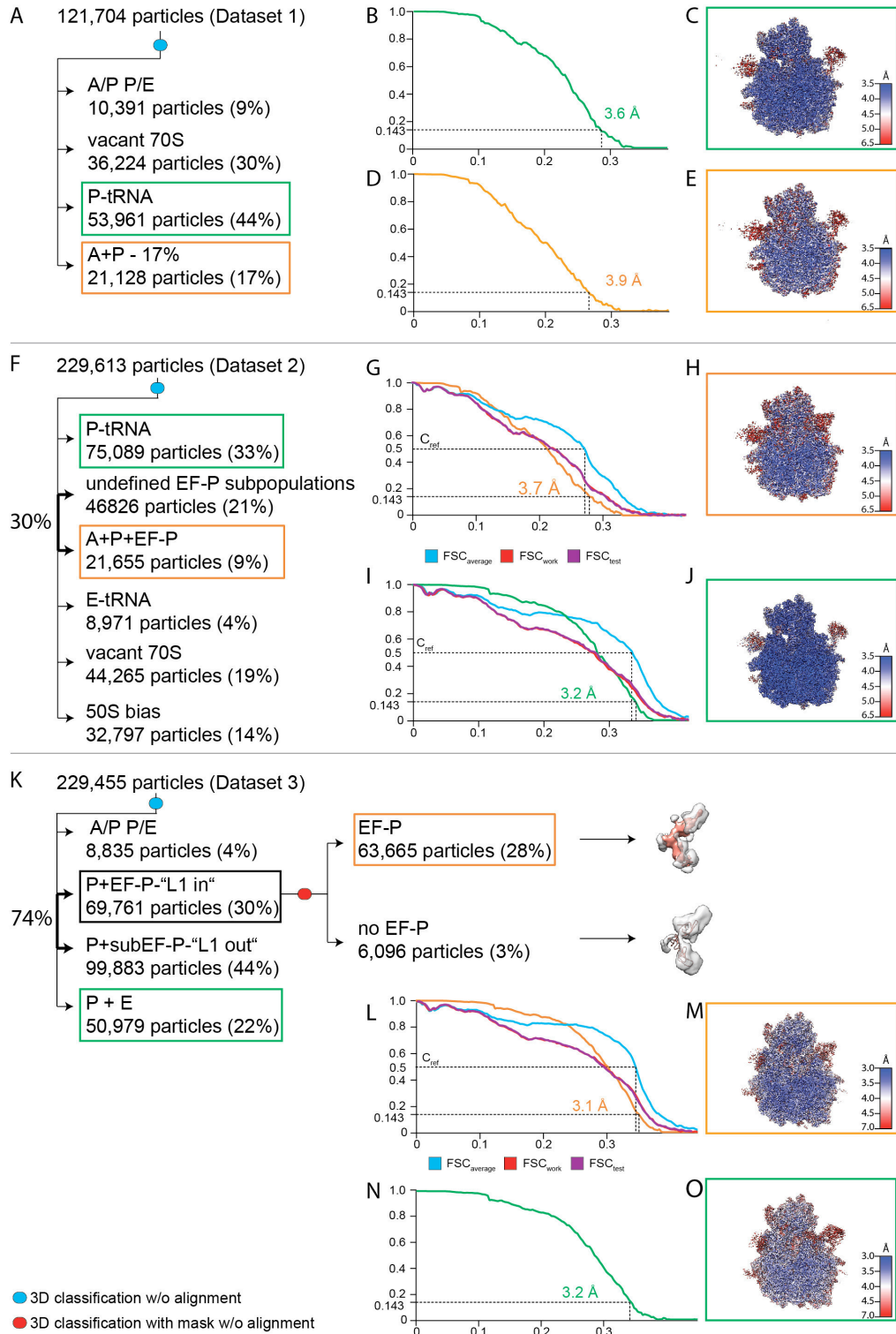


Figure S1 - Related to Figure 1-3. Data processing of the cryo-EM structures of polyproline-stalled ribosomes \pm EF-P. (A) *In silico* sorting procedure for Dataset 1 derived from the PPP-stalled ribosome complexes prepared in the absence of EF-P. (B) Fourier-shell-correlation (FSC) curve (green) and (C) transverse section of the P-site tRNA only structure colored according to local resolution. (D) FSC curve (orange) and (E) transverse section of the A- and P-site tRNAs containing structure colored according to local resolution. In (B) and (D), the resolution at FSC=0.143 is indicated with a dashed line. (F) *In silico* sorting procedure for Dataset 2 derived from the PPP-SRC prepared in the presence of EF-P. (G) FSC curve (orange), as well as self and cross-validated correlations FSC_{work} (red) and FSC_{test} (purple), respectively. The resolutions at FSC=0.143 and FSC=0.5 (C_{ref}) are indicated with dashed lines. (H) Transverse section of the A- and P-site tRNA- and EF-P-containing structure colored according to local resolution. (I) FSC curve (green), as well as self and cross-validated correlations as in (G) but for the P-site tRNA only structure. (J) as (H) but for P-site tRNA only structure. (K) *In silico* sorting procedure for Dataset 3 derived from the PP-SRC prepared in the presence of EF-P. (L) FSC curve (orange), as well as self and cross-validated correlations FSC_{work} (red) and FSC_{test} (purple), respectively. The resolutions at FSC=0.143 and FSC=0.5 (C_{ref}) are indicated with dashed lines. (M) Transverse section of the P-site tRNA and EF-P structure colored according to local resolution. (N) FSC curve (green) for the P- and E-site tRNA containing structure. (O) as (M) but for P- and E-site tRNA containing structure.

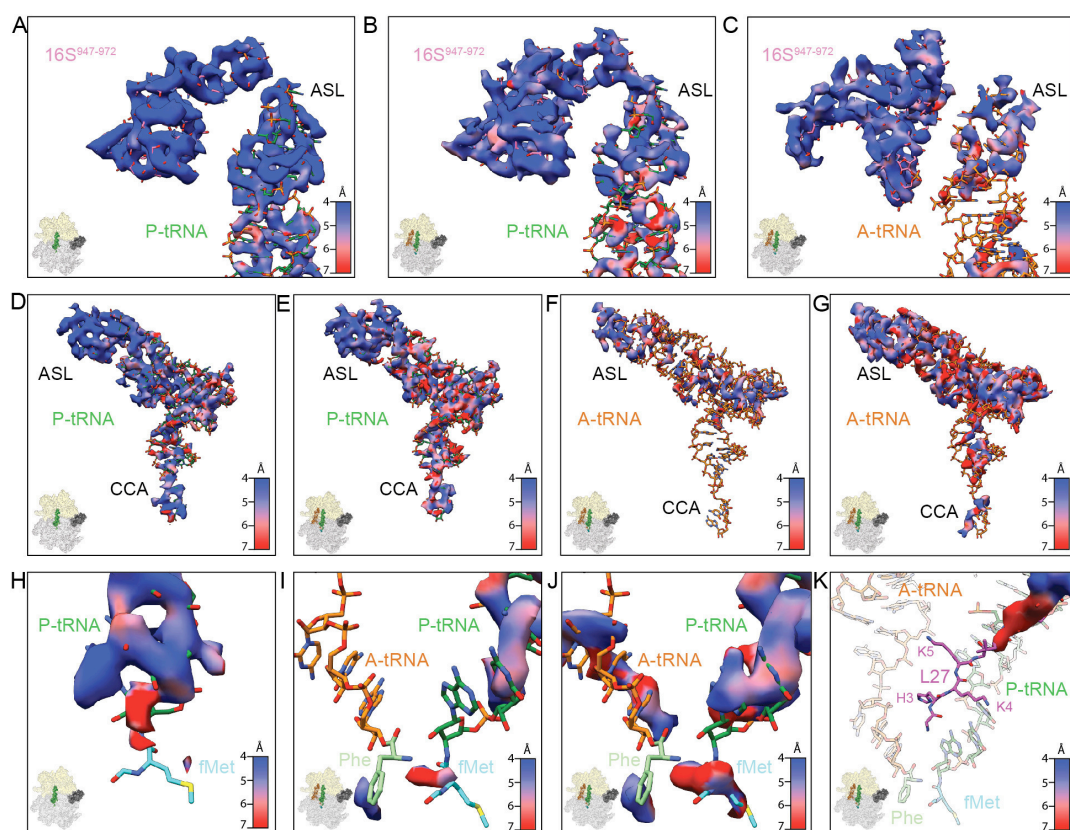


Figure S2 - Related to Figure 1. Flexibility of tRNA^{Pro} in A- and P-sites in the absence of EF-P. (A-C) Cryo-EM densities coloured according to local resolution of the ASL of P-site tRNA^{Pro} (green) or A-site tRNA^{Pro} (orange) in comparison to nucleotides 947-972 (purple) of the 16S rRNA at high threshold (7σ). (D-G) Cryo-EM densities of (D and E) P-site tRNA^{Pro} (green) and (F and G) tRNA^{Pro} (orange) coloured according to local resolution at (D-F) high (7σ) or (G) low threshold (3.5σ). (H-J) Cryo-EM densities of the CCA-ends of (H) P-site tRNA or (I and J) P- and A-site tRNAs including modeled fMet (cyan) and Phe (green) (from PDB: 1V4Y) (Polikanov et al., 2014), coloured according to local resolution. (K) Cryo-EM density colored according to local resolution for the N-terminus of ribosomal protein L27 (purple).

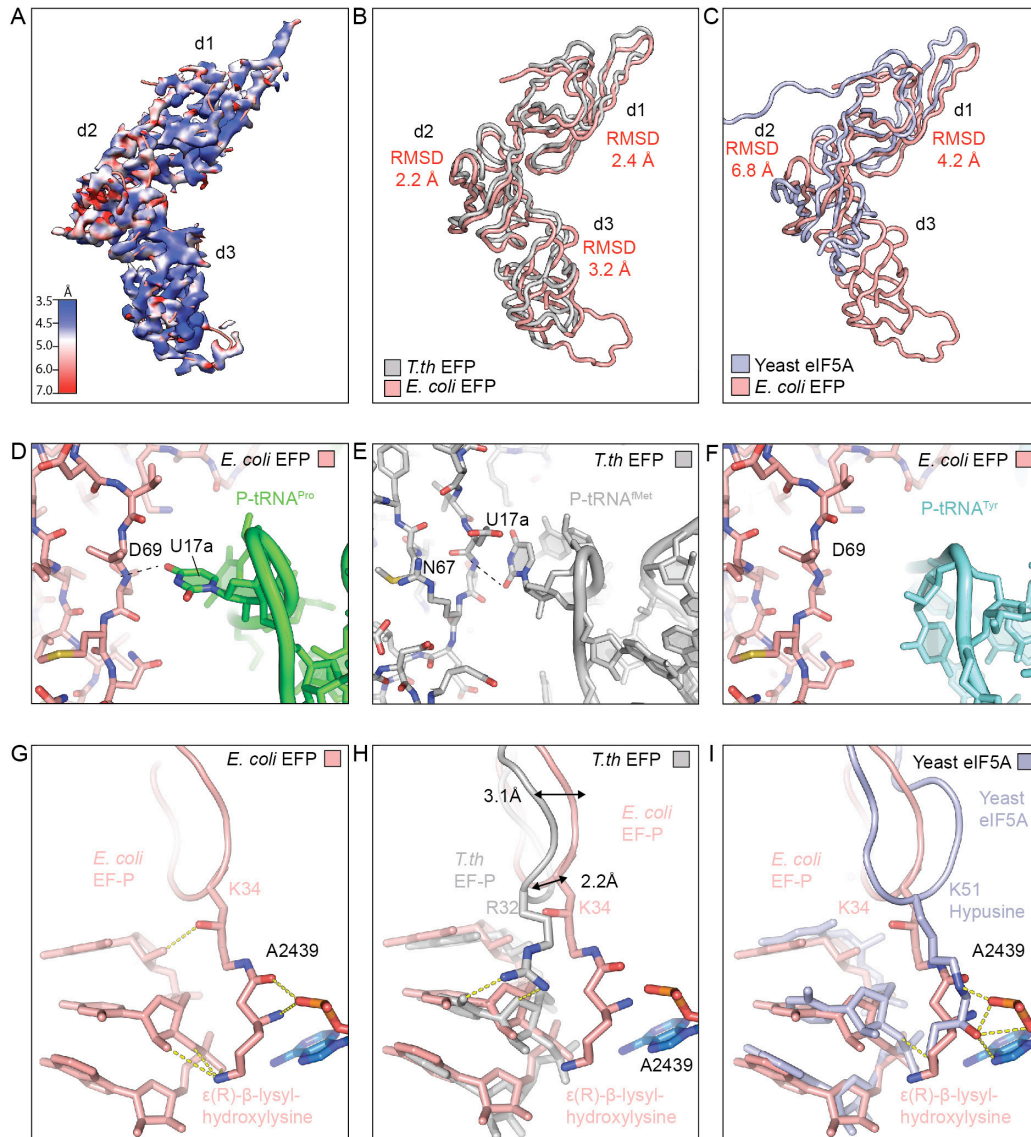


Figure S3 - Related to Figure 4. Comparison of *E. coli* EF-P, *T. thermophilus* EF-P and yeast eIF5A on the ribosome. (A) Cryo-EM density for EF-P coloured according to local resolution, with EF-P domains labeled (d1-d3). (B and C) Superimposition of ribosome-bound conformations of *E. coli* EF-P (salmon) with (B) *T. thermophilus* EF-P (grey) (PDB: 3HUX) (Blaha et al., 2009) and (C) yeast eIF5A (light blue) (PDB: 5GAK)(Schmidt et al., 2016). Root mean square deviations (RMSD) for the individual domains are indicated. (D) Interaction of D69 of *E. coli* EF-P with nucleotide U17a of the

D-loop of P-site tRNA^{Pro} (green). (E) Interaction of N67 of *T. thermophilus* with nucleotide U17a of the D-loop of P-site tRNA^{Met} (grey)(PDB: 3HUX) (Blaha et al., 2009). (F) Absence of interaction of D69 of *E. coli* EF-P with the D-loop of a tRNA^{Tyr} (cyan, PDB: 4WQ1) modeled into the P-site of the ribosome. (G-I) Interaction of (G) *E. coli* EF-P, (H) *T. thermophilus* EF-P (grey)(PDB: 3HUX) (Blaha et al., 2009) and (I) yeast eIF5A (light blue) (PDB: 5GAK) (Schmidt et al., 2016), with the CCA-end of P-site tRNA as well as A2439 (blue) of 23S rRNA (A2808 of 28S rRNA in yeast).

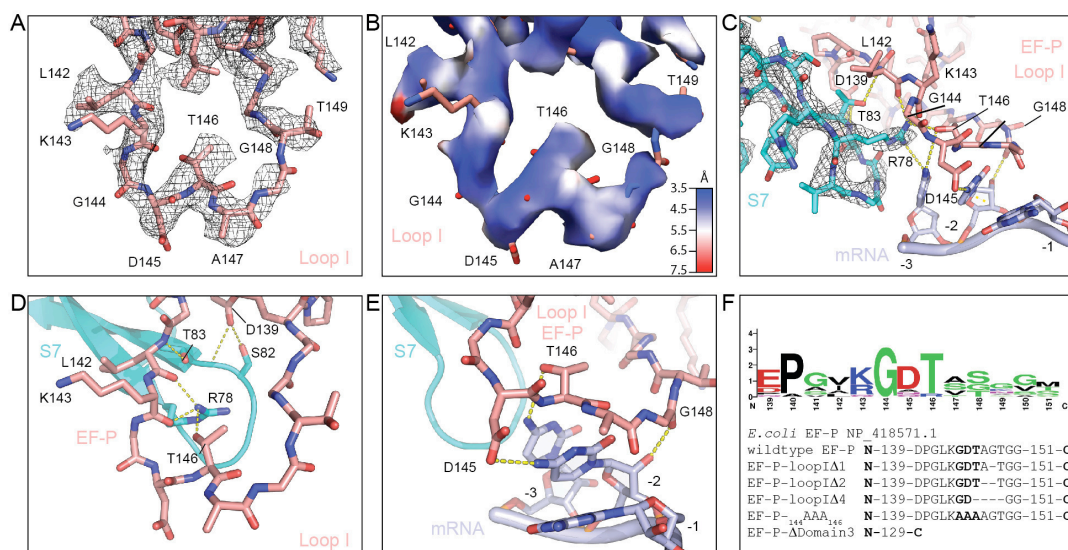


Figure S4 - Related to Figure 4. Interactions of Loop I of domain 3 with S7 and the E-site codon. (A) Electron density (grey mesh) for loop I of domain 3 (salmon). (B) Same as (A) but coloured according to local resolution. (C) Potential hydrogen bonds between loop I of EF-P (salmon), S7 (cyan) and the E-site codon (light blue) are indicated as dashed lines. (D) as (C) but only focusing on interactions between S7 and loop I of EF-P. (E) as (C) but only focusing on the interactions between the E-site codon and loop I. In (C) and (E), -1, -2 and -3 nucleotides of the E-site codon are relative to the first position of the P-site codon. (F) Weblogo of residues of EF-P loop I (based on 12 different bacterial EF-P sequences) and mutation scheme for EF-P variants.

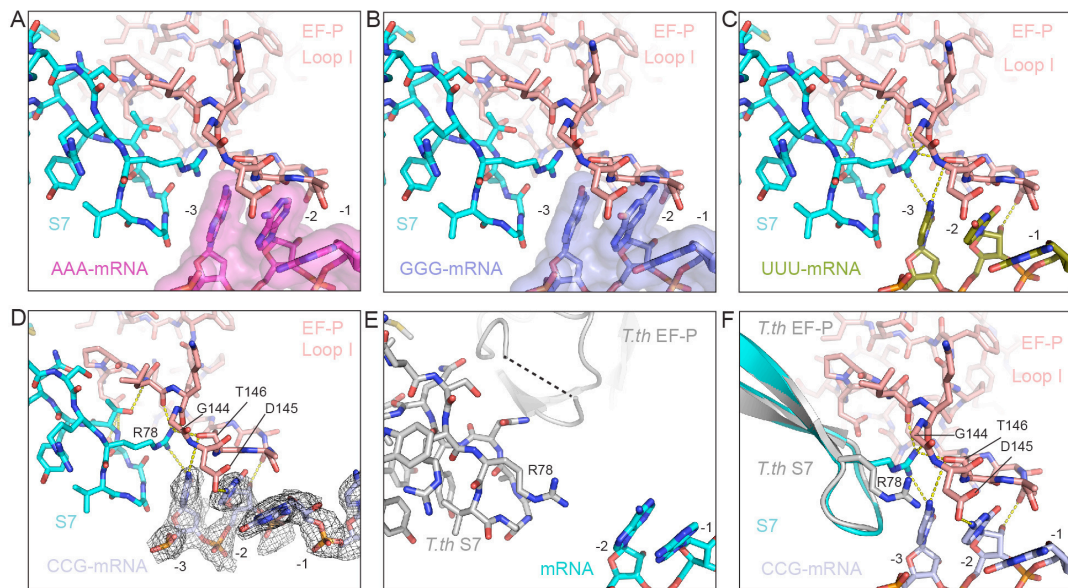


Figure S5 - Related to Figure 4. Interaction of Loop I of EF-P with the E-site codon.

(A and B) Modeling of an (A) AAA (magenta) or (B) GGG (blue) codon in the E-site suggests a steric clash with residues within loop I of EF-P (salmon). (C and D) Interaction of (C) UUU (olive) or (D) CCG (light blue) codon in the E-site with loop I of EF-P and S7 (cyan). Potential hydrogen bonds are indicated with dashed yellow lines. Note an additional interaction of loop I of EF-P with the -2 position of the (D) proline codon CCG, as compared with (C) phenylalanine UUU codon. (E) Lack of interaction of *T. thermophilus* (grey) loop I of EF-P with S7 and mRNA (PDB: 3HUX) (Blaha et al., 2009). (F) Comparison of position of R78 of S7 (grey) from the *T. thermophilus* EF-P (grey) 70S structure (PDB: 3HUX) (Blaha et al., 2009) or S7 (cyan) from our *E. coli* EF-P-PP-70S structure.

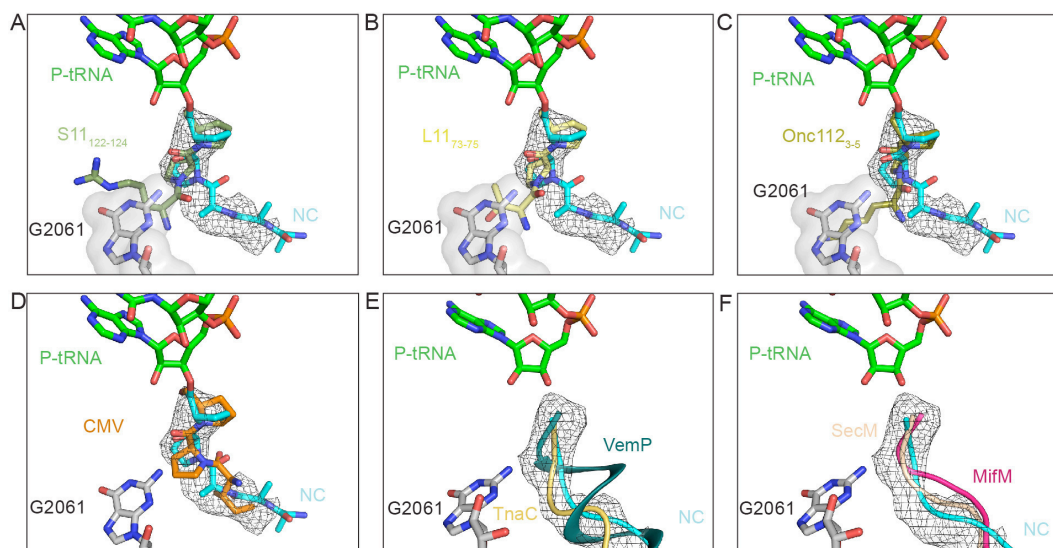


Figure S6 - Related to Figure 5. Conformation of polyproline nascent chain on the ribosome. (A-D) Comparison of cryo-EM density (mesh) and model for Pro-Pro nascent chain (cyan) compared with conformation of diprolyl residues found in (A) S11 (residues 122-124, deep olive), (B) L11 (residues 73-75, yellow), (C) the antimicrobial peptide Onc112 (residues 3-5, olive, PDB: 4ZER) (Seefeldt et al., 2015), and (D) the CMV-stalling peptidyl-tRNA (orange, PDB: 5A8L) (Matheisl et al., 2015). (E and F) Comparison of cryo-EM density (mesh) and model for Pro-Pro nascent chain (cyan ribbon) with (E) TnaC (yellow, PDB: 4UY8) (Bischoff et al., 2014), VemP (dark green, PDB: 5NWY) (Su et al., 2017) as well as (F) MifM (pink, PDB: 3J9W) (Sohmen et al., 2015) and SecM (tan, PDB: 3JBV) (Zhang et al., 2015). The relative position of nucleotide G2061 (grey) of the 23S rRNA is shown for reference.

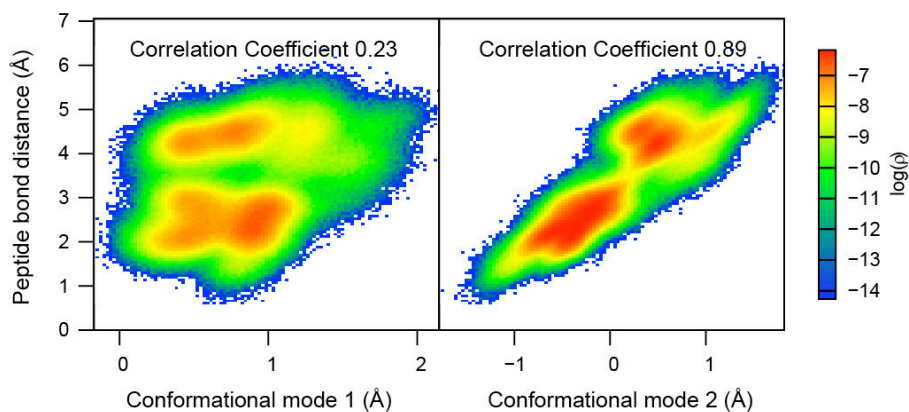


Figure S7 - Related to Figure 6. Conformation of polyproline nascent chain on the ribosome. Logarithm of the probability of finding a given peptide bond distance along the first (left panel) or the second (right) conformational mode of the CCA-end and the C-terminal proline backbone atoms obtained from all the simulations. Mode 2 highly correlates ($cc=0.89$) with the peptide bond distance, while mode 1 describes motions that are largely uncorrelated with the peptide bond distance ($cc=0.23$).